An Euler-Lagrangian concept for transport processes in coupled hydrosystems

Dissertation

zur Erlangung des Grades eines Doktors der Naturwissenschaften

der Geowissenschaftlichen Fakultät
der Eberhard-Karls-Universität Tübingen

vorgelegt von
Dipl.-Phys. Jens-Olaf Delfs
aus Heilbronn

2010

Tag der mündlichen Prüfung: 21. Januar 2010

Dekan: Prof. Dr. rer. nat. Peter Grathwohl

1. Berichterstatter: Prof. Dr.-Ing. Olaf Kolditz

2. Berichterstatter: Prof. Dr.-Ing. Olaf Cirpka

Summary

Understanding and predicting water quality require the concomitant knowledge of water origin and flow paths as stream and catchment hydrology are intimately linked. Bridging of various temporal and spatial scales is a key challenge in the numerical investigation of the terrestrial hydrologic cycle. A physically based numerical model for coupled surface and subsurface water flow with heat and mass transport has been developed in the software toolbox OpenGeoSys. The hydrological processes surface water flow, unsaturated, and saturated flow are described by diffusion type equations and solved with finite element and finite volume methods. New is the application of Lagrangian stochastic particles (random walk particle tracking) for the simulation of advective-diffusive/dispersive transport in coupled hydrosystems. Alternatively, Euler methods can be used. The coupling concept is a compartment approach. Typically, the hydrosphere is subdivided in surface, soil, and aquifer compartments, which interact via exchange fluxes at common interfaces. Each process is numerically solved with its own spatial and temporal discretization and an additional coupling loop is executed (partitioned coupling). A key to the object-oriented implementation of the compartment approach is a hierarchy of geometric, topologic (discretization meshes), and process libraries designed for multiphysics problems. The object-oriented environment of OpenGeoSys for high performance computing was used in the development of a regional hydraulic soil model. A central part of this work is the examination of the novel model with several application examples spanning hydrological and transport processes from laboratory to catchment scales: Two benchmark tests on Horton and Dunne overland flow, a modeling study on Cryptosporidium parvum oocysts, and three case studies - at the Lahn river basin in Germany, the Borden site in Canada, and the Beerze-Reusel drainage basin in the Netherlands.

Zusammenfassung

Das Verstehen und die Prognose von Wasserqualität bedingen eine gleichzeitige Kenntnis von Wasserherkunft und Fließwegen, da die Hydrology von Strömen und Einzugsgebieten eng miteinander verknüpft sind. Die Überbrückung verschiedenartiger Zeit- und Raumskalen ist eine der Hauptherausforderungen bei der numerischen Untersuchung des Wasserkreislaufes der Erde. Ein physikalisch basiertes numerisches Model zur Kopplung von Oberflächen- und Grundwasser einschließlich des Stoff- und Wärmetransportes wurde innerhalb des Programmpaketes OpenGeoSys entwickelt. Die hydrologischen Prozesse Oberflächen-, gesättigte und ungesättigte Strömung werden durch Diffusionsgleichungen beschrieben und mit Finite-Elemente und Finite-Volumen Verfahren gelöst. Neu ist die Anwendung von Lagrangeschen stochastischen Partikeln (random walk particle tracking) zur Simulation von advektiv-diffusivem/dispersivem Transport in gekoppelten Hydrosystemen. Alternativ können auch Eulersche Methoden verwendet werden. Das Kopplungskonzept ist ein Kompartiment-Ansatz. Typischerweise wird die Hydrosphäre in Oberflächen-, Boden- und Aquifer-Kompartimente aufgeteilt, welche über Austauschflüsse an gemeinsamen Schnittstellen interagieren. Jeder Prozess wird mit seiner eigenen räumlichen und zeitlichen Diskretisierung gelöst und eine weitere Kopplungsschleife wird ausgeführt (partitionierte Kopplung). Ein Schlüssel zur objektorientierten Implementierung des Kompartiment-Ansatzes ist eine Hierarchie von geometrischen, topologischen (Diskretisierungsnetzen) und Prozessbibliotheken, welche für Multiphysik-Probleme entworfen wurden. Die objektorientierte Umgebung von OpenGeoSys für Hochleistungsrechnen wurde bei der Entwicklung eines regionalen hydraulischen Bodenmodelles genutzt. Ein zentraler Teil dieser Arbeit ist die Untersuchung des neuen Modelles mit einigen Anwendungsbeispielen, welche hydrologische und Transportprozesse von Labor- bis Einzugsgebietsskala umspannen: Zwei Benchmark-Tests zu Horton'schem und Dunn'schem Oberflächenabfluss, eine Modellierungsstudie zu Cryptosporidium parvum Oozysten und drei Fallstudien - am Flussbecken der Lahn in Deutschland, dem Untersuchungsgebiet Borden in Kanada und dem Beerze-Reusel Einzugsgebiet in den Niederlanden.

Contents

1 Introduction

Hydrological systems belong to the most complex, dynamic and fragile environmental systems affected by both natural and human pressures. The hydrosphere can be subdivided roughly into surface water, vadose zone and aquifer compartments (Fig. 1). The hydrological processes on the surface are related to lakes as well as rivers and overland flow. In the subsurface unsaturated flow occurs in soils and groundwater flow in porous as well as fractured aquifers. The hyporheic interstitial is a region beneath and lateral to a stream bed, where there is mixing of shallow groundwater and surface water The hydrosphere directly interacts with the biosphere and the atmosphere. Water exchange with the atmosphere occurs via evaporation and precipitation whereas root water uptake and transpiration represent links to the biosphere. The transport of contaminants in the hydrosystems strongly depends on the water movement through the compartments. An integrated process understanding is required in order to evaluate impact of anthropogenic influences and the evolution of hydrosystems (Chen et al., 2006). Two of the most difficult and challenging topics in hydrosystem analysis are scale bridging and process coupling.

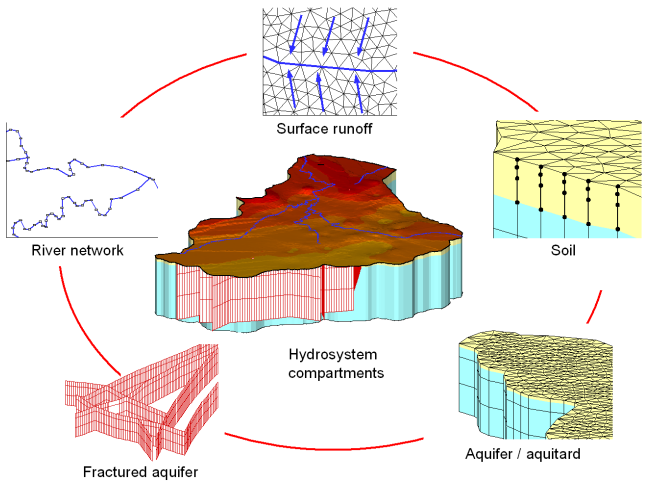

Figure 1: Compartments of environmental hydrosystems

1.1 State of the art

Coupled surface-subsurface flow models have been developed since they were first outlined in Freeze and Harlan (1969). Examples of existing conceptual models and numerical codes include MODFLOW2000 (MODular three finite-difference ground-water FLOW model, Harbaugh et al. (2000)), TOPMODEL (physically based runoff production model, Bertoldi et al. (2004)), Feflow (Wasy Ltd., Wasy Software (2004)), MIKE-SHE (Système Hydrologique Européen, Abbott et al. (1986)), Hydrosphere (Sudicky et al. (2000); Hydrosphere (2006)), SWAT (Arnold et al., 1998), HSPF (Gunduz and Aral (2005); Donigian and Imhoff (2006)), and ParFlow (Kollet and Maxwell, 2006), to mention a few.

Several methods for hydraulic coupling of surface and subsurface compartments have been developed in the past, which can be classified according to their concepts for the hydraulic compartment interaction: (i) The surface water flow equation is treated as a source/sink term in the subsurface water balance equation (Kollet and Maxwell, 2006). (ii) The surface water depth acts as a transient boundary condition for the subsurface water balance equation. The resulting soil water flux provides a source/sink term for the surface flow equation (Smith and Woolhiser, 1971b; Akan and Yen, 1981; Govindaraju and Kavvas, 1991; Singh and Bhallamudi, 1998; Morita and Yen, 2002; Thoms, 2003). (iii) Flux through a thin interface layer provides source/sink terms for both the surface and subsurface flow equations (VanderKwaak, 1999; VanderKwaak and Loague, 2001; Therrien et al., 2004; Gunduz and Aral, 2005; Jones et al., 2006). (iv) Continuity of pressure and water flux across the surface/subsurface water interface (Dawson, 2006). (v) Interface boundary conditions by Beavers and Joseph (1967) for velocity slip at the surface of a porous medium (Discacciati et al., 2002; Miglio, 2003). Two algorithms exist to couple the two water balance equations. In a monolithic scheme, both equations are assembled into a single equation system (Thoms, 2003; Therrien et al., 2004). Monolithic algorithms are particularly suited for strongly coupled processes. In a partitioned (staggered) scheme the equations are coupled in an iterative manner (Smith and Woolhiser, 1971b; Akan and Yen, 1981; Govindaraju and Kavvas, 1991; Singh and Bhallamudi, 1998; Morita and Yen, 2002; Miglio, 2003).

Transport between surface and subsurface compartments has been subject of various studies including numerical investigations with Euler methods (e.g. Richards and Parr (1988); Wallach et al. (1989); Govindaraju (1996); VanderKwaak (1999); Therrien et al. (2004)). Random-walk particle tracking (RWPT) methods have been used extensively to simulate transport of conservative solutes in groundwater systems, and are particularly advantageous in cases of heterogeneous flow and advection-dominated transport (e.g. Kinzelbach (1987); Hoteit et al. (2002); Hassan and Mohamed (2003); Delay et al. (2005)).

Object-oriented programming (OOP) has proven to be a key concept in developing complex software not only in engineering computation (e.g. Forde et al. (1990)) but also in hydrogeology (Desitter et al., 2000; Wang and Kolditz, 2007a). Its advantages become particularly visible in the context of large developer teams and for the reuse, maintenance and extension of codes. In the field of water resources and hydrology, recent object-oriented software developments include models for flood analysis (Alfredsen and Saether, 2000), topographically based watershed analysis (Wang et al., 2005), surface water quality (Elshorbagy and Ormsbee, 2006), and pollutant transport in mine spoil heaps (Gandy and Younger, 2007). The discussion on the literature will be continued later on.

1.2 Thesis objectives and scope

The objective of this thesis is the development and evaluation of a physically based numerical model for coupled surface and subsurface water flow with heat and mass transport. The numerical model is implemented in the object-oriented software toolbox GeoSys/Rockflow. A focus of the thesis is the elaboration and examination of a compartment coupling approach, especially the use of exchange fluxes at common compartment interfaces. Therefore, a sensitivity analysis of hydraulic interface parameters was conducted. A novel part of this thesis is the simulation of transport processes in coupled hydrosystems with various methods, the (control volume) finite element method (FEM) and Lagrangian stochastic particles (RWPT). The numerical scheme is verified with the laboratory experiments by Smith and Woolhiser (1971b) on Horton flow and Abdul and Gilham (1984) on Dunne flow. The thesis includes three case studies: A numerical investigation of thermal signatures in the Lahn river bed to determine hyphorheic exchange. A coupled overland/soil/aquifer system of the Borden field and a parallelized regional hydraulic soil model PRHSM of the Beerze-Reusel drainage basin were developed.

2 Theory of coupled hydrosystems

The same physical principles apply to water movement and contaminant transport in surface and subsurface hydrosystems. Thus, physically and chemically based mass, momentum and energy conservation laws expressed by partial differential equations are used to describe the processes (Abbott et al. (2001); Lees (2000)). We consider the hydrological processes groundwater flow, flow in the unsaturated zone, and surface water flow. Surface water flow comprises overland flow and rivers. We cover heat transport in the subsurface (aquifer and soil) and mass transport on the surface and in the subsurface. The governing equations, which describe the flow processes, are spatially discretized with finite element methods, in particular overland flow with the control volume finite element method. In order to simulate transport processes, finite elements and stochastic particles (RWPT) are used.

The process coupling concept is based on a compartment approach. The hydrosphere is subdivided in surface, soil, and aquifer compartments according to the flow processes surface flow, groundwater flow, and flow in the unsaturated zone, respectively. Heat and mass transport processes can be included in the compartments. The compartments interact with exchange fluxes at common interfaces. Sub-time steps allow to bridge temporal scales. Flexibility in the spatial resolution is achieved by discretizing each process on its own mesh. The discretized governing equations are solved separately with an additional iteration loop (partitioned coupling).

2.1 Mathematical modeling

We describe groundwater flow, flow in the unsaturated zone, and overland flow with diffusion equations. For heat and mass transport we use advection-diffusion/dispersion equations.

2.1.1 Flow

Groundwater Flow in aquifers is described by a three-dimensional fluid mass balance equation with fluxes given by Darcy's law. Laminar flow in rigid saturated porous media is described by (Bear, 1988)

$$\phi S_0 \frac{\partial h^{\mathrm{gf}}}{\partial t} + \nabla \cdot \mathbf{q}^{\mathrm{gf}} = q_s^{\mathrm{gf}} \tag{1}$$

where h^{gf}, hydraulic head, is used as a primary variable for groundwater flow, ϕ is the aquifer porosity, S_0 is the aquifer storativity which accounts for the porous medium matrix and the fluid compression, ∇ is the three-dimensional nabla operator and q_s^{of} is a source/sink term. The groundwater flux $\mathbf{q}^{\mathrm{gf}}$ is given according to Darcy (1856) by

$$\mathbf{q}^{\mathrm{gf}} = -K \nabla h^{\mathrm{gf}} \tag{2}$$

where K is the aquifer hydraulic conductivity tensor.

Unsaturated zone The Richards model is used in order to describe water flow in the unsaturated zone. The Richards model considers flow of the fluid phase with constant air phase pressure and makes use of a generalized form of Darcy's equation used in the groundwater model presented above. It is based on empirical capillary pressure-saturation and relative permeability-saturation functions, e.g. by van Genuchten (1980). Furthermore we assume that the fluid is incompressible and the porous matrix is non-deformable. Therefore the pressure-based Richards equation reads (Warrick, 2003)

$$\phi \frac{\partial S}{\partial t} + \nabla \cdot \mathbf{q}^{\mathrm{sf}} = q_s^{\mathrm{sf}} \tag{3}$$

where ϕ is porosity, S is soil water saturation, q_s^{sf} is a source/sink term. The flux $\mathbf{q}^{\mathrm{sf}}$ is given by

$$\mathbf{q}^{\mathrm{sf}} = -k_r K \nabla \left(h^{\mathrm{sf}} - z \right) \tag{4}$$

where h^{sf}, C, is used as a primary variable for unsaturated flow, k_r denotes relative permeability, K the saturated soil conductivity. Two material dependent constitutive relationships for saturation and permeability are required to close the fluid mass balance equation. The van Genuchten-Mualem soil-water characteristic curves $h^{\mathrm{sf}}(S)$ and $k_r(S)$ are used. With the effective saturation

$$S_e = \max\left(0, \frac{S - S_r}{1 - S_r}\right) \tag{5}$$

where S_r is the residual saturation, the empirical relationships for the capillary pressure h_c and relative permeability k_r read

$$\begin{aligned} h_c(S) &= -h^{\mathrm{sf}} = \frac{1}{\alpha}\left(S_e^{1/m} - 1\right)^{1-m} \\ k_r(S) &= S_e^{1/2}\left[1 - \left(1 - S_e^{1/m}\right)^m\right]^2 \end{aligned} \tag{6}$$

where α and m are soil material parameters.

Surface For the simulation of surface flow a two-dimensional diffusive wave approximation of the Saint-Venant equations is used. The Saint-Venant equations are derived by depth integration of the Reynolds averaged Navier-Stokes equations with the main assumptions of a hydrostatic pressure distribution, small morphology variations and empirical flow resistance distributions Vreugdenhil (1994); Gerbeau and Perthame (2001). These equations are hyperbolic and capable of handling extreme conditions such as dam breaks LeVeque (2002). The diffusive wave approximation of the Saint-Venant equations is parabolic and is derived by neglecting the inertial terms such that they are restricted to subcritical flow conditions Beinhorn (2005). For runoff simulations and flood predictions in rivers they have proven their reliability VanderKwaak (1999). Criteria for the applicability of this equation as well as the kinematic wave equation are given in Ponce et al. (1978); Singh (1994). The diffusive wave shallow water equation is given by (VanderKwaak, 1999)

$$\phi^{\mathrm{of}} \frac{\partial h^{\mathrm{of}}}{\partial t} + \bar{\nabla} \cdot \mathbf{q}^{\mathrm{of}} = q_s^{\mathrm{of}} \tag{7}$$

where h^{of}, hydraulic head, is used as a primary variable for surface water flow, $H = \max(h^{\mathrm{of}} - a - b, 0)$ is the mobile surface water depth, a is the immobile depth, b the bottom elevation, $0 \leq \phi^{\mathrm{of}}(H_a)$ $leq1$ the surface porosity which is unity for flow over a flat plane and varies between zero and unity for flow over an uneven surface, $H_a = h^{\mathrm{of}} - b$ is the surface water depth. $\bar{\nabla}$ is the two-dimensional horizontal nabla operator and q_s^{of} is a source/sink term for surface water. Empirical resistance to flow relationships for bottom friction have the general form (VanderKwaak, 1999)

$$\mathbf{q}^{\mathrm{of}} = -\frac{C_r H^l}{S_s^{1-k}} \bar{\nabla} h^{\mathrm{of}} \tag{8}$$

where

$$S_s = \left[\left(\frac{\partial h^{\mathrm{of}}}{\partial x}\right)^2 + \left(\frac{\partial h^{\mathrm{of}}}{\partial y}\right)^2\right]^{1/2}. \tag{9}$$

The resistance to flow relationship by Manning-Strickler (Manning, 1891) is given by $k = 1/2$, $l = 2/3$ and $C_r = 1/n$, where n

is the Manning friction parameter. The relationship by Darcy-Weisbach (Weisbach, 1845) for laminar flow leads to $k = 1$ and $l = 2$. For a one-dimensional description of rivers equation (8) becomes (Julien, 2002)

$$\mathbf{q}^{\mathrm{of}} = -\frac{C_r R^l}{|\partial h^{\mathrm{of}}/\partial x|^{1-k}} \frac{\partial h^{\mathrm{of}}}{\partial x} \tag{10}$$

where $R = A_F/P$ is the hydraulic radius, A_F the river cross section, and P the wetted perimeter.

General form The previously introduced governing equations for groundwater, soil, and overland flow belong to the general class of (non-linear) diffusion type partial differential equations which can be written as

$$A(u)\frac{\partial u}{\partial t} - \nabla \cdot B(u)\nabla u = Q(u) \tag{11}$$

where u is the unknown field function (primary variable), A is a capacitance matrix (representing time dependencies), B is a conductivity matrix (representing space dependencies), Q is a source/sink term. In general A, B and Q are dependent on the unknown field function u which results in nonlinearities.

2.1.2 Transport

Mass Various processes govern transport of solutes in the liquid phase. Most important are advection (transport with the moving fluid), molecular diffusion (Brownian molecular motion), and mechanical dispersion (spreading of solutes due to tortuosity of the flow path). Furthermore, adsorption onto a porous medium and decay may occur. Interaction with the flow field can occur, if the solute density affects the water density. In the following, we restrict to exponential decay and linear, reversible advection. The transport of solutes in the aquifer is described by (Bear, 1988):

$$\begin{aligned} R_d\phi\frac{\partial c_{\mathrm{st}}^{\mathrm{gf}}}{\partial t} + \mathbf{q}^{\mathrm{gf}} \cdot \nabla c_{\mathrm{st}}^{\mathrm{gf}} - \nabla \cdot \left(\phi\kappa_{\mathrm{st}}^{\mathrm{gf}}\nabla c_{\mathrm{st}}^{\mathrm{gf}}\right) & \\ + R_d\phi k_\lambda c_{\mathrm{st}}^{\mathrm{gf}} &= q_{s\,\mathrm{st}}^{\mathrm{gf}} \end{aligned} \tag{12}$$

where $c_{\mathrm{st}}^{\mathrm{gf}}$, the concentration in water, is used as a primary variable for mass transport in the aquifer, k_λ the decay constant, and $q_{s\,\mathrm{st}}^{\mathrm{gf}}$ a source/sink term. The retardation term R_d describes adsorption. The dispersion coefficient tensor $\kappa_{\mathrm{st}}^{\mathrm{gf}}$ reads

$$\begin{aligned} \kappa_{\mathrm{st}\,ij}^{\mathrm{gf}} &= \lambda_{\mathrm{st}}\tau_{ij} + D_{ij}^{\mathrm{gf}} \\ D_{ij}^{\mathrm{gf}} &= \delta_{ij}\alpha_T|\mathbf{q}^{\mathrm{gf}}| + (\alpha_L - \alpha_T)\frac{q_i^{\mathrm{gf}} q_j^{\mathrm{gf}}}{|\mathbf{q}^{\mathrm{gf}}|} \end{aligned} \tag{13}$$

where λ_{st} is the molecular diffusion coefficient, τ the tortuosity, D^{gf} the dispersion tensor, α_T and α_L the transverse and longitudional dispersivities. The transport of solutes in the unsaturated zone is described by (Bear, 1988):

$$\begin{aligned} R_d\phi\frac{\partial S c_{\mathrm{st}}^{\mathrm{sf}}}{\partial t} + \mathbf{q}^{\mathrm{sf}} \cdot \nabla c_{\mathrm{st}}^{\mathrm{sf}} - \nabla \cdot \left(\phi S\kappa_{\mathrm{st}}^{\mathrm{sf}}\nabla c_{\mathrm{st}}^{\mathrm{sf}}\right) & \\ + R_d\phi S k_\lambda c_{\mathrm{st}}^{\mathrm{sf}} &= q_{s\,\mathrm{st}}^{\mathrm{sf}} \end{aligned} \tag{14}$$

where $c_{\mathrm{st}}^{\mathrm{sf}}$, the concentration in water, is used as a primary variable for mass transport in the unsaturated zone, and $q_{s\,\mathrm{st}}^{\mathrm{sf}}$ is a source/sink term. The dispersion coefficient tensor $\kappa_{\mathrm{st}}^{\mathrm{sf}}$ and the dispersion tensor D^{sf} for molecular diffusion and mechanical dispersion in the liquid phase read

$$\begin{aligned} \kappa_{\mathrm{st}\,ij}^{\mathrm{sf}} &= \lambda_{\mathrm{st}}\tau_{ij} + D_{ij}^{\mathrm{sf}} \\ D_{ij}^{\mathrm{sf}} &= \delta_{ij}\alpha_T|\mathbf{q}^{\mathrm{sf}}| + (\alpha_L - \alpha_T)\frac{q_i^{\mathrm{sf}} q_j^{\mathrm{sf}}}{|\mathbf{q}^{\mathrm{sf}}|}. \end{aligned} \tag{15}$$

The transport of solutes on the surface is described by (VanderKwaak, 1999)

$$\begin{aligned} \frac{\partial \phi^{\mathrm{of}} H c_{\mathrm{st}}^{\mathrm{of}}}{\partial t} + \phi^{\mathrm{of}} H\mathbf{q}^{\mathrm{of}} \cdot \nabla c_{\mathrm{st}}^{\mathrm{of}} & \\ -\nabla \cdot \left(\phi^{\mathrm{of}} H\kappa_{ij}^{\mathrm{of}}\nabla c_{\mathrm{st}}^{\mathrm{of}}\right) + \phi^{\mathrm{of}} H k_\lambda c_{\mathrm{st}}^{\mathrm{of}} &= \phi^{\mathrm{of}} H q_{s\,\mathrm{st}}^{\mathrm{of}} \end{aligned} \tag{16}$$

where $c_{\mathrm{st}}^{\mathrm{of}}$, the concentration in water, is used as a primary variable for mass transport on the surface and $q_{s\,\mathrm{st}}^{\mathrm{of}}$ is a source/sink term. Molecular diffusion and mechanical dispersion in the fluid phase are described by the dispersion coefficient tensor $\kappa_{\mathrm{st}}^{\mathrm{of}}$ and the dispersion tensor D^{of} according to

$$\begin{aligned} \kappa_{\mathrm{st}\,ij}^{\mathrm{of}} &= \lambda_{\mathrm{st}} + D_{ij}^{\mathrm{of}} \\ D_{ij}^{\mathrm{of}} &= \delta_{ij}\alpha_T|\mathbf{q}^{\mathrm{of}}| + (\alpha_L - \alpha_T)\frac{q_i^{\mathrm{of}} q_j^{\mathrm{of}}}{|\mathbf{q}^{\mathrm{of}}|}. \end{aligned} \tag{17}$$

Heat For heat transport also advection and diffusion are important physical processes. A difference to mass transport is, that the thermal diffusion coefficient is about three orders of magnitude smaller. Dispersion in the subsurface is usually negligible. Usually there is significant heat transport in the solid phase. We restrict this work on heat transport in the soil and aquifer. Heat transport in the aquifer is described by (Bear, 1988)

$$\frac{\partial C^{\mathrm{gf}} T^{\mathrm{gf}}}{\partial t} + c^f\rho^f\mathbf{q}^{\mathrm{gf}} \cdot \nabla T^{\mathrm{gf}} - \nabla \cdot \left(\kappa_{\mathrm{ht}}\nabla T^{\mathrm{gf}}\right) = q_{s\,\mathrm{ht}}^{\mathrm{gf}} \tag{18}$$

where T^{gf} is the temperature, which is used as a primary variable for heat transport in the aquifer. The superscripts f refers to the fluid phase and s to the solid phase, κ^{ht} is the thermal diffusivity and $q_{s\,\mathrm{ht}}^{\mathrm{gf}}$ a heat source/sink term. The heat capacity C^{gf} is given by

$$C^{\mathrm{gf}} = \phi c^f\rho^f + (1-\phi)c^s\rho^s \tag{19}$$

where c is the specific heat capacity and ρ bulk densities. The thermal diffusivity $\kappa_{\mathrm{ht}}^{\mathrm{gf}}$ reads

$$\begin{aligned} \kappa_{\mathrm{ht}\,ij}^{\mathrm{gf}} &= \lambda_{\mathrm{ht}}^{\mathrm{gf}}\tau_{ij} + c^f\rho^f D_{ij}^{\mathrm{gf}} \\ \lambda_{\mathrm{ht}}^{\mathrm{gf}} &= \phi\lambda_{\mathrm{ht}}^f + (1-\phi)\lambda_{\mathrm{ht}}^s \end{aligned} \tag{20}$$

where $\lambda_{\mathrm{ht}}^{\mathrm{gf}}$ is the thermal conductivity for heat transport in the aquifer. The dispersion tensor D^{gf} is given in equations (13). Heat transport in the unsaturated zone is described by (Bear, 1988)

$$\frac{\partial C^{\mathrm{sf}} T^{\mathrm{sf}}}{\partial t} + c^f\rho^f\mathbf{q}^{\mathrm{sf}} \cdot \nabla T^{\mathrm{sf}} - \nabla \cdot \left(\kappa_{\mathrm{ht}}^{\mathrm{sf}}\nabla T^{\mathrm{sf}}\right) = q_{s\,\mathrm{ht}}^{\mathrm{sf}} \tag{21}$$

where T^{gf} the temperature is used as a primary variable for heat transport in the unsaturated zone and $q_{s\,\mathrm{ht}}^{\mathrm{sf}}$ is a heat source/sink term. The thermal capacity C^{sf} reads

$$C^{\mathrm{sf}} = \phi(Sc^f\rho^f + (1-S)c^g\rho^g) + (1-\phi^{\mathrm{sf}})c^s\rho^s \tag{22}$$

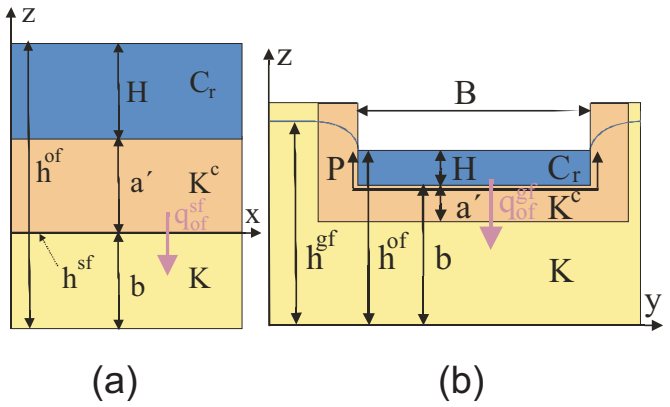

Figure 2: Exchange fluxes between (a) overland flow and unsaturated zone ,(b) river and aquifer. Interface layer (with conductivity K^c) between surface flow (Friction coefficient C_r) and soil/aquifer (conductivity K) for the calculation of coupling fluxes $q^{\mathrm{sf}}_{\mathrm{of}}$ (Eqn. 25), $q^{\mathrm{gf}}_{\mathrm{of}}$ (Eqn. 26).

where the superscript g refers to the gaseous phase. The thermal diffusivity $\kappa^{\mathrm{sf}}_{\mathrm{ht}}$ and the thermal diffusion coefficient $\lambda^{\mathrm{sf}}_{\mathrm{ht}}$ read

$$\begin{aligned} \kappa^{\mathrm{sf}}_{\mathrm{ht}\,ij} &= \lambda^{\mathrm{sf}}_{\mathrm{ht}}\tau_{ij} + c^f\rho^f D^{\mathrm{sf}}_{ij} \\ \lambda^{\mathrm{sf}}_{\mathrm{ht}} &= \phi(S\lambda^f_{\mathrm{ht}} + (1-S)\lambda^g_{\mathrm{ht}}) + (1-\phi)\lambda^s_{\mathrm{ht}} \end{aligned} \tag{23}$$

where the dispersion tensor D^{sf} is given in equations (15).

General form The previously introduced governing equations for mass and heat transport are advection-diffusion equations of the general form

$$A\frac{\partial u}{\partial t} + \mathbf{q}^*\nabla u - \nabla\cdot B\nabla u = Q \tag{24}$$

where u is the unknown field function (primary variable), A is a capacitance matrix (representing time dependencies), B is a conductivity matrix (representing space dependencies), Q is a source/sink term. The fluxes $\mathbf{q}^*$ in the advection term are given by equation (2) for groundwater flow, equation (4) for the unsaturated zone, and equation (8) for transport on the surface.

2.1.3 Coupling fluxes

For the definition of an exchange flux at a common compartment boundary an interface is introduced (Fig. 2). First order exchange fluxes between overland flow and flow in the unsaturated zone read (VanderKwaak, 1999)

$$q^{\mathrm{sf}}_{\mathrm{of}} = k_{a'}\Lambda\left(h^{\mathrm{of}} - h^{\mathrm{sf}}\right), \qquad \Lambda = \frac{K^c}{a'}, \qquad q^{\mathrm{of}}_{\mathrm{sf}} = -q^{\mathrm{sf}}_{\mathrm{of}} \tag{25}$$

where Λ is the leakance, K^c is the interface conductivity, and a' is the interface layer thickness. $0 \le k_{a'}(H_a) \le 1$ is a scaling factor to ensure that infiltration is not exceeding the available surface liquid. The scaling factor $k_{a'}$ varies between zero for dry and unity for fully saturated interface ($H_a \ge a$). The exchange fluxes between river and aquifer compartments are given by (Gunduz and Aral, 2005)

$$q^{\mathrm{gf}}_{\mathrm{of}} = \frac{P}{B}\Lambda\left(h^{\mathrm{of}} - h^{\mathrm{gf}}\right), \qquad q^{\mathrm{of}}_{\mathrm{gf}} = -q^{\mathrm{gf}}_{\mathrm{of}} \tag{26}$$

where B is the river breadth. Is the groundwater level below the river bottom, the exchange fluxes become

$$q^{\mathrm{gf}*}_{\mathrm{of}} = \Lambda H, \qquad q^{\mathrm{of}*}_{\mathrm{gf}} = -q^{\mathrm{gf}*}_{\mathrm{of}}. \tag{27}$$

The coupling fluxes (25), (26) and (27) provide source/sink terms in the equations (1) for groundwater flow, (3) for flow in the unsaturated zone and (7) for surface water flow.

In the coupling of transport processes solely advective exchange is considered (Therrien et al., 2004). Diffusive exchange was investigated for example by Richards and Parr (1988), Wallach et al. (1989), Govindaraju (1996) and VanderKwaak (1999). The exchange fluxes for mass transport between the overland flow and soil compartments read for example

$$q^{\mathrm{sf}}_{\mathrm{of\,st}} = q^{\mathrm{sf}}_{\mathrm{of}}\frac{c^{\mathrm{of}}_{\mathrm{st}} - c^{\mathrm{sf}}_{\mathrm{st}}}{a'}, \qquad q^{\mathrm{of}}_{\mathrm{sf\,st}} = -q^{\mathrm{sf}}_{\mathrm{of\,st}} \tag{28}$$

where $q^{\mathrm{sf}}_{\mathrm{of}}$ is given by equation (25).

2.2 Numerical methods

A variety of finite difference, finite element, and finite volume methods are available to solve the partial differential equations appearing in hydrosystems (Weiyan, 1992; Vreugdenhil, 1994; LeVeque, 2002; Quarteroni and Valli, 1994; Starke, 2005). In general, either of these methods leads to a (non-linear) algebraic system of equations. In order to resolve non-linearities in the governing equations, Picard and Newton-Raphson iteration schemes are used. For a comparison of both see for instance Paniconi et al. (1991). Also for transport processes finite difference, finite element, and finite element methods are used (Huyakorn and Pinder, 1983; Bear and Verruijt, 1987; Quarteroni and Valli, 1994) and additionally random walk particle tracking methods (Kinzelbach, 1987).

We use FEMs, more specifically the Galerkin and the control volume finite element method (CVFEM) with Picard and Newton-Raphson iteration, respectively, to solve the governing equations of the form (11) since finite elements are well suited for problems with complex geometries. For time discretisation a weighting parameter enables the choice between fully explicit and implicit Euler stepping schemes. Usually time stepping for parabolic equations is chosen in accordance with the Neumann criterium (e.g. Quarteroni and Valli (1994)). For transport processes we use both FEM and RWPT according to Hoteit et al. (2002). If the advection-diffusion equation is solved with an Eulerian method (e.g. FEM) the spatial discretization has also to satisfy the Peclet criterium (e.g. Quarteroni and Valli (1994)). We will introduce the finite element method for the simulation of the flow processes (Eqn. 11) and the particle tracking method concerning transport processes (Eqn. 24).

2.2.1 Finite element method

The FEM is based on the weak formulation of a partial differential equation, which allows the search for generalised solutions in Sobolev spaces. These contain discontinuous solutions and allow the assignment of discontinuous functions for material properties. The model domain is subdivided into small subdomains, the finite elements. The division can be performed according to geological structures, hydrological structures or other requirements. Calculations for these finite elements are performed after a transformation to a basis element. On each element the solution is locally approximated with piecewise polynomial functions forming the basis of an approximated solution space. The equation system for the solution of the unknown field function u is assembled from all element contributions.

Galerkin finite element method The standard Galerkin FEM is used for the subsurface compartments (soil and groundwater) because of the slow water movement. In order to obtain

the weak formulation of the general diffusion equation, the expression (11) is multiplied with test functions v and integrated over the domain Ω giving

$$\int_\Omega v\left(A\frac{\partial u}{\partial t} - \nabla\cdot B\nabla u\right) d\Omega = \int_\Omega vQ\, d\Omega \tag{29}$$

Applying Green's formula gives

$$\begin{aligned}&\int_\Omega vA\frac{\partial u}{\partial t}\, d\Omega + \int_\Omega \nabla v\cdot B\nabla u\, d\Omega \\ &= \int_\Gamma v\,(B\nabla u)\cdot \mathbf{n}_\Gamma\, d\Gamma + \int_\Omega vQ\, d\Omega\end{aligned} \tag{30}$$

where $\Gamma = \partial\Omega$ is the domain boundary and $\mathbf{n}_\Gamma$ the unit outward normal vector on Γ. These equations are valid for all test functions v in the Sobolev space $H^1(\Omega)$. In the Galerkin FEM and CVFEM the unknown field functions u as well as test functions v belong to the same Sobolev space. For the numerical solution u and v are approximated on a finite dimensional subspace spanned by polynomial basis functions. This reads

$$\begin{aligned}u(t,x,y,z) &\approx \hat{u}(t,x,y,z) = \sum_{j=1}^{ng}\phi_j(x,y,z)\,u_j(t) = \sum_{j=1}^{ng}\phi_j\,u_j \\ v(t,x,y,z) &\approx \hat{v}(t,x,y,z) = \sum_{i=1}^{ng}\phi_i(x,y,z)\,v_i(t) = \sum_{i=1}^{ng}\phi_i\,v_i\end{aligned} \tag{31}$$

where $\hat{u}$ and $\hat{v}$ are the approximate solutions, ϕ_i the basis functions and ng the dimension of the subspace which is equal to the number of grid nodes in the finite element discretisation. Therefore, equation (30) is transformed into an algebraic equation system.

$$\begin{aligned}&\sum_{j=1}^{ng}\left(\left[\int_\Omega \phi_i A\phi_j\, d\Omega\right]\frac{du_j}{dt} + \left[\int_\Omega \nabla\phi_i\cdot B\nabla\phi_j\, d\Omega\right]u_j\right) \\ &= \int_{\partial\Omega}\phi_i\,(B\nabla u)\cdot\mathbf{n}_\Gamma\, d\Gamma + \int_\Omega \phi_i Q\, d\Omega, \quad i = 1,\ldots,ng.\end{aligned} \tag{32}$$

The basis functions are subdivided into local basis functions for each element e with the domain Ω^e giving

$$\begin{aligned}&\sum_{s=1}^{ne}\left(\left[\int_{\Omega^e}\phi_r A\phi_s\, d\Omega\right]\frac{du_s}{dt} + \left[\int_{\Omega^e}\nabla\phi_r\cdot B\nabla\phi_s\, d\Omega\right]u_s\right) \\ &= \int_{\partial\Omega^e}\phi_r\,(B\nabla u)\cdot\mathbf{n}_\Gamma\, d\Gamma + \int_{\Omega^e}\phi_r Q\, d\Omega, \quad r = 1,\ldots,ne\end{aligned} \tag{33}$$

where ne is the number of element nodes. Equation (33) can be written as

$$\sum_{s=1}^{ne}\left(A^e_{rs}\frac{du_s}{dt} + B^e_{rs}u_s\right) = g^e_r + s^e_r + r^e_r \quad , \quad r = 1,\ldots,ne \tag{34}$$

where A^e_{rs} is the capacitance matrix, B^e_{rs} the conductance matrix, g^e_r accounts for the gravity term, s^e_r for the source terms and r^e_r for the boundary fluxes. The integrals are calculated with the Gaussian integration scheme yielding for the capacitance matrix entries

$$\begin{aligned}A^e_{rs} &= \int_{\Omega^e}\phi_r A\phi_s\, d\Omega = \int_{\hat{\Omega}^e}\hat{\phi}_r\hat{A}\hat{\phi}_s\,\det J\, d\hat{\Omega} \\ &= \sum_{k=1}^{gp} W_k(\hat{x}_k)\,\hat{\phi}_r(\hat{x}_k)\hat{A}(\hat{x}_k)\hat{\phi}_s(\hat{x}_k)\,\det J(\hat{x}_k)\end{aligned} \tag{35}$$

with the Jacobian matrix J of the coordinate transformation from the basis element domain $\hat{\Omega}$ to the element domain $\hat{\Omega}^e$ and the Gauss weights W_k. Entries of capacitance matrix as well as of gravity, source and boundary flux vector are calculated accordingly. Applying an Euler finite difference scheme to equation (34) for the approximation of the time derivative yields

$$\begin{aligned}&\sum_{s=1}^{ne}\left(\frac{A^e_{rs}}{\Delta t} + \theta B^e_{rs}\right)u^{n+1}_s = g^e_r + s^e_r + r^e_r \\ &+\sum_{s=1}^{ne}\left(\frac{A^e_{rs}}{\Delta t} - (1-\theta)B^e_{rs}\right)u^n_s, \quad r = 1,\ldots,ne\end{aligned} \tag{36}$$

where θ is an implicit-explicit weighting parameter. Frequently mass lumping schemes are employed in order to stabilize the numerical method. Defining

$$M^e_r = \int_{\Omega^e} A\phi_r\, d\Omega, \tag{37}$$

the mass matrix lumped form of equation (34) reads

$$M^e_r\frac{du_r}{dt} + \sum_{s=1}^{ne}B^e_{rs}u_s = g^e_r + s^e_r + r^e_r, \quad r = 1,\ldots,ne. \tag{38}$$

Control volume finite element method for surface flow The traditional FEMs such as the Galerkin and Petrov-Galerkin schemes tend to show non-physical oscillations for overland flow simulations (Di Giammarco et al., 1996; Beinhorn, 2005). On the other hand, finite volume methods have shown to handle these difficulties (LeVeque, 2002). Di Giammarco et al. (1996) suggested the CVFEM which effectively combines the finite element with the finite volume method. It avoids oscillations by mass matrix lumping as well as conductivity term upwinding (Forsyth and Kropinski, 1997) and guarantees local mass conservation. Using Lagrange polynominal basis functions ϕ_r where $\sum\phi_r = 1$, for the numerical approximation of the solution u and for the test function v, we have

$$\nabla\sum_{s=1}^{ne}u_s\phi_s = \nabla\sum_{s\neq r}\phi_s(u_s - u_r). \tag{39}$$

This allows to express the diffusion term in equation (33) as a function of the primary variable difference between node r and its neighbors. Using this scheme, the lumped mass matrix equation (38) becomes

$$V^e_r\frac{du_r}{dt} + \sum_{s\neq r}B^e_{rs}(u_s - u_r) = s^e_r + r^e_r \quad , \quad r = 1,\ldots,ne \tag{40}$$

where

$$V^e_r = \int_{\Omega^e}\phi_r\, d\Omega. \tag{41}$$

The conductance term can be written as $B = k^{\mathrm{of}}_r K^{\mathrm{of}}$, where $k^{\mathrm{of}}_r(u)$, K^{of} represent primary variable dependent and independent parts in equation (8). Therefore, equation (40) becomes

$$\begin{aligned}V^e_r\frac{du_r}{dt} &= \sum_{s\neq r}\lambda_{rs+1/2}\gamma^e_{rs}\,(u_s - u_r) + s^e_r + r^e_r \\ &\qquad\qquad r = 1,\ldots,ne\end{aligned} \tag{42}$$

where

$$\begin{aligned}\gamma^e_{rs} &= \int_{\Omega^e}\nabla\phi_r K^{\mathrm{of}}\nabla\phi_s d\Omega \\ &= \int_{\hat{\Omega}^e}\hat{\nabla}\hat{\phi}_r\hat{K}^{\mathrm{of}}\hat{\nabla}\hat{\phi}_s\,\det J\, d\hat{\Omega} \\ &= \sum_{k=1}^{gp}W_k(\hat{x}_k)\,\hat{\nabla}\hat{\phi}_r(\hat{x}_k)d\hat{K}^{\mathrm{of}}(\hat{x}_k)\hat{\nabla}\hat{\phi}_s(\hat{x}_k)\,\det J(\hat{x}_k)\end{aligned} \tag{43}$$

and upwinding is implemented by

$$\lambda_{rs+1/2} = \begin{cases} k_{r\,s} & \text{if } \gamma_{rs}(u_s - u_r) > 0 \\ k_{r\,r} & \text{if } \gamma_{rs}(u_s - u_r) < 0 \end{cases} \tag{44}$$

such that k_r represents a weighted conductivity. The right-hand-side terms s_r^e, r_r^e are coupling terms to the soil compartment. The Euler time stepping scheme gives

$$\frac{V_r^e}{\Delta t} u_r^{n+1} + \theta \sum_{s \neq r} \lambda_{rs+1/2}^{n+1} \gamma_{rs}^e \left(u_s^{n+1} - u_r^{n+1}\right) \tag{45}$$
$$= s_r^e + r_r^e - \frac{V_{rs}^e}{\Delta t} u_s^n - (1-\theta) \sum_{s \neq r} \lambda_{rs+1/2}^n \gamma_{rs}^e \left(u_s^n - u_r^n\right), \quad r = 1, \ldots, ne$$

with the implicit-explicit weighting parameter θ. For linearisation a Newton-Raphson scheme is applied. The Jacobian matrix in this iteration is approximated by a numerical derivative, which provides an effective matrix assembly method (Forsyth et al., 1995).

2.2.2 Random Walk Particle Tracking

In order to solve the advection-diffusion equation, we use the RWPT method by Hoteit et al. (2002). The position $\mathbf{x}$ of each particle for the new time step is determined for each component $i \leq d$ according to the stochastic equation (Kinzelbach, 1987)

$$\begin{aligned} x_i(t + \Delta t) &= x_i(t) + \left(q_i^*(\mathbf{x}) + \sum_{j=1}^{d} \frac{\partial \kappa_{*\,ij}^*}{\partial x_j} \right) \Delta t \\ &+ \sum_{j=1}^{d} \sqrt{2 \kappa_{*\,ij}^* \Delta t} Z_j \end{aligned} \tag{46}$$

where Δt is the time step length, $d = 2, 3$ the dimension and Z_i d random variables with the mean value of 0 and the variance 1. The fluxes $\mathbf{q}^*$ in aquifer, soil, and on the surface are given by equations (2), (4), and (8), respectively. The fluxes are calculated at the discretization nodes with finite elements (Park et al., 2008b). The dispersion coefficient tensor κ_*^* is given by equations 13, 15, 17 for mass transport and by equations 20, 23 for heat transport.

2.3 Compartment coupling approach

The coupling concept for the analysis of hydrosystems is based on a compartment approach. The hydrosphere is subdivided in aquifer, soil and surface compartments which host the corresponding flow and transport processes (secs. 2.1.1, 2.1.2). In this section we briefly summarize the key features of the coupling concept.

Multi-meshing To keep flexibility in the spatial resolution, each process is solved with a mesh optimized for its geological, hydrological structures, and numerical constraints. The implementation of the multi-mesh concept will be described in Sec. 3.1.3. A demonstration example will be given with the application to the Borden field site (Sec. 4.5). The most important requirement of a spatial discretization of the advection-diffusion equation (24) is the Peclet criterium. The Peclet number reads (Quarteroni and Valli, 1994)

$$Pe := \frac{|\mathbf{q}^*| \Delta l}{2D} \tag{47}$$

where Δl is a characteristic length scale of the spatial discretisation and D is a process-related diffusivity coefficient. The solution of equation (24) with the Galerkin FEM exhibits ocillatory behavior for $Pe > 1$. The Peclet criterium can be circumvented with RWPT.

Exchange fluxes Processes of adjacent compartments interact with coupling fluxes (sec. 2.1.3). Within hydraulically relevant time periods the water has to be passed through the common domain boundaries which reads for the overland and soil process coupling for example

$$Q_{\mathrm{sf}}^{\mathrm{of}} \Delta t = Q_{\mathrm{of}}^{\mathrm{sf}} \Delta t = \int_{\Delta t} \int_{A^{of}} q_{\mathrm{sf}}^{\mathrm{of}} \, d\Gamma \, dt \tag{48}$$

where $A^{\mathrm{of}} = A^{\mathrm{sf}}$ is the common overland and soil water flow compartment boundary. An important requirement for flux coupling is topological consistency, specifcally, the interface area between coupled compartments has to be the same for both. The implementation of this requirement will be described in Sec. 3.1.2.

If transport processes are simulated with RWPT, the ratio of water content and coupling flux gives a probability for a particle to cross a compartment interface. For example in case of infiltration the probability that a particle in the surface compartment enters the unsaturated zone is given by $q_{\mathrm{of}}^{\mathrm{sf}} \Delta t / H$ for $a = 0$.

Sub-time stepping The temporal discretization needs to meet process-specific requirements. The Neumann criterium for maximum time steps in diffusion type partial differential equations (11) reads (Quarteroni and Valli, 1994)

$$\Delta t = \frac{1}{2} \frac{\Delta l^2}{D}. \tag{49}$$

The sub-time stepping method by Bhallamudi et al. (2003) allows to deal with the different time scales in hydrosystems. Table 1 illustrates a typical situation with fast overland flow, Richards flow, and groundwater flow as the slowest process. The time step size can be determined adaptively (Du and Kolditz, 2005).

Table 1: Coupling scheme for time discretization of a surface/soil/aquifer system.

Δt	OF	SF	GF	Coupling
1	Δt_1^{of}			
⋮	⋮			
i	Δt_i^{of}	Δt_1^{sf}		OF/SF
⋮	⋮	⋮		
j	Δt_j^{of}	Δt_k^{sf}	Δt_1^{gf}	OF/SF/GF
⋮	⋮	⋮	⋮	

Partitioned coupling In general two concepts exist for equation coupling: Monolithic schemes for strongly coupled systems (e.g. Wang and Kolditz (2007a)) and partitioned (or staggered) techniques for weakly connected systems. In partitioned coupling an additional iteration loop is executed. Since the hydrological compartments interact weakly, we have adopted a partitioned coupling scheme for hydrosystems modelling. For a surface/soil/aquifer hydrosystem the equation system becomes

$$\begin{aligned} \left[P^{\mathrm{of}}\right] \left[u^{\mathrm{of}}\right] &= \left[r^{\mathrm{of}} + r^{\mathrm{of/sf}}\right] \\ \left[P^{\mathrm{sf}}\right] \left[u^{\mathrm{sf}}\right] &= \left[r^{\mathrm{sf}} + r^{\mathrm{sf/of}} + r^{\mathrm{sf/gf}}\right] \\ \left[P^{\mathrm{gf}}\right] \left[u^{\mathrm{gf}}\right] &= \left[r^{\mathrm{gf}} + r^{\mathrm{gf/sf}}\right]. \end{aligned} \tag{50}$$

where P^*, u^*, r^* are system matrix, solution vector, and RHS vector for overland, soil, and groundwater flow, respectively.

3 Computational methods

The compartment coupling approach (sec. 2.3) has been implemented in the object-oriented toolbox OpenGeoSys (Kolditz and Bauer, 2004; Wang and Kolditz, 2007b; Park et al., 2008a). GeoSys is a scientific open source software with an internet based Wikipedia platform. Software verification examples for the compartment approach are provided in Kolditz and Shao (2009). A key to the implementation of the compartment approach is a library hierarchy (sec. 3.1) which separate geometric data (e.g., points, polylines), discretization meshes, and process related information (e.g., matrix assembly, primary and secondary variables). An essential tool for large-scale applications is parallelization (sec. 3.2).

3.1 Object-orientation

The general idea of object-oriented programming (OOP) is the projection of the domain of problems (e.g. solution of PDEs) to a hierarchic class concept. A basic feature of OOP is the inheritance of class properties. The object-oriented concept is designed for the solution of multi-field problems in the context of continuum mechanics. It has already been successfully applied in several areas of porous media mechanics, i.e. TH (Kolditz and Bauer, 2004), THM (Wang and Kolditz, 2007a) and THC processes (Xie et al., 2006), where T-H-M-C stands for thermo-hydro-mechanical-chemical processes.

The novel part in this work is the extension of the object-oriented concept to hydrological problems including heat and mass transport. This requires the solution of partial differential equations on different discretizations (MultiMSH concept, sec. 3.1.3) and an appropriate coupling concept of the separate compartments at their common interfaces (secs. 2.1.3, 2.3). For the sake of clarity we make use of object input files for the explanation of the data structures and software implementation.

3.1.1 Object libraries

A key to the implementation of the compartment approach for hydrological systems modeling is the library concept. The GeoSys/RockFlow code consists of the following libraries:

- GEOLib: Geometric objects which are points, polylines, surfaces and volumes as well as related operations (level 1). Base classes are `CPoint,CPolyline,CSurface,CVolume`.
- MSHLib: Topological objects which are meshes, mesh nodes and elements as well as related methods and material properties (level 2). Base classes are `CNode` and `CElement`.
- PCSLib: Objects to solve partial differential equations based on numerical and related methods (level 3). Base class is `CProcess`.

Library hierarchy and access control are as follows: GEOLib is completely independent, MSHLib is allowed to use GEOLib data and methods, PCSLib is allowed to use MSHLib and GEOLib data and methods (Fig. 3). GEOLib (level 1) is accessible from all compartments. MSHLib (level 2) is related to specific compartments. Coupling between adjacent compartments is implemented by a common geometric interface. PCSLib (level 3) is compartment specific. Level 3 implementations benefit from this hierarchy in many ways. As an example, every FEM kernel needs geometric, topological and material-related operations, such as element volume calculations, shape functions and element-dependent material properties for the algebraic equation assembly. Hierarchic encapsulation of these steps leads to simple implementations even in coupled multi-field problems, as shown in previous work (Wang and Kolditz, 2007b).

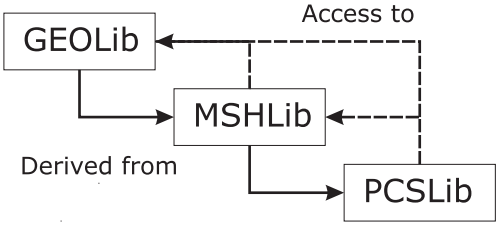

Figure 3: Hierarchy of object libraries and data access.

3.1.2 GEOLib concept

The geometric model for the compartment approach has to meet the following requirements: ensure topological consistency of the compartment structure (sec. 2.3) and provide geometric descriptions for initial and boundary conditions, source terms as well as data output. The topological consistency of the compartment structure for flux coupling is guaranteed using the same geometric instance as a common interface.

In Table 2 the geometric surface `GROUND_SURFACE` is defined which is shared by the surface and soil compartments as their interface. Similarly the geometric surface `WATER_TABLE` separates the soil and groundwater compartments. In the GEOLib two possibilities are given to define a geometric surface: unstructured TINs (triangular irregular networks) and polygons. The latter consist of closed polylines which are defined by an ordered set of points. In Table 2, lower data set, the surface `BC_LEFT_SFC` is defined with the polyline `BC_LEFT_PLY` consisting of points with the numbers $p_0, p_1, \ldots$. The points with their coordinates are created with the keyword `#POINTS`. Polygons can be used only for planar surfaces. For source terms and coupling flux assignments at the compartment interface TINs have to be used in realistic applications. The definition of the surface `GROUND_SURFACE` by a TIN is given in Table 2 (upper data set). In general, GEOLib objects are referenced by IDs defining object names.

Table 2: GEO data.

```
--------------------
#SURFACE
 $ID
  GROUND_SURFACE
 $TIN
  GROUND_SURFACE.tin
--------------------
#SURFACE
 $ID
  BC_LEFT_SFC
 $POLYLINE
  BC_LEFT_PLY
#POLYLINE
 $ID
  BC_LEFT_PLY
 $POINTS
  p_0
  p_1
  ...
#POINTS
 0 x_0 y_0 z_0
 1 x_1 y_1 z_1
 ...
#STOP
--------------------
```

3.1.3 MultiMSH concept

As the compartment approach relies on individual spatial discretizations for each compartment, a new `MSH` object is introduced, which is represented by the `CMesh` class.

Data members of `CMesh` as well as their relationship to `GEO` and `PCS` objects are explained based on Table 3 for a coupled overland-soil-aquifer system. Data sets for meshes are separated by `#FEM_MESH` keywords. The appearance of this keyword results in the creation of a new `MSH` instance, which is kept in a mesh vector. Standard mesh member data are `$NODES` and `$ELEMENTS`. The former simply contains the coordinates x, y, z of the n_{nod} nodes. The latter contains material property index, geometric element type and node numbers $n0, n1, n2$ of the n_{elem} elements. As commonly done, nodes (`CNode` instances)

and elements (CElement instances) are stored in vectors. In addition to standard mesh data, mesh-to-process (MSH-PCS) and mesh-to-mesh relations are required for the compartment approach. Mesh-to-process relations are set by a mesh $ID, which refers to a PCS object by process name. Mesh-to-mesh relations are defined by a geometric member variable $GEO_TYPE, which denotes the compartment interface. As mentioned above, the common geometric interface assures the topological consistency of adjacent meshes, which is important for the subsequent meshing procedure. The triangulation of the ground surface for the simulation of overland flow is generated from the geometric surface GROUND_SURFACE. Then the triangulation is mapped according to the digital elevation model (DEM). From this surface triangulation line elements are generated for the soil compartment. Each column consists of n_{lay}^{sf} lines and its top is located at the gravity center of a triangle. In general, soil elements can also be generated from patches of triangles in order to represent specific soil types and/or infiltration patterns. In that case the triangulation for the overland flow area A^{of} is generated from the surface A^{of}. The area of the related soil elements A^{sf} is derived from the same surface A^{of}. Hence, the exchange area for both compartments is identical to A^{of}.

Table 3: MSH data.

```
#FEM_MSH
 $ID
  OVERLAND_FLOW
 $GEO_TYPE
  SURFACE GROUND_SURFACE
 $NODES
  n_nod
  0 x_0 y_0 z_0
  1 x_1 y_1 z_1
  ...
 $ELEMENTS
  n_elem
  0  mat_0 type_0 n0_0 n1_0 n2_0
  1  mat_1 type_1 n0_1 n1_1 n2_1
  ...
#FEM_MSH
 $PCS_TYPE
  RICHARDS_FLOW
 $GEO_TYPE
  POLYLINE REGIONAL
 $LAYER
  n_lay^sf
#FEM_MSH
 $PCS_TYPE
  GROUNDWATER_FLOW
 $GEO_TYPE
  SURFACE WATER_TABLE
 $LAYER
  n_lay^gf
...
#STOP
```

The $GEO_TYPE of the Richards flow mesh can take two character strings, POLYLINE and REGIONAL. With the first string line elements are generated for the one-dimensional flow process in the unsaturated zone. With the second a regional soil model, i.e. several one-dimensional soil columns for one process, is generated. For the groundwater aquifer a prism mesh of n_{lay}^{gf} layers is generated from the surface WATER_TABLE. The vertical distance between GROUND_SURFACE and WATER_TABLE corresponds to the soil thickness distribution. Ultimately, the meshes referenced by $GEO_TYPE define also the location of source/sink terms for the compartment exchange fluxes.

3.1.4 MultiPCS concept

The central idea of process object-orientation is that the basic steps of the solution procedure for PDEs can be generalized, i.e. are independent of the specific physical problem (Kolditz and Bauer, 2004). Typically, the procedure is decomposed into time stepping, linearization, algebraic equation system assembly, incorporation of boundary conditions and source terms as well as calculation of secondary variables.

Table 4 illustrates the coding of the staggered process execution. PCS instances m_pcs are stored in the pcs_vector. The process base class, CProcess, provides very general methods to solve PDEs.

Table 4: MultiPCS execution.

```
PCSExecute()
{
  CProcess* m_pcs = NULL;
  for(i=0;i<pcs_vector.size();i++)
  {
    m_pcs = pcs_vector[i];
    m_pcs->Execute();
  }
}
```

Figure 4 shows the specification of processes for the coupled overland/soil/groundwater flow problem. Two additional loops are nested within the time loop (left box). In the first one the resolution of non-linearities of the shallow water and Richards equations are conducted. The second one hosts the coupling over all processes. The numerical solution of PDEs is conducted by the member function PCS::Execute() (Fig. 4, middle box) with the corresponding basic steps mentioned above. Specific properties of the problem, such as equation type, primary and secondary variables and material functions, are assigned during process configuration. For global assembly the element contributions of the MSH instance of the referencing process are summed up in the element loop (Fig. 4, right box). The specific PCS types are derived from the base class, i.e. class CProcessSpecific:public CProcess. The coupling between different processes is implemented by a new member function of the process object, PCS::IncorporateCPL() (Fig. 4, middle box), which is incorporating additional source/sink terms. This function is similar to the function PCS::IncorporateST(), which is adding right-hand-side (RHS) contributions for source/sink terms for the original process.

The input file for process data is shown in Table 5. The appearance of the keyword #PROCESS results in the creation of a PCS instance. In this example three processes are defined: OVERLAND_FLOW, RICHARDS_FLOW and GROUNDWATER_FLOW - all indicated by the subkeyword $PCS_TYPE. A new member $CPL_TYPE is added to the CProcess class to define process coupling relations. Processes can be coupled with more than one PCS object, e.g. Richards flow is linked with overland flow and groundwater flow.

Table 5: PCS file.

```
#PROCESS
 $PCS_TYPE
  OVERLAND_FLOW
 $CPL_TYPE
  RICHARDS_FLOW
#PROCESS
 $PCS_TYPE
  RICHARDS_FLOW
 $CPL_TYPE
  OVERLAND_FLOW
  GROUNDWATER_FLOW
#PROCESS
 $PCS_TYPE
  GROUNDWATER_FLOW
 $CPL_TYPE
  RICHARDS_FLOW
#STOP
```

To explain the process coupling procedure, we consider two PCS instances: m_pcs - the treated process, and

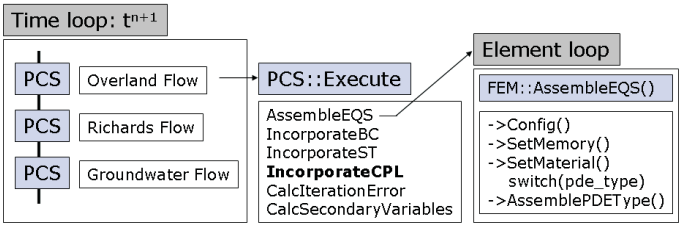

Figure 4: Implementation of the PCS solution algorithm.

`m_pcs_cpl` - the coupled process. The coupling function `m_pcs->IncorporateCPL()` has different tasks: (1) determination of mesh nodes and elements from the coupled process `m_pcs_cpl` at the compartment interface, (2) calculation of the nodal source/sink terms based on nodal values of the treated and coupled processes,(3) manipulation of the RHS vector of the current process based on step (1) and (2). The required data for this process coupling are provided by the corresponding source term (`ST`) objects. Table 6 shows the structure of the `ST` file for the definition of source/sink term objects. There are five `ST` objects of two different types created by the keyword `#SOURCE_TERM`. The first data set (6.1), related to the `OVERLAND_FLOW` process, is for precipitation. These source terms

Table 6: ST file.

```
---------------------------------
#SOURCE_TERM // 6.1 Precipitation
 $PCS_TYPE
  OVERLAND_FLOW
 $GEO_TYPE
  SURFACE GROUND_SURFACE
 $DIS_TYPE
  FILE precipitation.dat
---------------------------------
#SOURCE_TERM // 6.2 Flux coupling
 $PCS_TYPE
  OVERLAND_FLOW
 $GEO_TYPE
  SURFACE surface
 $CPL_TYPE
  RICHARDS_FLOW
#SOURCE_TERM // 6.3 Flux coupling
 $PCS_TYPE
  RICHARDS_FLOW
 $GEO_TYPE
  SURFACE surface
 $CPL_TYPE
  OVERLAND_FLOW
#SOURCE_TERM // 6.4 Flux coupling
 $PCS_TYPE
  RICHARDS_FLOW
 $GEO_TYPE
  SURFACE water_table
 $CPL_TYPE
  GROUNDWATER_FLOW
#SOURCE_TERM // 6.5 Flux coupling
 $PCS_TYPE
  GROUNDWATER_FLOW
 $GEO_TYPE
  SURFACE WATER_TABLE
 $CPL_TYPE
  RICHARDS_FLOW
#STOP
---------------------------------
```

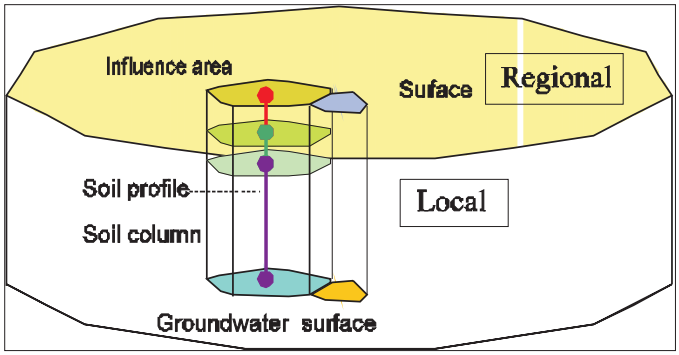

Figure 5: Regional hydrological soil model. Regional richards process consists of numerous lokal richards processes with influence areas for source term assignments.

are applied to the `GROUND_SURFACE` and imported from the file `precipitation.dat`. The remaining data sets (6.2-5) describe the flux coupling. Only three properties need to be specified by subkeywords: (1) which process (`$PCS_TYPE`), (2) which geometry (`$GEO_TYPE`), and (3) coupled to which process (`$CPL_TYPE`). For example, in 6.5 groundwater flow is coupled to the Richards flow and the compartment interface is defined by the geometric object `WATER_TABLE`.

3.2 High performance computing

Large scale modeling with adequate resolution can lead to a enormous computational demand. An example is provided by the study on the Beerze-Reusel drainage basin (sec. 4.6, Kolditz et al. (2007)[**EP5**], Du et al. (2008)[**EP3**]) where a extremely high vertical resolution in the soil system is required to obtain an adequate resolution in groundwater recharge patterns. We use MPI (message passing interface) to develop a parallelized regional hydrological soil model which consists of numerous vertical soil columns (Fig. 5). Table 7 illustrates the parallel process execution at each time step. Since each local Richards process is independent, there is no data exchange necessary during computation execution. However, the job scheduling and computational load distribution is handled by the parallelized code. For any given number p ($p > 0$) of processors a round-robin approach is used: For a total of nlocal Richards processes we have p-1 groups of local Richards processes, which have to be calculated sequentially by a single processor. The remaining $\mod(n, p)$ local Richards processes are distributed to the pth processor. Upon completion of all local Richards processes message passing is carried out to forward the results to the regional Richards process.

Table 7: Parallel process execution.

```
-----------------------------------------------------
pcs_local_vector = CreateLocalProcesses(m_pcs_global);

for(i=0;i<pcs_local_vector.size();i++)
{
  m_pcs_local = pcs_local_vector[i];
  m_pcs_local->Execute();
}

for(i=0;i<pcs_local_vector.size();i++)
 MPI_Bcast((void *)values, no_local_nodes,
    MPI_DOUBLE, i, MPI_COMM_WORLD);
-----------------------------------------------------
```

4 Applications

We present six application examples of the compartment approach introduced in Sec. 2 which go from laboratory to catchment scale (Tab. 8). The laboratory experiments by Smith and Woolhiser (1971b) and Abdul and Gilham (1984) provide benchmark test cases for the coupling of the compartments for overland flow and flow in the unsaturated zone. With the laboratory experiments by Smith and Woolhiser (1971b) the parameters of the hydraulic interface in the coupling flux calculation (sec. 2.1.3), the friction, and capillarity processes are investigated for Horton (infiltration excess) overland flow (sec. 4.1). Mass transport in the laboratory experiments by Abdul and Gilham (1984) on Dunne (saturation excess) overland flow (sec. 4.2) is simulated with RWPT. In the following example hyporheic exchange in the Lahn riverbed is determined based on temperature signatures (sec. 4.3). In Sec. 4.4 fate and transport of pathogens through the unsaturated zone are simulated with RWPT. A coupled overland/soil/aquifer system is introduced with the Borden field site example in Sec. 4.5. Finally, a parallelized regional hydraulic soil model of the Beerze-Reusel basin is presented (sec. 4.6).

4.1 Labororatory experiments by Smith and Woohiser

The classic experiments by Smith and Woolhiser (1971b) have been used in many studies to examine coupling of overland flow with the unsaturated (Smith and Woolhiser (1971b); Akan and Yen (1981); Govindaraju and Kavvas (1991); Singh and Bhallamudi (1998); Morita and Yen (2002); Thoms (2003); Therrien et al. (2004)). Smith and Woolhiser (1971a,b) conducted infiltration experiments in a soil flume with a length of 12.2 m, a width of 5.1 cm, and a slope of 0.01 (Fig. 6). Infiltration excess overland (Hortonian) flow was generated by 15 minutes of artificial precipitation at a rate of 4.2 mm min^{-1} which was roughly 2-3 times the saturated soil conductivity. To prevent algal growth in the soil a light oil instead of water was used. The viscosity of this light oil was about twice the water viscosity. Seepage was allowed at both flume ends. As the water table was about 1 m below the surface, it was assumed that the capillary fringe did not influenced the infiltration process. The soil material was a locally obtained river-deposited sand known as Poudre fine sand. Soil bulk density measurements at four sections of the flume indicated a considerable horizontal and vertical heterogeneity. Soil density increased with depth. Soil water characteristic curves, i.e., capillary pressure and relative permeability dependencies on water content, were measured for different soil densities. Overland friction parameters were determined in the laboratory for water depths higher than 4 mm.

Simulated and measured hydrographs at the outlet of the flume for initially drained conditions are compared in Figure 7. Overland flow initialization starts after about 7 minutes. The

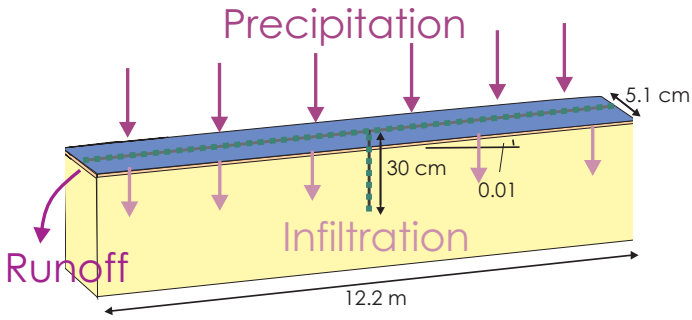

Figure 6: Setup, processes, and spatial discretization of the laboratory experiments by Smith and Woolhiser (1971b) regarding Horton overland flow.

finite length of the soil flume causes a flattening in the hydrograph after about 10 min. The hydrograph can be split into three flow stages: (I) Overland flow initialization, (II) Hydrograph rise, (III) Hydrograph flattening Since lateral flow effects in the soil compartment (i.e., interflow) due to heterogeneity were shown to be marginal, we used the simplest geometric representation of the experiment by coupling two 1-D models

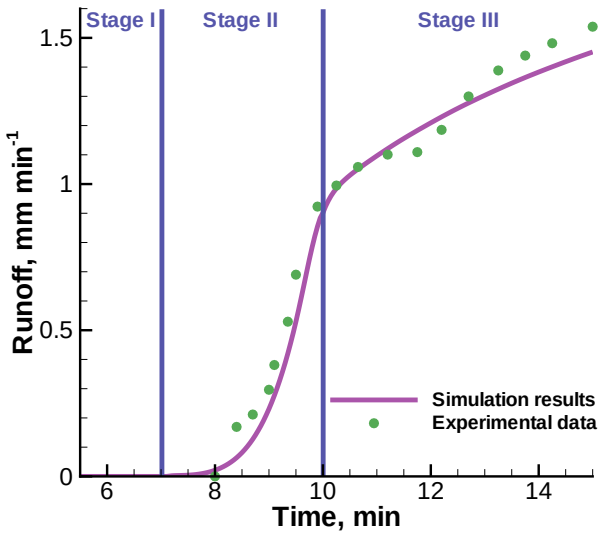

Figure 7: Comparison of experimental and simulated runoff in the laboratory experiments by Smith and Woolhiser (1971b). The runoff q_{ab}^{of} is given by $q_{ab}^{of} = Q_{krit}^{of}/A$, where $Q_{krit}^{of} = \sqrt{gH^3}B$ is the critical flux (Julien, 2002) at the outlet, B the flume breadth, and A the flume surface.

Table 8: Application examples, processes and domain sizes.

Application	Compartments	Transport	Size
Smith & Woolhiser (1971)	OF/SF		$10 \times 0.05 \times 0.2$ m^3
Abdul & Gilham (1984)	OF/SF	ST	$1.4 \times 1 \times 0.08$ m^3
Lahn riverbed	GF	HT	1.5 m
Fate and transport of Cryptosporidium parvum oocysts	RF	ST	3×6 m^2
Borden field site	OF/SF/GF		$80 \times 20 \times 2$ m^3
Beerze-Reusel drainage basin	SF		440m^2 $\times$ 2m

for overland flow and the unsaturated zone, which is represented by an array of soil columns (Fig. 6). The parameters used for the analysis of the Smith & Woolhiser experiment are given in Delfs et al. (2009c) [**EP1**]. The impact of friction processes, capillarity and hydraulic interface parameters on runoff and coupling flux have been investigated. Therefore, logarithmic sensitivities $\frac{\mathcal{P}_j}{\mathcal{O}_i}\frac{\Delta\mathcal{O}_i}{\Delta\mathcal{P}_j}$ were calculated, where $\mathcal{O}_i$ are output functions and $\mathcal{P}_j$ are model parameters. The relative change in output $d\mathcal{O}_i/\mathcal{O}_i$ depends on the relative change of input parameters $d\mathcal{P}_j/\mathcal{P}_j$ in first order according to

$$\frac{d\mathcal{O}_i}{\mathcal{O}_i} = \sum_j \left(\frac{\mathcal{P}_j}{\mathcal{O}_i}\frac{\partial\mathcal{O}_i}{\partial\mathcal{P}_j}\right)\frac{d\mathcal{P}_j}{\mathcal{P}_j}. \tag{51}$$

The system output functions of the sensitivity analysis are coupling flux $\mathcal{O}_1$ and surface runoff by overland flow $\mathcal{O}_2$ at the critical depth boundary. The sensitivity study of the model parameters focused on the effects of friction processes, soil capillarity, and the hydraulic interface introduced in the coupling flux calculation (sec. 2.1.3). Logarithmic sensitivities are weighted with uncertainties identified by Smith and Woolhiser (1971b) for parameter ranking (Delfs et al. (2009c) [**EP1**]) As a result of the sensitivity study we found that soil parameters ($\mathcal{P}_1$, $\mathcal{P}_3$-$\mathcal{P}_7$) have a stronger influence than overland flow parameters for the coupling flux $\mathcal{O}_1$ (Fig. 8). Due to the low impact of overland flow on infiltration (Philip, 1957) the runoff data can be reproduced with simpler approaches. Results obtained with the model by Green and Ampt (1911) are shown in Delfs et al. (2009b). Most important is the soil hydraulic conductivity K ($\mathcal{P}_1$). Overland friction parameter C ($\mathcal{P}_2$), interface layer thickness ($\mathcal{P}_8$), and immobile depth a ($\mathcal{P}_{10}$) are ranked as important in the second flow stag for runoff $\mathcal{O}_2$ (Fig. 9). The sensitivity to all parameters $\mathcal{P}_1$-$\mathcal{P}_{10}$ is larger in flow stage II than in flow stage III with the flattening hydrograph. We found that the impact of the parameters in the calculation of the coupling flux (25) on runoff and coupling flux is low.

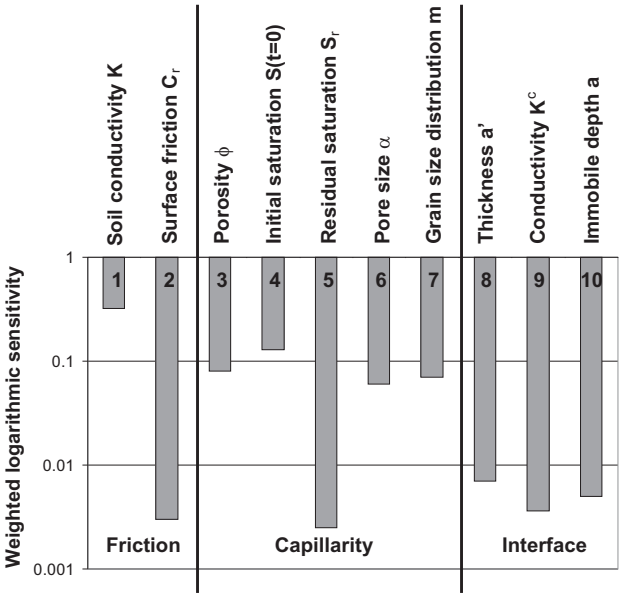

Figure 8: Parameter ranking for coupling flux of the laboratory experiments by Smith and Woolhiser (1971b).

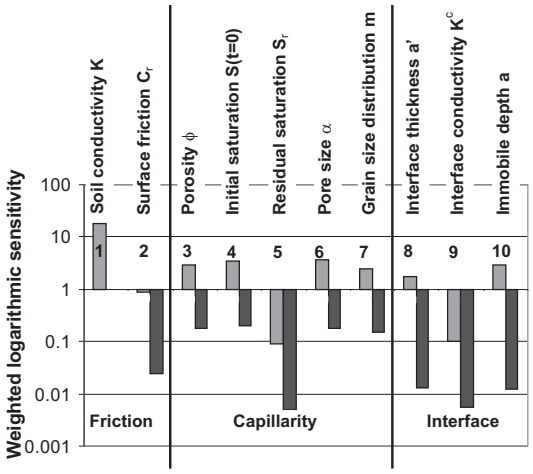

Figure 9: Parameter ranking for runoff prediction of the laboratory experiments by Smith and Woolhiser (1971b).

4.2 Laboratory experiments by Abdul and Gilham

The laboratory experiments by Abdul and Gilham (1984) were designed to examine the role of capillary fringe on runoff generation processes. Simulations have been performed by Abdul (1985), VanderKwaak (1999), and Kollet and Maxwell (2006). Precipitation was applied for 20 min on a soil flume with a length of 1.4 m, a width of 8 cm, and a slope of 0.12 (Fig. 10). The precipitation had a concentration of $c^{of}_{nsw\,\mathrm{st}} = 60.6$ mg/l of chloride as a tracer in order to determine the event/pre-event water ratio in runoff. The groundwater level was initially located at outlet height such that immediately Dunne (saturation excess) overland flow develops. Hydrographs and chlorographs at the outlet were continuously recorded. Water content-pressure relationships were determined for the used sand.

In the application of the model introduced in section 2, overland flow was simulated 1D and flow in the unsaturated zone 1D. Particle tracking (sec. 2.2.2) was applied to simulate advective mass transport. Therefore, each time step $\Delta t = 1$ s $N_{nsw} = 140$ particles were uniformly distributed on the surface. Particlefluxes are illustrated in Figure 11. The used parameters are given in Delfs et al. (2009a)[**EP2**].

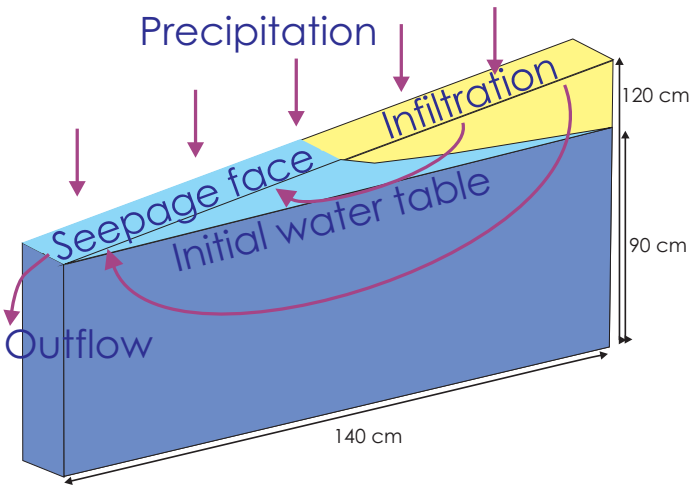

Figure 10: Setup of the laboratory experiments by Abdul and Gilham (1984) regarding Dunne overland flow.

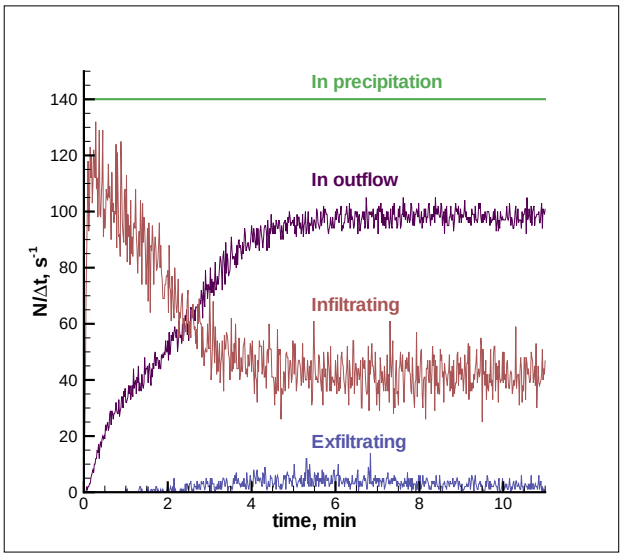

Figure 11: Particle fluxes in the simulations of the laboratory experiments by Abdul and Gilham (1984). Number of particles N which enter the flume each time step Δt through precipitation, leave the flume with the outflow, infiltate and exfiltrate.

Figure 12 compares simulation results with experimental data for three soil hydraulic conductivities K. The results indicate that exfiltration from the soil immediately dilute the precipitation water. Results are shown for 11 minutes, later the flow field is steady and chloro/hydrographs reached maxima. The maxima are well reproduced by the model. The maximum outflow is independent of the soil hydraulic conductivity. Differences between measured and simulated chloride concentrations occur at the beginning during the rising part of the chlorograph due to the neglect of diffusion/dispersion.

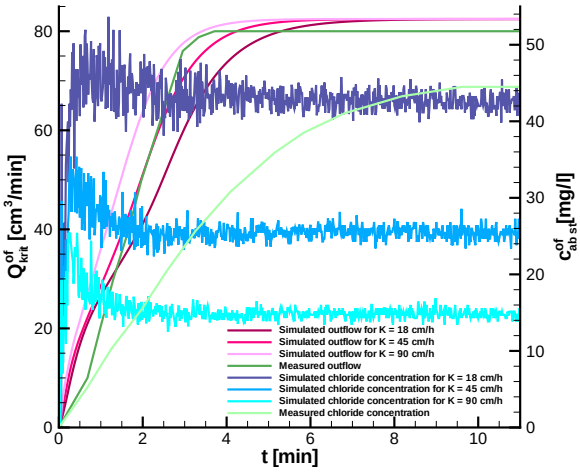

Figure 12: Comparison of measured and simulated hydrographs and chlorographs. Simulation results of three soil hydraulic conductivities K are shown. Shown is the critical flow $Q^{of}_{krit} = \sqrt{gH^3B}$ (Julien, 2002) at the outlet and its chlorid concentration $c^{\mathrm{of}}_{ab\,\mathrm{st}} = N_{ab}c^{of}_{nsw\,\mathrm{st}}q^{of}_{nsw}A/N_{nsw}Q^{of}_{krit}$, where N_{ab} are the number of particles at the outlet, A the flume surface, and B the flume breadth.

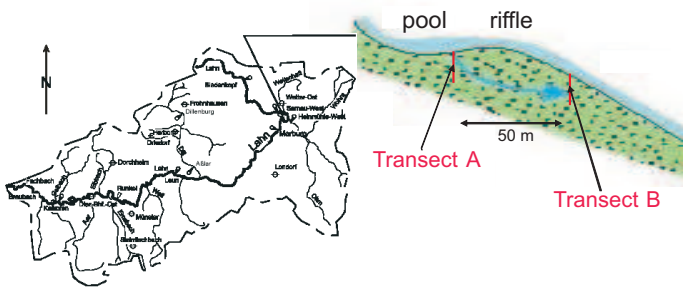

Figure 13: Area of investigation in the Lahn river basin close to Marburg (50°49'N,8°46'E).

4.3 Heat transport experiments in the Lahn riverbed

The hyporheic zone is the region beneath and lateral to a stream bed, where shallow groundwater and surface water mix. There has already been a considerable research on hyporheic exchange at a stretch of the Lahn river in Germany, e.g. concerning ingress of fines by Saenger and Zanke (2008) and biotic colmation (growth of biomass in river sediments) by Ibisch et al. (2008). Temperature signatures have been proven to be a valuable tool for the determination of hyporheic exchange (Constantz and Stonestrom, 2003).

Temperature time series were continuously recorded and averaged every 30 minutes between the summer of 2000 and the spring of 2001 at two transects upstream and downstream of a riffle (Fig. 13). The temperature sensors were located in the riverbed at depths of up to 1.5 meters at the center of the river and between the center and riverbank. Stream and groundwater levels were measured at each transect, the latter at both riverbanks (2 meters from the river).

Heat transport (Eqn. 20) is simulated in 1-D vertically for saturated porous media (Fig. 14). The temperature at the river bottom and at 1.5 meters depth in the river sediments provide boundary conditions. A homogeneous representation was used for the river sediments and dispersion neglected since the influence on daily temperature patterns is small (Cardenas and Wilson, 2007). The used parameters can be found in Delfs et al. (2009a)[**EP2**].

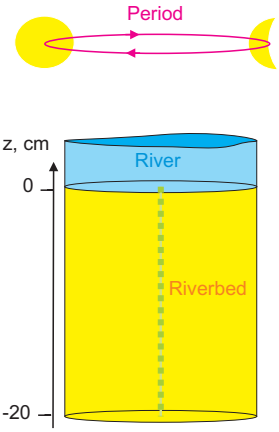

Figure 14: Model setup for the simulations of hyporheic exchange in the Lahn riverbed.

Figure 15(b) compares temperature signatures in the river sediments simulated with different velocity profiles (Fig. 15a) for a sinusoidal upper boundary condition. An analytical solution of equation (20) for constant velocity with a sinusoidal boundary condition on a semi-infinite column with homogeneous parametrization is given by (Logan and Zlotnik (1996))

$$T(z,t) = \exp\left(\frac{q^{\mathrm{gf}}z}{2\kappa} - \frac{z}{2\kappa}\sqrt{\frac{\alpha+\left(q^{\mathrm{gf}}\right)^2}{2}}\right)\sin\left(\frac{2\pi t}{\tau} + \frac{z}{2\kappa}\sqrt{\frac{\alpha-(q^{\mathrm{gf}})^2}{2}}\right) \quad (52)$$

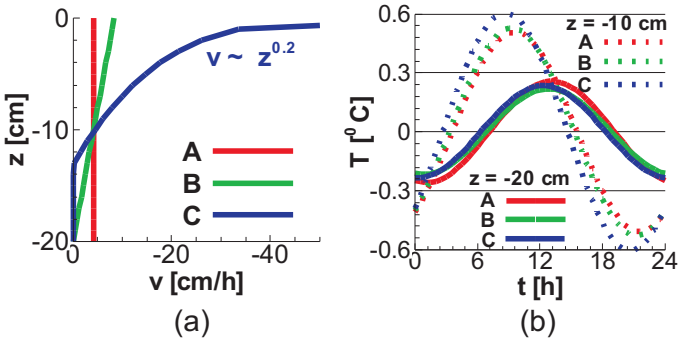

Figure 15: Influence of vertical velocity profile on hyporheic exchange. (a) Profiles A, B, C and (b) corresponding thermal signatures at $z = -10$ cm $z = -20$ cm depth for a sinusoidal upper boundary condition.

where

$$\alpha = \sqrt{\left(q^{\mathrm{gf}}\right)^4 + \left(\frac{8\pi}{\kappa\tau}\right)^2} \qquad (53)$$

$$\kappa = \frac{\lambda_{\mathrm{ht}}}{C^{\mathrm{gf}}}$$

and τ is the period (Amplitude is unity, $z = 0$ at river bottom). The advective-diffusive transport leads to a damping of the amplitude and a phase shift with depth. The increased advection in the upper part of the linear profile (green color) leads to a larger amplitude and smaller phase shift in the temperature field for $z = -10$ cm (dashed line) compared to the constant profile (red color). With the reduced advection in the lower part the temperature field for $z = -20$ cm (solid line) has a smaller amplitude in combination with a smaller phase shift. The profile with a strong velocity decay with depth (blue color) shows a more reduced phase shift (solid line).

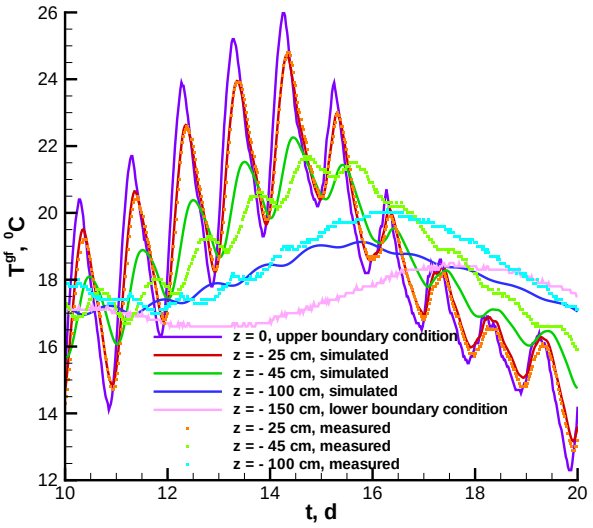

Figure 16: Comparison of simulation results and measurement data of the Lahn riverbed (July, 17th-27th 2000). Vertical velocity decreases linearly with depth in the simulations between $0 > z > -30$ cm.

Simulation and measurement data of the river Lahn are compared in Figure 16 for a 10 days period in June 2000. Temperature data upstream of the riffle at the center of the river were taken. The selected scenario represents a typical summer situation with strong temperature amplitudes and small variations in the river flow rate. Good agreement of simulation and measurement data could be achieved for small depths ($z = -20$ cm). Deviations increase with depth which indicates for lateral flow in the deeper sediments. Figure 17 compares calibrated vertical velocity values with the river flow rate. The determined vertical velocities decrease at river flow peaks in winter and at the end of september 2000, when a pool of an adjacent water treatment plant was filled.

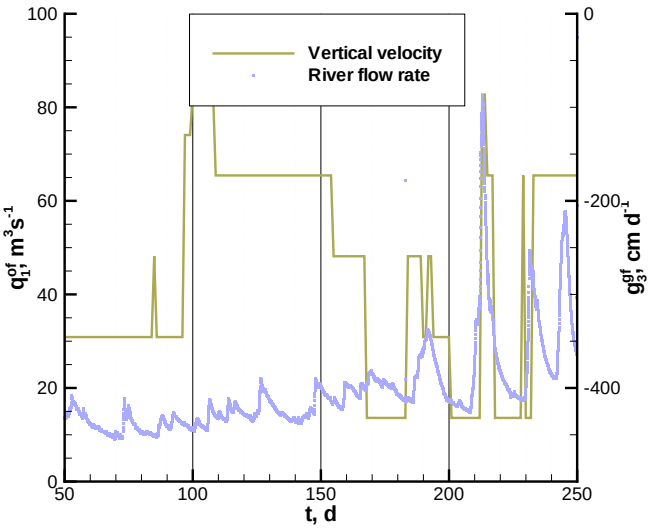

Figure 17: River flow rate q_1^{of} and vertical fluxes q_3^{gf} in the Lahn riverbed at Transect A (July, 27th 2000 - February, 12th 2001).

4.4 Fate and transport of Cryptosporidium parvum oocysts

Cryptosporidium parvum is a spore-forming coccidian protozoan. Oocysts are excreted in feces and are the infectious form. Cryptosporidium parvum oocysts are a threat concerning river and groundwater quality since a small number of particles are sufficient for infection (Schijven et al., 2004). The biggest known outbreak occurred in Milwaukee in 1993 and infected more than 400 000 people.

Fate and transport of Cryptosporidium parvum oocysts were simulated through the unsaturated zone with particle tracking. Sorption/desorption are included with the two rate model from Johnson et al. (1995):

$$N/N_0 = A_k e^{-k_1 t} + (1 - A_k) e^{-k_2 t} \qquad (54)$$

where N is the number of particles in the water at time t, N_0 is the initial number of oocysts, k_1, k_2 are fast and slow sorption rate coefficients and A_k is a weighting factor. Filtering and die-off are combined with

$$N/N_0 = e^{-(k_d + \lambda_t)t} \qquad (55)$$

where λ_t is the filtration coefficient and k_d the die-off rate coefficient.

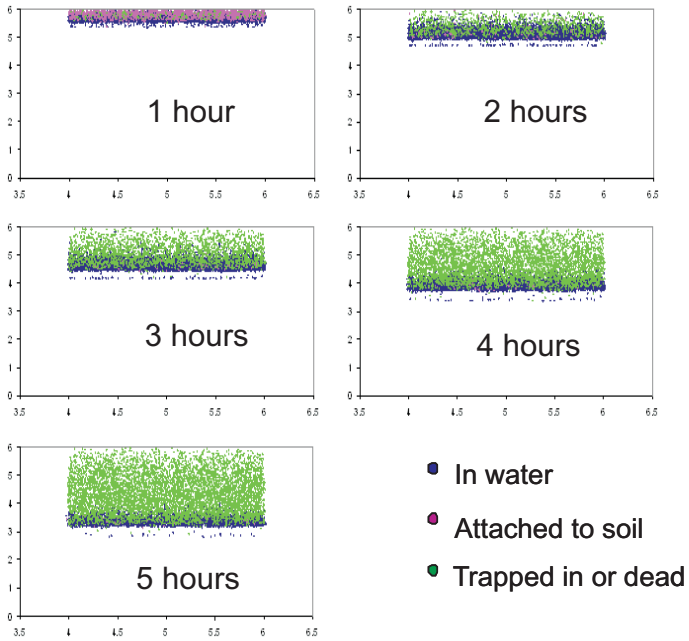

Figure 18: Status of the Cryptosporidium parvum oocysts.

The status of the particles is shown in Figure 18 for one hour steps. Parameters are given in Park et al. (2008c)[**EP4**]. Breakthrough curves at the groundwater table are shown in Figure 19. Sorption/desorption leads to a delay, filtering and die-off which reduces the number of particles reaching the groundwater table significantly.

4.5 Field experiments by Abdul and Gilham at the Borden site

The measurement data at the Canadian Forces Base Borden in Ontario by Abdul (1985) and Abdul and Gilham (1989) concerning the effect of capillary fringe on runoff were for instance used by Jones et al. (2006). The overland/soil/aquifer system is used as a demonstration example for the compartment coupling approach (sec. 2.3) in Kolditz et al. (2008). Under investigation is a stretch of 80 times 20 m^2 with a man-made channel of 1.2 m depth surrounded by grass-covered land. Figure 20 shows the result of the multi-mesh discretization described in Sec. 3.1.3. Prior to the beginning of the experiment the channel is dry. Then uniform artificial precipitation is applied at a rate of 0.02 meters per hour over the entire area for 50 minutes. Characteristic saturation-pressure relationships of the underlying porous medium were determined. Three topologically coupled meshes were used for the surface, soil, and groundwater compartments (Fig. 20). The multi-mesh system (Sec. 3.1.3) consists of the following numbers and types of elements: 2651 triangles for the surface, 106040 line elements for the soil, and 26510 prisms for the aquifer. Each soil column has 40 line elements and the groundwater compartment is split into 10 element layers. The groundwater table was fixed at 2 meter depth. The parameters used in the simulations are given in Kolditz et al. (2008)[**EP6**]. Due to the different temporal scales in the overland, soil, and groundwater compartments (Figs. 21-23) a sub-timing scheme (Sec. 2.3) was applied. The governing equations were solved fully implicitly with fixed time steps of $\Delta t = 10^2$ s and $\Delta t = 10^4$ s for overland flow and groundwater flow, respectively. For soil water flow a self- adaptive time stepping was applied resulting in time steps of the order of $\Delta t = 10^3$ s.

In the coupling flux calculation (Eqn. 25) for the overland

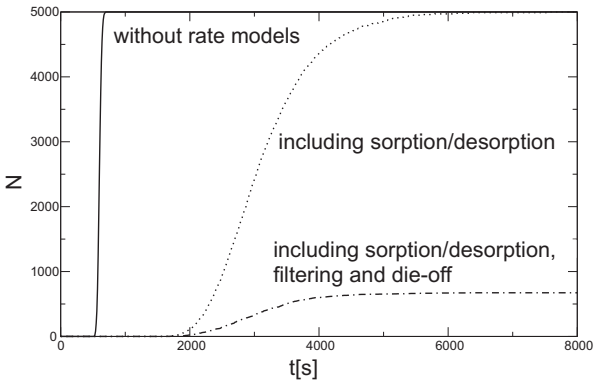

Figure 19: Breakthrough curves at the groundwater table in the simulations of the Cryptosporidium parvum oocysts.

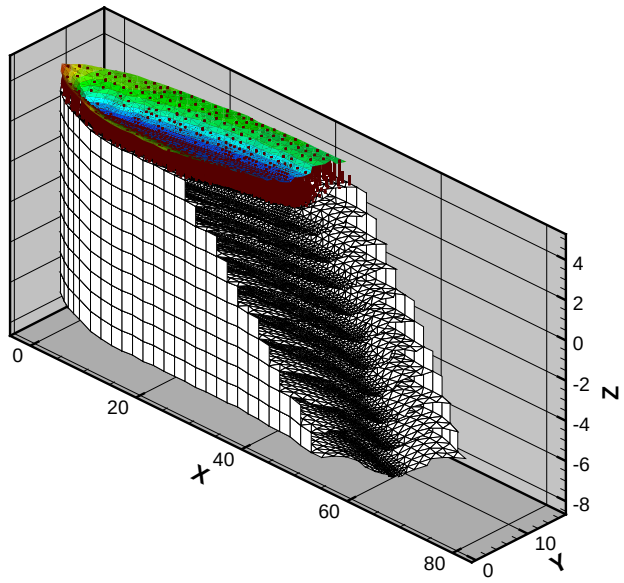

Figure 20: Finite element discretization meshes of the overland/soil/aquifer system in the Borden field site example.

and soil compartment only hydrostatic surface water pressure was considered. Due to topography water flows fast into the ditch (Fig. 21) where it infiltrates (Fig. 22). Most retardation in the response shows the groundwater compartment (Fig. 23).

4.6 Soil system of the Beerze-Reusel basin

A parallelized regional hydrological soil model was developed as a tool for large-scale unsaturated zone investigations (Du et al. (2008)[**EP3**] and Kolditz et al. (2007)[**EP5**]). The study region with an area of 440km^2 is located in the Province of North Brabant in the southern half of the Netherlands. An overview of the Beerze-Reusel drainage basin itself is given in Figure 24. A comprehensive database for soil and aquifer properties is available (Wösten et al., 2001). The subsoil mainly consists of sandy deposits formed in the Pleistocene. The flat region gently slopes in a north to northeast direction, from an altitude of 45 m+NAP (m above Mean Sea Level) down to 3.7 m+NAP.

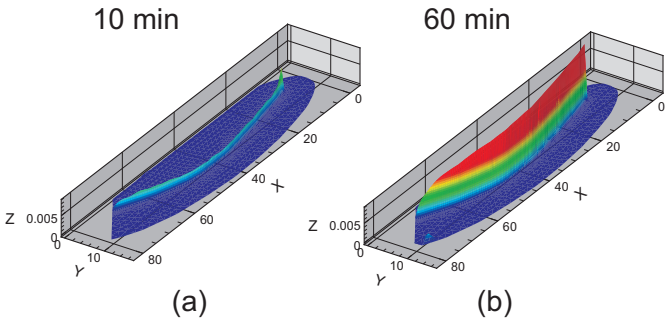

Figure 21: Overland flow water depths in the simulations of the overland/soil/aquifer system after (a) 10 min (b) 60 min.

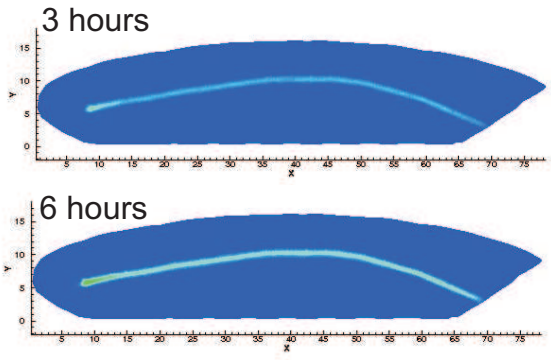

Figure 22: Soil saturation at 1 m depth in the simulations of the overland/soil/aquifer system after (a) 3 hours (b) 6 hours.

There are several aeolian sand ridges up to a few meters in height that are orientated in a west to east direction. These ridges have a large impact on the geomorphology of the stream valleys, as they are situated transversely to the general slope and drainage pattern of the area. In the valleys alluvial soils have been formed consisting of redeposited sand, loam and peat.

As a time-dependent boundary condition to the regional soil model precipitation and evaporation time-series are used. The raw data of time series were obtained from ECA&C (2006) for the stations in De Bilt, Twenthe, Vlissingen, Eindhoven, and Maastricht. Potential evaporation is computed with the method by Makkink (1957). The used parameters are given in Kolditz et al. (2007)[**EP5**].

The regional hydrological soil model of the Beerze-Reusel drainage basin consists of 12210 individual soil columns, which can be categorized into 61 different kinds of soil profiles composed of 56 soil types. The database is illustrated in Figure 25. The horizontal distribution of soil profiles is represented by in-

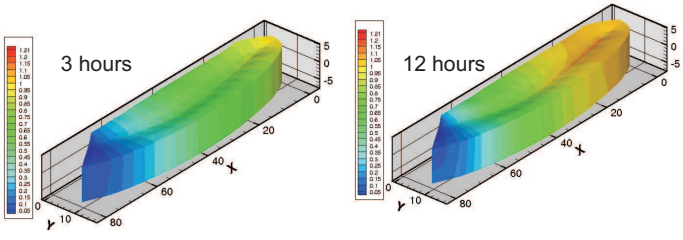

Figure 23: Groundwater hydraulic heads in the simulations of the overland/soil/aquifer system after (a) 3 hours (b) 12 hours.

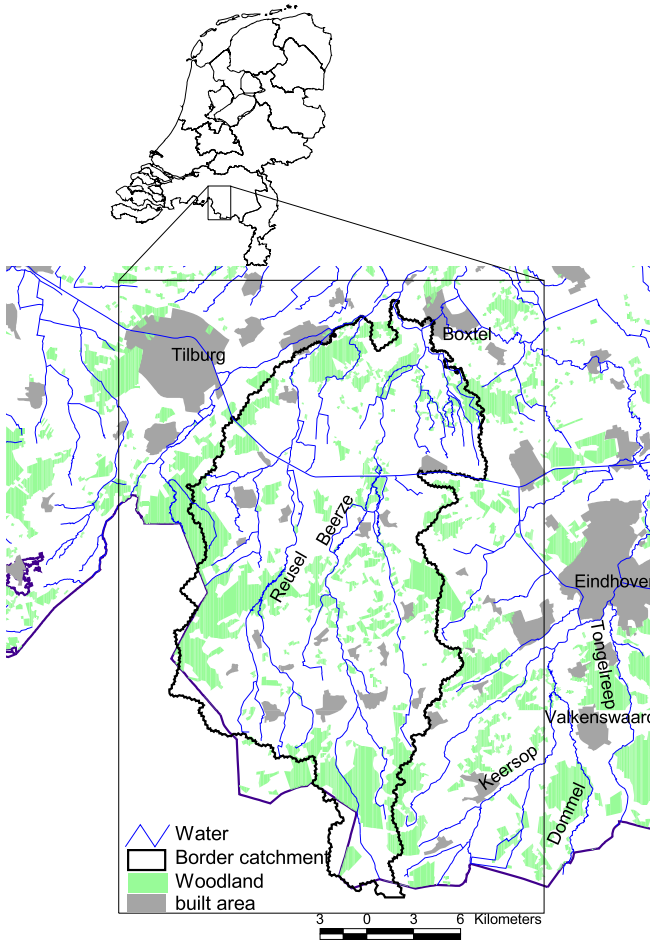

Figure 24: Beerze-Reusel study area in the Meuse basin. (vertical direction is North, geographic data: Tilburg (51°33'N,5°5'E), Boxtel (51°35'N,5°19'E) Eindhoven (51°27'N,5°27'E)).

fluence areas (Fig. 25, left). A first data table gives the relation between influence area and soil profile number (profile code) (Fig. 25, right, upper). A second data table describes the soil structure (Fig. 25, right, middle) (vertical distribution, depth). The soil profiles consist of several soil types, which are coded for instance as H03, H07, H20. A third data table gives the van

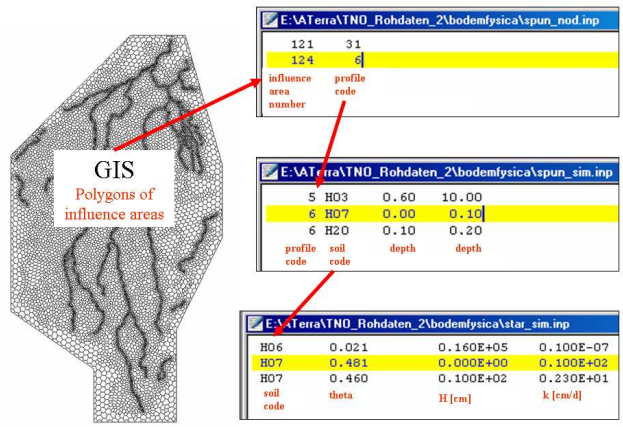

Figure 25: Database for the hydraulic soil properties of the Beerze-Reusel drainage basin.

Genuchten curves (Eqns. 6) for each soil type (Fig. 25, right, lower). Several typical soil profiles, which are located at different parts in the region, are selected. The typical soil profiles are composed by 4, 2 and 3 different soil layers, and the specific soil profile codes are defined as 16, 14 and 46, respectively. Each soil column with the corresponding daily precipitation series is simulated for the whole 2000 year period. Due to the soil heterogeneity a very different evolution of moisture occurs with locally varying infiltration into the groundwater compartment (Fig. 26).

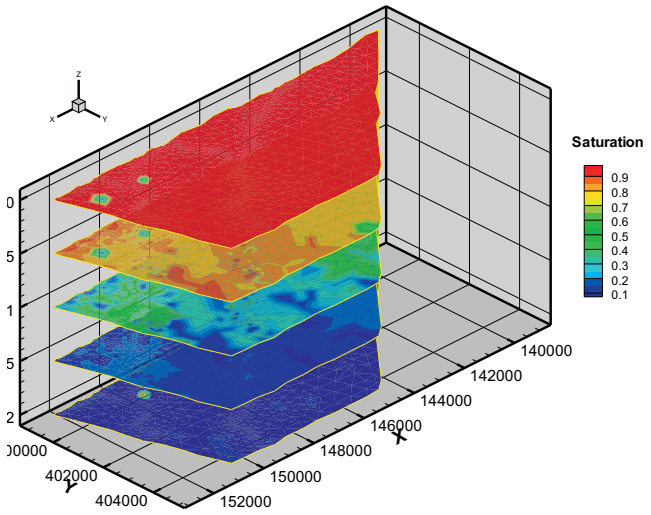

Figure 26: Regional water saturation distribution in the Beerze-Reusel drainage basin after 150 days.

5 Synopsis

In this work the scientific software toolbox OpenGeoSys was extended for numerical modeling of coupled surface and subsurface water flow and transport with Euler-Lagrange methods. The new physically based model was evaluated with several application examples at a laboratory, field, and regional scale.

The hydrological processes groundwater flow, unsaturated zone flow, and surface water flow are described by diffusion type equations, e.g. the diffusion-wave model for surface water flow which is suited for the numerical investigation of overland runoff and river floods. The diffusion type equations are spatially discretized with finite elements, in particular the control volume finite element method is used in the diffusion-wave surface water flow model. Advective-diffusive/dispersive mass and heat transport are simulated with both finite elements and Lagrangian stochastic particles.

The coupled hydrological model is based on a compartment approach where the hydrosphere is subdivided into surface, soil, and aquifer compartments (Fig. 27). New, and a characteristic feature of the compartment approach is that the governing equations of different compartments are spatially discretized on their own mesh. This allows to solve each process with a mesh optimized for its geological, hydrological structures, and numerical constraints. Flow and transport processes of adjacent compartments interact at their common interface with exchange fluxes which are implemented as source/sink terms in the governing equations. The library hierarchy in the object-oriented implementation provides a flexible framework for multi-process problems. For example topological consistency, i.e. the same area has to be assigned to the source terms of both coupled processes in the calculation of exchange fluxes (Fig. 27), is guaranteed, since source/sink term objects at a common interface use the same geometric instance (e.g., point, polyline).

The new model was examined with six application examples spanning scales from laboratory experiments to catchments. The coupling concept was analyzed with the laboratory experiments by Smith and Woolhiser (1971b) on Horton overland flow. The influence of hydraulic interface parameters in the coupling flux calculation on runoff and infiltration prediction was found to be low compared to

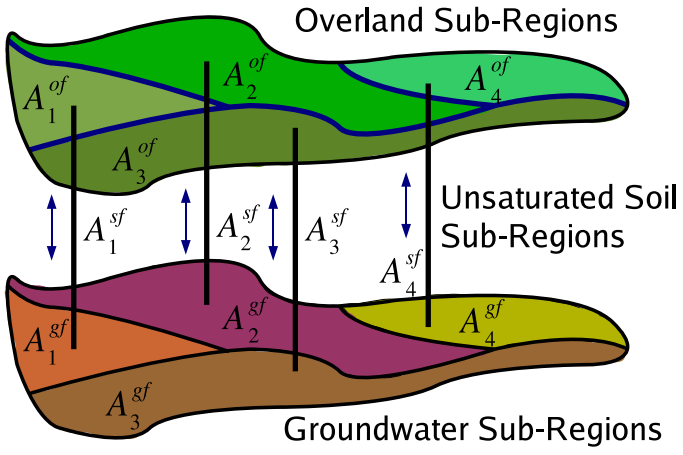

Figure 27: Compartment approach for a typical watershed. The hydrosphere consists of overland, soil, and groundwater compartments which are subdivided in sub-regions. The flow processes interact with exchange fluxes at common compartment interface areas $A_i^{\mathrm{of}} = A_i^{\mathrm{sf}} = A_i^{\mathrm{gf}}$ for $i = 1 \ldots 4$.

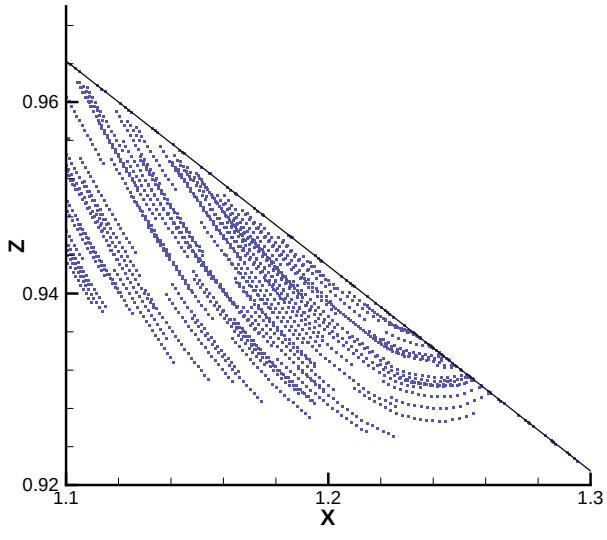

Figure 28: Particle path lines in the simulations of the laboratory experiments by Abdul and Gilham (1984).

uncertainties in friction and capillarity parameterizations. New in the simulations of the laboratory experiments by Abdul and Gilham (1984) on Dunne overland flow is the use of Lagrangian stochastic particles in coupled hydrological modeling (Fig. 28). The experimental tracer data could be well reproduced for the steady flow field with solely advective mass transport between the overland and variably saturated soil compartments. Hyporheic exchange was determined for a year period in a numerical investigation of thermal signatures in the Lahn riverbed. The conceptual model consist of vertical heat transport in saturated porous media were (daily) temperature variations are assigned as boundary conditions. The new model was also used to simulate fate and transport of Cryptosporidium parvum oocysts through the unsaturated zone. The highly infectious pathogens are subject to filtering and adsorption/desorption on the porous matrix as well as die-off. A coupled overland/soil/aquifer model of the Borden field site was presented as a demonstration example of the compartment coupling approach. The spatial scale of this example is considered as the upper limit for numerical modeling of coupled overland and subsurface water flow with the presented physically based model. Finally, a parallelized regional hydraulic soil model was developed. In the application to the Beerze-Reusel basin groundwater recharge was calculated with extremely high vertical resolution for a year period at a regional scale based on rainfall-evaporation data.

The practical experiences also showed limitations of the physically based approach. One issue is that scale differences of coupled hydrological processes cause numerical errors in the coupling flux calculation. Applications at catchment scale showed that in particular the experimental determination of bottom friction parameters in the shallow water equations is problematic.

Numerical investigations of large scale hydrosystems are possible in principle, as shown recently by a series of studies (Sudicky et al., 2008; Li et al., 2008; Park et al., 2008d). However, the question remains of how we can deal with the large scale parametrization since an experimental determination of the parameters is complex. The hydrographs in the applications at laboratory scale showed significant sensitivity on the bottom friction parametrization.

Coupling of different approaches, which are currently used in the numerical investigation of hydrosystems, appears promising. In the analysis of soil and groundwater systems Euler methods (finite differences, volumes, and elements) are common. In surface hydrology stochastic methods are faster and easier to parameterize (e.g. Samaniego and Bárdossy (2007)). Furthermore, we pursuit a numerical investigation of the soil-plant-atmosphere interface by coupling the scientific software toolbox OpenGeoSys with a plant water uptake model (Schneider et al., 2009)[**EP7**].

The main achievements of this thesis are:

- Development and implementation of a physically based numerical model for coupled surface and subsurface water flow with heat and mass transport in the scientific software toolbox OpenGeoSys.
- Evaluation of the implemented compartment coupling concept with a sensitivity analysis of hydraulic interface parameters in the coupling flux calculation.
- Simulation of transport processes in coupled hydrosystems with both finite elements and Lagrangian stochastic particles (random walk particle tracking).
- Determination of hyphoreic exchange in a numerical investigation of temperature signatures in a riverbed.
- Development and application of a parallelized regional hydrologic soil model for the calculation of highly resolved groundwater recharge.

References

Abbott, M. B., Babovic, V. M., Cunge, J. A., 2001. Towards the hydraulics of the hydroinformatics era. J. Hydraul. Res. 39 (4), 339–349.

Abbott, M. B., Bathurst, J. C., Cunge, J. A., O'Connell, P. E., Rasmussen, J., 1986. An introduction to the european hydrological system - Système Hydrologique Européen, 'SHE', 2: Structure of a physically-based, distributed modelling system. J. Hydrol. 87 (2), 61–77.

Abdul, A. S., 1985. Experimental and Numerical Studies of the Effect of the Capillary Fringe on Streamflow Generation. Ph.D. thesis, Department of Earth Sciences, University of Waterloo.

Abdul, A. S., Gilham, R. W., 1984. Laboratory studies of the effects of the capillary fringe on streamflow generation. Water Resour. Res. 20 (6), 691–698.

Abdul, A. S., Gilham, R. W., 1989. Field studies of the effects of the capillary fringe on streamflow generation. J. Hydrol. 112, 1–18.

Akan, A. O., Yen, B. C., 1981. Mathematical model of shallow water flow over porous media. J. Hydraul. Div. ASCE 107 (4), 479–494.

Alfredsen, K., Saether, B., 2000. An object-oriented application framework for building water resource information and planning tools applied to the design of a flood analysis system. Environ. Modell. Softw. 15 (3), 215–224.

Arnold, J. G., Sirinivasan, R., Muttiah, R. S., Williams, J. R., 1998. Large area hydrologic modeling and assessment, part 1 - model development. J. AWRA 34 (1), 73–89.

Bear, J., 1988. Dynamics of Fluids in Porous Media, 2nd Edition. Dover Publications Inc., New York.

Bear, J., Verruijt, A., 1987. Modeling Groundwater Flow and Pollution. In J. Bear (Ed.), Theory and Applications of Transport in Porous Media, Vol. 2. Reidel Publishing Company, Dordrecht.

Beavers, G. S., Joseph, D. D., 1967. Boundary conditions at a naturally permeable wall. J. Fluid Mech. 30, 197–207.

Beinhorn, M., 2005. Non-linear Flow Processes in Subsurface and Surface Hydrosystems. Ph.D. thesis, Center for Applied Geoscience, University of Tübingen, Germany.

Bertoldi, G., Tamanini, D., Zanotti, F., Rigon, R., 2004. GEOtop, A Hydrological Balance Model, Technical Description and Programs Guide (Version 0.875). Department of Civil and Environmental Engineering, University of Trento.

Bhallamudi, S. M., Panday, S., Huyakorn, P. S., 2003. Sub-timing in fluid flow and transport simulations. Adv. Water Res. 26 (5), 477–489.

Cardenas, M. B., Wilson, J. L., 2007. Effects of current-bed form induced fluid flow on the thermal regime of sediments. Water Resour. Res. 43, W08431, doi:10.1029/2006WR005343.

Chen, Q., Morales-Chaves, Y., Li, H., Mynett, A., 2006. Hydroinformatics techniques in eco-environmental modelling and management. J. Hydroinf. 8 (4), 297316.

Constantz, J., Stonestrom, D., 2003. Heat as a tracer of water movement near streams, in: Heat as a tool for studying the movement of ground water near streams, edited by Stonestrom, D. and Constantz J. USGS Survey Circular 1260.

Darcy, H. P. G., 1856. Les Fontaines Publiques de la Ville de Dijon. Victor Dalmont, Paris.

Dawson, C., 2006. Analysis of discontinuous finite element methods for ground water/surface water coupling. SIAM J. Numer. Anal. 52, 63–88.

Delay, F., Ackerer, P., Danquigny, C., 2005. Simulating solute transport in porous or fractured formations using random walk particle tracking: a review. Vadose Zone J. 4 (2), 360–379.

Delfs, J.-O., Kalbus, E., Park, C.-H., Kolditz, O., 2009a. Ein physikalisch basiertes Modellkonzept zur Transportmodellierung in gekoppelten Hydrosystemen. Grundwasser (in print).

Delfs, J.-O., Park, C.-H., Kolditz, O., 2009b. Benchmarking of flow and transport in coupled surface/subsurface hydrosystems. Tech. rep., Helmholtz Centre for Environmental Reserach - UFZ Leipzig, Germany.

Delfs, J.-O., Park, C.-H., Kolditz, O., 2009c. A sensitivity analysis of Hortonian overland flow. Adv. Water Res. (in print).

Desitter, A., Bates, P. D., Anderson, M. G., Hervouet, J. M., 2000. Development of one, two, and three-dimensional finite element groundwater models within a generalized object-oriented framework. Hydrological Processes 14 (13), 2245–2259.

Di Giammarco, P., Todini, P. E., Lamberti, P., 1996. A conservative finite elements approach to overland flow: The control volume finite element formulation. J. Hydrol. 175, 267–291.

Discacciati, M., Miglio, E., Quarteroni, A., 2002. Mathematical and numerical models for coupling surface and groundwater flows. Apl. Num. Math. 43, 57–74.

Donigian, A. S., Imhoff, J., 2006. History and evolution of watershed modeling derived from the Stanford Watershed Model. CRC Press, Boca Raton, In Watershed Models edited by Singh V.P. and Frevert D.

Du, Y., Delfs, J.-O., Park, C.-H., Wang, W., Kolditz, O., 2008. A parallelized regional soil model: Conceptional approach and application. J. Environ. Hydrol. 17 (Paper 7).

Du, Y., Kolditz, O., 2005. Time discretization for Richards flow modelling. Tech. Rep. 2005-50, Center of Applied Geoscience, University of Tübingen, GeoSys -Preprint.

ECA&C, 2006.
`http://eca.knmi.nl/dailydata/index.php`.

Elshorbagy, A., Ormsbee, L., 2006. Object-oriented modeling approach to surface water quality management. Env. Modell. Softw. 21 (5), 689–698.

Forde, B. W. R., Foschi, R. O., Stiemer, S. F., 1990. Object-oriented finite element analysis. Computers & Structures 34 (3), 355–374.

Forsyth, P. A., Kropinski, M. C., 1997. Monotonicity considerations for saturated-unsaturated subsurface flow. SIAM J. Sci. Comp. 18, 1328–1354.

Forsyth, P. A., Wu, Y. S., Pruess, K., 1995. Robust numerical methods for saturated-unsaturated flow with dry initial conditions in heterogeneous media. Adv. Water Res. 18, 25–38.

Freeze, R. A., Harlan, R. L., 1969. Blueprint for a physically based, digitally-simulated hydrological response model. J. Hydrol. 9, 237–258.

Gandy, C., Younger, P., 2007. An object-oriented particle tracking code for pyrite oxidation and pollutant transport in mine spoil heaps. J. Hydroinf. 9 (4), 293–304.

Gerbeau, J.-F., Perthame, B., 2001. Derivation of viscous Saint Venant system for laminar shallow water: Numerical validation. Discr. Cont. Dyn. Syst. Ser. B 1 (1), 89–102.

Govindaraju, R. S., 1996. Modeling overland flow contamination by chemicals mixed in shallow soil horizons under variable source area hydrology. Water Resour. Res. 32 (3), 753758.

Govindaraju, R. S., Kavvas, M. L., 1991. Dynamics of moving boundary overland flows over infiltrating surfaces at hillslopes. Water Resour. Res. 27 (8), 1885–1898.

Green, W. A., Ampt, G. A., 1911. Studies on soil physics I. The flow of air and water through soils. J. of Agr. Sci. 4, 1–24.

Gunduz, O., Aral, M. M., 2005. River networks and groundwater flow: simultaneous solution of a coupled system. J. Hydrol. 301 (1-4), 216–234.

Harbaugh, A. W., Banta, E. R., Hill, M. C., McDonald, M. G., 2000. MODFLOW-2000, the U.S. geological survey modular ground-water model – user guide to modularization concepts and the groundwater flow process. Tech. Rep. 00-92, U.S. Geological Survey, Open-File Report.

Hassan, A. E., Mohamed, M. M., 2003. On using particle tracking methods to simulate transport in single-continuum and dual continua porous media. J. Hydrol. 275, 242–260.

Hoteit, H., Mose, R., Younes, A., Lehmann, F., Ackerer, P., 2002. Three-dimensional modeling of mass transfer in porous media using the mixed hybrid finite elements and the random-walk methods. Math Geol 34 (4), 435–456.

Huyakorn, P., Pinder, G., 1983. Computational methods in subsurface flow. Academic Press, New York.

Hydrosphere, 2006.
`http://sciborg.uwaterloo.ca/ mclaren/public/ or`
`http://www.modhms.com/software/hydrosphere.html`.

Ibisch, R. B., Borchardt, D., Seydell, I., 2008. Influence of periphyton biomass dynamics on biological colmation processes in the hyporheic zone of a gravel bed river (River Lahn, Germany). Fundam. Appl. Limnol. (in press).

Johnson, W. P., Blue, K. A., Logan, B. E., 1995. Modeling bacterial detachment during transport through porous media as a residence-time-dependent process. Water Resour. Res. 31 (11), 2649–2658.

Jones, J. P., Sudicky, E. A., Brookfield, A. E., Park, Y. J., 2006. An assessment of the tracer-based approach to quantifying groundwater contributions to streamflow. Water Resour. Res. 42, W02407.

Julien, P. Y., 2002. River mechanics. Cambridge University Press, Cambridge.

Kemmler, D., 2009. High-Performance Computing in Geoscience - Data Preprocessing by Domain Decomposition and Load Balancing. Ph.D. thesis, Institute of Geoscience, University of Tübingen, Germany.

Kinzelbach, W., 1987. Numerische Methoden zur Modellierung des Transports von Schadstoffen im Grundwasser. Oldenburg Verlag, München und Wien.

Kolditz, O., Bauer, S., 2004. A process-orientated approach to compute multi-field problems in porous media. J. Hydroinf. 6, 225–244.

Kolditz, O., Delfs, J.-O., Bürger, C., Beinhorn, M., Park, C.-H., 2008. Numerical analysis of coupled hydrosystems based on an object-oriented compartment approach. J. Hydroinf. 10 (3), 227–244.

Kolditz, O., Du, Y., Bürger, C., Delfs, J.-O., Kuntz, D., Beinhorn, M., Hess, M., Wang, W., vanderGrift, B., teStroet, C., 2007. Development of a regional hydrologic soil model and application to the Beerze-Reusel drainage basin. J. Environ. Pollut.

Kolditz, O., Shao, H., 2009. (eds) OpenTHMC - Developer Benchmark Book based on GeoSys/RockFlow Version 4.9.06. Tech. Rep. 15, Helmholtz Centre for Environmental Reserach - UFZ Leipzig, Germany.

Kollet, S. J., Maxwell, R. M., 2006. Integrated surface-groundwater flow modeling: A free-surface overland flow boundary condition in a parallel groundwater flow model. Adv. Water Res. 29 (7), 945–958.

Lees, M., 2000. Data-based mechanistic modelling and forecasting of hydrological systems. J. Hydroinf. 2 (1), 15–34.

LeVeque, R. J., 2002. Finite Volume Methods for Hyperbolic Problems. Cambridge University Press, Cambridge.

Li, Q., Unger, A., Sudicky, E., 2008. Simulating the multi-seasonal response of a large-scale watershed with a 3D physically-based hydrologic model. J. Hydrol. 357 (3-4), 317–336.

Logan, J. D., Zlotnik, V. A., 1996. Time-periodic transport in heterogeneous porous media. Appl. Math. Comput. 75, 119–138.

Makkink, G. F., 1957. Testing the Penman formula by means of lysimeters. J. Inst. Wat. Engrs. 11, 277–288.

Manning, R., 1891. On the flow of water in open channels and pipes. Trans., Inst. of Civ. Engrs. of Ireland 20, 161–207.

Miglio, E., 2003. Coupling of free surface and groundwater flows. Comput. Fluids, 73–83.

Morita, M., Yen, B. C., 2002. Modeling of conjunctive two-dimensional surface-three-dimensional subsurface flows. J. Hydraul. Eng., ASCE 128 (2), 184–200.

Paniconi, C., Aldama, A. A., E, E. W., 1991. Numerical evaluation of iterative and noniterative methods for the solution of nonlinear richards equation. Water Resour. Res. 27, 1147–1163.

Park, C.-H., Beyer, C., Bauer, S., Kolditz, O., 2008a. A study of preferential flow in heterogeneous media using random walk particle tracking. Geosci. J. 12 (3), 285–297.

Park, C.-H., Beyer, C., Bauer, S., Kolditz, O., 2008b. Using global node-based velocity in random walk particle tracking in variably saturated porous media: Application to contaminant leaching from road constructions. Environ. Geol. 55, 1755–1766.

Park, C.-H., Delfs, J., Kolditz, O., 2008c. Particle tracking of cryptosporidium oocysts from surface to groundwater. Groundwater quality 2007 proceedings, IAHS Publ. 324, 47–54.

Park, Y., Sudicky, E., Panday, S., 2008d. Application of implicit sub-time stepping to simulate flow and transport in fractured porous media. Adv. Water Res. 31 (7), 995–1003.

Philip, J. R., 1957. The theory of infiltration: 6. Effect of water depth over soil. Soil Science 85, 278–286.

Ponce, V. M., Ruh-Ming, L., Simmons, D. B., 1978. Applicability of kinematic and diffusion models. J. Hydraul. Div. ASCE 104, 353–360.

Quarteroni, A., Valli, A., 1994. Numerical approximation of Partial Differential Equations. Springer, Heidelberg.

Richards, C. P., Parr, A. D., 1988. Modified fickian model for solute uptake by runoff. J. Env. Engrg. 114 (4), 792–809.

Saenger, N., Zanke, U. C., 2008. A depth - oriented view of hydraulic exchange patterns between surface water and the hyporheic zone: analysis of field experimants at the River Lahn, Germany. Arch. Hydrobiol. (in press).

Samaniego, L., Bárdossy, A., 2007. Exploratory modelling applied to integrated water resources management. Proceedings 3rd International Symposium on Integrated Water Resources Management, Bochum, Germany, September 2006 IAHS Publ. 317.

Schijven, J. F., Bradford, S. A., Yang, S., 2004. Release of cryptosporidium and giardia from dairy cattle manure: physical factors. J. Environ. Qual. 33, 1499–1508.

Schneider, C., Attinger, S., Delfs, J.-O., Hildebrandt, A., 2009. Implementing small scale processes at the soil-plant interface - the role of root architectures for calculating root water uptake profiles. Hydrol. Earth Syst. Sci. Discuss. 6, 4233–4264.

Singh, V., Bhallamudi, S. M., 1998. Conjunctive surface-subsurface modeling of overland flow. Adv. Water Res. 21 (7), 567–579.

Singh, V. P., 1994. Derivation of errors of kinematic-wave and diffusion-wave approximations for space-independent flows. Water Resour. Manage 8, 57–82.

Smith, R. E., Woolhiser, D. A., 1971a. Mathematical Simulation of Infiltrating Watersheds. Tech. rep., Colorado State University, Fort Colins.

Smith, R. E., Woolhiser, D. A., 1971b. Overland flow on an infiltrating surface. Water Resour. Res. 7 (4), 899–913.

Starke, G., 2005. A first-order system least-squares finite element method for the shallow water equations. SIAM J. Numer. Anal. 42, 2387–2407.

Sudicky, E., Jones, J., Park, Y., 2008. Simulating complex flow and transport dynamics in an integrated surface-subsurface modeling framework. Geosc. J. 12 (2), 107–122.

Sudicky, E. A., Jones, J. P., McLaren, R. G., Brunner, D. S., VanderKwaak, J. E., 2000. A fully-coupled model of surface and subsurface water flow: Model overview and application to the laurel creek watershed. In: Balkema, A. A. (Ed.), Computational Methods in Water Resources. No. 2. pp. 1093–1099.

Therrien, R., McLaren, R. G., Sudicky, E. A., Panday, S., 2004. HydroSphere: A Three-dimensional Numerical Model Describing Fully-integrated Subsurface and Surface Flow and Solute Transport, Users Guide. Université Laval and University of Waterloo.

Thoms, R. B., 2003. Simulating fully coupled overland and variably saturated subsurface flow using MODFLOW. MSc thesis, OGI School for Science and Engineering, Oregon Health & Science University, Beaverton.

van Genuchten, M. T., 1980. A closed-form equation for predicting the hydraulic conductivity of unsaturated soil. Soil Sci. Soc. Am. J. 44, 892–898.

VanderKwaak, J. E., 1999. Numerical Simulation of Flow and Chemical Transport in Integrated Surface-Subsurface Hydrologic Systems. Ph.D. thesis, Department of Earth Sciences, University of Waterloo, Ontario, Canada.

VanderKwaak, J. E., Loague, K., 2001. Hydrologic-response simulations for the R-5 catchment with a comprehensive physics-based model. Water Resour. Res. 37 (4), 999–1013.

Vreugdenhil, C. B., 1994. Numerical Methods for Shallow-Water Flow. Kluwer Academic Publishers, Dordrecht.

Wallach, R., van Genuchten, T., Spencer, W., 1989. Modelling solute transfer from soil to surface runoff: The concept of effective depth of transfer. J. Hydrol. 109, 307–317.

Wang, J., Endreny, T. A., Hassett, J. M., 2005. A flexible modeling package for topographically based watershed hydrology. J. Hydrol. 314 (1-4), 78–91.

Wang, W., Kolditz, O., 2007a. Object-oriented finite element analysis of thermo-hydro-mechanical (thm) problems in porous media. Int. J. Numer. Methods Eng. 69 (1), 162–201.

Wang, W., Kolditz, O., 2007b. Object-oriented finite element analysis of thermo-hydro-mechanical (THM) problems in porous media. Int. J. Numer. Methods Eng. 69 (1), 162–201.

Warrick, J. W., 2003. Soil Water Dynamics. Oxford University Press Inc., New York.

Wasy Software, 2004. IFMMIKE11 1.1, User Manual. Wasy GmbH, Institute for Water Resources Planning and System Research.

Weisbach, J., 1845. Lehrbuch der Ingenieur- und Maschinen-Mechanik. Water & Power Press, Braunschweig.

Weiyan, T., 1992. Shallow Water Hydrodynamics. Water & Power Press, Hong Kong.

Wösten, J. H. M., Veerman, G. J., de Groot, W. J. M., Stolte, J., 2001. Water retention and conductivity characteristics of upper en deeper soil layers in the netherlands (in dutch). Alterra report 153.

Xie, M., Bauer, S., Kolditz, O., Nowak, T., Shao, H., 2006. Numerical simulation of reactive processes in an experiment with partially saturated bentonite. J. Contam. Hydrol. 83, 122–147.

6 List of enclosed publications

[**EP1**] **J.-O. Delfs**, C.-H. Park and O. Kolditz (2009): A sensitivity analysis of Hortonian flow, Advances in Water Resources 32, 1386-1395, doi: 10.1016/j.advwatres.2009.06.005.

[**EP2**] **J.-O. Delfs**, E. Kalbus, C.-H. Park and O. Kolditz (2009): Ein physikalisch basiertes Modellkonzept zur Tranportmodellierung in gekoppelten Hydrosystemen, Grundwasser 14(3), 227-244, doi: 10.1007/s00767-009-0114-0.

[**EP3**] Y. Du, **J.-O. Delfs**, W. Wang, C.-H. Park and O. Kolditz (2009): A regional hydrological soil model for large-scale applications: Computational concept and implementation, Journal of Environmental Hydrology 17, Paper 7.

[**EP4**] C.-H. Park, **J.-O. Delfs** and O. Kolditz (2008): Particle tracking of Cryptosporidium oocysts from surface to groundwater, Groundwater quality 2007 proceedings, IAHS Publication 324, 47-54.

[**EP5**] O. Kolditz, Y. Du, C. M. Bürger, **J.-O. Delfs**, D. Kunz, M. Beinhorn, M. Hess, W. Wang, B. van der Grift and C. te Stroet (2007): Development of a regional hydrologic soil model and application to the Beerze-Reusel drainage basin, Journal of Environmental Pollution 148(3), 855-866.

[**EP6**] O. Kolditz, **J.-O. Delfs**, C. M. Bürger, M. Beinhorn, C.-H. Park (2007): Numerical analysis of coupled hydrosystems based on an object-oriented compartment approach. Journal of Hydroinformatics 10(3), 227-244.

[**EP7**] C. Schneider, S. Attinger, **J.-O. Delfs** and A. Hildebrandt (2010): Implementing small scale processes at the soil-plant interface - the role of root architectures for calculating root water uptake profiles, Hydrology and Earth System Sciences 14(2), 279-289.

Enclosed Publication

[EP1] **J.-O. Delfs**, C.-H. Park and O. Kolditz (2009): *A sensitivity analysis of Hortonian overland flow*, Advances in Water Resources 32, 1386-1395, doi: 10.1016/j.advwatres.2009.06.005.

Advances in Water Resources 32 (2009) 1386–1395

Contents lists available at ScienceDirect

Advances in Water Resources

journal homepage: www.elsevier.com/locate/advwatres

A sensitivity analysis of Hortonian flow

J.-O. Delfs [a,b,*], C.-H. Park [b], O. Kolditz [b,c]

[a] Center for Applied Geoscience, University of Tübingen, Germany
[b] Helmholtz Centre for Environmental Research – UFZ, Department of Environmental Informatics, Leipzig, Germany
[c] Environmental System Analysis, TU Dresden, Germany

ARTICLE INFO

Article history:
Received 6 February 2009
Received in revised form 12 June 2009
Accepted 13 June 2009
Available online 21 June 2009

Keywords:
Sensitivity analysis
Smith and Woolhiser experiment
Coupled hydrosystem modeling
Infiltration excess overland flow

ABSTRACT

We present a sensitivity analysis for infiltration excess (Hortonian) overland flow based on a classic laboratory experiment by Smith and Woolhiser [Smith RE, Woolhiser DA. Overland flow on an infiltrating surface. Water Resour Res 1971;7(4):899–913]. The model components of the compartment approach are comprised of a diffusive wave approximation to the Saint–Venant equations for overland flow, a Richards model for flow in the variably saturated zone, and an interface coupling concept that combines the two components. In the coupling scheme a hydraulic interface is introduced to allow the definition of an exchange flux between the surface and the unsaturated zone. The effects of friction processes, soil capillarity, hydraulic interface, and vertical soil discretization on both infiltration and runoff prediction are investigated in detail. The corresponding sensitivity analysis is conducted using a small-perturbation method. As a result the importance of the hydraulic processes and related parameters are evaluated for the coupled hydrosystem.

1. Introduction

Research of overland flow on infiltrating surfaces has been subject of the hydrological science for several decades, pioneered, e.g. by Philip [33] and Smith and Woolhiser [40]. Recent studies include the work of Smith et al. [39], Jones et al. [15], Park et al. [30] and Delfs et al. [5]. The classic experiment by Smith and Woolhiser [41] has been used in many studies to examine coupled surface/subsurface flow models [41,1,10,38,27,45,44]. Overland flow on inclined planes can be described by both the kinematic and diffusive wave approximations of the Saint–Venant equations [51,28,9]. Fluid flow in the unsaturated soil zone (e.g., of air and water) is usually described by Richards models [35] with both van Genuchten–Mualem and Brooks–Corey soil–water characteristic-curves. Details of soil–water characteristic-curves in oil–air systems have been investigated, e.g. by Liu et al. [23]. A more complex approach to model fluid movement in the vadose zone (e.g., of non-aqueous phase liquids) considers multi-phase flow behavior [26,13]. The above mentioned studies of the Smith and Woolhiser experiment show some discrepancies in the parametrization of capillary forces (initial saturation, porosity, soil–water characteristic-curves) and friction processes (overland friction parameters and soil permeability). The importance of capillarity parameters for runoff predictions were shown, e.g. by Panday and Huyakorn [29]. Smith and Woolhiser [40] have already investigated the effects of soil parametrization and discretization on infiltration. A discretization limit was specified by Vogel and Ippisch [48]. The effects of subsurface heterogeneities on runoff prediction were considered in Singh and Bhallamudi [38], Kollet and Maxwell [20] and Maxwell and Kollet [25]. However, a systematic comparative study of parameter sensitivities for Hortonian flow does not exist so far.

Several methods for hydraulic coupling of surface flow with the variably saturated zone have been developed in the past: (i) The overland flow equation is treated as a source/sink term in the soil water balance equation [20]. (ii) The overland water depth acts as a transient boundary condition for the soil water balance equation. The resulting soil water flux provides a source/sink term for the overland flow equation [41,1,10,38,27,45]. (iii) Flux through a thin interface layer provides source/sink terms for both the overland flow and the Richards equations [47,44,14]. Two algorithms exist to couple the two water balance equations. In a monolithic scheme, both equations are assembled into a single equation system [45,44]. Monolithic algorithms are particularly suited for strongly coupled processes. In a partitioned (staggered) scheme the equations are coupled in an iterative manner [41,1,10,38,27]. In this study we use a compartment approach [19] which is designed for multi-scale problems. The hydrologic compartments (surface, soil, aquifer) individually host the different flow processes, which are described by diffusion type equations. In this new approach, the governing equations of different compartments are spatially discretized on their own mesh. The hydraulic compartments interact via coupling fluxes (method (iii)) at a common interface in a partitioned coupling scheme.

* Corresponding author. Address: Helmholtz Centre for Environmental Research – UFZ, Leipzig Permoserstr. 15 04318 Leipzig, Germany. Tel.: +49 3412351886; fax: +49 3412351939.
E-mail address: jens-olaf.delfs@ufz.de (J.-O. Delfs).

0309-1708/$ - see front matter © 2009 Elsevier Ltd. All rights reserved.
doi:10.1016/j.advwatres.2009.06.005

Nomenclature

a	immobile water depth (m)	m	van Genuchten–Mualem parameter for grain size distribution (–)
a'	interface layer thickness (m)	q	source/sink term ($m\ s^{-1}$)
b	bottom elevation (m)	q_c	coupling flux ($m\ s^{-1}$)
C	surface friction coefficient ($m^{-1}\ s^{-1}$)	q_d	surface outflow ($m\ s^{-1}$)
f	Darcy–Weisbach friction factor (–)	q_p	precipitation rate ($m\ s^{-1}$)
F_0	Froude number (–)	q_r	surface runoff ($m\ s^{-1}$)
g	gravitational acceleration ($m\ s^{-2}$)	Re	Reynolds number (–)
h	surface water head (m)	S	soil saturation (–)
H	mobile water depth (m)	S_e	effective soil saturation (–)
H_0	normal depth (m)	S_i	initial soil saturation (–)
H_a	surface water depth (m)	S_r	residual soil saturation (–)
j	surface friction coefficient (–)	S_0	bottom slope (–)
k	kinematic wave number (–)	u	depth-averaged velocity ($m\ s^{-1}$)
k_f	surface roughness coefficient (–)	u_0	normal velocity ($m\ s^{-1}$)
k_r	relative permeability (–)	α	van Genuchten–Mualem parameter for pore size (m^{-1})
$k_{a'}$	scaling factor in the coupling flux (–)	Λ	leakance (s^{-1})
K	saturated soil hydraulic conductivity ($m\ s^{-1}$)	ϕ	soil porosity (–)
K^c	interface conductivity ($m\ s^{-1}$)	ϕ_a	surface porosity (–)
l	surface friction coefficient (–)	Ψ	matric head (m)
L	flume length (m)		

Sensitivity analysis is a proven method for the assessment of parameter and model uncertainties in surface as well as subsurface hydrology (e.g., [16,18,12]). In a small-perturbation method the sensitivities of output functions to input parameters are approximated by differential quotients. The first-order sensitivity analysis assumption gives a total sensitivity as a sum of the partial sensitives to the different input parameters. The small-perturbation method was used for instance by Sun et al. [43], Sanz and Voss [37]. Other popular approaches are direct [34,18], (semi-)analytical [16,17,12], adjoint [4,52,24], and large-perturbation methods [11,3].

The structure of this paper is as follows. After a brief description of the classic Smith and Woolhiser experiment (Section 2), the model equations for coupled overland flow and flow in unsaturated porous media are summarized in Section 3. The numerical model and benchmark exercise for code verification based on the Smith and Woolhiser experiment are provided in Section 4. A detailed model sensitivity analysis for Hortonian flow is presented in Section 5. The focus is examining the sensitivities of surface runoff and infiltration flux to friction processes and soil capillarity. This includes a study of the impact of hydraulic interface properties in the coupling scheme and the vertical discretization of the soil system on the results.

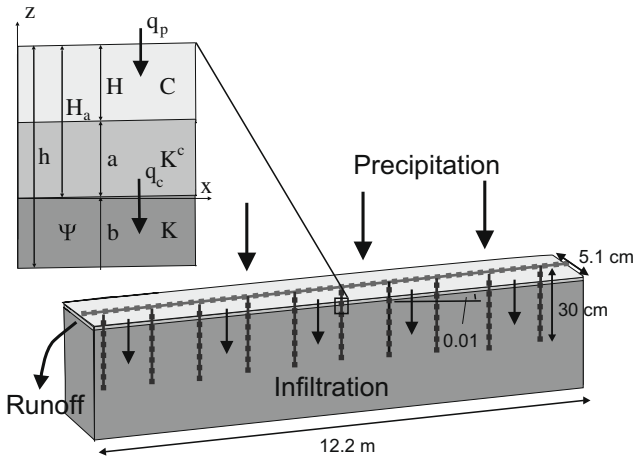

Fig. 1. Soil flume of the laboratory experiments by Smith and Woolhiser [41] with focus on overland flow, hydraulic interface, and soil parameters. The model domains for overland flow and flow in the unsaturated zone consist of two coupled one-dimensional meshes.

2. Laboratory experiments by Smith and Woolhiser

Smith and Woolhiser [40,41] conducted infiltration experiments in a soil flume with a length of 12.2 m, a width of 5.1 cm, and a slope of 0.01 (Fig. 1). Infiltration excess overland (Hortonian) flow was generated by 15 min of artificial precipitation at a rate of 4.2 mm min^{-1} which was roughly 2–3 times the saturated soil conductivity. To prevent algal growth in the soil a light oil instead of water was used. The viscosity of this light oil was about twice the water viscosity. Seepage was allowed at both flume ends. As the water table was about 1 m below the surface, it was assumed that the capillary fringe did not influenced the infiltration process. The soil material was a locally obtained river-deposited sand known as Poudre fine sand. Soil bulk density measurements at four sections of the flume indicated a considerable horizontal and vertical heterogeneity. Soil density increased with depth. Soil water characteristic curves, i.e., capillary pressure and relative permeability dependencies on water content, were measured for different soil densities. Overland friction parameters were determined in the laboratory for water depths higher than 4 mm. A surface runoff collector was mounted at the lower end of the flume (experimental data in Fig. 2). The vertical movement of moisture in the soil was monitored at a vertical cross-section in the middle of the flume by saturation gauging through gamma-ray attenuation (experimental data in Fig. 3). Experimental results were obtained under both drained and undrained initial conditions. Drained conditions were ensured by letting the flume drain for several weeks. Lateral flow effects in the soil compartment (i.e., interflow) due to heterogeneity were shown to be marginal for the Smith and Woolhiser experiment by Singh and Bhallamudi [38], which was confirmed by our own numerical results. Therefore, we used the simplest geometric representation of the experiment by coupling two 1-D models for overland flow and the unsaturated zone, which is represented by an array of soil columns (Fig. 1). The parameters used for the analysis of the Smith and Woolhiser experiment are summarized in Table 1.

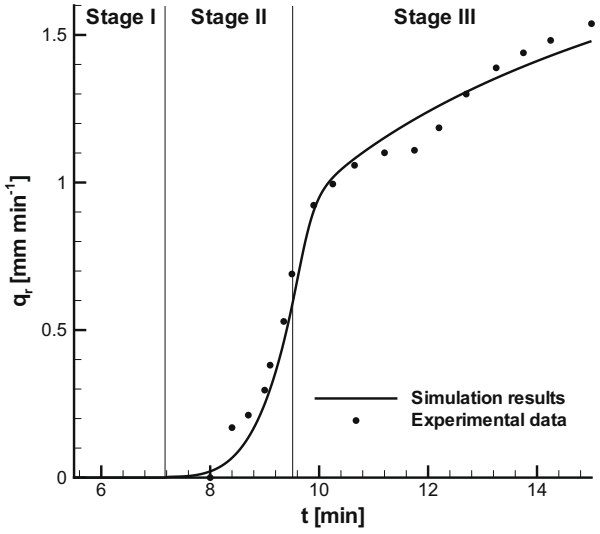

Fig. 2. Comparison of hydrograph simulation results q_r with experimental data by Smith and Woolhiser [41] and definition of flow stages.

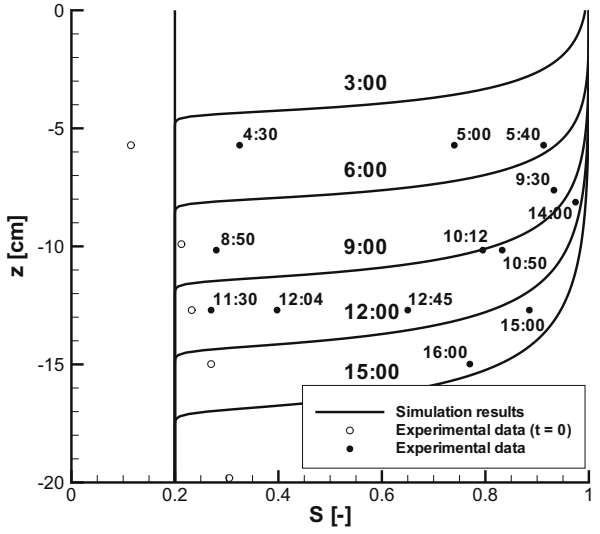

Fig. 3. Comparison of moisture front simulation results with experimental data by Smith and Woolhiser [41]. $z = 0$ at soil top.

Table 1
Hydraulic parameters of the laboratory experiment by Smith and Woolhiser [41].

Items	Symbol	Setting	Unit
Fluid			
Kinematic viscosity	ν	177	mm^2 min^{-1}
Density	ρ	0.756	g mm^{-3}
Overland flow			
Surface friction	C	80,000	mm^{-1} min^{-1}
	j	1	–
	l	2	–
Unsaturated flow			
Porosity	ϕ	0.42	–
Residual saturation	S_r	0.05	–
Hydraulic conductivity	K	1.7	mm min^{-1}
Pore size	α	0.006	mm^{-1}
Grain size distribution	m	0.75	–
Interface			
Conductivity	K^c	1.7	mm min^{-1}
Thickness	a'	1	mm
Immobile depth	a	1	mm

3. Conceptual model

The conceptual model consists of three components: diffusive wave approximation to the Saint–Venant equations for overland flow (Section 3.1), Richards model for fluid movement in the unsaturated soil (Section 3.2), and the interface layer concept for coupling (Section 3.3).

3.1. Overland flow

Overland flow is described by the diffusive and kinematic wave approximations of the Saint–Venant equations [51,28,9]. The Saint–Venant formulation is derived from the Reynolds-averaged Navier–Stokes equations by depth integration and the assumption of a hydrostatic pressure distribution. Further negligence of the (eddy) viscosity tensor and use of empirical relationships for bottom friction lead to a set of two hyperbolic equations (e.g. [49,8,7]). The Saint–Venant equations for mass and momentum balance in the normal depth normalized representation read

$$\phi_a \frac{\partial H_*}{\partial t_*} + \frac{\partial H_* u_*}{\partial x_*} = q_* \tag{1}$$

$$\frac{\partial u_*}{\partial t_*} + u_* \frac{\partial u_*}{\partial x_*} + \frac{1}{F_0^2}\frac{\partial h_*}{\partial x_*} = k\left[1 - \left(\frac{u_*}{H_*^l}\right)^{1/j}\right] - \frac{q_* u_*}{H_*} \tag{2}$$

Asterisks denote dimensionless variables defined as

$$H_* = \frac{H}{H_0}, \quad h_* = \frac{h}{H_0}, \quad u_* = \frac{u}{u_0}, \quad x_* = \frac{x}{L}, \quad t_* = \frac{t u_0}{L}, \quad q_* = \frac{qL}{H_0 u_0} \tag{3}$$

where H is mobile water depth, H_0 is normal depth, h is surface water head, u is depth-averaged velocity, u_0 is normal velocity, x is horizontal coordinate, L is flume length, t is time, and q is a source/sink term. $0 \leqslant \phi_a(H_a) \leqslant 1$ is the surface porosity which is unity for flow over a flat plane and varies between zero and unity for flow over an uneven surface. Surface roughness is parameterized with the immobile depth a such that the surface water depth is given by $H_a = h - b$ and the mobile water depth by $H = \max(h - a - b, 0)$ where b is bottom elevation (Fig. 1). Bottom friction is expressed by power laws of the general form

$$u = C S_0^j H^l \tag{4}$$

where S_0 is the bottom slope parameter. The friction coefficients C, j, and l are evaluated from the Darcy–Weisbach relationship

$$u^2 = \frac{8gHS_0}{f} \tag{5}$$

where $g = 9.81\ \mathrm{m\,s^{-2}}$ is the gravitational acceleration and f the Darcy–Weisbach friction factor. Under laminar flow we can assume $f = k_f/Re$ where k_f is a surface roughness coefficient and Re the Reynolds number, such that $j = 1$, $l = 2$.

The Froude number F_0, which expresses the relation between the inertial and the head-gradient term, as well as the kinematic wave number k, which expresses the relation between the inertial term and the gravity as well as the bottom friction term, are defined as

$$F_0 = \frac{u_0}{\sqrt{gH_0}}, \quad k = \frac{S_0 L}{H_0 F_0^2} \tag{6}$$

Neglecting advection and lateral inflow in the momentum balance equation (2) and using Eq. (4) lead to the diffusive wave approximation

$$\phi_a \frac{\partial H}{\partial t} - \frac{\partial}{\partial x}\frac{C H^{l+1}}{|\partial h/\partial x|^{1-j}}\frac{\partial h}{\partial x} = q_p - q_c - q_d \tag{7}$$

where water head h is used as a primary variable in the overland flow calculation, q_p is the precipitation rate, q_c is the coupling flux, and outflow at the lower boundary is determined with the critical depth $q_d = \sqrt{gH^3}$. The non-dimensional momentum balance equation (2) shows that the diffusive wave solution approaches the Saint–Venant equations for $F_0 \to 0$ and $k \to \infty$. Further neglecting the head-gradient term in Eq. (2) leads to the hyperbolic kinematic wave approximation. The Froude and kinematic numbers for the Smith and Woolhiser experiment are in the ranges of $0 < F_0(H) < 1$ and $k(H) > 30$, respectively. For this range both the diffusive and kinematic wave approximations are applicable [51,28]. The estimations depend on the maximum flow depth along the soil flume. Simulations affirmed that the use of a normal depth condition $\tilde{q}_d = CS_0^j H^l$, which preserves the flow depth at the outlet, affects the following results insignificantly.

3.2. Flow in the variably saturated zone

In this study we consider infiltration of light oil into a unsaturated porous medium. The assumption that the air phase moves under a negligible pressure gradient leads to the Richards equation

$$\phi \frac{\partial S}{\partial t} - \frac{\partial}{\partial z} k_r K \left(\frac{\partial \Psi}{\partial z} + 1 \right) = q_c \tag{8}$$

where Ψ is matric head, which is used as a primary variable for unsaturated flow, ϕ is soil porosity, S is saturation, k_r is relative permeability, K is saturated hydraulic conductivity of the soil, and z is the vertical coordinate (positive upwards). Two soil-dependent constitutive relationships for saturation and relative permeability are required to close Eq. (8). With the effective saturation

$$S_e = \max\left(0, \frac{S - S_r}{1 - S_r}\right) \tag{9}$$

where S_r is the residual saturation, the van Genuchten–Mualem soil–water characteristic-curves read

$$S_e(\Psi) = \left(1 + |\alpha \Psi|^{\frac{1}{1-m}}\right)^{-m} \tag{10}$$

$$k_r(S) = \sqrt{S_e}\left[1 - \left(1 - S_e^{1/m}\right)^m\right]^2 \tag{11}$$

where α is a pore size parameter and m is a grain size distribution parameter. In both the oil–air and the water–air system the liquid is the wetting fluid. A substantial difference, however, is the lower surface tension between oil and air. A scaling for the oil–air system leads to a higher value for α and a lower value for m in Eq. (10) for the capillary pressure [21]. Eq. (11) for the relative permeability, however, is independent of the specific liquid [23].

3.3. Hydraulic interface layer

In this study an interface layer is introduced at the common boundary of the overland and soil compartments. This interface layer allows the definition of a discrete exchange flux to couple both flow processes mutually. The coupling flux is given by

$$q_c = -k_{a'} \Lambda \Psi, \quad \Lambda = \frac{K^c}{a'} \tag{12}$$

where Λ is the leakance, K^c is the interface conductivity, and a' is the interface layer thickness. The coupling flux (Eq. (12)) depends on the hydraulic head in the upper soil Ψ. $0 \leqslant k_{a'}(H_a) \leqslant 1$ is a scaling factor to ensure that infiltration is not exceeding the available surface liquid. The scaling factor $k_{a'}$ varies between zero for dry and unity for fully saturated interfaces ($H_a \geqslant a$). A first-order exchange flux (e.g. [46]) includes an additional term for hydrostatic surface water pressure. In this work the coupling flux (Eq. (12)) is used as sink term in the overland flow equation (7) and a source term in the Richards equation (8).

4. Numerical scheme

We use two different finite element methods for numerical analysis of the coupled problem: a Control Volume finite element method for the solution of the shallow water equation (7) and a standard Galerkin finite element method for solving the Richards equation (8) [19]. As this paper focuses on a sensitivity analysis of the coupled hydrosystem we skip a detailed description of the numerical schemes and refer to VanderKwaak [46], Beinhorn et al. [2], Wang and Kolditz [50]. The numerical models for both flow in the variably saturated zone and overland flow are tested against several benchmark examples [6]. Due to the different characteristics of the shallow water and Richards equations, specific discretizations are necessary to obtain accurate numerical solutions for the coupled problem.

4.1. Scheme verification

In order to verify the presented numerical scheme for coupling overland flow and flow in the variably saturated zone, we compare the simulation results with data from the classic laboratory experiment by Smith and Woolhiser [41] (see Section 2). The soil system is represented homogeneously with a uniform initial water saturation of $S_i = 0.2$. Hydraulic friction parameters are used as suggested from additional measurements by Smith and Woolhiser [40] corresponding to the laminar Darcy–Weisbach equation (4). Interface thickness a' and interface conductivity K^c are set according to the immobile water depth a and the soil conductivity K, respectively (Section 5.2.3). The hydraulic parameters for the surface–subsurface system are summarized in Table 1.

Fig. 2 shows the numerical simulation results and experimental data for the runoff hydrograph

$$q_r = \frac{q_d H}{L} \tag{13}$$

with initially drained conditions. A no-flow and constant pressure boundary condition were specified at the upper overland flow boundary and at the soil bottom, respectively. The numerical results are in good agreement with the experimental data and other findings existing in the literature [41,1,10,38,27,45,44]. Overland flow initialization starts after about 7 min. The finite length of the soil flume causes a flattening in the hydrograph after about 10 min. The hydrograph can be split into three flow stages: (I) Overland flow initialization, (II) Hydrograph rise, (III) Hydrograph flattening, which will be used for the following sensitivity analysis (Section 5).

Fig. 3 depicts the simulated propagation of the moisture front into the soil in comparison to the measurements. Experimental data are available for some depths along a vertical profile in the middle of the flume. Calculated saturation values are shown at 3-min intervals. In general, the simulations are close to the measured data and other existing study results [41,1,10,38,27,45,44]. The calculated saturation front is a little ahead of the measured data. This deviation is in the range of accuracy of the measurements as reported by Smith and Woolhiser [41].

The coupling flux (Eq. (12)) is the most important quantity in order to describe the hydraulic exchange process between the surface and the soil compartments. Fig. 4 shows the temporal evolution of the coupling flux q_c as a function of surface water depth H_a and matric head in the soil Ψ during the continuous precipitation q_p. In the first flow stage (I), capillary pressure (initially $\Psi = -300$ mm – dot-dashed line), which dominates the infiltration process, induces a large infiltration capacity. Therefore, q_c (solid line) corresponds at the beginning to the precipitation rate

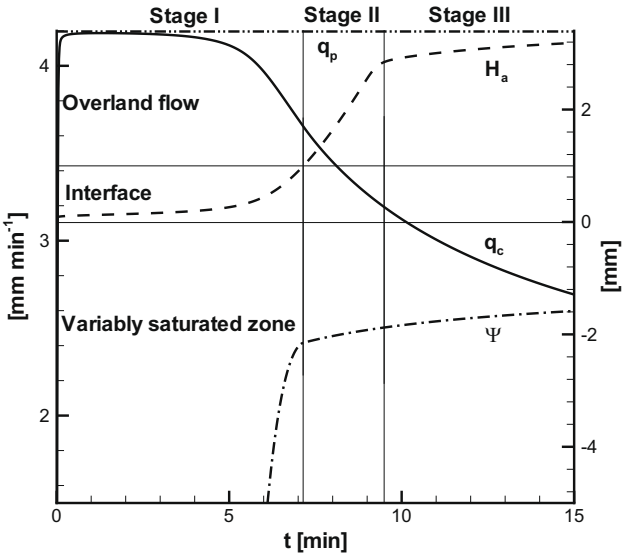

Fig. 4. Temporal evolution of coupling flux q_c, surface water depth H_a and matric head Ψ during continuous precipitation q_p.

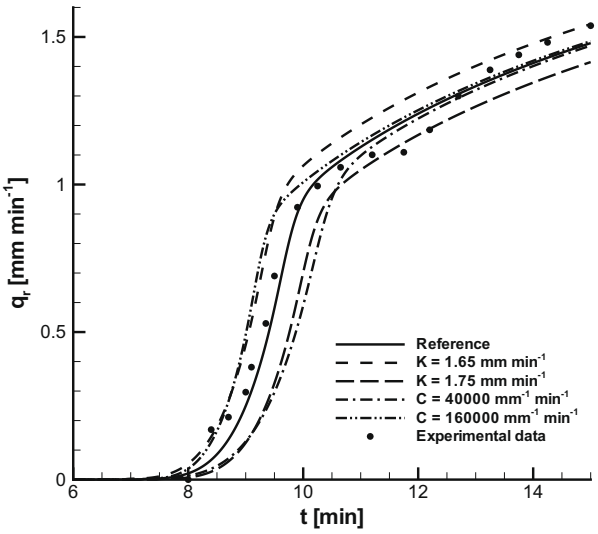

Fig. 5. Influence of friction parameter variations (overland friction and soil hydraulic conductivity) on surface runoff. Reference simulation (solid line) corresponds to parametrization given in Table 1.

$q_p = 4.2$ mm min^{-1}. Overland flow and stage II start after the interface layer is saturated (i.e. $H_a \geqslant a' = 1$ mm). In stage II, the matric potential Ψ approaches $-a' = -1$ mm and the coupling flux declines slowly. At the same time, the hydrograph rises steeply until later in stage III, the water depth curve and consequently the runoff hydrograph become flat (Fig. 2). At the end of the third flow stage, the coupling flux still exceeds 1.5 times the soil hydraulic conductivity $K = 1.7$ mm min^{-1}.

4.2. Discretization

At first, a 2-D finite element discretization was used for the soil compartment. In accordance to the findings of Singh and Bhallamudi [38], the ratio between lateral and vertical flow velocities did not exceed 0.05. For the sake of simplicity in the numerical model, we used the following spatial discretization: A one-dimensional grid ($\Delta x = 12.2$ cm) is aligned along the soil flume for overland flow, and one-dimensional vertical columns with a length of 30 cm are used for flow in the unsaturated zone (Fig. 1). The soil system requires a dense vertical discretization ($\Delta z = 1$ mm) for the sensitivity analysis (Section 5.3). We use an implicit Euler time marching procedure with a global step size of 1 s.

5. Sensitivity analysis

Laboratory and particularly field experiments involve uncertainties concerning the exact determination of model parameters. Previous studies of the Smith and Woolhiser experiment reveal several discrepancies in the model parametrization, e.g., concerning soil density (heterogeneity) increasing with depths; (initial) water saturation only known at a vertical cross-section at the middle of the flume, and friction parameters [41,1,10,38,27,45,44]. As an example, Fig. 5 shows the influence of parameter variations (overland friction coefficient C and soil conductivity K) on the surface runoff simulation. The parameters correspond to the range found in the literature. From Fig. 5 it can be clearly seen that the overland friction coefficient C influences the surface runoff mainly at the early time (hydrograph rise in the second flow stage), whereas the soil hydraulic conductivity K shows its influence at later times as well (hydrograph flattening in the final flow stage III) (Fig. 2).

In order to examine the influence of parameter uncertainties systematically, we present a parameter sensitivity study focussed on friction processes (overland flow friction and soil conductivity) (Section 5.2.1) and soil capillarity (Section 5.2.2). We study the influences of the model parameters on both surface runoff and infiltration flux using a small-perturbation method (Section 3). We study the impact of the parameters of the hydraulic interface and the vertical soil discretization on the results The importance of the parameters is evaluated and ranked (Section 5.2.4).

5.1. Small perturbation method

In general, sensitivity analysis considers the evolution of a system whose response $\mathcal{O}(\mathcal{P}_1, \mathcal{P}_2, \mathcal{P}_3, \ldots)$ depends on a set of input parameters $\mathcal{P}_i$. In the small-perturbation approach, a single input parameter $\mathcal{P}_i$ is systematically varied and the resulting system response $\mathcal{O}$ is investigated. The first-order sensitivity analysis is based on the following total differential

$$d\mathcal{O} = \sum_i \frac{\partial \mathcal{O}}{\partial \mathcal{P}_i} d\mathcal{P}_i \tag{14}$$

Sensitivity is defined as a derivative of the system output function to an input parameter

$$\frac{\partial \mathcal{O}}{\partial \mathcal{P}_i} \tag{15}$$

Logarithmic sensitivities

$$\frac{\mathcal{P}_i}{\mathcal{O}} \frac{\partial \mathcal{O}}{\partial \mathcal{P}_i} = \frac{\partial \ln(\mathcal{O})}{\partial \ln(\mathcal{P}_i)} \tag{16}$$

allow a comparison of input parameters and output functions in different dimensions. The total differential (Eq. (14)) can be rearranged to obtain the relative change of the system response

$$\frac{d\mathcal{O}}{\mathcal{O}} = \sum_i \left(\frac{\mathcal{P}_i}{\mathcal{O}} \frac{\partial \mathcal{O}}{\partial \mathcal{P}_i} \right) \frac{d\mathcal{P}_i}{\mathcal{P}_i} \tag{17}$$

which gives rise to the logarithmic sensitivities (Eq. (16)). In order to rank the model parameters we use these logarithmic sensitivities in the following analysis. The logarithmic sensitivities (Eq. (16)) are numerically computed by finite differences

$$\frac{\mathcal{P}}{\mathcal{O}}\frac{\partial \mathcal{O}}{\partial \mathcal{P}} \approx \frac{\mathcal{P}}{\mathcal{O}(\mathcal{P})}\frac{\mathcal{O}(\mathcal{P}[1+\epsilon]) - \mathcal{O}(\mathcal{P}[1-\epsilon])}{\mathcal{P}[1+\epsilon] - \mathcal{P}[1-\epsilon]} = \frac{\mathcal{O}(\mathcal{P}[1+\epsilon]) - \mathcal{O}(\mathcal{P}[1-\epsilon])}{2\epsilon\mathcal{O}(\mathcal{P})} \quad (18)$$

where ϵ is a discretization parameter. $\epsilon = 1\times10^{-3}$ and $\epsilon = 1\times10^{-4}$ were determined heuristically as suited in this study.

5.2. Results

In this study the sensitivities of coupling flux $q_c(=\mathcal{O}_1)$ and surface runoff $q_r(=\mathcal{O}_2)$ are investigated. The system input parameters $\mathcal{P}_i$ are listed in Table 2. Concerning friction processes, we consider the saturated soil hydraulic conductivity $K(=\mathcal{P}_1)$ and the surface friction coefficient $C(=\mathcal{P}_2)$. For the analysis of capillarity forces we vary the available pore space, i.e. porosity $\phi(=\mathcal{P}_3)$, initial saturation $S_i(=\mathcal{P}_4)$, and the residual saturation $S_r(=\mathcal{P}_5)$ as well as the van Genuchten–Mualem parameters concerning pore size $\alpha(=\mathcal{P}_6)$ and grain size distribution $m(=\mathcal{P}_7)$. Regarding the interface layer approach, we examine the interface layer thickness a' and the interface conductivity K^c in the coupling flux as well as the immobile depth a in the overland flow.

5.2.1. Friction processes

Three different friction processes are important to coupled surface/subsurface flow: hydraulic resistance due to bottom friction in overland water flow, hydraulic conductivity of soil, and fluid viscosity. As the values of fluid viscosity can be measured at high precision, we focus the sensitivity study on more uncertain friction parameters for the overland surface and the porous medium.

Fig. 6 shows the logarithmic sensitivities of coupling flux $(\mathcal{O}_1)$ on soil hydraulic conductivity $(\mathcal{P}_1)$ and of surface runoff $(\mathcal{O}_2)$ on both surface and subsurface friction parameters $(\mathcal{P}_1, \mathcal{P}_2)$. Soil hydraulic conductivity $K(\mathcal{P}_1)$ is the most sensitive friction parameter. The sensitivity of surface runoff on soil hydraulic conductivity $\left|\frac{K}{q_r}\frac{\Delta q_r}{\Delta K}\right|$ reaches a maximum in flow stage II after overland flow initialization and reduce between t = 9.5 min and t = 10.5 min by a factor of about 7. The ratio between the sensitivity of surface runoff to the overland flow friction coefficient $\frac{C}{q_r}\frac{\Delta q_r}{\Delta C}$ and to the soil hydraulic conductivity $\left|\frac{K}{q_r}\frac{\Delta q_r}{\Delta K}\right|$ remains during the hydrograph rise in flow stage II lower than 0.06. The decrease of the sensitivity $\frac{C}{q_r}\frac{\Delta q_r}{\Delta C}$ in the transition between the flow stages II and III is about 3.5 times higher than for $\left|\frac{K}{q_r}\frac{\Delta q_r}{\Delta K}\right|$. Long term simulations showed that the sensitivity of the coupling flux on soil hydraulic conductivity $\frac{K}{q_c}\frac{\Delta q_c}{\Delta K}$ approaches unity.

At first, we calculated the coupling flux (12) with an addition term for hydrostatic surface water pressure. We found logarithmic sensitivities of the coupling flux on the surface friction parameter $\left|\frac{C}{q_c}\frac{\Delta q_c}{\Delta C}\right|$ of about 0.003. Similar to the findings of [33] the influence of surface water on the soil system can be neglected.

Table 2
Parameter uncertainties $\overline{\Delta}\mathcal{P}_i/\mathcal{P}_i$ $(i = 1,\ldots,7)$ specified for the laboratory experiment by Smith and Woolhiser [41].

$\mathcal{P}_i$	Parameter	Symbol	Setting
$\mathcal{P}_1$	Soil hydraulic conductivity	$\overline{\Delta}K/K$	0.4
$\mathcal{P}_2$	Overland friction parameter	$\overline{\Delta}C/C$	1
$\mathcal{P}_3$	Porosity	$\overline{\Delta}\phi/\phi$	0.2
$\mathcal{P}_4$	Initial soil saturation	$\overline{\Delta}S_i/S_i$	1
$\mathcal{P}_5$	Residual soil saturation	$\overline{\Delta}S_r/S_r$	0.1
$\mathcal{P}_6$	Pore size	$\overline{\Delta}\alpha/\alpha$	0.4
$\mathcal{P}_7$	Grain size distribution	$\overline{\Delta}m/m$	0.05

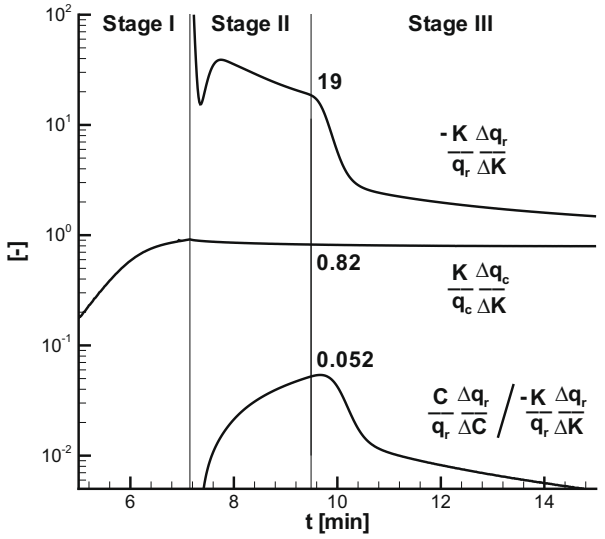

Fig. 6. Logarithmic sensitivities of coupling flux q_c and surface runoff q_r on friction parameters: Soil hydraulic conductivity K and surface friction parameter C. Numbers assigned to curves are sensitivity values at $t = 9.5$ min.

5.2.2. Soil capillarity

Soil capillarity has a major effect on infiltration processes (e.g. [35,32]). Capillarity is mainly influenced by the hydraulically available pore space, i.e., porosity $\phi(\mathcal{P}_3)$, initial saturation $S_i(\mathcal{P}_4)$ and residual saturation $S_r(\mathcal{P}_5)$ as well as the soil–water characteristic-curves for capillary pressure and relative permeability described by van Genuchten–Mualem parameters $(\mathcal{P}_6$–$\mathcal{P}_7)$.

Fig. 7 illustrates the effect of the saturation status and the capillarity parameters $(\mathcal{P}_3$–$\mathcal{P}_7)$ on the sensitivity of the coupling flux $(\mathcal{O}_1)$. Similar to the case of soil hydraulic conductivity $K(=\mathcal{P}_1)$ (Fig. 6), the sensitivities of the coupling flux on capillarity parameters $\left|\frac{\mathcal{P}_i}{q_c}\frac{\Delta q_c}{\Delta \mathcal{P}_i}\right| (i = 3,\ldots,7)$ increase with water accumulation in the interface layer (first flow stage). After the interface layer is saturated $(k_{a'}(H_a) = 1)$, the effect of capillarity declines slowly with time. Therefore, the sensitivities of the coupling flux on capillarity parameters are reduced during flow stage III by a factor of

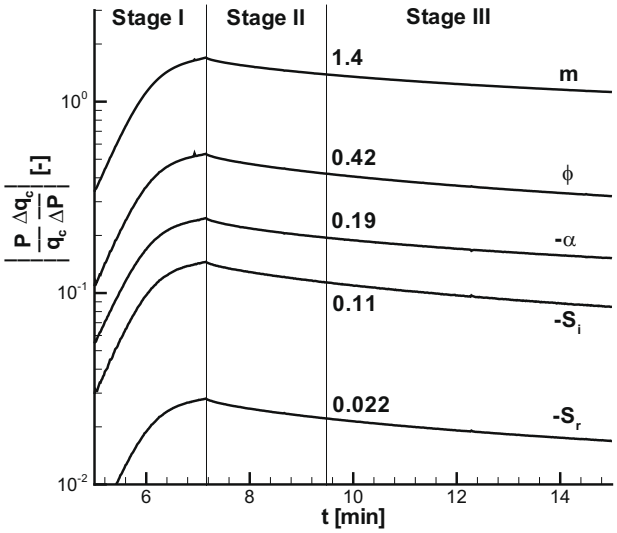

Fig. 7. Logarithmic sensitivities of coupling flux q_c on soil capillarity parameters: Pore size m, porosity ϕ, grain size distribution α, initial saturation S_i, and residual saturation S_r. Numbers assigned to curves are sensitivity values at $t = 9.5$ min.

approximately 4/3. The sensitivities on capillarity parameters drop between $t = 9.5$ min and $t = 10.5$ min by a factor which is about 15% higher than for the sensitivities on soil hydraulic conductivity $\left|\frac{K}{q_r}\frac{\Delta q_r}{\Delta K}\right|$. The van Genuchten parameter m has the largest sensitivity values.

Fig. 8 depicts the effect of the capillarity-related parameters $(\mathcal{P}_3-\mathcal{P}_7)$ on surface runoff $(\mathcal{O}_2)$. The sensitivities $\left|\frac{\mathcal{P}_i}{q_r}\frac{\Delta q_r}{\Delta \mathcal{P}_i}\right|$ $(i = 3,\ldots,7)$ are scaled with the sensitivity on soil hydraulic conductivity $\left|\frac{K}{q_r}\frac{\Delta q_r}{\Delta K}\right|$ (Fig. 6). The temporal behavior of the sensitivities is similar: Moderate decline during flow stage II, sharp decline when the hydrograph turns flat, and gradual decrease in the late part of the experiment (flow stage III). The van Genuchten parameter m has the largest effect on surface runoff again.

5.2.3. Hydraulic interface

In the definition of the coupling flux (12) we introduced additional parameters: interface thickness a', conductivity K^c, and immobile surface water depth a. We examine their effect on the coupling flux $q_c(=\mathcal{O}_1)$, runoff prediction $q_r(=\mathcal{O}_2)$ and their sensitivities on soil parameters $(\mathcal{P}_1, \mathcal{P}_3-\mathcal{P}_7)$. We present results for the soil porosity $\phi(=\mathcal{P}_3)$ as an example.

For the interface conductivity K^c we use the soil hydraulic conductivity K. Fig. 9 depicts the effects of interface conductivity variations on the coupling flux q_c and its sensitivity on soil porosity $\frac{\phi}{q_c}\frac{\Delta q_c}{\Delta \phi}$. An increase of the interface conductivity K^c by two orders of magnitude raises the coupling flux q_c by about 1% while the sensitivity at the transition between flow stages I and II becomes smoother. On the other hand, a decrease in the interface conductivity by two orders of magnitude reduces the coupling flux q_c and its sensitivity on soil porosity $\frac{\phi}{q_c}\frac{\Delta q_c}{\Delta \phi}$ by more than 50%.

For the interface thickness a' we use the immobile surface water depth a. Fig. 10 illustrates the effects of interface thickness variations on the coupling flux q_c and its sensitivities on soil porosity $\frac{\phi}{q_c}\frac{\Delta q_c}{\Delta \phi}$. An decrease in the interface thickness a' by one order of magnitude raises the coupling flux q_c by about 1% while the corresponding sensitivity on soil porosity shows a sharp peak at the transition between flow stages II and III. The sensitivity shows significant oscillations for $a' = 5$ mm and $t \leqslant 10$ s. The coupling flux q_c is reduced for $t \leqslant 7$ and overestimated later on.

Fig. 11 depicts the effects on runoff q_r and its sensitivities on soil porosity $\frac{\phi}{q_r}\frac{\Delta q_r}{\Delta \phi}$ if both interface thickness a' and immobile surface water depth a are varied with the condition that $a = a'$. The hydrograph shows a retardation of about 2 min for $a' = 10$ mm. Overland flow starts less than 0.5 min earlier for $a' = 0.1$ mm than for the interface layer used as a reference $(a' = 1$ mm). A finite interface leads to an increase in the sensitivity of the hydrograph on soil porosity $\left|\frac{\phi}{q_r}\frac{\Delta q_r}{\Delta \phi}\right|$ after overland flow initialization. The effect of the interface layer declines with time.

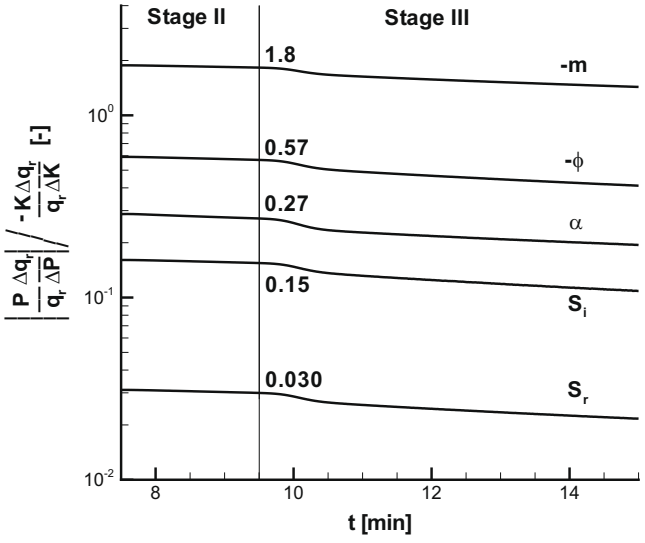

Fig. 8. Logarithmic sensitivities of surface runoff q_r on soil capillarity parameters: Pore size m, porosity ϕ, grain size distribution α, initial saturation S_i, and residual saturation S_r. Numbers assigned to curves are sensitivity values at $t = 9.5$ min.

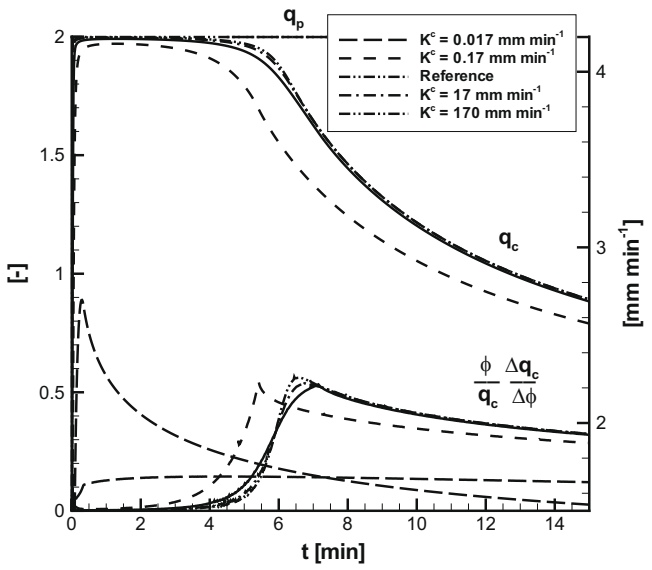

Fig. 9. Coupling flux q_c and logarithmic sensitivities on soil porosity $\frac{\phi}{q_c}\frac{\Delta q_c}{\Delta \phi}$ as dependent on interface conductivity K^c, chosen as soil hydraulic conductivity K in reference curve. q_p is precipitation rate.

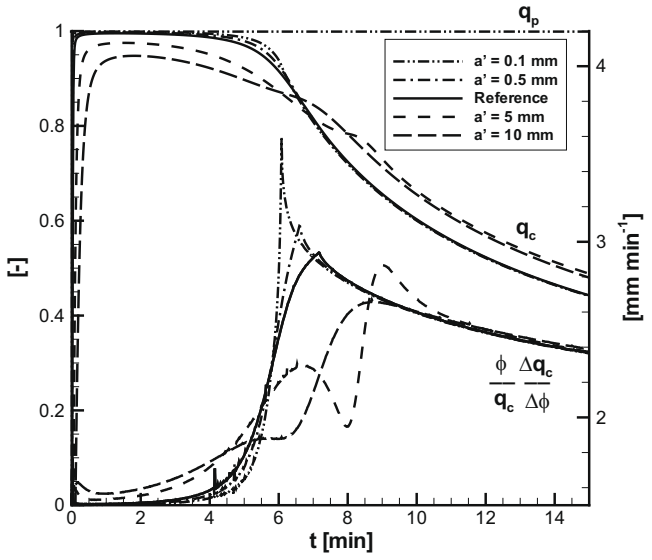

Fig. 10. Coupling fluxes q_c and logarithmic sensitivities on soil porosity $\frac{\phi}{q_c}\frac{\Delta q_c}{\Delta \phi}$ as dependent on interface thickness parameter a', chosen as immobile surface depth a in reference curve. q_p is precipitation rate.

5.2.4. Parameter ranking

In this section we provide a ranking of parameter sensitivities for coupling flux $(\mathcal{O}_1)$ and surface runoff $(\mathcal{O}_2)$. In order to rank the parameters $\mathcal{P}_1-\mathcal{P}_7$, we scale the logarithmic sensitivities (Eq. (16)) of soil parameters $\mathcal{P}_1, \mathcal{P}_3-\mathcal{P}_7$ with values identified by Smith and Woolhiser [41] (Table 2).

The ranking of the friction parameters $\mathcal{P}_1-\mathcal{P}_2$ and the capillarity parameters $\mathcal{P}_3-\mathcal{P}_7$ for surface runoff $(\mathcal{O}_2)$ is shown in Fig. 12.

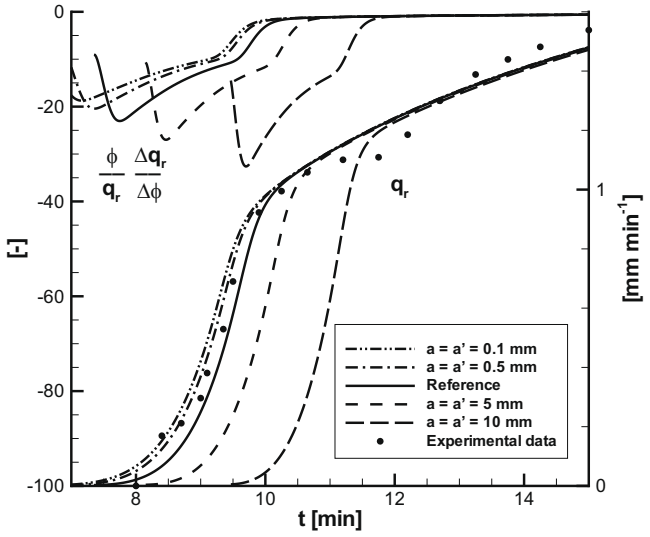

Fig. 11. Surface runoff q_r and logarithmic sensitivities on soil porosity $\frac{\phi}{q_r}\frac{\Delta q_r}{\Delta \phi}$ as dependent on interface thickness parameter a' with the condition that $a' = a$, where a is immobile surface depth. Reference curve corresponds to $a' = 1$ mm.

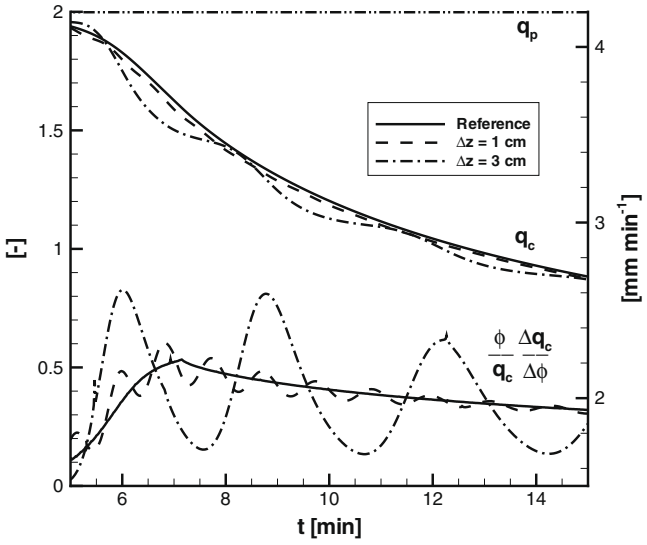

Fig. 13. Coupling flux q_c and logarithmic sensitivities on soil porosity $\frac{\phi}{q_c}\frac{\Delta q_c}{\Delta \phi}$ as dependent on vertical soil discretization Δz during continuous precipitation q_p. Reference curve corresponds to $\Delta z = 1$ mm.

For the logarithmic sensitivities $\frac{\mathcal{P}_i}{q_r}\frac{\Delta q_r}{\Delta \mathcal{P}_i}$ $(i = 1, \ldots, 7)$ values at the end of flow stage II ($t = 9.5$ min) are taken to avoid the effects of the finite interface layer (Fig. 2) and the finite flume length (Fig. 6). Latter reduces the sensitivities on soil parameters $\mathcal{P}_1, \mathcal{P}_3 - \mathcal{P}_7$ and the surface friction parameter $C(= \mathcal{P}_2)$ after 10 min simulation time by a factor of about 7 and 25, respectively. The ranking for coupling flux $(\mathcal{O}_1)$ is similar (Figs. 7 and 8) except of the surface friction parameter C which influence has been neglected. The influence of capillarity parameters $\mathcal{P}_3 - \mathcal{P}_7$ reduces during flow stage III by a factor of 4/3.

The soil hydraulic conductivity K, which describes friction in the porous medium, has the largest influence on the results (ranking value 1). The capillarity parameters porosity ϕ, initial saturation S_i, pore size α, and grain size distribution m follow with a ranking values between 0.23 and 0.38. The ranking value for the surface friction parameter C is 0.13. Residual saturation S_r is rated of lower importance (ranking value 0.013).

5.3. Vertical soil discretization

The sensitivity analysis requires a dense vertical discretization ($\Delta z = 1$ mm). Fig. 13 illustrates the influence of vertical soil discretization on the coupling flux q_c and its sensitivity soil parameters. A resolution of $\Delta z = 1$ cm produces already oscillations in sensitivity on the soil porosity $\frac{\phi}{q_c}\frac{\Delta q_c}{\Delta \phi}$ with amplitudes up to 0.3 and reduces the coupling flux by approximately 1%. For $\Delta z = 3$ oscillations reduce the coupling flux up to 3% in the displayed time frame. The errors caused by vertical soil discretization reduce with time.

6. Summary and conclusions

In this work, we presented a sensitivity analysis for infiltration excess overland (Hortonian) flow. The conceptual model consists of the diffusive wave approximation to the Saint–Venant equations for overland flow (Eq. (7)) and the Richards model for flow in the unsaturated zone (Eq. (8)). Both compartments are coupled with an hydraulic interface layer concept (Eq. (12)). The data basis for the numerical study is taken from the classic experiment by Smith and Woolhiser [41] representing Hortonian flow with short-term infiltration in a rather homogeneous sand.

Concerning the numerical accuracy we found that certain relationships of time and space discretization are necessary for the coupled compartment approach. A high spatial resolution

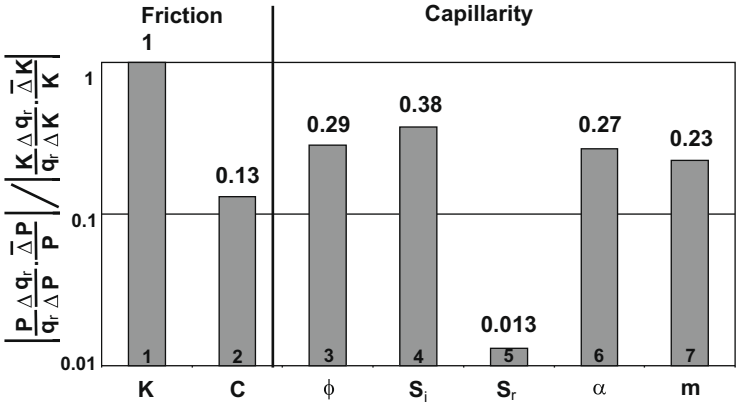

Fig. 12. Ranking values with logarithmic sensitivities of surface runoff $\frac{\mathcal{P}_i}{q_r}\frac{\Delta q_r}{\Delta \mathcal{P}_i}$ at $t = 9.5$ min weighted by parameter uncertainties $\overline{\Delta}\mathcal{P}_i/\mathcal{P}_i$ $(i = 1, \ldots, 7)$. Results are scaled with sensitivity and uncertainty values obtained for soil hydraulic conductivity $\frac{K}{q_r}\frac{\Delta q_r}{\Delta K}, \overline{\Delta}K/K$. Numbers i in the bars correspond to parameters $\mathcal{P}_i$, respectively.

($\Delta z = 1$ mm) of the soil compartment is required for solving the Richards equation precisely in comparison to the resolution required for overland flow ($\Delta x = 12.2$ cm). A global time step size of $\Delta t = 1$ s is used for flow in the unsaturated zone and overland flow.

The sensitivity study of the model parameters ($\mathcal{P}_i$) was focused on the effects of friction processes and soil capillarity. The impact of vertical soil discretization and a interface layer, which is used for the calculation of the coupling flux, is investigated. The system output functions of the sensitivity analysis are coupling flux $q_c(\mathcal{O}_1)$ and surface runoff by overland flow $q_r(\mathcal{O}_2)$ at the outlet of the flume.

The sensitivity of surface runoff q_r to all parameters $\mathcal{P}_1$—$\mathcal{P}_7$ is larger in flow stage II than in flow stage III (Fig. 2) with the flattening hydrograph due to the finite flume length. More specifically, the logarithmic sensitivity of surface runoff on soil hydraulic conductivity $K(\mathcal{P}_1)$ declines by a factor of about 7. This factor is 15% higher for capillarity parameters ($\mathcal{P}_3$—$\mathcal{P}_7$) and 3.5 times higher for surface friction $C(\mathcal{P}_2)$. The influence of soil capillarity on infiltration declines with time such that the logarithmic sensitivities of the coupling flux q_c and surface runoff q_r on soil capillarity parameters ($\mathcal{P}_3$—$\mathcal{P}_7$) are reduced during flow stage III (4.5 min) by 4/3. We found logarithmic sensitivities of the coupling flux q_c on the surface friction parameter C of about 0.003 which is two orders of magnitude lower than the corresponding logarithmic sensitivity on soil hydraulic conductivity K. Therefore, we could simplify the coupling flux by neglecting the influence of surface water on the soil system. As suited parameters for the interface layer thickness a' and interface conductivity K^c were found the immobile surface water depth a and soil hydraulic conductivity K, respectively. Lower interface layer values $a' < a$ led to numerical oscillations and lower interface conductivities $K^c < K$ hindered infiltration. An interface layer thickness of $a = a' = 1$ mm was found as suitable for the sensitivity study.

In order to rank the friction and capillarity parameters, the calculated logarithmic sensitivities at the end of stage II are weighted with parameter uncertainties in the experiment by Smith and Woolhiser [41]. The soil hydraulic conductivity $K(\mathcal{P}_1)$ is ranked as the most important parameter and assigned the ranking value 1. The capillarity parameters $\phi(\mathcal{P}_3), S_i(\mathcal{P}_4)$ for pore space and $\alpha(\mathcal{P}_6), m(\mathcal{P}_7)$ in the soil–water characteristic curves by van Genuchten–Mualem are assigned ranking values between 0.23 and 0.38. Overland friction parameter $C(\mathcal{P}_2)$ was found as important for the runoff prediction q_r in flow stage II (ranking value 0.13). Residual saturation $S_r(\mathcal{P}_5)$ was found to be of low importance throughout (ranking value 0.013).

Numerical investigations of large scale hydrosystems are possible in principle, as shown recently by a series of excellent studies [42,22,31]. Essential is a precise determination of the soil hydraulic conductivity in the analysis of coupled hydrosystems, especially for long term simulations. However, the hydrograph in the application at laboratory scale showed significant sensitivity on the surface friction parametrization.

Coupling of different conceptional approaches, which are currently used in the numerical investigation of hydrosystems, appears promising. In the analysis of soil and groundwater systems Euler methods (finite differences, volumes, and elements) are common. In surface hydrology stochastic methods are faster and easier to parameterize (e.g. [36]).

Acknowledgement

This work was partly funded by the European Union FP6 Integrated Project "AquaTerra" (Project No. 505428) and the German Ministry of Education and Research (BMBF) Project "IWAS - International Water Research Alliance Saxony" (Project No. 02WM1027). The authors thank the editor and the reviewers for constructive comments that improved the paper.

References

[1] Akan AO, Yen BC. Mathematical model of shallow water flow over porous media. J Hydraul Div, Am Soc Civ Eng 1981;107(4):479–94.
[2] Beinhorn M, Dietrich P, Kolditz O. 3-D numerical evaluation of density effects on tracer tests. J Contam Hydrol 2005;81(1–4):89–105.
[3] Boateng S, Crawlfield JD. Two-dimensional sensitivity analysis of contaminant transport in the unsaturated zone. Ground Water 1999;37(2):185–93.
[4] Cacuci DG, Weber CF, Oblov EM, Marable JH. Sensitivity theory for general systems of nonlinear equations. Nucl Sci Eng 1980;75:88–110.
[5] Delfs J-O, Kalbus E, Park C-H, Kolditz O. A physically based model concept for transport modelling in coupled hydrosystems [in German]. Grundwasser, in press. doi:10.1007/s00767-009-0114-0.
[6] Delfs J-O, Park C-H, Kolditz O. Benchmarking of flow and transport in coupled surface/subsurface hydrosystems. Tech. rep., Helmholtz Centre for Environmental Reserach – UFZ Leipzig, Germany. 2008.
[7] Ferrari S, Saleri F. A new two-dimensional shallow water model including pressure effects and slow varying bottom topography. Math Modell Numer Anal 2004;38(2):211–34.
[8] Gerbeau J-F, Perthame B. Derivation of viscous Saint Venant system for laminar shallow water: Numerical validation. Discrete Contin Dyn Syst Ser B 2001;1(1):89–102.
[9] Govindaraju RS, Jones SE, Kavvas ML. On the diffusion wave model for overland flow 1. Solution for steep slopes. Water Resour Res 1998;24(5):734–44.
[10] Govindaraju RS, Kavvas ML. Dynamics of moving boundary overland flows over infiltrating surfaces at hillslopes. Water Resour Res 1991;27(8):1885–98.
[11] Griggs JE, Peterson FL. Groundwater-flow dynamics and development strategies at the atoll scale. Ground Water 1993;31(2):209–20.
[12] Guinot V, Cappalaere B. Sensitivity analysis of 2D steady-state shallow water flow. Application to free surface flow model calibration. Adv Water Resour 2009;32:540–60.
[13] Helmig R. Multiphase flow and transport processes in the subsurface. Berlin/Heidelberg/New York: Springer; 1997.
[14] Jones JP, Sudicky EA, Brookfield AE, Park YJ. An assessment of the tracer-based approach to quantifying groundwater contributions to streamflow. Water Resour Res 2006;42:W02407.
[15] Jones JP, Sudicky EA, McLaren RG. Application of a fully-integrated surface–subsurface flow model at the watershed-scale: a case study. Water Resour Res 2008;44:W03407.
[16] Kabala ZJ. Sensitivity analysis of a pumping test on a well with wellbore storage and skin. Adv Water Resour 2001;24(5):483–504.
[17] Kabala ZJ, El-Sayegh HK, Gavin HP. Sensitivity analysis of a no-crossflow model for the transient flowmeter test. Stochast Environ Res Risk Assess 2002;16(6):399–424.
[18] Kabala ZJ, Milly PCD. Sensitivity analysis of flow in unsaturated heterogeneous porous media: theory, numerical model, and its verification. Water Resour Res 1990;26(4):593–610.
[19] Kolditz O, Delfs J-O, Bürger C, Beinhorn M, Park C-H. Numerical analysis of coupled hydrosystems based on an object-oriented compartment approach. J Hydroinf 2008;10(3):227–44.
[20] Kollet SJ, Maxwell RM. Integrated surface-groundwater flow modeling: a free-surface overland flow boundary condition in a parallel groundwater flow model. Adv Water Resour 2006;29(7):945–58.
[21] Leverett MC. Capillary behavior in porous soils. Trans Am Inst Min Met Eng 1941;142:152–69.
[22] Li Q, Unger A, Sudicky E. Simulating the multi-seasonal response of a large-scale watershed with a 3D physically-based hydrologic model. J Hydrol 2008;357(3–4):317–36.
[23] Liu YP, Hopmans JW, Grismer ME, Chen JY. Direct estimation of air–oil and oil–water capillary pressure and permeability relations from multi-step outflow experiments. J Contam Hydrol 1998;32:223–45.
[24] Martien PT, Harley RA, Cacuci DC. Adjoint sensitivity analysis for a three-dimensional photochemical model: implementation and method comparison. Trans Inst Civil Eng Ireland 2006;20:161–207.
[25] Maxwell RM, Kollet SJ. Quantifying the effects of three-dimensional subsurface-heterogeneity on Hortonian runoff processes using a coupled numerical, stochastic approach. Adv Water Resour 2008;31:807–17.
[26] Morel-Seytoux HJ, Billica JA. A two-phase numerical model for prediction of infiltration: Applications to a semi-infinite column. Water Resour Res 1985;21(4):607–15.
[27] Morita M, Yen BC. Modeling of conjunctive two-dimensional surface-three-dimensional subsurface flows. J Hydraul Eng 2002;128(2):184–200.
[28] Morris EM, Woolhiser DA. Unsteady one-dimensional flow over a plane: partial equilibrium and recession hydrographs. Water Resour Res 1980;16(2):355–60.
[29] Panday S, Huyakorn PS. A fully coupled physically-based spatially-distributed model for evaluating surface/subsurface flow. Adv Water Resour 2004;27:361–82.
[30] Park C-H, Delfs J-O, Kolditz O. Particle tracking of cryptosporidium oocysts from surface to groundwater. Groundwater quality: securing groundwater quality in urban and industrial environments. In: Proceedings 6th

international groundwater quality conference held in Fremantle, Western Australia, December 2007, IAHS Publ. 324. 2008. p. 47–54.
[31] Park Y, Sudicky E, Panday S. Application of implicit sub-time stepping to simulate flow and transport in fractured porous media. Adv Water Resour 2008;31(7):995–1003.
[32] Philip JR. The theory of infiltration: 4. Sorptivity and algebraic infiltration equation. Soil Sci 1957;84:257–64.
[33] Philip JR. The theory of infiltration: 6. Effect of water depth over soil. Soil Sci 1957;85:278–86.
[34] Reuven Y, Smooke MD, Rabitz H. Sensitivity analysis of one-dimensional mixed initial-boundary value problems: applications to freely propagating premixed laminar flames. J Sci Comput 1987;2(4):345–70.
[35] Richards LA. Capillary conduction of liquids through porous mediums. J Phys 1931;1:318–33.
[36] Samaniego L, Bárdossy A. Exploratory modelling applied to integrated water resources management. In: Proceedings 3rd international symposium on integrated water resources management, Bochum, Germany, September 2006, IAHS Publ. 317. 2007.
[37] Sanz E, Voss CI. Inverse modeling for seawater intrusion in coastal aquifers: insights about parameter sensitivities, variances, correlations and estimation procedures derived from the henry problem. Adv Water Resour 2005;29(3):439–57.
[38] Singh V, Bhallamudi SM. Conjunctive surface–subsurface modeling of overland flow. Adv Water Resour 1998;21(7):567–79.
[39] Smith RE, Smettern KRJ, Broadbridge P, Woolhiser DA. Infiltration theory for hydrologic applications. Water series monograph series, vol. 15. Washington, DC: American Geophysical Union; 2002.
[40] Smith RE, Woolhiser DA. Mathematical simulation of infiltrating watersheds. Tech. rep., Colorado State University, Fort Colins. 1971.
[41] Smith RE, Woolhiser DA. Overland flow on an infiltrating surface. Water Resour Res 1971;7(4):899–913.
[42] Sudicky E, Jones J, Park Y. Simulating complex flow and transport dynamics in an integrated surface–subsurface modeling framework. Geosci J 2008;12(2):107–22.
[43] Sun N, Sun N-Z, Elimelech M, Ryan JN. Sensitivity analysis and parameter identifiability for colloid transport in geochemically heterogeneous porous media. Water Resour Res 2001;37(2):209–22.
[44] Therrien R, McLaren RG, Sudicky EA, Panday SM. Hydrosphere, a three-dimensional numerical model describing fully-integrated subsurface and surface flow and solute transport. Tech. rep., Université Laval and University of Waterloo, Canada. 2004.
[45] Thoms RB. Simulating fully coupled overland and variably saturated subsurface flow using MODFLOW. MSc thesis. OGI School for Science and Engineering, Oregon Health & Science University, Beaverton. 2003.
[46] VanderKwaak JE. Numerical simulation of flow and chemical transport in integrated surface–subsurface hydrologic systems. PhD thesis, Department of Earth Sciences, University of Waterloo, Ontario, Canada. 1999.
[47] VanderKwaak JE, Loague K. Hydrologic-response simulations for the R-5 catchment with a comprehensive physics-based model. Water Resour Res 2001;37(4):999–1013.
[48] Vogel H-J, Ippisch O. Estimation of a critical spatial discretization limit for solving Richards' equation at large scales. Vadose Zone J 2008;7(1):112–4.
[49] Vreugdenhil CB. Numerical methods for shallow-water flow. Dordrecht: Kluwer Academic Publishers; 1994.
[50] Wang W, Kolditz O. Object-oriented finite element analysis of thermo-hydro-mechanical (THM) problems in porous media. Int J Numer Meth Eng 2007;69(1):162–201.
[51] Woolhiser DA, Liggett JA. Unsteady, one-dimensional flow over a plane – the rising hydrograph. Water Resour Res 1967;3(3):753–71.
[52] Yeh TCJ, Zhang JQ. A geostatistical inverse method for variably saturated flow in the vadose zone. Water Resour Res 1996;32(9):2757–66.

Enclosed Publication

[EP2] **J.-O. Delfs**, E. Kalbus, C.-H. Park and O. Kolditz (2009): *Ein physikalisch basiertes Modellkonzept zur Tranportmodellierung in gekoppelten Hydrosystemen*, Grundwasser 14(3), 227-244, doi: 10.1007/s00767-009-0114-0.

Grundwasser – Zeitschrift der Fachsektion Hydrogeologie
DOI 10.1007/s00767-009-0114-0

FACHBEITRAG

Ein physikalisch basiertes Modellkonzept zur Transportmodellierung in gekoppelten Hydrosystemen

Jens-Olaf Delfs · Edda Kalbus · Chan-Hee Park · Olaf Kolditz

Eingang des Beitrages: 12. 12. 2008 / Eingang des überarbeiteten Beitrages: 6. 4. 2009

Kurzfassung Hydrosysteme sind komplexe Systeme, in denen eine Vielzahl von Prozessen gleichzeitig auf unterschiedlichen Raum- und Zeitskalen ablaufen. In diesem Artikel stellen wir ein Kompartimentkonzept zur Simulation von Stoff- und Wärmetransportprozessen in gekoppelten Hydrosystemen vor. Das Konzept beinhaltet die Kopplung von Strömungs- und Transportprozessen über die Grenzflächen der Kompartimente (oder der Prozessdomäne) unter Beibehaltung der rechentechnischen Anforderungen und Optimierungen für die numerische Lösung jedes einzelnen Prozesses. Neu ist auch die Verwendung stochastischer Partikelmethoden (random walk particle tracking – RWPT) zur Analyse von Stofftransport in gekoppelten Hydrosystemen. Wir stellen zunächst kurz die verwendete RWPT-Methode und die maßgeblichen Gleichungen für Strömung, Wärme- und Stofftransport in der gesättigten und der ungesättigten Zone sowie auf der Landoberfläche vor. Fließvorgänge werden durch (z. T. nichtlineare) Diffusionsgleichungen beschrieben (Darcy-Gleichung für Grundwasserströmung, Richards-Gleichung für Strömung in der ungesättigten Zone und diffusive Wellengleichung für Oberflächenabfluss) und über Austauschterme (Flüsse) gekoppelt. Transportprozesse werden durch Advektions-Diffusionsgleichungen beschrieben und advektiv gekoppelt. Wir stellen drei Anwendungsbeispiele für Strömungs-, Stoff- und Wärmetransportvorgänge in gekoppelten Hydrosystemen vor basierend auf Hortonschen und Dunneschen Oberflächenabflüssen sowie hyporheischen Fließvorgängen.

Dipl.-Phys. J.-O. Delfs (✉) · Ph.D. C.-H. Park · Prof. Dr. O. Kolditz
Helmholtz-Zentrum für Umweltforschung – UFZ Leipzig,
Department Umweltinformatik,
Permoserstr. 15, 04318 Leipzig, Deutschland
E-Mail: jens-olaf.delfs@ufz.de, chanhee.park@ufz.de,
olaf.kolditz@ufz.de

M.Sc. E. Kalbus
Helmholtz-Zentrum für Umweltforschung – UFZ Leipzig,
Department Hydrogeologie,
Permoserstr. 15, 04318 Leipzig, Deutschland
E-Mail: edda.kalbus@ufz.de

A physically based model concept for transport modelling in coupled hydrosystems

Abstract Hydrosystems are very complex systems with numerous processes occuring simultaneously at different spatial and temporal scales. In this paper we present the concept of a compartment approach for the analysis of coupled hydrosystems including heat and mass transport. In this concept, flow and transport processes are coupled via their compartment (or process domain) boundaries without giving up the computational necessities and optimisations for the numerical solution of each individual process. In this new approach, random walk particle tracking (RWPT) methods are integrated into the coupled hydrosystem analysis. We briefly introduce the RWPT method and the governing equations for water flow, heat, and mass transport in aquifers, soils and on surfaces. Flow processes are described by diffusion equations (Darcy equation for groundwater flow, Richards equation for flow in the unsaturated zone, and the diffusive wave approximation for overland flow) which are coupled by exchange fluxes. Transport processes are described by advection-diffusion equations and coupled with the exchange fluxes by advection. We present three application examples concerning flow, mass and heat transport in coupled hydrosystems based on Horton- and Dunne overland flow as well as on hyporheic flows.

Keywords Coupled hydrosystems · heat and mass transport · random walk particle tracking · hyporheic zone

Published online: 18 July 2009

Einleitung

Hydrosysteme sind sehr komplexe, dynamische und empfindliche Umweltsysteme, die durch natürliche Einflüsse sowie durch die Einwirkung des Menschen belastet werden. Die Hydrosphäre kann grob in drei Kompartimente unterteilt werden: das Oberflächenwasser, das Wasser in der ungesättigte Zone und das Grundwasser (Abb. 1). Oberflächenwasser setzt sich aus Seen, Flüssen, sowie dem Oberflächenabfluss zusammen (Anderson & Burt 1985, Singh & Frevert 2005). Im Untergrund treten Strömung durch die ungesättigten Zonen (Simunek et al. 1999) sowie Grundwasserströmung durch poröse Aquifere und Karstaquifere auf (Huyakorn & Pinder 1983, Teutsch 1988). Einen Übergangs- und Pufferbereich zwischen Flüssen und dem Grundwasserkörper bildet die hyporheische Zone (Brunke & Gonser 1997).

Ein integriertes Prozessverständnis ist erforderlich um die Auswirkungen anthropogener Einflüsse auf die Entwicklung von Hydrosystemen abschätzen zu können (Chen et al. 2006). Zwei der schwierigsten Herausforderungen in der Analyse von Hydrosystemen sind die Überbrückung von verschiedenen Skalen sowie die Kopplung der einzelnen Prozesse. Da sich die Fließgeschwindigkeiten innerhalb der einzelnen Kompartimente stark voneinander unterscheiden, finden Stoff- und Wärmetransportprozesse auf mehreren Zeitskalen statt. Als vielversprechend erscheint hier die Verwendung stochastischer Partikel (engl.: random walk particle tracking – RWPT) (Delay et al. 2005, Park et al. 2008b).

Gekoppelte Grundwasser-Oberflächenwasser-Modelle wurden seit ihrer ersten Erwähnung in Freeze & Harlan (1969) kontinuierlich weiterentwickelt, so auch zur Simulation von Transportprozessen. Beispiele für zur Verfügung stehende konzeptionelle Modelle und numerische Codes sind MODFLOW2000 (Harbaugh et al. 2000), TOPMODEL (Bertoldi et al. 2004), Feflow (Wasy GmbH, Wasi Software 2004), MIKE-SHE (Système Hydrologique Européen, Abbott et al. 1986), Hydrosphere (Sudicky et al. 2000, Therrien et al. 2004), SWAT (Arnold et al. 1998), HSPF (Gunduz & Aral 2005) und ParFlow (Kollet & Maxwell 2006), um nur einige zu nennen.

Kolditz et al. (2008) stellten zur Simulation gekoppelter Hydrosysteme einen Kompartimentenansatz vor, bei dem jeder Prozess mit seiner eigenen zeitlichen und räumlichen Skale berücksichtigt wird. Innerhalb der einzelnen Kompartimente finden Fließ- und Transportprozesse in einer gemeinsamen Prozessdomäne statt (z. B. Oberfläche, Boden, Aquifer). Sowohl die Fließ- als auch die Transportprozesse werden durch Diffusionsgleichungen beschrieben. Neu und kennzeichnend für diesen Ansatz ist insbesondere, dass die Prozesse innerhalb der unterschiedlichen Kompartimente auf unterschiedlichen Gittern räumlich diskretisiert werden. Die Simulationszeitschritte werden ebenfalls dem Prozess entsprechend angepasst, da schnellere Prozesse kleinere Zeitschritte erfordern. Zur Kopplung benachbarter Kompartimente werden Austauschflüsse an gemeinsamen Grenzflächen berechnet und eine zusätzliche Kopplungs-Iteration durchgeführt (partitionierte Kopplung). Der sog. „Global implicit"-Algorithmus,

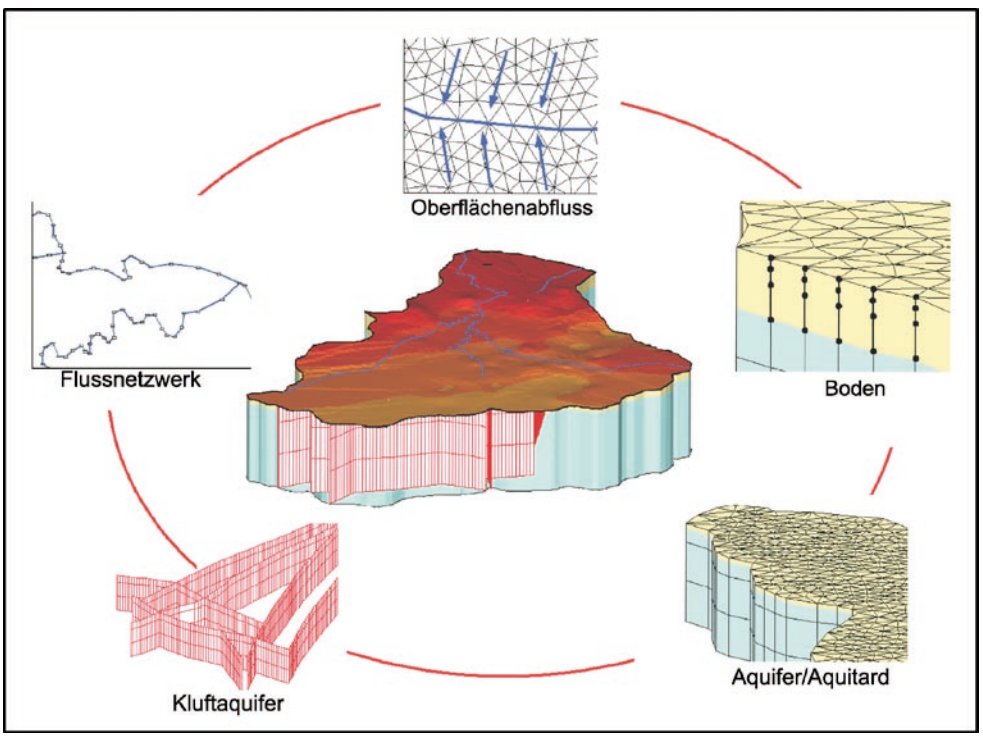

Abb. 1 Kompartimente von Hydrosystemen (Numerische Diskretisierungen)

der durch Sudicky et al. (2008) und Li et al. (2008) entwickelt wurde, löst die gekoppelten Gleichungen für die ober- und unterirdischen Abflüsse in einem Rechenschritt. Die Separation der Zeitskalen der unterschiedlichen Prozesse erfolgt durch ein sog. „Sub-time stepping"-Konzept (Park et al. 2008c).

In dieser Arbeit wird ein Modell zur Analyse gekoppelter Hydrosysteme vorgestellt, welches sowohl Strömung als auch Stoff- und Wärmetransport umfasst. Nach einer kurzen Erläuterung des Modellkonzepts und der verwendeten Gleichungen werden drei Anwendungsbeispiele vorgestellt, die die Anwendbarkeit des Modells für Fragestellungen im Bereich Oberflächen-Boden-Aquifer-Wechselwirkungen demonstrieren. Die Beispiele umfassen zwei Benchmark-Tests basierend auf den klassischen Experimenten von Smith & Woolhiser (1971) und Abdul & Gilham (1984) sowie eine Anwendung von Wärmetransport im Flussbett der Lahn zur Untersuchung hyporheischer Fließvorgänge.

Modellkonzept

Für Strömungs- und Transportprozesse in Oberflächen-, Boden- und Grundwassersystemen gelten die gleichen physikalischen und chemischen Prinzipien. In dieser Arbeit werden die physikalischen Gesetze der Erhaltung von Masse, Impuls und Energie angewandt, um mittels Differentialgleichungen die Fließ- und Transportprozesse in Raum und Zeit zu beschreiben (Lees 2000, Abbott et al. 2001). Es werden Grundwasserströmung, Strömung in der ungesättigten Bodenzone sowie Oberflächenströmung betrachtet, die durch nichtlineare Diffusionsgleichungen beschrieben und mithilfe von Austauschflüssen gekoppelt werden. Die Kompartimente setzen sich entsprechend den hydrologischen Bedingungen aus Subgebieten zusammen (Abb. 2). Den Strömungsvorgängen lassen sich jeweilig Wärme- und Stofftransportprozesse zuordnen, die durch Advektions-Diffusions-Gleichungen beschrieben und mittels Quell-/Senkentermen gekoppelt werden. Die Transportgleichungen werden entweder deterministisch mit finiten Elementen oder stochastisch mittels RWPT gelöst.

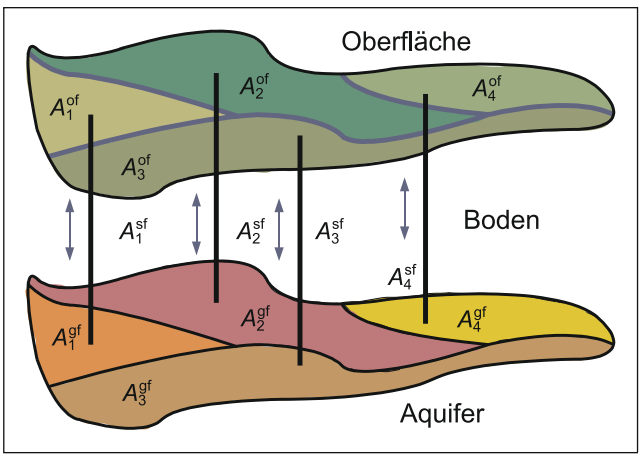

Abb. 2 Einzugsgebiet bestehend aus Oberflächen-, Boden,- und Aquiferkompartimenten. Oberflächen- und Bodenkompartimente werden in Subgebiete unterteilt und jeweils Bodensäulen zugewiesen. Der Wasseraustausch erfolgt durch Kopplungsflüsse über die gemeinsamen horizontalen Grenzflächen $A_i^{of} = A_i^{gf} = A_i^{sf}$ für $i = 1, \ldots, 4$

Hydraulik

Die Grundwasserströmung wird durch eine Massenbilanzgleichung beschrieben, in welcher der spezifische Durchfluss nach dem Gesetz von Darcy enthalten ist. Die folgende Gleichung ist gültig für laminare Fließvorgänge in starren porösen Medien (Bear 1988):

$$[1] \quad \phi S_0 \frac{\partial h^{gf}}{\partial t} + \nabla \cdot \mathrm{q}^{gf} = q_s^{gf},$$

wobei h^{gf} als Druckhöhe die Primärvariable der Grundwasserströmungsgleichung darstellt, φ die Porosität des Aquifers, S_0 der Speicherkoeffizient, der die Matrix des porösen Mediums sowie die Kompression des Liquids berücksichtigt, ∇ der dreidimensionale Nabla-Operator und q_s^{gf} ein Quellen-/Senkenterm ist. Der spezifische Grundwasserfluss q^{gf} ergibt sich aus dem Gesetz von Darcy (1856) zu

$$[2] \quad \mathrm{q}^{gf} = -K \nabla h^{gf},$$

wobei K die hydraulische Leitfähigkeit des Aquifers darstellt.

Zur Beschreibung von Fließvorgängen in der ungesättigten Zone wird das Modell von Richards (1931) verwendet. Es berücksichtigt die Strömung der wässrigen Phase bei konstantem Gasdruck und nutzt eine verallgemeinerte Form der zuvor beschriebenen Darcy-Gleichung (Gl. 2) für die Grundwasserströmung. Das Richards-Modell beruht auf empirisch ermittelten Relationen zwischen Kapillardruck und Wassersättigung sowie relativer Durchlässigkeit und Sättigung. Die Druck-basierte Richards-Gleichung ergibt sich für ein starres poröses Medium somit zu (Warrick 2003):

$$[3] \quad \phi \frac{\partial S}{\partial t} + \nabla \cdot \mathrm{q}^{sf} = q_s^{sf},$$

wobei φ die Porosität, S die Wassersättigung des Bodens und q_s^{sf} ein Quellen-/Senkenterm ist. Der spezifische Durchfluss q^{sf} ergibt sich aus Bear (1988):

$$[4] \quad \mathrm{q}^{sf} = -k_r K \nabla \left(h^{sf} - z \right),$$

wobei h^{sf} als Druckhöhe des Bodenwassers die Primärvariable der Gleichung für Strömung in der ungesättigten Zone darstellt, k_r die relative Durchlässigkeit, K die hydraulische

Leitfähigkeit des gesättigten Bodens. Materialabhängige Beziehungen zwischen Druckhöhe und Sättigung h^{sf} (S) sowie relativer Durchlässigkeit und Sättigung k_r (S) sind erforderlich, um die Massenbilanzgleichung (Gl. 3) zu lösen. Die funktionalen Beziehungen nach van Genuchten (1980) werden hierzu verwendet. Mit der effektiven Sättigung

$$[5] \quad S_e = \max\left(0, \frac{S - S_r}{1 - S_r}\right),$$

wobei S_r die residuale Sättigung darstellt, ergeben sich die empirischen Funktionen für die Kapillardruckhöhe h_{cap} und die relative Durchlässigkeit zu

$$[6] \quad h_{cap} = -h^{sf} = \frac{1}{\alpha}\left(S_e^{1/m} - 1\right)^{1-m},$$

$$[7] \quad k_r(S) = S_e^{1/2}\left[1 - \left(1 - S_e^{1/m}\right)^m\right]^2,$$

wobei α und m Materialeigenschaften des Bodens sind.

Die Simulation des Oberflächenabflusses erfolgt durch die diffusive Wellenapproximation der Saint-Venant-Gleichungen. Die Saint-Vernant-Gleichungen werden durch Integration der Navier-Stokes-Gleichungen unter der Annahme einer hydrostatischen Druckverteilung, geringen Änderungen der Morphologie und empirischen Fließformeln hergeleitet (Vreugdenhil 1994, Gerbeau & Perthame 2001). Bei den Saint-Venant-Gleichungen handelt es sich um ein hyperbolisches Gleichungssystem, das auch für extreme Bedingungen wie z. B. Dammdurchbrüche verwendet werden kann (LeVeque 2002). Die diffusive Wellenapproximation ist dagegen parabolisch und wird unter Vernachlässigung des Advektionstermes aus den Saint-Venant-Gleichungen hergeleitet. Sie lässt sich sehr zuverlässig zur Simulation von Oberflächenabflüssen und Flutwellen in Flüssen anwenden. Kriterien zur Anwendbarkeit dieser Gleichung sowie der kinematischen Wellengleichung sind beispielsweise in Ponce et al. (1978) und Singh (1994) angegeben. Die diffusive Wellengleichung ergibt sich zu

$$[8] \quad \phi^{of}\frac{\partial h^{of}}{\partial t} + \overline{\nabla}\cdot\left(H\mathrm{q}^{of}\right) = q_s^{of},$$

wobei h^{of} als Druckhöhe die Primärvariable des Oberflächenabflusses darstellt, $H = \max(h^{of} - a - b, 0)$ die Tiefe des beweglichen Oberflächenwassers, a eine Schichtdicke, b die geodätische Höhe, $\overline{\nabla}$ der zweidimensionale horizontale Nabla-Operator und q_s^{of} ein Quellen-/Senkenterm ist. Mit der Oberflächenporosität φ^{of} und der Schichtdicke a lassen sich Oberflächenstrukturen beschreiben (Therrien et al. 2004). Die Oberflächenporosität φ^{of} liegt zwischen 0 für trockene und 1 für vollständig gesättigte Zwischenschichten. Die Verwendung der empirischen Fließformeln ergibt den spezifischen Oberflächenfluss q^{of}, der bei Vernachlässigung von Scherkräften durch Sohlformen die Form (Vander-Kwaak 1999)

$$[9] \quad \mathrm{q}^{of} = -\frac{C_r H^l}{S_s^{1-k}}\overline{\nabla}h^{of}$$

hat, wobei C_r, k und l Oberflächenreibungsbeiwerte sind und der Betrag des Druckhöhengradienten S_s durch

$$[10] \quad S_s = \left[\left(\frac{\partial h^{of}}{\partial x}\right)^2 + \left(\frac{\partial h^{of}}{\partial y}\right)^2\right]^{1/2}$$

gegeben ist. Bei Verwendung der Fließformel nach Manning-Strickler (Manning 1891) ist $k = 1/2, l = 2/3$ und $C_r = 1/n$, wobei n der Manning-Beiwert ist. Die Darcy-Weisbach-Formel (Weisbach 1845) für laminare Strömungen führt zu $k = 1$ und $l = 2$. Für die eindimensionale Beschreibung von Flüssen wird Gleichung 9 zu (Julien 2002)

$$[11] \quad \mathrm{q}^{of} = -\frac{C_r R^l}{|\partial h^{of}/\partial x|^{1-k}}\frac{\partial h^{of}}{\partial x},$$

wobei $R = A_F/P$ den hydraulischen Radius, A_F den Flussquerschnitt und P den benetzten Umfang darstellen.

Die Gleichungen 1 und 3 für Strömung im Boden werden mit Galerkin-Finite-Elemente-Methoden räumlich diskretisiert. Die räumliche Diskretisierung von Gleichung 8 für den Oberflächenabfluss erfolgt durch das Kontroll-Volumen-Finite-Elemente-Verfahren (Forsyth et al. 1995).

Transport

Beim Transport gelöster Stoffe in der wässrigen Phase können je nach Problemstellung eine Reihe physikalischer Prozesse wirksam werden. Neben Quellen und Senken sowie der reinen Advektion (der konvektiven Verschleppung eines Stoffes durch ein Strömungsfeld) müssen in aller Regel auch molekulare Diffusion (Brownsche Molekularbewegung) sowie mechanische Dispersion (Verbreiterung der Konzentrationsfront aufgrund unterschiedlicher Wege im porösen Medium) berücksichtigt werden. Darüber hinaus können auch Adsorption eines Stoffes am Porengerüst, Lösung und Fällung von Matrixbestandteilen in und aus der Flüssigkeit, sowie Zerfall bzw. Abbau des Stoffes wichtig sein. Zudem kann es zur Rückkopplung auf das Strömungsfeld kommen, wenn die Konzentration des gelösten Stoffes die Dichte des Wassers merklich ändert. Es werden exponentielle Zerfallsreaktionen sowie sofortige, lineare, reversible Adsorption betrachtet. Der Stofftransport im Aquifer ist gegeben durch (Bear 1988):

$$[12] \quad R_d\phi\frac{\partial c_{st}^{gf}}{\partial t} + \mathrm{q}^{gf}\cdot\nabla c_{st}^{gf} - \nabla\cdot\left(\phi\kappa_{st}^{gf}\nabla c_{st}^{gf}\right) + R_d\phi k_\lambda c_{st}^{gf} = q_{s\,st}^{gf},$$

wobei $c_{\mathrm{st}}^{\mathrm{gf}}$ als Stoffkonzentration die Primärvariable der Gleichung für Stofftransport im Aquifer darstellt, k_λ eine Zerfallsrate und $q_s{}^{\mathrm{gf}}{}_{\mathrm{st}}$ ein Quellen-/Senkenterm ist. Der Retardationsfaktor R_d dient zur Beschreibung der Adsorption. Die Diffusivität gelöster Stoffe $\kappa_{\mathrm{st}}^{\mathrm{gf}}$ ergibt sich aus

$$[13]\quad \kappa_{\mathrm{st}\,ij}^{\mathrm{gf}} = \lambda_{\mathrm{st}}\tau_{ij} + D_{ij}^{\mathrm{gf}},$$
$$D_{ij}^{\mathrm{gf}} = \delta_{ij}\alpha_T\,|\,\mathrm{q}^{\mathrm{gf}}\,| + (\alpha_L - \alpha_T)\frac{q_i^{\mathrm{gf}} q_j^{\mathrm{gf}}}{|\,\mathrm{q}^{\mathrm{gf}}\,|},$$

wobei λ_{st} der molekulare Diffusionskoeffizient gelöster Stoffe, τ die Tortuosität, D^{gf} der Dispersionstensor und α_T und α_L die transversalen und longitudinalen Dispersivitäten sind. Der Stofftransport in der ungesättigten Bodenzone ergibt sich aus (Bear 1988):

$$[14]\quad R_d\phi\frac{\partial S c_{\mathrm{st}}^{\mathrm{sf}}}{\partial t} + \mathrm{q}^{\mathrm{sf}}\cdot\nabla c_{\mathrm{st}}^{\mathrm{sf}} - \nabla\cdot\left(\phi S\kappa_{\mathrm{st}}^{\mathrm{sf}}\nabla c_{\mathrm{st}}^{\mathrm{sf}}\right) + R_d\phi S k_\lambda c_{\mathrm{st}}^{\mathrm{sf}} = q_s{}^{\mathrm{sf}}{}_{\mathrm{st}},$$

wobei $c_{\mathrm{st}}^{\mathrm{sf}}$ als Stoffkonzentration in der wässrigen Phase die Primärvariable der Gleichung für Stofftransport in der ungesättigten Bodenzone darstellt und $q_s{}^{\mathrm{sf}}{}_{\mathrm{st}}$ ein Quellen-/Senkenterm ist. Die Diffusivität $\kappa_{\mathrm{st}}^{\mathrm{sf}}$ und der Dispersionstensor D^{sf} zur Beschreibung der molekularen Diffusion und mechanischen Dispersion in der wässrigen Phase sind durch

$$[15]\quad \kappa_{\mathrm{st}\,ij}^{\mathrm{sf}} = \lambda_{\mathrm{st}}\tau_{ij} + D_{ij}^{\mathrm{sf}},$$
$$D_{ij}^{\mathrm{sf}} = \delta_{ij}\alpha_T\,|\,\mathrm{q}^{\mathrm{sf}}\,| + (\alpha_L - \alpha_T)\frac{q_i^{\mathrm{sf}} q_j^{\mathrm{sf}}}{|\,\mathrm{q}^{\mathrm{sf}}\,|}$$

gegeben. Der Stofftransport in der Oberflächenströmung ergibt sich aus (VanderKwaak 1999)

$$[16]\quad \frac{\partial\phi^{\mathrm{of}} H c_{\mathrm{st}}^{\mathrm{of}}}{\partial t} + \phi^{\mathrm{of}} H\mathrm{q}^{\mathrm{of}}\cdot\nabla c_{\mathrm{st}}^{\mathrm{of}} - \nabla\cdot\left(\phi^{\mathrm{of}} H\kappa_{ij}^{\mathrm{of}}\nabla c_{\mathrm{st}}^{\mathrm{of}}\right) + \phi^{\mathrm{of}} H k_\lambda c_{\mathrm{st}}^{\mathrm{of}} = \phi^{\mathrm{of}} H q_s{}^{\mathrm{of}}{}_{\mathrm{st}},$$

wobei $c_{\mathrm{st}}^{\mathrm{of}}$ als Stoffkonzentration die Primärvariable der Gleichung für Stofftransport in der Oberflächenströmung darstellt und $q_s{}^{\mathrm{of}}{}_{\mathrm{st}}$ ein Quellen-/Senkenterm ist. Molekulare und turbulente Diffusion werden durch die Diffusivität $\kappa_{\mathrm{st}}^{\mathrm{of}}$ und den Dispersionstensor D^{of} beschrieben:

$$[17]\quad \kappa_{\mathrm{st}\,ij}^{\mathrm{of}} = \lambda_{\mathrm{st}} + D_{ij}^{\mathrm{of}},$$
$$D_{ij}^{\mathrm{of}} = \delta_{ij}\alpha_T\,|\,\mathrm{q}^{\mathrm{of}}\,| + (\alpha_L - \alpha_T)\frac{q_i^{\mathrm{of}} q_j^{\mathrm{of}}}{|\,\mathrm{q}^{\mathrm{of}}\,|}.$$

Auch beim Wärmetransport sind Diffusion, Advektion, sowie Quellen und Senken wichtige physikalische Prozesse. Ein wesentlicher Unterschied zum Stofftransport ist, dass der thermische Diffusionskoeffizient ungefähr drei Größenordnungen größer ist als die molekulare Diffusionskonstante. Der Beitrag der Dispersion in Boden und Aquifer ist dagegen meist vernachlässigbar klein. Im Allgemeinen tritt auch erhebliche Wärmeleitung in der Matrix auf. Wir beschränken uns in dieser Arbeit auf den Wärmetransport in Boden und Aquifer. Die Gleichung zur Beschreibung des Wärmetransports im Aquifer stellt sich folgendermaßen dar (Bear 1988):

$$[18]\quad \frac{\partial C^{\mathrm{gf}} T^{\mathrm{gf}}}{\partial t} + c^f\rho^f\mathrm{q}^{\mathrm{gf}}\cdot\nabla T^{\mathrm{gf}} - \nabla\cdot\left(\kappa_{\mathrm{ht}}\nabla T^{\mathrm{gf}}\right) = q_s{}^{\mathrm{gf}}{}_{\mathrm{ht}},$$

wobei T^{gf} als Temperatur die Primärvariable für Wärmetransport im Aquifer darstellt. Das hochgestellte *f* bezeichnet die wässrige Phase, *s* die Feststoffphase, κ^{ht} die thermische Diffusivität und $q_s{}^{\mathrm{gf}}{}_{\mathrm{ht}}$ eine Wärmequelle/-senke. Die Wärmekapazität C^{gf} ergibt sich aus

$$[19]\quad C^{\mathrm{gf}} = \phi c^f\rho^f + (1-\phi)c^s\rho^s,$$

wobei c spezifische Wärmekapazitäten und ρ Massendichten sind. Die thermische Diffusivität $\kappa_{\mathrm{ht}}^{\mathrm{gf}}$ ist gegeben durch:

$$[20]\quad \kappa_{\mathrm{ht}\,ij}^{\mathrm{gf}} = \lambda_{\mathrm{ht}}^{\mathrm{gf}}\tau_{ij} + c^f\rho^f D_{ij}^{\mathrm{gf}},$$
$$\lambda_{\mathrm{ht}}^{\mathrm{gf}} = \phi\lambda_{\mathrm{ht}}^f + (1-\phi)\lambda_{\mathrm{ht}}^s,$$

wobei $\lambda_{\mathrm{ht}}{}^{\mathrm{gf}}$ der molekulare Diffusionskoeffizient für den Wärmetransport im Aquifer und der Dispersionstensor D^{gf} in den Gleichungen 13 gegeben sind. Wärmetransport in der ungesättigten Bodenzone ist gegeben durch (Bear 1988):

$$[21]\quad \frac{\partial C^{\mathrm{sf}} T^{\mathrm{sf}}}{\partial t} + c^f\rho^f\mathrm{q}^{\mathrm{sf}}\cdot\nabla T^{\mathrm{sf}} - \nabla\cdot\left(\kappa_{\mathrm{ht}}^{\mathrm{sf}}\nabla T^{\mathrm{sf}}\right) = q_s{}^{\mathrm{sf}}{}_{\mathrm{ht}},$$

wobei T^{gf} als Temperatur die Primärvariable für Wärmetransport im Boden und $q_s{}^{\mathrm{sf}}{}_{\mathrm{ht}}$ eine Wärmequelle/-senke darstellt. Die Wärmekapazität C^{sf} ergibt sich aus

$$[22]\quad C^{\mathrm{sf}} = \phi(Sc^f\rho^f + (1-S)c^g\rho^g) + (1-\phi^{\mathrm{sf}})c^s\rho^s,$$

wobei sich das hochgestellte *g* auf die Gasphase bezieht. Die thermische Diffusivität $\kappa_{\mathrm{ht}}^{\mathrm{sf}}$ und der molekulare Diffusionskoeffizientist $\lambda_{\mathrm{ht}}^{\mathrm{sf}}$ sind gegeben durch:

$$[23]\quad \kappa_{\mathrm{ht}\,ij}^{\mathrm{sf}} = \lambda_{\mathrm{ht}}^{\mathrm{sf}}\tau_{ij} + c^f\rho^f D_{ij}^{\mathrm{sf}},$$
$$\lambda_{\mathrm{ht}}^{\mathrm{sf}} = \phi(S\lambda_{\mathrm{ht}}^f + (1-S)\lambda_{\mathrm{ht}}^g) + (1-\phi)\lambda_{\mathrm{ht}}^s,$$

wobei sich der Dispersionstensor D^{sf} in den Gleichungen 15 findet.

Die Gleichungen 12, 14 und 16 für den Stofftransport sowie 18 und 21 für den Wärmetransport werden entweder mittels der Galerkin-Finite-Elemente-Methode räumlich diskretisiert oder es wird die RWPT-Methode nach Hoteit et al. (2002) angewandt. Bei der RWPT-Methode wird die Position × jedes Partikels im neuen Zeitschritt jeweils für die Komponenten $i \le d$ durch (Kinzelbach 1987)

$$[24]\quad x_i(t+\Delta t) = x_i(t) + \left(q_i^*(\mathrm{x}) + \sum_{j=1}^{d}\frac{\partial\kappa_{ij}^{\mathrm{st}}}{\partial x_j}\right)\Delta t + \sum_{j=1}^{d}\sqrt{2\kappa_{ij}^{\mathrm{st}}\Delta t}\,Z_j$$

bestimmt, wobei Δt die Zeitschrittweite, d = 2, 3 die Dimension und Z_i die Zufallsvariablen mit einem Mittelwert von 0 und einer Varianz von 1 sind. Die spezifischen Flüsse q* in Aquifer, Boden und in der Oberflächenströmung sind gegeben durch die Gleichungen 2, 4 und 9. Ausgehend von der Druckverteilung wird die Geschwindigkeitsverteilung an den Knotenpunkten mittels finiter Elemente berechnet (Park et al. 2008b).

Kopplung

Zur Beschreibung eines Austauschflusses an den Kompartimentgrenzen wird eine Grenzschicht definiert (Abb. 3). Die Austauschflüsse zur Kopplung von Oberflächenabfluss und Strömung in der ungesättigten Zone ergeben sich aus (VanderKwaak 1999)

$$[25]\quad q_{\mathrm{of}}^{\mathrm{sf}} = k_{a'}\Lambda\left(h^{\mathrm{of}} - h^{\mathrm{sf}}\right),\quad \Lambda = \frac{K^c}{a'},\quad q_{\mathrm{sf}}^{\mathrm{of}} = -q_{\mathrm{of}}^{\mathrm{sf}},$$

wobei Λ der Leakage-Faktor, K^c die Leitfähigkeit der Grenzschicht und a' die Dicke der Grenzschicht ist. $0 \le k_{a'}(h^{\mathrm{of}}) \le 1$ ist ein Skalierungsfaktor, welcher sicherstellt, dass die Infiltration die zur Verfügung stehende Menge an Oberflächenwasser nicht übersteigt. Der Skalierungsfaktor $k_{a'}$ liegt zwischen 0 für trockene und 1 für vollständig gesättigte Grenzschichten. Die Austauschflüsse zur Kopplung von Flüssen mit dem Grundwasser sind gegeben durch (Gunduz & Aral 2005):

$$[26]\quad q_{\mathrm{of}}^{\mathrm{gf}} = \frac{P}{B}\Lambda\left(h^{\mathrm{of}} - h^{\mathrm{gf}}\right),\quad q_{\mathrm{gf}}^{\mathrm{of}} = -q_{\mathrm{of}}^{\mathrm{gf}},$$

wobei B die Flussbreite darstellt. Liegt der Grundwasserspiegel unterhalb des Flussbettes berechnen sich die Austauschflüsse aus

$$[27]\quad q_{\mathrm{of}}^{\mathrm{gf}^*} = \Lambda H,\quad q_{\mathrm{gf}}^{\mathrm{of}^*} = -q_{\mathrm{of}}^{\mathrm{gf}^*}.$$

Die Kopplungsflüsse (Gl. 25, 26 und 27) stellen Quellen-/Senkenterme in den Gleichungen für Grundwasserströmung (Gl. 1), für Strömung in der ungesättigten Zone (Gl. 3) und für Oberflächenabfluss (Gl. 8) dar. Alternative Kopplungsansätze beinhalten eine Druckrandbedingung (z. B. Morita & Yen 2002, Dawson 2006, Kollet & Maxwell 2006). Zeitskalendifferenzen angrenzender Strömungsprozesse lassen sich durch Unterzeitschritte nach dem Verfahren von Bhallamudi et al. (2003) berücksichtigen. Zeitschrittweiten lassen sich mittels einer adaptiven Zeitschritt-Kontrolle bestimmen (Du & Kolditz 2005). Gekoppelte Strömungsprozesse werden durchweg mittels implizitem Eulerverfahren zeitlich diskretisiert.

Zur Kopplung von Transportprozessen wird gemäß Therrien et al. (2004) ausschließlich advektiver Austausch berücksichtigt. Diffusiver Austausch wird beispielsweise in Richards & Parr (1988), Wallach et al. (1989), Govindaraju (1996) und VanderKwaak (1999) betrachtet. Bei der Verwendung von finiten Elementen zur räumlichen Diskretisierung der Transportgleichungen wird ein spezifischer Austauschfluss berechnet. Die Austauschflüsse für die Kopplung von Stofftransport zwischen Oberflächenströmung und Strömung in der ungesättigten Zone ergeben sich zu

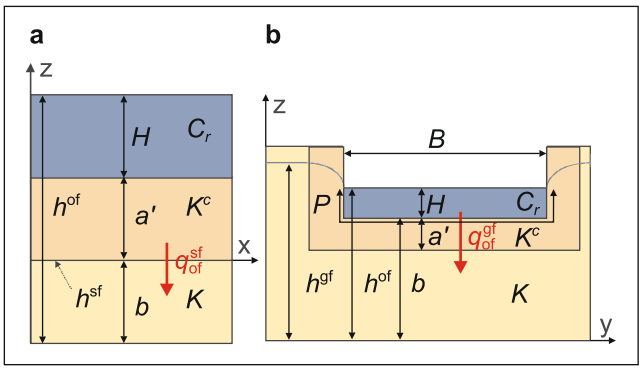

Abb. 3 Austauschflüsse zwischen (a) Oberflächenströmung und Boden, (b) Fluss und Aquifer. Grenzschicht (mit der Leitfähigkeit K^c) zwischen Oberflächenströmung (mit dem Reibungskoeffizienten C_r) und Boden bzw. Aquifer (Leitfähigkeit K) zur Berechnung der Kopplungsflüsse $q_{\mathrm{of}}^{\mathrm{st}}$, $q_{\mathrm{of}}^{\mathrm{gf}}$ über die Differenzen der Druckhöhen (Gl. 25 und 26)

$$[28]\quad q_{\mathrm{of\,st}}^{\mathrm{sf}} = q_{\mathrm{of}}^{\mathrm{sf}}\frac{c_{\mathrm{st}}^{\mathrm{of}} - c_{\mathrm{st}}^{\mathrm{sf}}}{a'},\quad q_{\mathrm{sf\,st}}^{\mathrm{of}} = -q_{\mathrm{of\,st}}^{\mathrm{sf}},$$

wobei $q_{\mathrm{of}}^{\mathrm{sf}}$ aus Gleichung 25 resultiert. Bei der Verwendung stochastischer Partikel ergibt sich die Wahrscheinlichkeit, dass ein Partikel zu einem angrenzenden Strömungsprozess überspringt, aus dem Verhältnis von Wassergehalt und Austauschfluss. Für das Beispiel der Infiltration ergibt sich die Wahrscheinlichkeit, dass ein Partikel aus dem Oberflächenwasser in die ungesättigte Zone eintritt, aus $q_{\mathrm{of}}^{\mathrm{sf}}\,\Delta t/H$ für $a = 0$.

Implementierung

Das Kompartiment-Konzept für die Modellierung von gekoppelten Hydrosystemen (Oberflächen-Boden-Grundwasser) wurde im Kontext des objekt-orientierten Programmsystems GeoSys/RockFlow implementiert (Kolditz & Bauer 2004, Wang & Kolditz 2007, Park et al. 2008a). GeoSys ist eine wissenschaftliche Open-Source-Software, deren Entwicklung über eine internetbasierte Wikipedia-Subversion-Plattform erfolgt. Für den Zugriff auf die Entwicklungsplattform GeoSys/Trac ist ein Browser-Zertifikat auf der Basis der Open-Source-Regeln erforderlich. Die in dieser Publikation präsentierten Anwendungen sind Bestandteil der GeoSys-Benchmarksammlung (Kolditz & Shao 2009).

Modellanwendungen

Wir stellen in dieser Arbeit drei Beispiele vor, welche die Anwendbarkeit des Modellkonzepts zur Analyse von gekoppelten Hydrosystemen einschließlich Wärme- und Stofftransport zeigen. Die Kopplung von Oberflächenströmung mit der ungesättigten Bodenzone wird mit den Laborversuchen von Smith & Woolhiser (1971) für Hortonschen Oberflächenabfluss (Abluss durch Infiltrationsüberschuss) untersucht. Dunnescher Oberflächenabfluss (Sättigungsflächenabfluss) mit Stofftransport wird mit den Laborversuchen von Abdul & Gilham (1984) simuliert. Im letzten Beispiel werden hyporheische Fließvorgänge im Flussbett der Lahn mittels Temperatursignaturen in den Flusssedimenten identifiziert.

In der vorliegenden Arbeit konzentrieren wir uns auf kleinskalige Modellanwendungen (d. h. Auswertung von Laborexperimenten). Die Übertragbarbeit des Kompartiment-Konzepts auf größere Maßstäbe wurde z. B. von Kolditz et al. (2008) für den Bordenaquifer (Abdul & Gilham 1989) demonstriert. Eine weitere Anwendung des Kompartiment-Konzepts ist in Delfs et al. (2008) zu finden, worin ein großräumiges Fluss-Aquifer-System (Gunduz & Aral 2005) modelliert wird. Auf die Limitationen dieses Konzept-Modells gehen wir im Ausblick am Ende der Arbeit näher ein.

Laborversuche von Smith & Woolhiser (1971)

Die klassischen Versuche von Smith & Woolhiser (1971) wurden bereits in mehreren Arbeiten zur Untersuchung der Kopplung des Oberflächenabflusses mit der ungesättigten Zone und zum Test numerischer Modelle verwendet (Smith & Woolhiser 1971, Akan & Yen 1981, Govindaraju & Kavvas 1991, Singh & Bhallamudi 1998, Morita & Yen 2002, Thoms 2003, Delfs et al. 2009). Smith & Woolhiser (1971) führten Infiltrationsversuche in einer mit Bodenmaterial gefüllten Rinne mit einer Länge von 12,2 m, einer Breite von 5,1 cm und einem Gefälle von 0,01 durch (Abb. 4). Oberflächenabfluss durch Infiltrationsüberschuss (Hortonscher Abfluss) wurde durch 15-minütige Beregnung mit einer Intensität von 25,2 cm/min erzeugt, was etwa dem zwei- bis dreifachen der Leitfähigkeit des gesättigten Bodens entspricht. Zur Verhinderung von Algenwachstum im Boden wurde ein Leichtöl an Stelle von Wasser benutzt, dessen Viskosität etwa dem zweifachen der Viskosität von Wasser entspricht. Da der Wasserspiegel etwa einen Meter unterhalb der Oberfläche lag, wurde angenommen, dass der Kapillarsaum keinen Einfluss auf den Infiltrationsprozess hat. Das Bodenmaterial bestand aus lokal gewonnenem fluviatilem Sand. Messungen der Schüttdichte an vier Stellen in der Rinne zeigten eine ausgeprägte horizontale und vertikale Heterogenität. Die Dichte nahm mit der Tiefe zu. Charakteristische Boden-Wasser-Beziehungen, wie z. B. die Abhängigkeit des Kapillardrucks und der relativen Durchlässigkeit vom Wassergehalt, wurden für verschiedene Dichten aufgestellt. Parameter der Oberflächenreibung wurden für Wasserstände höher als 4 mm ermittelt.

Simulierte und gemessene Abflussganglinien am Auslass der Rinne bei drainierten Anfangsbedingungen sind in Abbildung 5 dargestellt. Die Initialisierung des Oberflächenabflusses beginnt nach etwa 7 Minuten. Die begrenzte Länge der Rinne bewirkt eine Abflachung der Abflussganglinie nach etwa 10 Minuten. Die Ganglinie kann in drei Phasen eingeteilt werden: (I) Initialisierung des Oberflächenabflusses, (II) steiler Anstieg der Ganglinie und (III) Abflachung der Ganglinie. Da laterale Fließvorgänge bedingt durch Heterogenitäten des Bodens vernachlässigbar waren, wählten wir die einfachste geometrische Darstellung des Experiments in Form einer Kopplung von zwei 1D-Modellen für Oberflächenabfluss und ungesättigte Zone. Die ungesättigte Zone wird durch eine Reihe von Bodensäulen dargestellt (Abb. 4). Tabelle 1 zeigt die Parameter, die zur Simulation

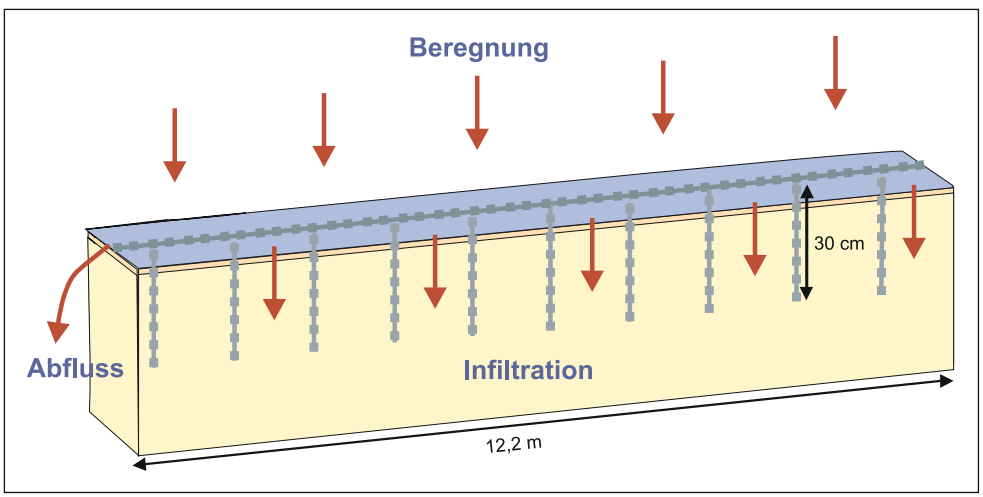

Abb. 4 Aufbau, Prozesse und Diskretisierungsgitter der Laborversuche von Smith & Woolhiser (1971) zum Hortonschen Oberflächenabfluss

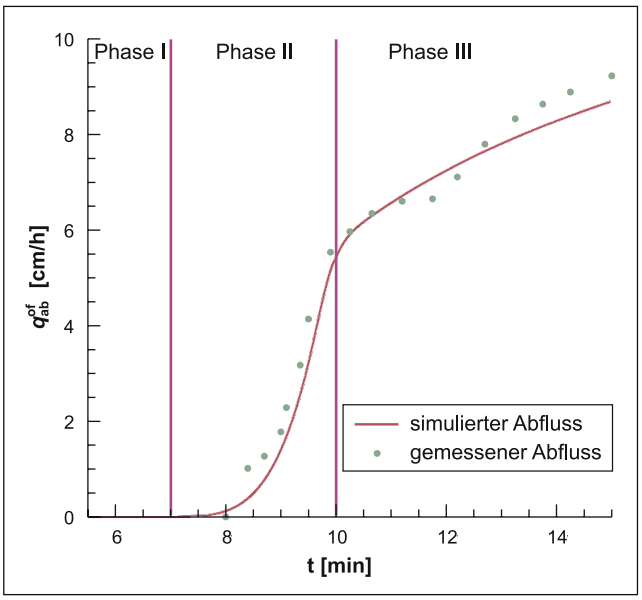

Abb. 5 Vergleich von gemessenen und simulierten Abflussganglinien zu den Laborversuchen von Smith & Woolhiser (1971). Der Abfluss q_{ab}^{of} ist gegeben durch $q_{ab}^{of} = Q_{krit}^{of}/A$, wobei $Q_{krit}^{of} = \sqrt{gH^3}B$ den kritischen Abfluss (Julien 2002), B die Rinnenbreite und A die Rinnenoberfläche bezeichnen

Tabelle 1 Eigenschaften des gekoppelten Oberflächen-Boden-Hydrosystems zur Simulation der Laborversuche von Smith & Woolhiser (1971)

Parameter	Symbol	Wert	Einheit
Oberflächenkompartiment			
Reibungsbeiwert	C_r	$4{,}8 \cdot 10^7$	1/cmh
Dicke der Oberflächenstrukturschicht	a	0,1	cm
Bodenkompartiment			
Porosität	φ	0,42	–
Residuale Sättigung	S_r	0,053	–
Hydraulische Leitfähigkeit	K	4,08	cm/h
Van Genuchten-Parameter	α	6	1/m
Van Genuchten-Parameter	m	0,75	–
Kopplungsgrenzschicht			
Leitfähigkeit	K^c	4,08	cm/h
Dicke	a'	0,1	cm

des Smith & Woolhiser-Experiments verwendet wurden. Die Darcy-Weisbach-Formel für laminare Strömungen wird für die Oberflächenreibung verwendet.

Der Einfluss von Reibungsprozessen, Bodenkapillarität und hydraulischer Grenzschicht auf den Kopplungs- sowie Oberflächenabfluss am Auslass der Rinne wurde untersucht. Dazu wurden logarithmische Sensitivitäten $\frac{P_i}{O}\frac{\Delta O}{\Delta P_i}$ berechnet, wobei O die Ausgabefunktion und P_i die dazugehörigen Modellparameter sind. Damit lässt sich die relative Änderung der Ausgabefunktion dO/O gemäß

$$[29] \quad \frac{dO}{O} = \sum_i \left(\frac{P_i}{O}\frac{\partial O}{\partial P_i} \right) \frac{dP_i}{P_i}$$

aus den Störungen (pertubations) der Parameter dP_i/P_i in erster Ordnung ermitteln. Die logarithmischen Sensitivitäten wurden mittels finiter Differenzen berechnet und mit Unsicherheiten, die von Smith & Woolhiser (1971) ermittelt wurden, gewichtet (Tab. 2). Die Parameter werden in den Abbildungen 6 und 7 miteinander verglichen. Für den Parametervergleich bezüglich des Kopplungsflusses wird ein Wert angegeben, der die Phasen II und III repräsentiert, da die logarithmischen Sensitivitäten in diesem Simulationszeitraum nur geringfügig variieren. Für den Oberflächenabfluss (Abb. 7) werden die logarithmischen Sensitivitäten für die Phasen II und III getrennt betrachtet. In der Abbildung 6 sieht man, dass die Bodenparameter (P_1, P_3–P_7) einen deutlich größeren Einfluss auf den Kopplungsfluss O_1 haben als die Parameter der Oberflächenreibung C_r (P_2) und Grenzschicht (P_8–P_{10}). Die Strömungsverhältnisse werden also überwiegend durch die Kapillarität und Reibung im Boden bestimmt. Da die Infiltration in den Boden in diesem Fall nur wenig von der Oberflächenströmung abhängt (Philip 1957), läßt sich der Oberflächenabfluss auch mit einfacheren Ansätzen reproduzieren wie zum Beispiel einer Kopplung der diffusiven Wellenapproximation (Gl. 8) mit dem Model von Green & Ampt (1911). Diese

Tabelle 2 Gewichtungsfaktoren für den Parametervergleich in der Sensitivitätsstudie zu den Laborversuchen von Smith & Woolhiser (1971)

P_i	Parameter	Symbol	Unsicherheit
P_1	Hydraulische Leitfähigkeit des Bodens	$\Delta K/K$	0,4
P_2	Oberflächenreibungskoeffizient	$\Delta C_r/C_r$	1
P_3	Porosität des Bodens	$\Delta\varphi/\varphi$	0,2
P_4	Anfangssättigung des Bodens	$\Delta S(t=0)/S(t=0)$	1
P_5	Residuale Sättigung des Bodens	$\Delta S_r/S_r$	0,1
P_6	Van Genuchten-Parameter	$\Delta\alpha/\alpha$	0,4
P_7	Van Genuchten-Parameter	$\Delta m/m$	0,05
P_8	Dicke der Kopplungsgrenzschicht	$\Delta a'/a'$	1
P_9	Hydraulische Leitfähigkeit der Kopplungsgrenzschicht	$\Delta K^c/K^c$	1
P_{10}	Dicke der Oberflächenstrukturschicht	$\Delta a/a$	1

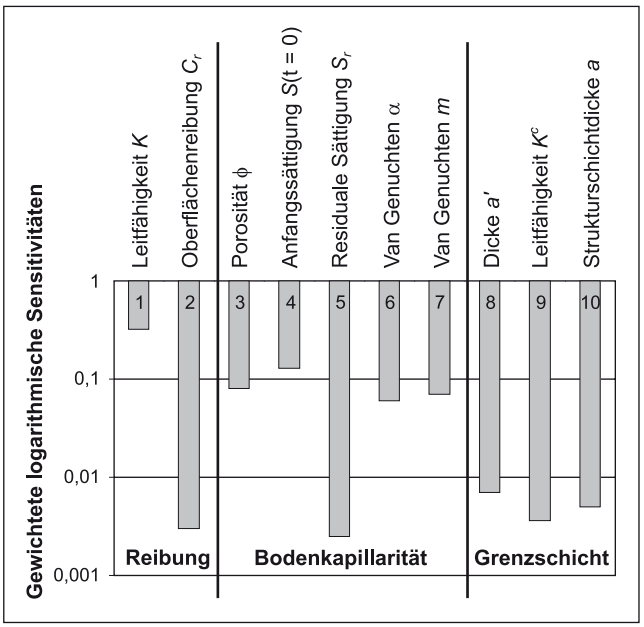

Abb. 6 Bewertung der Parameter für den Kopplungsfluss in den Simulationen der Laborversuche von Smith & Woolhiser (1971). Logarithmische Sensitivitäten (29) werden mit Parameterunsicherheiten (Tab. 2) gewichtet

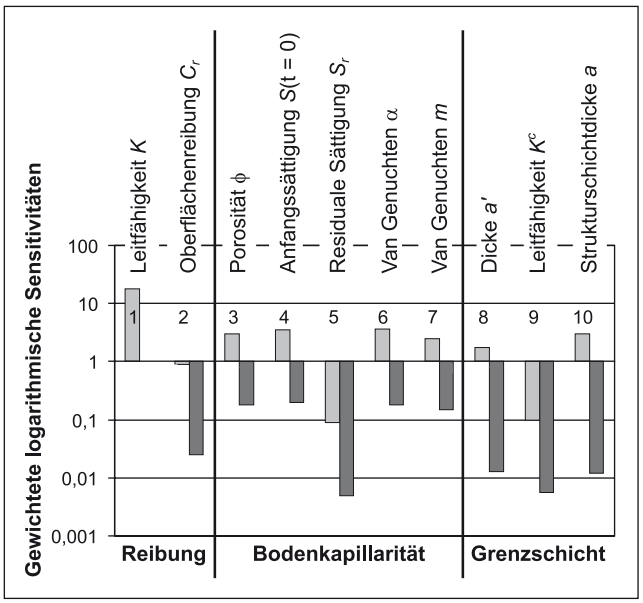

Abb. 7 Bewertung der Parameter für die Oberflächenabflussvorhersage in den Simulationen der Laborversuche von Smith & Woolhiser (1971) für Phase II (helle Balken) und Phase III (dunkle Balken). Logarithmische Sensitivitäten (Gl. 29) werden mit Parameterunsicherheiten (Tab. 2) gewichtet

Modellvereinfachung ist in Delfs et al. (2008) näher erläutert. Oberflächenreibungskoeffizient C_r (P_2), die Dicke der Grenzschicht *a'* (P_8) und die Dicke der Oberflächenstrukturschicht *a* (P_{10}) sind in Phase II als wichtig für den Oberflächenabfluss O_2 anzusehen (Abb. 3 und 7). Danach hat das Wasser vom oberen Rinnenende den Auslass erreicht und der Abfluss wird unabhängig von der Oberflächenbeschaffenheit. In Phase II ist die Sensitivität aller Parameter P_1–P_{10} größer als in Phase III bei abflachender Ganglinie. Den größten Einfluss auf den Kopplungsfluss O_1 sowie den Oberflächenabfluss O_2 hat die hydraulische Leitfähigkeit des Bodens K (P_1). Der Einfluss der zusätzlich eingeführten Grenzschichtparameter in der Berechnung des Kopplungsflusses (Gl. 25) erwies sich als gering.

Laborversuche von Abdul & Gilham (1984)

Ziel der Laborversuche von Abdul & Gilham (1984) war die Untersuchung des Einflusses des Kapillarsaums auf die Abflussbildung. Numerische Simulationen der Versuche wurden von Abdul & Gilham (1984), VanderKwaak (1999) und Kollet & Maxwell (2006) durchgeführt. Ein gleichmäßiger Niederschlag von $q_s^{\mathrm{of}}{}_{nsw} = 4{,}3$ cm/h wurde auf ein Gerinne gefüllt mit Bodenmaterial für 20 min aufgebracht. Die Rinne hatte eine Länge von 1,4 m, eine Breite von 8 cm und ein Gefälle von 0,12 (Abb. 8). Der Grundwasserspiegel lag zu Beginn auf Höhe des Auslasses, sodass unmittelbar Sättigungsflächenabfluss (Dunnescher Abfluss) entstand. Der Niederschlag wurde mit Chlorid mit der Konzentration $c_{nsw}^{\mathrm{of}}{}_{\mathrm{st}} = 60{,}6$ mg/l versetzt, um den Anteil des Niederschlages (Ereigniswassers) und des bereits vor dem Ereignis im Boden gespeicherten Wassers (Vorereigniswassers) im Ausfluss festzustellen. Am Auslass der Rinne wurden Abflussganglinien und Chlorographen aufgezeichnet. Weiterhin wurden die Kapillardruck-Sättigungs-Beziehungen für den verwendeten Sand bestimmt.

Bei der Anwendung des gekoppelten Modells wurde der Oberflächenabfluss in 1D und die Strömung in der ungesättigten Zone in 2D simuliert. Rein advektiver Stofftransport wurde mittels RWPT berechnet. Dazu wurden in jedem Zeitschritt $\Delta t = 1$ s $N_{nsw} = 140$ Partikel gleichmäßig auf der Rinne verteilt. Die Tabelle 3 zeigt die verwendeten Parameter für die Modellierung. Die Darcy-Weisbach-Formel für laminare Strömungen wird für die Oberflächenreibung verwendet. Die relative Durchlässigkeit des Bodens k_r und Bodensättigung S werden mit einem Parameter p durch $k_r = S_e^p$ verknüpft. Zur Illustration des Dunneschen Strömungsprozesses (Infiltration und Exfiltration) veranschaulicht die Abbildung 9 Stromlinien im stationären Zustand durch die berechneten Partikelbahnen in der Übergangszone zwischen Infiltrationsbereich und Sättigungsfläche (die vertikale Dimension ist überhöht dargestellt).

Simulierte und gemessene Abflussganglinien sowie die Chloridkonzentrationen im Abfluss sind in Abbildung 10 für drei hydraulische Leitfähigkeiten des Bodens aufgetragen. Die Ergebnisse zeigen, dass durch den hohen Anfangsgrundwasserspiegel das aus dem Boden exfiltrierende Wasser die

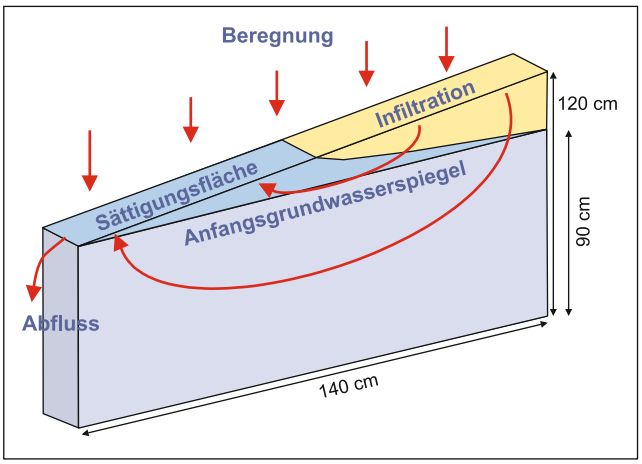

Abb. 8 Aufbau der Laborversuche von Abdul & Gilham (1984) zum Dunneschen Oberflächenabfluss

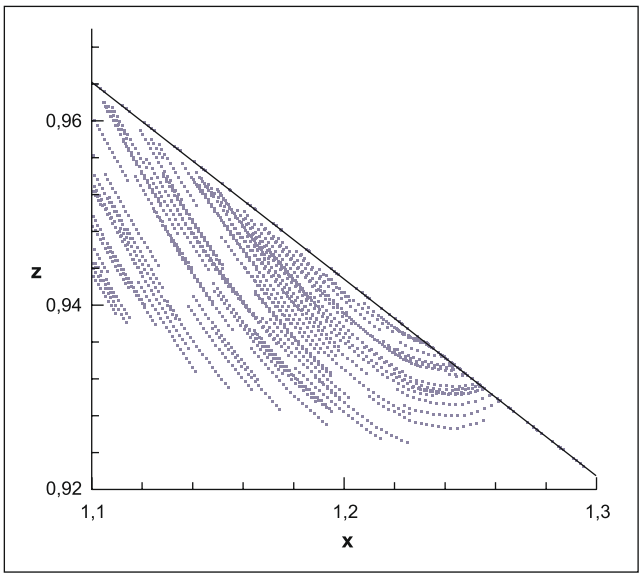

Abb. 9 Simulierte Partikelbahnen zu den Laborversuchen von Abdul & Gilham (1984) im stationären Strömungsfeld

Tabelle 3 Modellparameter zur Simulation der Laborversuche von Abdul & Gilham (1984)

Parameter	Symbol	Wert	Einheit
Oberflächenströmung			
Reibungsbeiwert	C_r	$4{,}8 \cdot 10^7$	1/cmh
Dicke der Oberflächenstrukturschicht	a	0	cm
Bodenströmung			
Porosität	φ	0,34	–
Residuale Sättigung	S_r	0	–
Hydraulische Leitfähigkeit	K	18	cm/h
Van Genuchten-Parameter	α	2,4	1/m
Van Genuchten-Parameter	m	0,8	–
Parameter für Durchlässigkeit-Sättigungs-Beziehung	p	0,8	–
Kopplungsgrenzschicht			
Leitfähigkeit	K^c	18	cm/h
Dicke	a'	0,1	cm

Chloridkonzentrationen im Oberflächenabfluss unmittelbar ‚verdünnt'. Die Grafik beschränkt sich auf die ersten 11 Minuten, danach ist die Strömung stationär. Nach dieser Zeit haben gemessener Abfluss und deren Chloridkonzentration beide den Maximalwert angenommen. Für die von Abdul & Gilham (1984) vorgeschlagene hydraulische Leitfähigkeit von K = 18 cm/h lassen sich diese Maximalwerte mit dem Modell gut reproduzieren. Unterschiede gibt es in der Anfangsphase während des Anstiegs des Oberflächenabflusses (siehe auch VanderKwaak 1999). In den Simulationsergebnissen fallen in dieser Phase die Chloridkonzentrationen ab, während die Messergebnisse einen Anstieg zeigen. Der Versuch, die Infiltration mit einer Erhöhung der Bodenleitfähigkeit zu verstärken, zeigt, dass der Maximalabfluss von diesem Parameter unabhängig ist. Der Chloridanteil im Oberflächenwasser reduziert sich erheblich, d. h. der Anteil

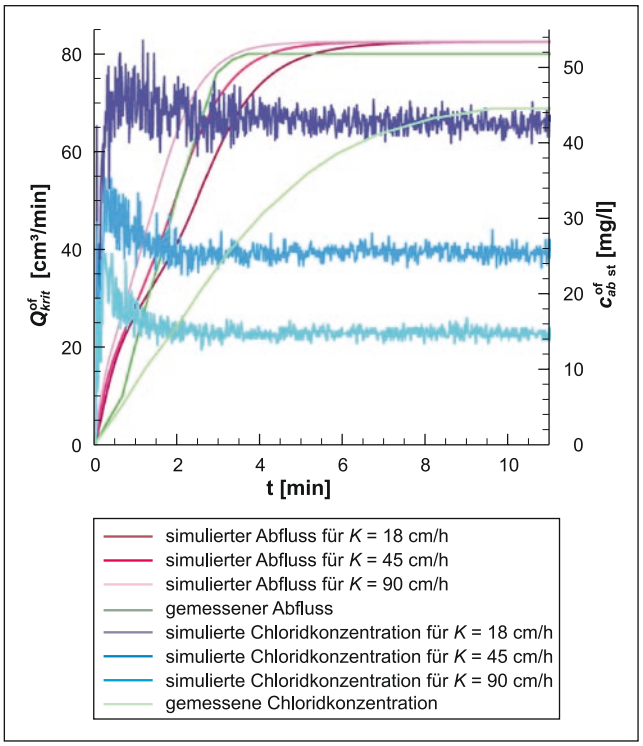

Abb. 10 Vergleich von gemessenen und simulierten Abflussganglinien mit deren Chloridkonzentrationen zu den Laborversuchen von Abdul & Gilham (1984). Aufgetragen ist für die Simulationsergebnisse der kritische Abfluss $Q_{krit}^{of} = \sqrt{gH^3}B$ (Julien 2002) sowie dessen Chloridkonzentration $c_{ab\ st}^{of} = N_{ab}c_{nsw\ st}^{of}q_{nsw}^{of}A/N_{nsw}Q_{krit}^{of}$, wobei N_{ab} die am unteren Rinnenende gezählten Teilchen, A die Rinnenoberfläche und B die Rinnenbreite bezeichnen. Für die hydraulische Leitfähigkeit K des Bodens wurden drei verschiedene Werte angenommen, um deren Einfluss zu zeigen

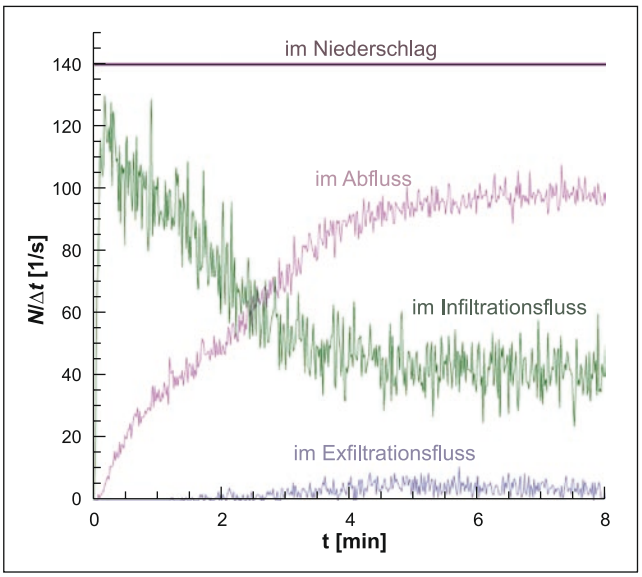

Abb. 11 Simulierte Partikelflüsse zu den Laborversuchen von Abdul & Gilham (1984). Anzahl der Partikel N, welche im Zeitschritt Δt über einen Strömungsquellterm q_s^{of}, q_s^{gf} neu hinzukommen (im Niederschlag), die Rinne über die Oberflächenströmung verlassen (im Abfluss), in den Boden gelangen (im Infiltrationsfluss) oder wieder zurück an die Oberfläche gelangen (im Exfiltrationsfluss)

des Vorereigniswassers ist stark erhöht. Abbildung 11 stellt die Partikelflüsse dar. Mit zunehmender Sättigungsfläche sinkt die Anzahl der infiltrierenden Partikel. Infiltrierte Partikel verweilen nahezu ausschließlich im Boden. Die Modellergebnisse zeigen, dass die Hydro- und Chlorographen im stationären Zustand gut reproduziert werden können, die Separierung des Ereignis- und Vorereigniswassers in den Boden- und Oberflächen-Kompartimenten in der instationären Fließphase allerdings noch nicht richtig erfasst wird. Hier sind weitere Modellverbesserungen erforderlich.

Hyporheische Fließvorgänge im Flussbett der Lahn

Das hyporheische Interstitial eines Flusses ist der durchflossene Porenraum, der an das Oberflächengewässer anschließt. Es bildet den Übergangsbereich zum Grundwasserkörper. Hyporheische Austauschprozesse wurden an der Lahn bereits in einigen Arbeiten untersucht. Beispielsweise untersuchten Sänger & Zanke (2008) den Einfluss von Feinsedimenten und Ibisch et al. 2008 die Wirkung von Algenwachstum im Flussbettsediment (Biokolmation). Die messtechnische Erfassung von Fließvorgängen zwischen Grundwasser und Flüssen gestaltet sich oft schwierig (Kalbus et al. 2006). Temperatursignaturen können hierfür ein wertvolles Werkzeug sein (Constantz & Stonestrom 2003). Am untersuchten Abschnitt der Lahn wurden kontinuierliche Temperaturzeitreihen an zwei Transekten ober- und unterstrom eines Riffels (Abb. 12) von Sommer 2000 bis

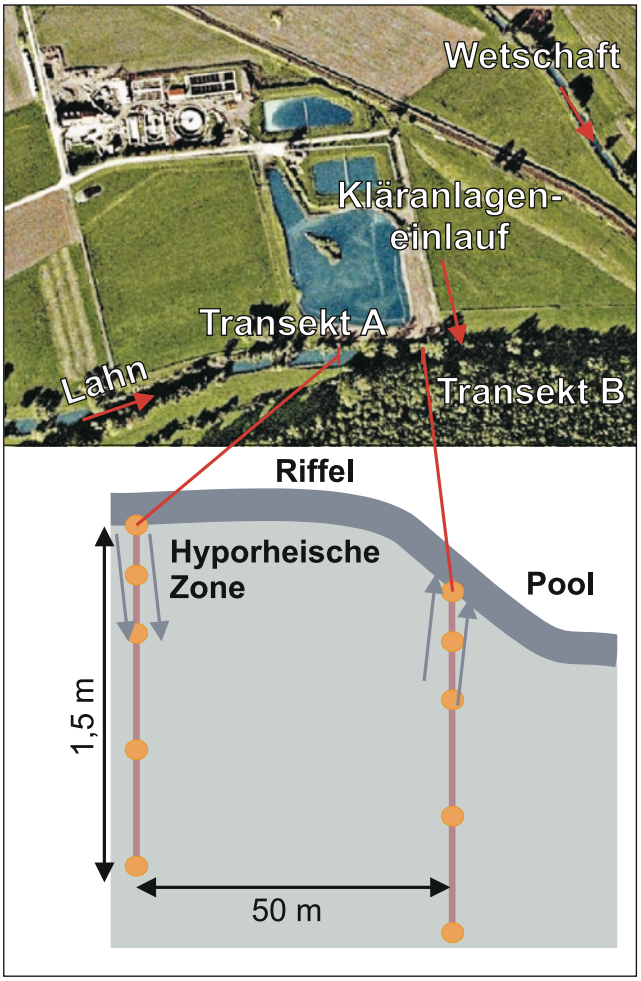

Abb. 12 Untersuchungsgebiet an der Lahn (Quelle: Google Earth 2009) mit Temperatursensoren (orange)

Frühjahr 2001 aufgezeichnet. An Transekt A lag Infiltration aus dem Fluss und in Transekt B Exfiltration in den Fluss vor. Die Temperatursensoren befanden sich in der Mitte des Flussbetts sowie zwischen Mitte und Ufer in Tiefen bis zu 1,5 m.

In einem eindimensionalen Modell (Abb. 13) wurde der vertikale Wärmetransport durch das wassergesättigte Flussbettsediment simuliert. Die Wassertemperatur an der Flusssohle und in 1,5 m Tiefe stellen Randbedingungen des Modells dar. Das Flussbettsediment wurde als homogen angenommen (Tab. 4). Dispersion wurde vernachlässigt, da der Einfluss auf die täglichen Temperaturmuster als gering eingeschätzt wird (Cardenas & Wilson 2007). Die Porosität des Sediments wurde anhand von Siebanalysen von Gefrierbohrkernen abgeschätzt. Für die Eigenschaften des Sediments (Dichte, Spezifische Wärmekapazität und Wärmeleitfähigkeit) wurden Literaturwerte für Quartz angenommen (Tab. 4). Die Eigenschaften des Wassers wurden für eine Temperatur von 20 °C übernommen.

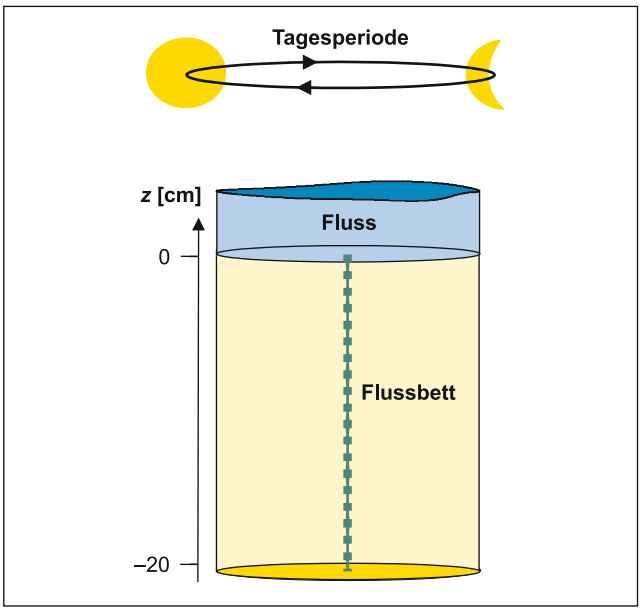

Abb. 13 Konzeptionelles Modell zur Simulation von Wärmetransport im Flussbett der Lahn

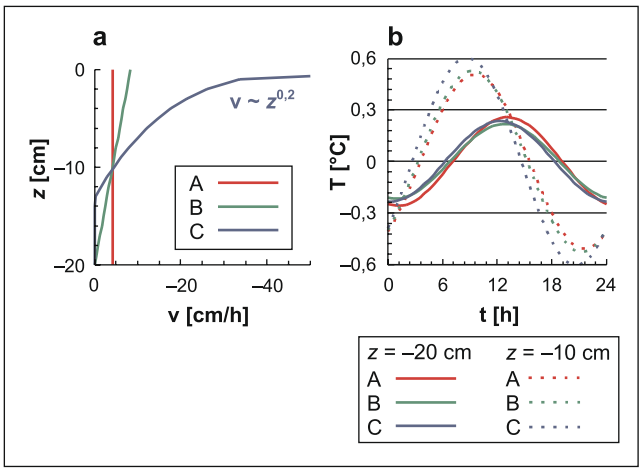

Abb. 14 Einfluss des vertikalen Durchflussprofiles auf die Temperatursignale im Flussbett. (a) Verwendete Profile zur Simulation von (b), dem Temperaturverlauf in verschiedenen Tiefen unterhalb der Flusssohle

Tabelle 4 Modellparameter zur Simulation von Wasser- und Wärmefluss im Flussbett der Lahn

Parameter	Symbol	Wert	Einheit
Wasser			
Spezifische Wärmekapazität	c^f	4,28	J/Kg
Massendichte	ρ^f	1	g/cm
Molekularer Diffusionskoeffizient	$\lambda_{ht}{}^f$	21,6	J/Kcmh
Sediment			
Porosität	φ	0,25	–
Spezifische Wärmekapazität	c^s	0,8	J/Kg
Massendichte	ρ^s	2,7	g/cm
Molekularer Diffusionskoeffizient	$\lambda_{ht}{}^s$	90	J/Kcmh

Der Einfluss der vertikalen Durchflüsse $q_3{}^{gf}$ auf die Temperatursignale im Flussbett wurde untersucht. Abbildung 14a zeigt folgende vertikale Profile: mit über die Tiefe gleichbleibendem Durchfluss (rot), mit über die Tiefe linear abnehmendem Durchfluss (grün), und mit über die Tiefe zunehmend geringer werdendem Durchfluss (blau). Abbildung 14b zeigt den Temperaturverlauf im Flussbett für die verschiedenen Profile in zwei Tiefen. Bei einem Vergleich der beiden Tiefen wird deutlich, dass der advektive-konduktive Wärmetransport zu einer Verringerung der Amplitude und zu einer Phasenverschiebung mit zunehmender Tiefe führt. Die Zunahme der Advektion im oberen Bereich des linearen Profils (grün) führt zu einer größeren Amplitude und einer kleineren Phasenverschiebung des Temperaturverlaufs in der Tiefe von $z = -10$ cm (gestrichelte Linien) im Vergleich zum konstanten Geschwindigkeitsprofil (rot).

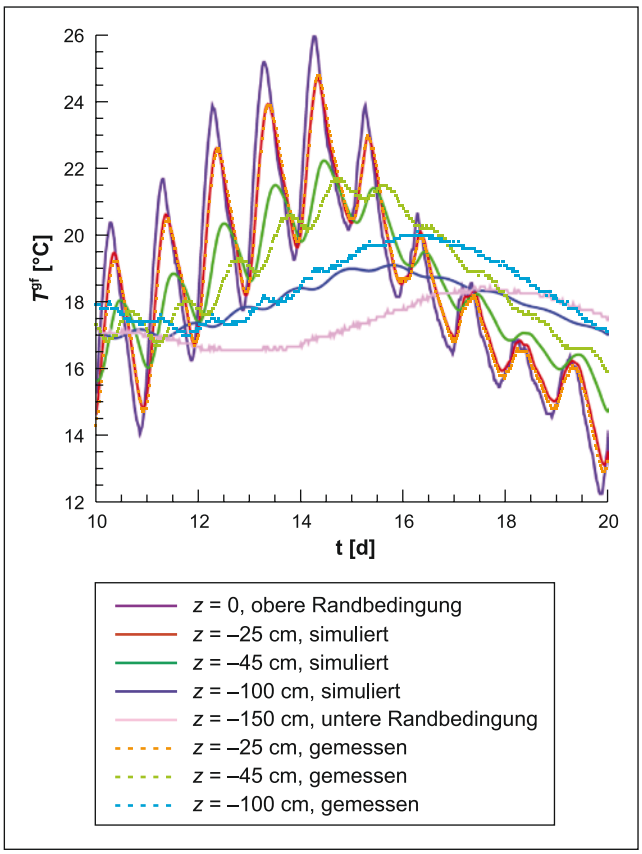

Abb. 15 Temperaturverlauf in verschiedenen Tiefen des Flussbetts der Lahn (17.–27. Juli 2000). Geschwindigkeitsprofil in den Simulationen fällt linear unterhalb der Flusssohle zwischen $0 > z > -30$ cm nach 0 ab

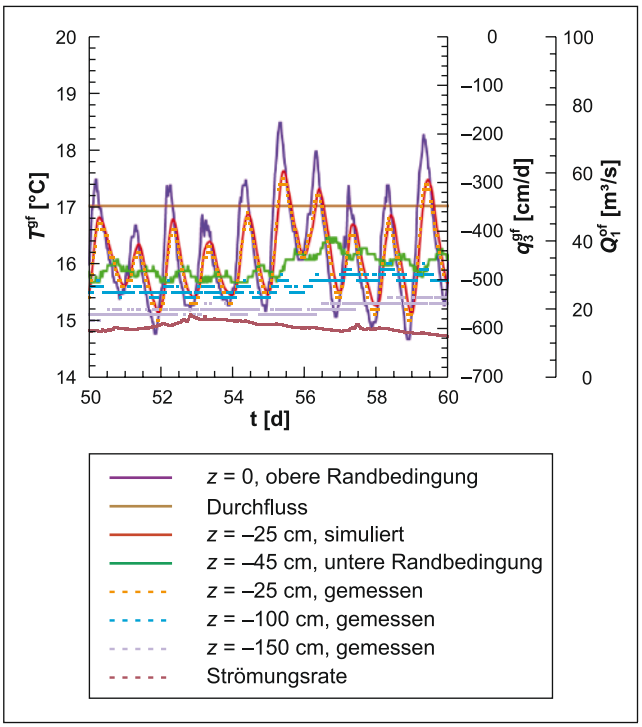

Abb. 16 Sommersituation an Transekt A der Lahn (27. Juli–6. August 2000). Temperaturverlauf in verschiedenen Tiefen des Flussbetts, kalibrierter vertikaler Durchfluss und Strömungsrate im Fluss

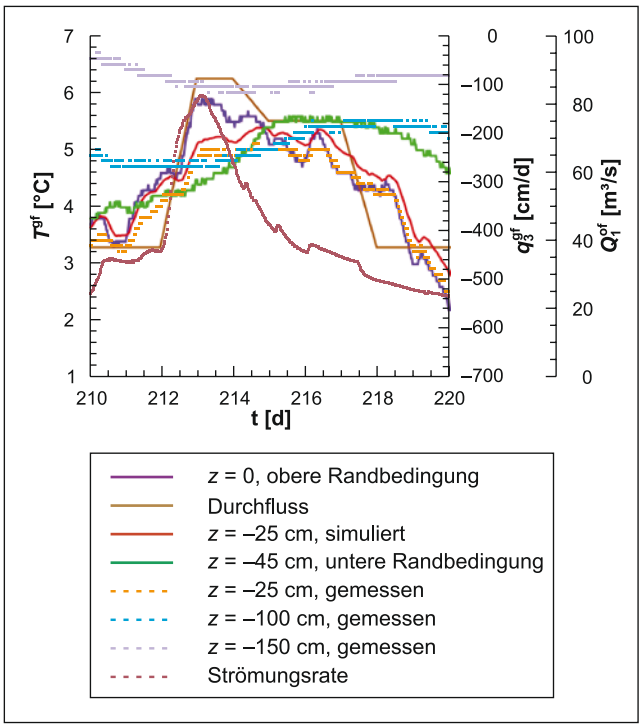

Abb. 17 Wintersituation an Transekt A der Lahn (3.–13. Januar 2001). Temperaturverlauf in verschiedenen Tiefen des Flussbetts, kalibrierter vertikaler Durchfluss und Strömungsrate im Fluss

In der Tiefe von $z = -20$ cm (Volllinien) führt die geringere Advektion im unteren Bereich zu einer kleineren Amplitude und einer geringeren Phasenverschiebung des Temperaturverlaufs. Ein stark abfallender Durchfluss in zunehmender Tiefe (blau) resultiert in einer stärker verringerten Phasenverschiebung. Vertikale Profile des Durchflusses im Flussbett der Lahn lassen sich wesentlich besser an Transekt A (Infiltration) als an Transekt B (Exfiltration) bestimmen. Abbildung 15 zeigt Simulations- und Messergebnisse über 10 Tage für ein Durchflussprofil, welches linear abfällt. Die Übereinstimmung gemessener und simulierter Daten ist am besten für die oberen Flusssedimente ($z = -25$ cm).

Eine typische Sommer- und Wintersituation ist in den Abbildungen 16 und 17 dargestellt. Im Sommer ist die Flusssohle wärmer und im Winter die tieferen Sedimente ($z = -150$ cm). Die Strömungsrate im Fluss q_1^{of} weist eine deutlich höhere Variabilität im Winter auf. Dagegen sind im Winter die Tagesamplituden schwächer ausgeprägt. Die Kalibrierung der vertikalen Geschwindigkeiten beruht hauptsächlich auf den längeren Perioden und ist daher für den gesamten Zeitraum (Mai 2000–Februar 2001) möglich (Abb. 18). Die Abbildungen 16–18 zeigen Kalibrationsergebnisse mit vertikal kontstanten Durchflussprofilen. Variationen im hyporheischen Austausch lassen sich größtenteils auf Kolmationsprozesse zurückführen (z. B. Sänger & Zanke 2008). Die ermittelten vertikalen Durchflüsse verringern

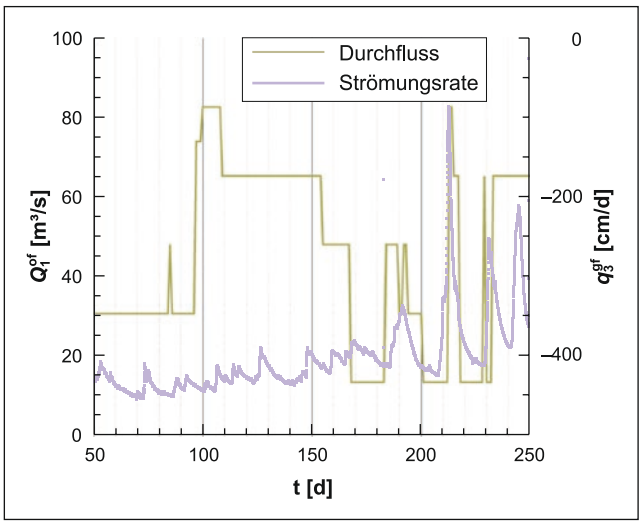

Abb. 18 Strömungsraten im Fluss Q_1^{of} und kalibrierte vertikale Durchflüsse q_3^{gf} an Transekt A der Lahn (27. Juli 2000–12. Februar 2001)

sich während der Phasen starker Flussströmung im Winter und zusätzlich als Ende September 2000 der Absetzteich der Kläranlage Sarnau in Richtung der Lahn gefüllt wurde. Mithilfe des einfachen Wärmetransportmodells können die vertikalen Durchflüsse in der hyporheischen Zone anhand von Temperatursignalen korrekt bestimmt werden.

Schlussfolgerungen und Ausblick

In dieser Arbeit wird das Kompartiment-Konzept zur Analyse gekoppelter Hydrosysteme (Kolditz et al. 2008) um Stoff- und Wärmetransportprozesse erweitert. Transportprozesse werden durch Advektions-Diffusionsgleichungen beschrieben. Die Transportgleichungen können alternativ mittels finiter Elemente oder RWPT gelöst werden. Damit steht ein flexibles numerisches Instrumentarium zur Berechnung von Strömungs- und Transportprozessen in gekoppelten Hydrosystemen zur Verfügung.

Die präsentierten Anwendungsbeispiele beschäftigen sich i. W. mit der Auswertung von kleinskaligen Laborversuchen. Dabei wurde die Genauigkeit der numerischen Modelle hinsichtlich der gekoppelten Hydraulik (Oberflächenabfluss und Bodenhydraulik) und des Stofftransports getestet. Am Beispiel der Lahn wurden thermische Signaturen im Flusssediment im Zeitraum eines Jahres mit dem neuen numerischen Modell erfolgreich ausgewertet. Zur Simulation der Laborversuche von Smith & Woolhiser (1971) wird Oberflächenabfluss mit der ungesättigten Zone gekoppelt. Der Einfluss von Reibungsprozessen, Bodenkapillarität und der hydraulischen Grenzschicht zur Berechnung des Kopplungsflusses wird für Hortonschen Abfluss untersucht. Stofftransport zwischen Oberflächenströmung und ungesättigter Bodenzone (Dunnescher Abfluss) wird am Beispiel der Laborversuche von Abdul & Gilham (1984) mittels RWPT simuliert.

Die Erfahrungen aus den Modellanwendungen haben aber auch gezeigt, dass dieser konzeptionelle Ansatz Grenzen besitzt. Der Grund für die Limitationen des Kompartiment-Konzepts sind zum einen die extrem unterschiedlichen Raum- und Zeitskalen der einzelnen Prozesse in den Oberflächen-, Boden- und Grundwassersystemen, die zwar mittels Kopplung über Quell-/Senkenterme abgebildet werden können, aber mit zunehmenden Skalendifferenzen zu größeren Kopplungsfehlern führen. Zum anderen haben Modellanwendungen auf der großen Skala (Watanabe 2008) gezeigt, dass insbesondere die Parametrisierung der Flachwasserwellengleichungen (Gl. 8–10) im Einzugsgebietsmaßstab problematisch ist.

Untersuchungen mit numerischen Modellen in größeren hydrologischen Systemen sind prinzipiell möglich. Dies wurde unlängst in einer Reihe von Arbeiten sehr erfolgreich demonstriert (Sudicky et al. 2008, Li et al. 2008, Park et al. 2008c). Dennoch stellt sich die Frage der Parametrisierung großskaliger hydrologischer Modelle. Die numerischen Experimente zeigen, dass Hydrographen schon im Labormaßstab sehr sensitiv gegenüber den Oberflächen-Boden-Parametern sind (Abb. 10). Eine großflächige experimentelle Bestimmung der hydrologischen Parameter für prozessbasierte Modellansätze ist nicht trivial.

Vielversprechend ist die Kopplung verschiedener konzeptioneller Methoden für die hydrologische Systemanalyse. In der Boden- und Grundwassermodellierung beispielsweise werden bevorzugt Euler-Verfahren (Finite Differenzen, Volumen oder Elemente) eingesetzt. In der Oberflächenhydrologie haben prozess-basierte stochastische Methoden Vorteile, da diese rechentechnisch effizient und leichter zu parametrisieren sind (z. B. Samaniego & Bárdossy 2007).

Symbolverzeichnis

a	Dicke der Oberflächenstrukturschicht (m)
a'	Dicke der Kopplungsgrenzschicht (m)
A	Rinnenoberfläche (m²)
A^{of}	Horizontale Kompartimentgrenzfläche (m²)
A^{gf}	Horizontale Kompartimentgrenzfläche (m²)
A^{sf}	Horizontale Kompartimentgrenzfläche (m²)
A_F	Flussquerschnitt (m²)
b	Geodätische Höhe (m)
B	Fluss-/Rinnenbreite (m)
c^f	Spezifische Wärmekapazität der wässrigen Phase (J/Kkg)
c^g	Spezifische Wärmekapazität der Gasphase (J/Kkg)
c^s	Spezifische Wärmekapazität der Feststoffphase (J/Kkg)
$c_{nsw}{}^{of}{}_{st}$	Stoffkonzentration im Niederschlagswasser (kg/m³)
$c_{st}{}^{of}$	Stoffkonzentration in Oberflächenströmung (kg/m³)
$c_{st}{}^{gf}$	Stoffkonzentration im Aquifer (kg/m³)
$c_{st}{}^{sf}$	Stoffkonzentration in wässriger Phase des Bodens (kg/m³)
C^{gf}	Wärmekapazität im Aquifer (J/Km³)
C^{sf}	Wärmekapazität im Boden (J/Km³)
C_r	Oberflächenreibungskoeffizient ($m^{1/3}$/s für Manning-Strickler und 1/ms für Darcy-Weisbach-Fließformel)
D^{of}	Dispersionstensor für Oberflächenströmung (m²/s)
D^{gf}	Dispersionstensor für Strömung im Aquifer (m²/s)
D^{sf}	Dispersionstensor für Strömung im Boden (m²/s)
h^{of}	Druckhöhe der Oberflächenströmung (m)
h^{gf}	Druckhöhe der Grundwasserströmung (m)
h^{sf}	Druckhöhe in der ungesättigten Bodenzone (m)
h_{cap}	Kapillardruckhöhe (m)
H	Tiefe des beweglichen Oberflächenwassers (m)
k	Oberflächenreibungskoeffizient (–)
$k_{a'}$	Skalierungsfaktor des Kopplungsflusses (–)
k_r	Relative Durchlässigkeit des Bodens (–)
k_λ	Zerfallsrate (1/s)
K	Hydraulische Leitfähigkeit des Aquifers und des gesättigten Bodens (m/s)
K^c	Leitfähigkeit der Kopplungsgrenzschicht (m/s)
l	Oberflächenreibungskoeffizient (–)
m	Van Genuchten-Parameter (–)
n	Manning-Beiwert ($1/m^{1/3}$)
N	Partikelanzahl (–)
N_{ab}	Partikelanzahl im Abfluss (–)

N_{nsw} Partikelanzahl im Niederschlagswasser (–)
O Ausgabefunktion in Sensitivitätsanalyse.
P Parameter in Sensitivitätsanalyse.
P Benetzter Umfang (m)
q^{of} Spezifische Oberflächenströmung (m/s)
q^{gf} Spezifische Grundwasserströmung nach Darcy (m/s)
q^{sf} Spezifischer Durchfluss nach Darcy (m/s)
$q_c{}^{st}$ Kopplungsfluss für den Stofftransport (kg/m³s)
q_r Oberflächenabfluss (m/s)
$q_s{}^{of}$ Quellen-/Senkenterm der Oberflächenströmungsgleichung (m/s)
$q_s{}^{gf}$ Quellen-/Senkenterm der Grundwassergleichung (1/s)
$q_s{}^{sf}$ Quellen-/Senkenterm der Gleichung für den Boden (m/s)
$q_{sf}{}^{of}$ Austauschfluss der Oberflächenströmungsgleichung für Kopplung mit Bodenströmung (m/s)
$q_{gf}{}^{of}$ Austauschfluss der Oberflächenströmungsgleichung für Kopplung mit Grundwasser (m/s)
$q_{gf}{}^{of}{}_*$ Austauschfluss der Oberflächenströmungsgleichung für Kopplung mit Grundwasser, Grundwasserspiegel unter Flusssohle (m/s)
$q_{of}{}^{sf}$ Austauschfluss der Gleichung für Bodenströmung für Kopplung mit Oberflächenströmung (m/s)
$q_{of}{}^{gf}$ Austauschfluss der Grundwassergleichung für Kopplung mit Oberflächenströmung (m/s)
$q_{of}{}^{gf}{}_*$ Austauschfluss der Grundwassergleichung zur Kopplung mit Oberflächenströmung, Grundwasserspiegel unter Flusssohle (m/s)
$q_{of}{}^{sf}{}_{st}$ Austauschfluss für Stofftransport im Boden zur Kopplung mit Oberflächenströmung (kg/m³s)
$q_{sf}{}^{of}{}_{st}$ Austauschfluss für Stofftransport in Oberflächenströmung zur Kopplung mit Boden (kg/m³s)
$q_s{}^{gf}{}_{ht}$ Quellen-/Senkenterm für Wärmetransport im Aquifer (J/m³s)
$q_s{}^{sf}{}_{ht}$ Quellen-/Senkenterm für Wärmetransport im Boden (J/m³s)
$q_s{}^{of}{}_{st}$ Quellen-/Senkenterm für Stofftransport in der Oberflächenströmung (kg/m³s)
$q_s{}^{gf}{}_{st}$ Quellen-/Senkenterm für Stofftransport im Aquifer (kg/m³s)
$q_s{}^{sf}{}_{st}$ Quellen-/Senkenterm für Stofftransport im Boden (kg/m³s)
Q_{crit} Kritischer Abfluss (m/s)
R Hydraulischer Radius (m)
R_d Retardationsfaktor (–)
S Wassersättigung des Bodens (–)
S_0 Speicherkoeffizient des Aquifers (1/m)
S_e Effektive Sättigung des Bodens (–)
S_r Residuale Sättigung des Bodens (–)
S_s Betrag des Druckhöhengradienten der Oberflächenströmung (–)
T^{gf} Temperatur im Aquifer (K)
T^{sf} Temperatur im Boden (K)
α Van Genuchten-Parameter (1/m)
α_L Longitudinaler Dispersionskoeffizient (m)
α_T Transversaler Dispersionskoeffizient (m)
$\kappa_{ht}{}^{gf}$ Thermische Diffusivität im Aquifer (J/Kms)
$\kappa_{ht}{}^{sf}$ Thermische Diffusivität im Boden (J/Kms)
$\kappa_{st}{}^{gf}$ Diffusivität gelöster Stoffe im Aquifer (m²/s)
$\kappa_{st}{}^{sf}$ Diffusivität gelöster Stoffe im Boden (m²/s)
$\kappa_{st}{}^{of}$ Diffusivität gelöster Stoffe in der Oberflächenströmung (m²/s)
$\kappa_{ij}{}^{ht}$ Thermische Diffusivität (J/Kms)
$\lambda_{ht}{}^{gf}$ Molekularer Diffusionskoeffizient für Wärmetransport im Aquifer (J/Kms)
$\lambda_{ht}{}^{sf}$ Molekularer Diffusionskoeffizient für Wärmetransport im Boden (J/Kms)
$\lambda_{ht}{}^{f}$ Wärmeleitfähigkeit der wässrigen Phase (J/Kms)
$\lambda_{ht}{}^{g}$ Wärmeleitfähigkeit der Gasphase (J/Kms)
$\lambda_{ht}{}^{s}$ Wärmeleitfähigkeit der Feststoffphase (J/Kms)
λ_{ht} Molekulare Diffusivität für Wärmetransport (J/Kms)
λ_{st} Molekularer Diffusionskoeffizient gelöster Stoffe (m²/s)
Λ Leakage-Faktor (1/s)
ρ^f Massendichte der wässrigen Phase (kg/m³)
ρ^g Massendichte der Gasphase (kg/m³)
ρ^s Massendichte der Feststoffphase (kg/m³)
τ_{ij} Tortuosität (–)
φ Porosität des Aquifers und Bodens (–)
φ^{of} Oberflächenporosität (–)

Danksagung Diese Arbeit wurde finanziell vom EU FP6 Projekt „AquaTerra“ (Projekt Nr. 505428) und dem Bundesministerium für Bildung und Forschung (BMBF)-Projekt „IWAS - Internationale WasserforschungsAllianz Sachsen“ (Projekt Nr. 02WM1027) gefördert. Wir danken den Gutachtern für ihre konstruktiven Hinweise und den Herausgebern für ihre Moderation.

Literatur

Abbott, M.B., Babovic, V.M., Cunge, J.A.: Towards the hydraulics of the hydroinformatics era.- J. Hydraul. Res **39**(4), 339–349 (2001)

Abbott, M.B., Bathurst, J.C., Cunge, J.A., O'Connell, P.E., Rasmussen, J.: An introduction to the european hydrological system – Systéme Hydrologique Européen, ‚SHE', 2: Structure of a physically-based, distributed modelling system.- J. Hydrol. **87**(2), 61–77 (1986)

Abdul, A.S., Gilham, R.W.: Laboratory studies of the effects of the capillary fringe on streamflow generation.- Water Resour. Res. **20**(6), 691–698 (1984)

Abdul, A.S., Gilham, R.W.: Field studies of the effects of the capillary fringe on streamflow generation.- J. Hydrol. **112**, 1–18 (1989)

Akan, A.O., Yen, B.C.: Mathematical model of shallow water flow over porous media.- J. Hydr. Div. ASCE **107**(4), 479–494 (1981)

Anderson, M.G., Burt, P.T.: Hydrological forecasting; Wiley Publisher, Berlin (1985)

Arnold, J.G., Sirinivasan, R., Muttiah, R.S., Williams, J.R.: Large area hydrologic modeling and assessment, part 1 – model development.- J. Am. Water Resour. Assoc. **34**(1), 73–89 (1998)

Bear, J.: Dynamics of fluids in porous media.- Dover Publications Inc. New York, 2. Aufl. (1988)

Bertoldi, G., Tamanini, D., Zanotti, F., Rigon, R.: GEOtop, A hydrological balance model, technical description and programs guide (Version 0.875). Department of Civil and Environmental Engineering, University of Trento (2004)

Bhallamudi, S.M., Panday, S., Huyakorn, P.S.: Sub-timing in fluid flow and transport simulations.- Adv. Water Resour. **26**(5), 477–489 (2003)

Brunke, M., Gonser, T.: The ecological significance of exchange processes between rivers and groundwater.- Freshwater Biol. **37**, 1–33 (1997)

Cardenas, M.B., Wilson, J.L.: Effects of current-bed form induced fluid flow on the thermal regime of sediments.- Water Resour. Res. **43**, W08431, doi:10.1029/2006WR005343 (2007)

Chen, Q., Morales-Chaves, Y., Li, H., Mynett, A.: Hydroinformatics techniques in eco-environmental modelling and management.- J. Hydroinf. **8**(4), 297–316 (2006)

Constantz, J., Stonestrom, D.: Heat as a tracer of water movement near streams.- In: Stonestrom, D., Constantz, J. (Hrsg.): Heat as a tool for studying the movement of ground water near streams.- USGS Survey Circular **1260** (2003)

Darcy, H.P.G.: Les fontaines publiques de la ville de Dijon; Victor Dalmont, Paris (1856)

Dawson, C.: Analysis of discontinuous finite element methods for groundwater/surface water coupling.- SIAM J. Num. Anal. **52**, 63–88 (2006)

Delay, F., Ackerer, P., Danquigny, C.: Simulating solute transport in porous or fractured formations using random walk particle tracking: a review.- Vadose Zone J. **4**(2), 360–379 (2005)

Delfs, J.-O., Park, C.-H., Kolditz, O.: A sensitivity analysis of Hortonian flow.- Adv. Water Resour., doi:10.1016/j.advwatres.2009.06.005 (2009, in Druck)

Delfs, J.-O., Park, C.-H., Kolditz, O.: Benchmarking of flow and transport in coupled surface/subsurface hydrosystems. Helmholtz Zentrum für Umweltforschung – UFZ; Leipzig (2008)

Donigian, A.S., Imhoff, J.: History and evolution of watershed modelling derived from the Stanford Watershed Model. CRC Press, Boca Raton.- In: Singh, V.P., Frevert, D. (Hrsg.): Watershed Models (2006)

Du, Y., Kolditz, O.: Time discretization for Richards flow modelling.- Tech. Rep. 2005-50; Center of Applied Geoscience, University of Tübingen, GeoSys-Preprint (2005)

Forsyth, P.A., Wu, Y.S., Pruess, K.: Robust numerical methods for saturated-unsaturated flow with dry initial conditions in heterogeneous media.- Adv. Water Resour. **18**, 25–38 (1995)

Freeze, R.A., Harlan, R.L.: Blueprint for a physically based, digitally-simulated hydrological response model.- J. Hydrol. **9**, 237–258 (1969)

Gerbeau, J.-F., Perthame, B.: Derivation of viscous Saint Venant system for laminar shallow water: Numerical validation.- Discrete Contin. Dyn. Syst. Ser. **B 1**(1), 89–102 (2001)

Govindaraju, R.S.: Modeling overland flow contamination by chemicals mixed in shallow soil horizons under variable source area hydrology.- Water Resour. Res. **32**(3), 753–758 (1996)

Govindaraju, R.S., Kavvas, M.L.: Dynamics of moving boundary overland flows over infiltrating surfaces at hillslopes.- Water Resour. Res. **27**(8), 1885–1898 (1991)

Green, W.A., Ampt, G.A.: Studies on soil physics I. The flow of air and water through soils.- J. of Agr. Sci. **4**, 1–24 (1911)

Gunduz, O., Aral, M.M., 2005. River networks and groundwater flow: simultaneous solution of a coupled system.- J. Hydrol. **301**(1–4), 216–234 (2005)

Harbaugh, A.W., Banta, E.R., Hill, M.C., McDonald, M.G.: MODFLOW-2000, the U.S. geological survey modular ground-water model – user guide to modularization concepts and the groundwater flow process.- Tech. Rep. 00-92, U.S. Geological Survey, Open-File Report (2000)

Hoteit, H., Mose, R., Younes, A., Lehmann, F., Ackerer, P.: Three-dimensional modeling of mass transfer in porous media using the mixed hybrid finite elements and the random-walk methods.- Math. Geol. **34**(4), 435–456 (2002)

Huyakorn, P., Pinder, G.: Computational methods in subsurface flow; Academic Press, New York (1983)

Ibisch, R.B., Borchardt, D., Seydell, I.: Influence of periphyton biomass dynamics on biological colmation processes in the hyporheic zone of a gravel bed river (River Lahn, Germany).- Fundam. Appl. Limnol. (2009, im Druck)

Julien, P.Y.: River mechanics.- Cambridge University Press; Cambridge (2002)

Kalbus, E., Reinstorf, F., Schirmer, M.: Measuring methods for groundwater – surface water interactions: a review.- Hydrol. Earth Syst. Sci. **10**(6), 873–887 (2006)

Kinzelbach, W.: Numerische Methoden zur Modellierung des Transports von Schadstoffen im Grundwasser; Oldenburg Verlag, München und Wien (1987)

Kolditz, O., Bauer, S.: A process-orientated approach to compute multi-field problems in porous media.- International J. Hydroinf. **6**, 225–244 (2004)

Kolditz, O., Delfs, J.-O., Bürger, C., Beinhorn, M., Park, C.-H.: Numerical analysis of coupled hydrosystems based on an object-oriented compartment approach.- J. Hydroinf. **10**(3), 227–244 (2008)

Kolditz, O., Shao, H. (Hrsg.): OpenTHMC – Developer Benchmark Book based on GeoSys/RockFlow Version 4.9.06. Report 15, Helmholtz Centre for Environmental Reserach – UFZ Leipzig (2009)

Kollet, S.J., Maxwell, R.M.: Integrated surface-groundwater flow modeling: A free-surface overland flow boundary condition in a parallel groundwater flow model.- Adv. Water Resour. **29**(7), 945–958 (2006)

Lees, M.: Data-based mechanistic modelling and forecasting of hydrological systems.- J. Hydroinf. **2**(1), 15–34 (2000)

LeVeque, R.J.: Finite volume methods for hyperbolic problems; Cambridge University Press, Cambridge (2002)

Li, Q., Unger, A., Sudicky, E.: Simulating the multi-seasonal response of a large-scale watershed with a 3D physically-based hydrologic model.- J. Hydrol. **357**(3–4), 317–336 (2008)

Manning, R.: On the flow of water in open channels and pipes.- Trans. Inst. Civil Eng. Ireland **20**, 161–207 (1891)

Morita, M., Yen, B.C.: Modeling of conjunctive two-dimensional surface-three-dimensional subsurface flows.- J. Hydraul. Eng. **128**(2), 184–200 (2002)

Park, C.-H., Beyer, C., Bauer, S., Kolditz, O.: A study of preferential flow in heterogeneous media using random walk particle tracking.- Geosci. J. **12**(3), 285–297 (2008a)

Park, C.-H., Beyer, C., Bauer, S., Kolditz, O.: Using global node-based velocity in random walk particle tracking in variably saturated porous media: Application to contaminant leaching from road constructions.- Environ. Geol. **55**, 1755–1766 (2008b)

Park, Y., Sudicky, E., Panday, S.: Application of implicit sub-time stepping to simulate flow and transport in fractured porous media.- Adv. Water Resour. **31**(7), 995–1003 (2008c)

Philip, J.R.: The theory of infiltration: 3. Moisture profiles and relation to experiment.- Soil Sci. **83**, 163–178 (1957)

Ponce, V.M., Ruh-Ming, L., Simmons, D.B.: Applicability of kinematic and diffusion models.- J. Hydr. Div. ASCE **104**, 353–360 (1978)

Richards, C.P., Parr, A.D.: Modified Fickian model for solute uptake by runoff.- J. Env. Engrg. **114**(4), 792–809 (1988)

Richards, L.A.: Capillary conduction of liquids through porous mediums.- Phys. **1**, 318–333 (1931)

Sänger, N., Zanke, U.C.: A depth – oriented view of hydraulic exchange patterns between surface water and the hyporheic zone: analysis of field experiments at the River Lahn, Germany.- Arch. Hydrobiol. (2009, in Druck)

Samaniego, L., Bárdossy, A.: Exploratory modelling applied to integrated water resources management. Proceedings 3rd International Symposium on Integrated Water Resources Management, Bochum, September 2006.- IAHS Publ. **317** (2007)

Simunek, J., Sejna, M., Genuchten, M. T. v.: The Hydrus-2D software package for simulating two-dimensional movement of water, head and multiple solutes in variably saturated media. Version 2.0, IGWMC-TPS-53. International GroundWater Modeling Center, Colorado School of Mines, Golden, Colorado (1999)

Singh, V., Bhallamudi, S. M.: Conjunctive surface-subsurface modeling of overland flow.- Adv. Water Resour. **21**(7), 567–579 (1998)

Singh, V. P.: Derivation of errors of kinematic-wave and diffusion-wave approximations for space-independent flows.- Water Resour. Manage. **8**, 57–82 (1994)

Singh, V. P., Frevert, D. K. (Hrsg.): Watershed Models; CRC, USA (2005)

Smith, R. E., Woolhiser, D. A.: Overland flow on an infiltrating surface.- Water Resour. Res. **7**(4), 899–913 (1971)

Sudicky, E., Jones, J., Park, Y.: Simulating complex flow and transport dynamics in an integrated surface-subsurface modeling framework.- Geosci. J. **12**(2), 107–122 (2008)

Sudicky, E. A., Jones, J. P., McLaren, R. G., Brunner, D. S., VanderKwaak, J. E.: A fully-coupled model of surface and subsurface water flow: Model overview and application to the Laurel Creek watershed.- In: Balkema, A. A. (Hrsg.): Computational methods in water resources Nr. 2, 1093–1099 (2000)

Teutsch, G.: Grundwassermodelle im Karst: Praktische Ansätze am Beispiel zweier Einzugsgebiete im Tiefen und Seichten Malmkarst der Schwäbischen Alb. Dissertation, Zentrum für Angewandte Geowissenschaften, Universität Tübingen (1988)

Therrien, R., McLaren, R. G., Sudicky, E. A., Panday, S.: HydroSphere: A three-dimensional numerical model describing fully-integrated subsurface and surface flow and solute transport; Université Laval and University of Waterloo (2004)

Thoms, R. B.: Simulating fully coupled overland and variably saturated subsurface flow using MODFLOW. Magisterarbeit, OGI School for Science and Engineering, Oregon Health & Science University, Beaverton, USA (2003)

van Genuchten, M. T.: A closed-form equation for predicting the hydraulic conductivity of unsaturated soil.- Soil Sci. Soc. of Am. J. **44**, 892–898 (1980)

VanderKwaak, J. E.: Numerical simulation of flow and chemical transport in integrated surface-subsurface hydrologic systems. Dissertation, Department of Earth Sciences, University of Waterloo, Ontario, Canada (1999)

Vreugdenhil, C. B.: Numerical Methods for Shallow-Water Flow. Kluwer Academic Publishers, Dordrecht (1994)

Wallach, R., van Genuchten, T., Spencer, W.: Modelling solute transfer from soil to surface runoff: The concept of effective depth of transfer.- J. Hydrol. **109**, 307–317 (1989)

Wang, W., Kolditz, O.: Object-oriented finite element analysis of thermo-hydro-mechanical (THM) problems in porous media.- Int. J. Numer. Methods Eng. **69**(1), 162–201 (2007)

Warrick, J. W., 2003.- Soil water dynamics. Oxford University Press Inc., New York.

Wasy Software: IFMMIKE11 1.1, User manual; Wasy GmbH, Institute for Water Resources Planning and System Research (2004)

Watanabe, N.: Mesh design for finite element analysis of geo-hydrological systems. Magisterarbeit, Graduate School of Environmental science, Okayama University, Japan (2008)

Weisbach, J.: Lehrbuch der Ingenieur- und Maschinen-Mechanik.- Water & Power Press, Braunschweig (1845)

Enclosed Publication

[EP3] Y. Du, **J.-O. Delfs**, W. Wang, C.-H. Park and O. Kolditz (2009): *A regional hydrological soil model for large-scale applications: Computational concept and implementation*, Journal of Environmental Hydrology 17, Paper 7.

JOURNAL OF
ENVIRONMENTAL HYDROLOGY
The Electronic Journal of the International Association for Environmental Hydrology
On the World Wide Web at http://www.hydroweb.com
VOLUME 17 2009

A REGIONAL HYDROLOGICAL SOIL MODEL FOR LARGE-SCALE APPLICATIONS: COMPUTATIONAL CONCEPT AND IMPLEMENTATION

Y. Du[1]
J-O. Delfs[2]
E. Kalbus[2]
W. Wang[2]
C-H. Park[2]
O. Kolditz[2]

[1]University of Plymouth, School of Engineering, UK
[2]Helmholtz Centre for Environmental Research - UFZ, Leipzig, Germany

A parallelized large-scale regional hydrologic soil model (RHSM) is developed as a tool for large-scale unsaturated zone investigations. It is applied to simulate the temporal and spatial responses of the unsaturated zone and the regional water budget under the forcing of realistic precipitation and evaporation scenarios. The Richards equation is used to describe the flow movement in the vadose zone and is solved using a finite element code. The RHSM provides a way to deal with the enormous discretization demand of unsaturated flow simulation at regional scales. The relatively thin soil cover is modeled vertically by 1D line elements with adequate resolution, whereas the large lateral dimensions are modeled as coarser grid patches, the so-called influence areas. In order to achieve reasonable computation times for a single model run the independence properties of the RHSM are elegantly exploited to realize a relatively uncomplex code parallelization. The parallelized RHSM runs on Linux supported symmetric multiprocessing computers using the message passing interface (MPI). This implementation attains a high performance computation of regional scale hydro-system models. In an application study at the Beerze-Reusel drainage basin (Netherlands), a high resolution of variably saturation distributions and wet front movements are obtained for the anisotropic field using the parallel RHSM. An analysis of the computational speed-up demonstrates the performance gain of the parallel RHSM.

INTRODUCTION

A large-scale hydrologic model is an indispensable research tool for hydrologists to investigate regional hydrological features under the influence of global climate change, anthropogenic alteration, or land-use change in recent decades. In hydrological analysis, unsaturated flow simulation is important since the vadose zone constitutes the interface between hydrosphere and atmosphere and governs transfer of water and contaminants from the atmosphere to the subsurface. As such, soil moisture patterns influence recharge to groundwater. On a larger scale wet-dry patterns in soil may also have an effect on convective cells in the atmospheric boundary layer (Patton et al., 2005). Moreover, it was demonstrated in a modeling study by Clark et al. (2004) that rainfall locations and intensities can be influenced by the presence and size of a wet soil patch down to scales of 10-15 km. A recent example of successful large-scale hydrologic modeling is the Altamaha river drainage basin study (Aral and Gunduz, 2003; Gunduz, 2004). Other macroscale hydrological models include the VIC-3L model, which was used for the upper Mississippi river basin (U.S.) (Srinivasan and Lakshmi, 2005), and the Xi'anjiang model, which is used in China chiefly for stream flow computations (Ren and Yuan, 2005).

Many different approaches have been developed to model water movement in the unsaturated zone. They can be summarized as: 1) quasi-linear analysis; 2) Green-Ampt (GA) method; 3) kinematic wave approximation; and 4) perturbation method. Quasi-linear analysis was first presented by Garden (1958) and later generalized and applied by Philip (1968, 1992). The GA method, originally developed by Green and Ampt (1911) for a one-dimensional domain and a single infiltration period, was extended to a more generally applicable model by Mein and Larson (1973). A large-scale application of GA was carried out by Govindaraju and Corradini (2000). Ogden and Sahafian (1997) introduced the GA redistribution (GAR) technique to estimate the soil water distribution during transient rainfall. The comparison of their results with those computed by numerically solving a Richards model showed a high level of agreement and demonstrated the accuracy of GAR. The kinematic wave approximation, brought forward first by Lighthill and Whitham (1955), handles wetting and draining waves travelling downwards through unsaturated soils. More recently, this method was used by Smith (1983), Levy and Germann (1988), Singh (1997), and Troch et al. (2002, 2003). The perturbation method was developed by Prasad and Romkens (1982). Of these methods, the Richards equation remains the most widely accepted framework for soil water flow analysis e.g. (Milly, 1988; Schüze et al., 2005). The numerical implementation of the solution of the Richards equation has been detailed extensively by Segol, (1993) and Kolditz (2002).

At large scales a significant temporal diversification of soil moisture contents is observed due to the variability of meteorological variables such as precipitation and evapotranspiration. The coupling of hydrological models with regional climate models was therefore undertaken to investigate the linkages between both systems (Stamm et al., 1994; Walker and Houser, 2001; Hurk et al., 2004), the sensitivity of the hydrosystem to climatic conditions (Gedney and Cox, 2003), and the feedback of soil moisture content to local or regional climate systems (Yeh et al., 1994; Schaer et al., 1999).

Apart from the meteorological forcing, the spatial variability of soil properties needs to be considered. With sophisticated data sampling techniques and tools for data processing and management at hand, large-scale distributed modeling is becoming a more and more viable option despite its enormous demand for data and computational resources. More and more models

choose parallelization as a practical tool to solve massive and large scale problems. The parallel integrated hydrologic model ParFLOW was developed by Ashby and Falgout (1996). The model exhibits higher parallel efficiency in solving small problems compared to large problems. Overland flow simulation requires considerably more computational effort compared to other processors, causing low parallel inefficiency. Dawson et al. (1997) brought forward a parallel implicit cell-centered method for two-phase flow with a preconditioned Newton-Krylov solver. In Jones and Woodward's (2001) work, the parallel computation results show the effectiveness of the entire nonlinear solution procedure and parallel efficiencies. As for other models, the sequential hydrological model SWMS_3D was upgraded to a parallelized version by Hardelauf et al. (2007), and its reliability was tested and performance and efficiency was compared with a single processor run. Once the computation efficiency was improved by parallelization, more integrated hydrological models became possible. Kollet and Maxwell (2006) incorporated an overland flow simulator into the parallel three-dimensional variable saturated subsurface flow code ParFlow. In addition, the influence of groundwater dynamics on the energy balance at the land surface was studied using this integrated, distributed modelling platform (Kollet and Maxwell (2008)).

In this study, we give a detailed description of the implementation of a parallelized regional hydrological soil model or RHSM, and present a class of solvers developed for the parallel solution of Richards' equation, the model chosen for variably saturated flow simulation. The parallelized RHSM provides an approach that meets the required vertical discretization demands on the one hand, and keeps the computational efforts realistic on the other hand. Additionally, the lateral spatial variability of meteorological input or soil parameters can be incorporated into the simulation with an appropriate level of detail.

Notwithstanding the parallelization, the RHSM remains computationally intensive for models of the size of river basins, and this approach is not only necessary, but is an integral part of the concept. Parallel computing has two paradigms in general: message passing (http://www.mpi-forum.org) and shared memory (http://www.ics.uci.edu/javid/dsm.html). In message passing the individual parallel processes exchange data via the computer network. In the shared memory model, parallel processes access one publicly available memory and pass information by coordinated reading and/or writing of the information stored. As the message passing model possesses several advantages, e.g. easy programmability, scalability and portability, we use this paradigm in this study.

In the following we first give a detailed description of the parallelized RHSM and then cover some of the implementation features used within the GeoSys/RockFlow (GS/RF) software platform (Kolditz, 2004; Wang and Kolditz, 2007). We perform a benchmark test for the validation of this implementation and apply it to the Beerze-Reusel area in the Netherlands, where a large scale comprehensive soil property data base was available. Finally, the computational efficiency of the parallelized code is investigated by determining speed-up factors for an increasing number of processors.

MODEL THEORY

Conceptual model

The basic concept of the RHSM is the use of a local one dimensional soil column as an effective model segment that is represented by a mesh of vertical line (finite) elements that approximate the (essentially vertical) movement of water through the three dimensional unsaturated zone. This

one dimensional column approximation is assumed to be valid for a certain lateral extent, the so-called influence area of the vertical column. The influence area may be outlined by a polygon and may be viewed as a function of topography, vegetation, as well as lateral soil profile variability. The origin of the finite element meshes for flow computation is the weight center of the influence area, and its vertical discretization can be made a function of the thickness of each soil layer. Further refinement may also be required due to numerical reasons. This concept is shown in Figure 1. The top of the soil column represents the topographic surface and the bottom is, by definition, the groundwater table. In order to maintain this configuration, the elements can shrink or elongate according to the groundwater table variations. The RHSM itself is the spatial arrangement of the numerous soil columns connected laterally by their respective influence areas. An important assumption of this approach is that flow within soil columns is independent of neighboring soil columns, which neglects lateral flow and is strictly only valid for flat or mildly sloping areas. Lateral flow may be incorporated by the use of prism elements. However, in order to represent lateral flow for large scales reasonably well, the advantage of the coarser discretization using influence areas is lost.

Data model

In order to fill the conceptual RHSM with the parameter information, an interface to a data management system has to be created and integrated into the RHSM framework. The required information is as follows:

- Spatially distributed meteorological time series of precipitation, air temperature and sunshine duration.
- Land-use and vegetation maps.
- A digital elevation model.
- Influence areas as well as soil type profiles (should include a description of pressure-saturation and permeability-saturation relationships; see Figure 1).
- Contaminant concentrations and properties (for additional transport computations only).

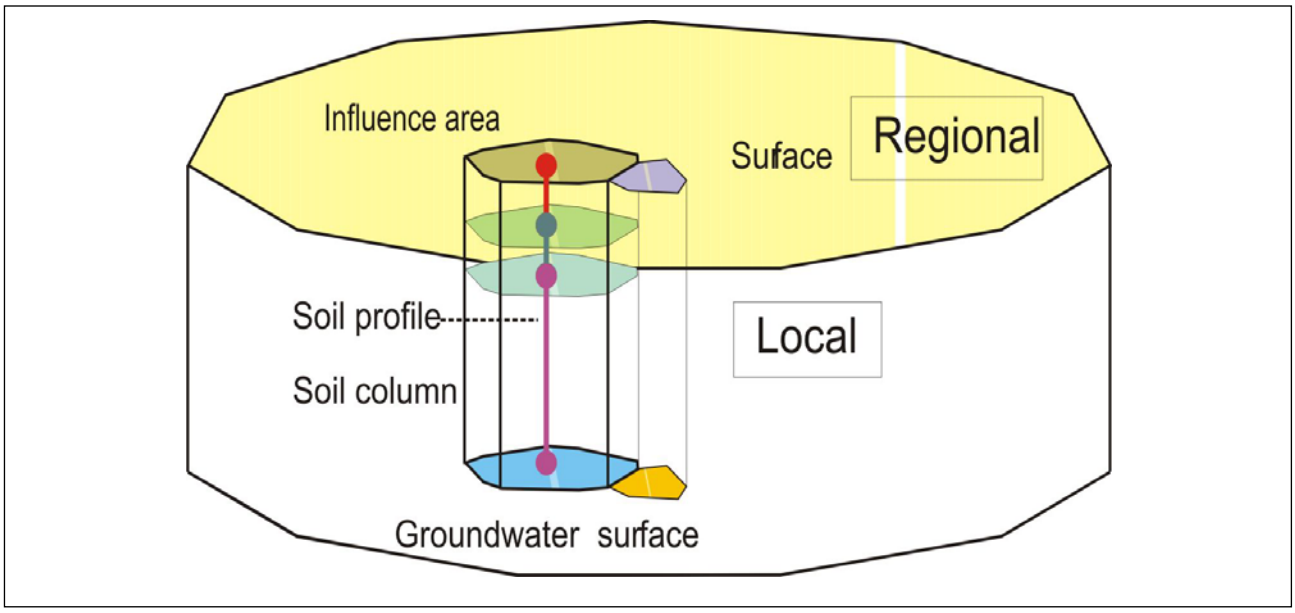

Figure 1. Illustration of the concept of the regional hydrologic soil model.

Mathematical model

The GS/RF software uses the Richards equation for unsaturated water flow computations. The Richards equation is obtained by combining Darcy's law with the law of mass conservation and the assumption that the air phase is at constant atmospheric pressure and not interfering with the water phase. Mathematically, the incompressible and non-deformable pressure-based Richards equation can be written as:

$$n\frac{\partial S}{\partial p}\frac{\partial p}{\partial t}-\nabla\cdot\left(\frac{k_{rel}\mathbf{k}}{\mu}\left(\nabla p-\rho^{l}\mathbf{g}\right)\right)=\frac{Q_p}{\rho} \tag{1}$$

in which n is the soil porosity, S is the soil water saturation, p is the soil water pressure, k_{rel} is the relative permeability, $\mathbf{k}$ is the saturated permeability, μ is the water viscosity, Q_p is a source/sink term, ρ is the water density, $\mathbf{g}$ is the gravitational acceleration, and t is time. Constitutive relationships describe saturation S as a function of (capillary) pressure and relative permeability k_{rel} as a function of S. The exact functional relationships may be obtained either from the empirical expressions given by van Genuchten (1980) or by an explicit description of soil water characteristic curves (SWCC). The SWCC provided in the available database define the functional relationships of $p(S)$ and $k_{\mathrm{rel}}(S)$, neglecting hysteresis, with the effective saturation being

$$S_{eff}=\max\left(0,\frac{S-S_r}{S_{\max}-S_r}\right) \tag{2}$$

where S_r is the residual saturation. The empirical functions for capillary pressure and relative permeability are given by,

$$p=\frac{\rho g}{\alpha}\left(S_{eff}^{1/m}-1\right)^{1-m} \tag{3}$$

and

$$k_{rel}(S)=S_{eff}^{1/2}\left[1-\left(1-S_{eff}^{1/m}\right)^{m}\right]^{2} \tag{4}$$

where α and m are the so-called van Genuchten parameters.

We solve the Richards equation numerically by a Galerkin finite element method. Mass lumping is employed to improve solution convergence and stability behavior. For the time discretization, we use an adaptive time stepping with an embedded error control as given in Kavetski et al. (2001).

Model verification

The implemented solution procedure within GS/RF was verified by a direct comparison to the MIN3P software (Mayer et al., 2002). The comparison was based on a laboratory experiment with soil samples from the Elbe River where pulsed artificial rainfall was applied to a 0.25 m high soil column. The artificial forcing is illustrated in Figure 2 along with the temporal evolution of soil water saturation at three selected observation points (z = 0.25, 0.1, 0.05 m). Within the modeling exercises the hydraulic head at the bottom of the soil column was set to be constantly zero. As shown by the simulation, the solutions of GS/RF are in excellent agreement with those of MIN3P. Additional benchmark results for unsaturated zone water flow using GS/RF can be found in Kolditz et al. (2006).

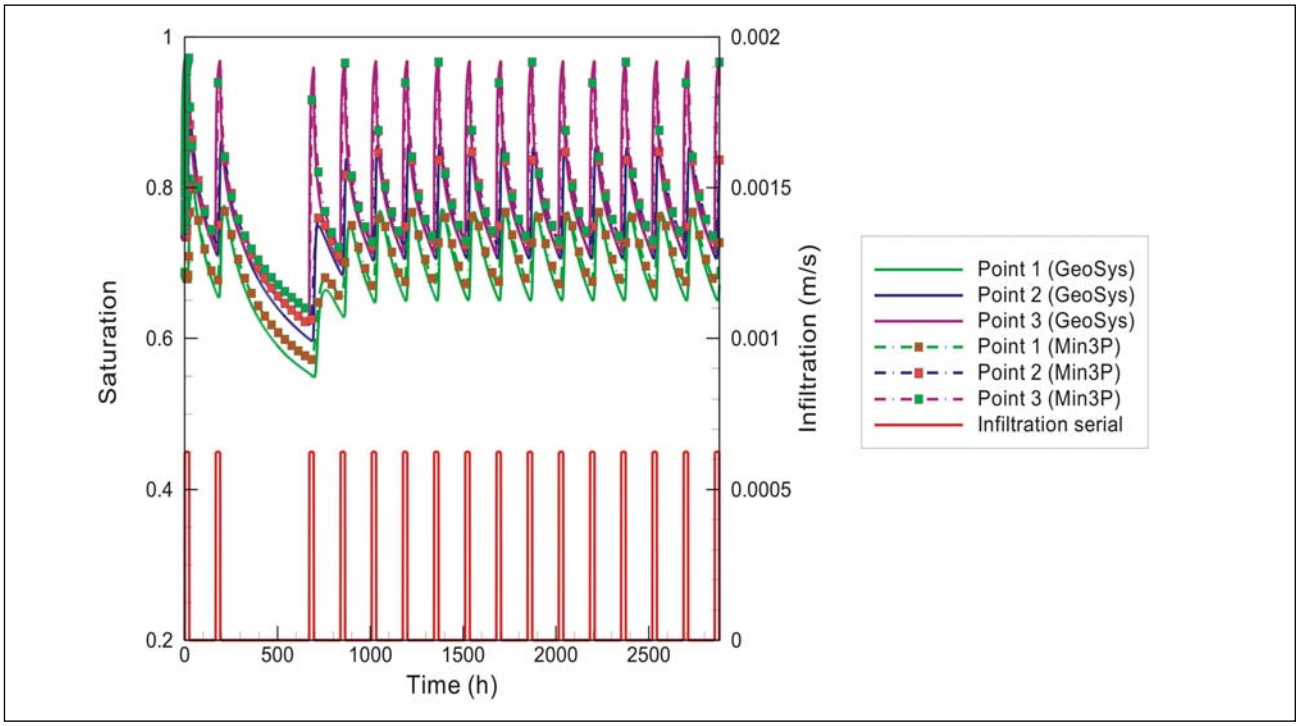

Figure 2. An inter-comparison of MIN3P and GS/RF for a transient Richards problem.

SOFTWARE CONCEPT

Object-orientated programming and implementation

Object-orientated programming understands the software as a collection of objects and their defined interactions. Hereby objects are instances of abstractly defined classes that contain both data (also called properties) and functions (also called methods) to manipulate this data. By this the encapsulation is achieved, as an object's properties can only be accessed by its own methods. Defined interaction between objects (also of objects belonging to different classes) is achieved by one object calling the other object's methods and vice versa. Another fundamental concept is inheritance, where new classes may be defined by inheriting properties and methods from already existing classes. If properly designed, these concepts achieve two of the big advantages of object-orientation: easy extendibility of the software's functionality and code-reuse ability.

In the GS/RF software individual processes are instances of the process class. The RHSM discerns between two process types: a regional (Richards) process and a local (Richards) process as depicted in Figure 1. The regional process defines a regional problem that also comprises components of the boundary condition (BC) object, initial condition (IC) object, source term (ST) object and equation object in its overall solution procedure. The single regional process also collects the geometric diversities inherent to the given local Richards processes. In other words, the definition of the regional Richards process also includes the arrangement of local Richards processes.

Database organization

The RHSM has an interface to a geographic information system, which stores the spatially related data such as influence area location and shape, as well as soil parameter profiles. As the spatial structure of the soil layer may contain numerous different soil types that may vary in complex patterns, an efficient organization of such databases is indispensable. Figure 3 shows the database organization of the RHSM using the ArcGIS software.

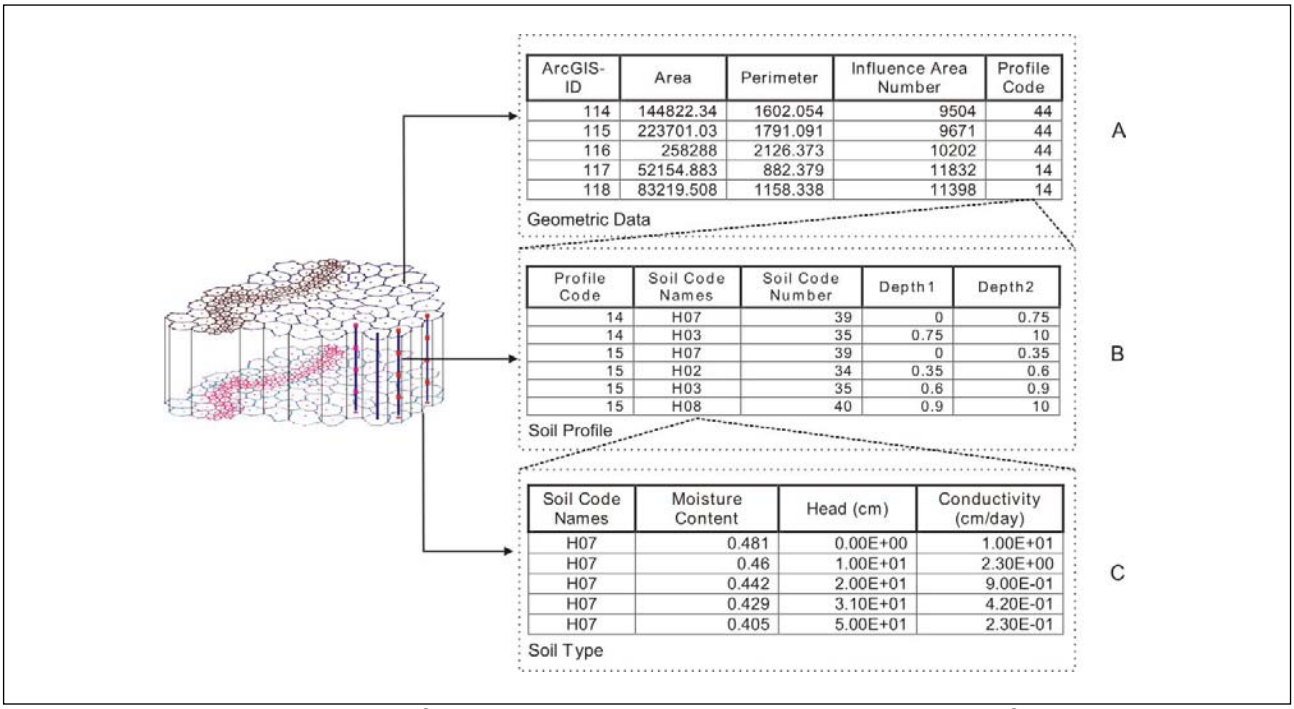

Figure 3. Database organization of RHSM. Data is grouped into (A) topographic information, (B) soil profile, and (C) soil type.

Topographic information. This table contains points and polygons that hold influence area locations and shapes. It is linked to vertical information via the soil profile code. (see Figure 3-A.)

Soil profiles. The soil profile table contains the vertical sequence of soil types with their respective thickness. This table is linked to soil property data via soil code names. (see Figure 3-B.)

Soil types. This basic table holds information on soil type flow characteristics (see Figure 3- C). These can either be given by SWCC or by van Genuchten parameters.

Parallelization approach

In this section the sequence of processing steps for the parallelized RHSM is outlined. The Algorithm 1 illustrates the pseudo-code of distributing the job of *N* loaded local Richards processes and their solution

The GS/RF software is coded in the C++ programming language, which makes inter-processor communication conveniently achievable by adding MPI statements to source code. The MPI implementation used within GS/RF is http://www-unix.mcs.anl.gov/mpi/mpich1. Since each local Richards process is independent, there is no data exchange necessary during computation execution. However, the job scheduling and computational load distribution is handled by the parallelized code. For any given number, P (P > 0), of processors a simple round-robin approach is used: For a total of N local Richards processes we have P-1 groups of v = [N/P] local Richards processes, which have to be calculated sequentially by a single processor. The remaining *mod* (N,P) local Richards processes are distributed to the P^{th} processor. Upon completion of all local Richards processes message passing is carried out to forward the results to the regional Richards process. The parallel scheduling is depicted in Figure 4 and a pseudo-code skeleton is provided in Algorithm 2.

Algorithm 1. Skeleton of regional soil model.

```
Time loop of the simulation
  if Regional and Richards
    Create local Richards processes
    for local Richards k (k ∈ [1, N])
      Load local Richards k: BC, IC, ST
      Solve the non-linear equation for Richards k
    end for
  end if
```

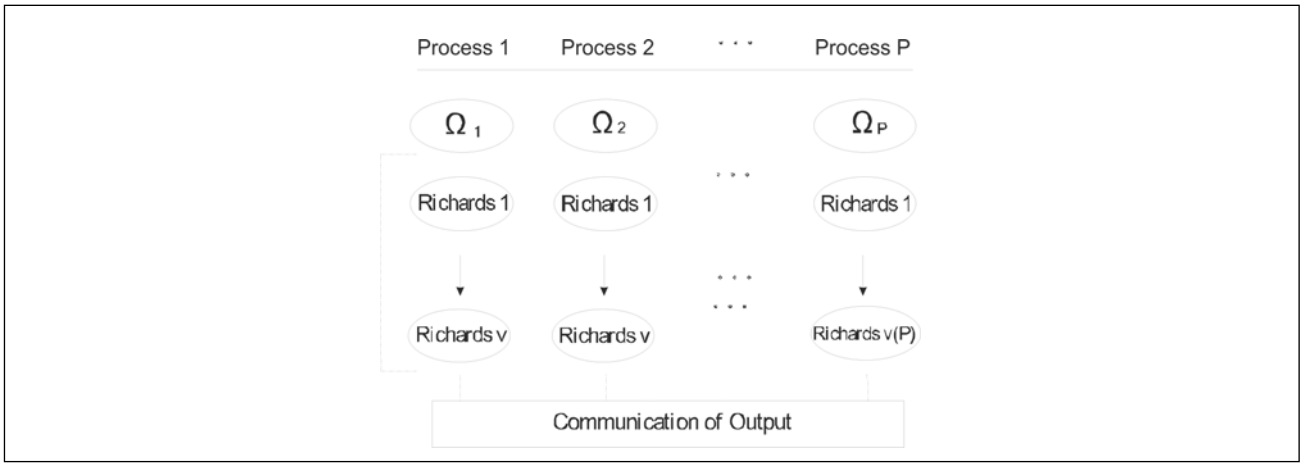

Figure 4. Schematic diagram of the parallel process execution of the RHSM.

Algorithm 2. Skeleton of parallel computation.

```
Time loop of the simulation
  if Regional and Richards
   Create local Richards process
   Divide the set of total Richards processes into P groups
   Start of parallel processing of group i, i ∈ [1, P]
     for local Richards k (k ∈ [1, ν(i)]) in group i
       Load local Richards k: BC, IC, ST
       Solve non-linear equation for local Richards k
       Communicate the computation result to the global space
     end for
   End of parallel processing of group i
  end if
```

Test environment

The application study and preliminary testing of the parallelized RHSM implementation was carried out on a small Linux cluster consisting of four dual-cpu nodes. Each node is equipped with two AMD Opteron 248 processors and four GB of memory. The nodes are connected by a gigabit ethernet. The system has a theoretical peak performance of 35.2 GFlop/s.

APPLICATION OF THE PARALLELIZED RHSM TO THE BEERZE-REUSEL AREA

Geomorphological setting of the basin

The Beerze-Reusel drainage basin belongs to the province of North Brabant which is located in the southern Netherlands. A geographic overview of the basin is given in the bottom inset of

Figure 5. The shallow subsurface geology mainly consists of sandy deposits formed during the Pleistocene. The generally flat region gently slopes towards the direction north/northeast, and spans an elevation range between 45 m MSL (Mean Sea Level) to 3.7 m MSL. There are several aeolian sand ridges of a few meters in height striking west-east. These ridges have a large impact on the morphology of the stream valleys, as they are situated transversely to the general slope and overall drainage pattern. In the valleys alluvial soils have formed consisting of redeposited sand, loam and peat. Because of the intensive agricultural drainage of the areas, these peaty soils are strongly oxidized and have often become very thin. The majority of the area consists of cultivated land with grassland and maize being the most frequently occurring crops.

The soil data for the Beerze-Reusel basin was categorized into more than 12,000 influence areas (Wöster et al., 2001). In the database these are given as GIS polygons whose spatial arrangement is shown in Figure 5 at the top-right corner. In the RHSM each influence area is linked to a vertical column of 40 line elements of uniform size that discretize the generally about 2 m

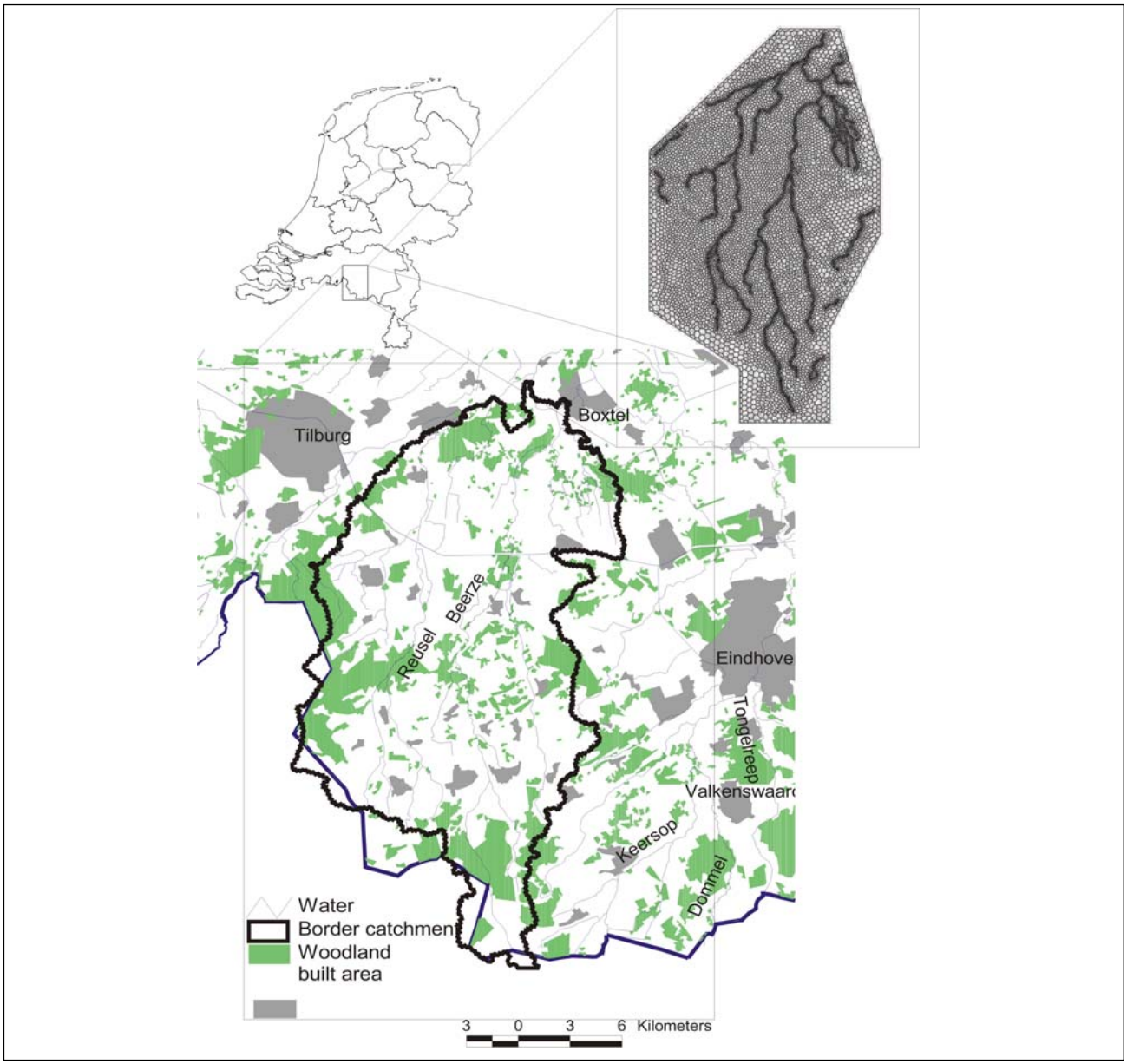

Figure 5. Map of the Meuse basin. Bottom inset shows the detailed map of the region. Top-right inset shows the influence area polygons.

thick soil layer. The database holds the SWCC for each soil type and their vertical arrangement through the model area. There are 56 distinct soil types discerned among the sand, loam and peat soils, which form 62 different soil profiles. The SWCC is pre-processed to describe the different soil properties specifically found in this basin. A complete description of all SWCC can also be found in Du et al. (2006).

Evaporation model

The RHSM simulation is driven by daily meteorological input data (precipitation, air temperature, sunshine duration) of the year 2000 in order to provide for a realistic system forcing. The raw time series data was taken from http://eca.knmi.nl/dailydata/index.php. From these data infiltration time series were calculated for the stations De Bilt, Twenthe, Vlissingen, Eindhoven, and Maastricht and transferred to the influence areas by inverse distance interpolation. By infiltration we refer to precipitation Pc minus potential evaporation E, if Pc > E, and zero infiltration otherwise. Figure 6 shows the precipitation amounts measured at Eindhoven over the year 2000 (top) and the corresponding calculated evaporation (bottom). It is important to note that it is the spatial variability of the infiltration series that makes every single local Richards problem unique in this study, i.e. even though only 62 distinct soil profiles exist, all roughly 12,000 local Richards problems have to be computed in order to achieve the correct regional representation of the Beerze-Reusel soil layer.

Potential evaporation, EMK, is computed by the Makkink method (Makkink, 1957), whose estimates are based on air temperature and the net shortwave radiation, Rs, only. Mathematically the Makkink estimate is defined as,

$$E_{MK} = C_{MK} \frac{1}{\lambda} \frac{R_s s}{s+\gamma} \tag{5}$$

where λ is the latent heat of water evaporation, γ is the psychrometric constant and s is the slope of saturated vapor pressure curve (a function of air temperature). The method assumes a constant ratio between net radiation and net shortwave radiation. The Makkink parameter, CMK = 0.63, was

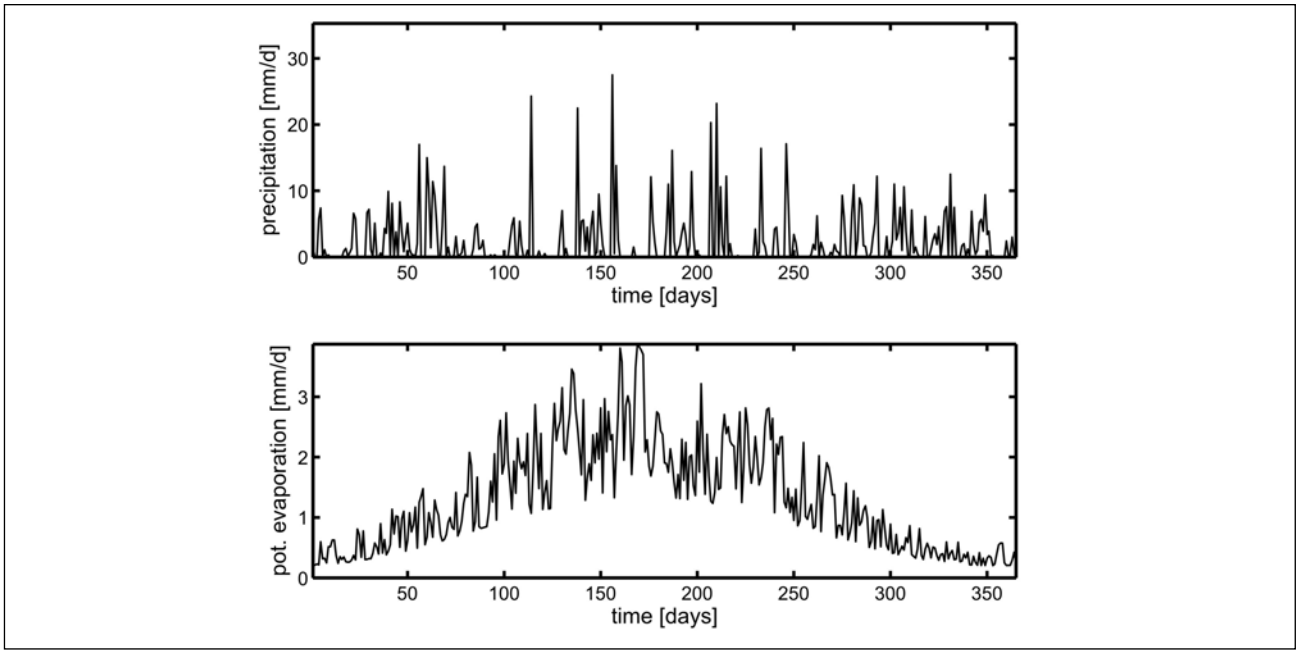

Figure 6. Precipitation and potential evaporation during the year 2000 for station Eindhoven.

chosen according to the findings of van Kraalingen and Stol (1997) for the Netherlands. Daily net shortwave radiation values are calculated based on the equations and recommendations given in Allen et al. (1998). A general albedo parameter of 0.23 is assumed, being representative of wet sand (Buttner and Sutter, 1935; Graser and Bavel, 1982) or dry grey soil (Kondrat'ev, 1954).

Simulation results

Single soil column

From the roughly 12,000 1D Richards problems two examples are shown below in Figure 7 together with their corresponding SWCC (i.e. capillary pressure- and relative permeability-saturation relationships). The top row of Figure 7 represents the functional behavior of a typical soil profile from the north of the basin, whereas the bottom row reflects the characteristics of the central region. Both soil profiles contain vertical changes of soil types (layered soil), hence, changing SWCC.

The simulation illustrates the difference in hydrologic response of both sites, which is mainly attributed to the soil heterogeneity in this case, rather than to the infiltration difference. Nevertheless, the parallelized RHSM provides a general means of computing spatially variable recharge patterns to groundwater created either by soil heterogeneity and/or the variation in water infiltration.

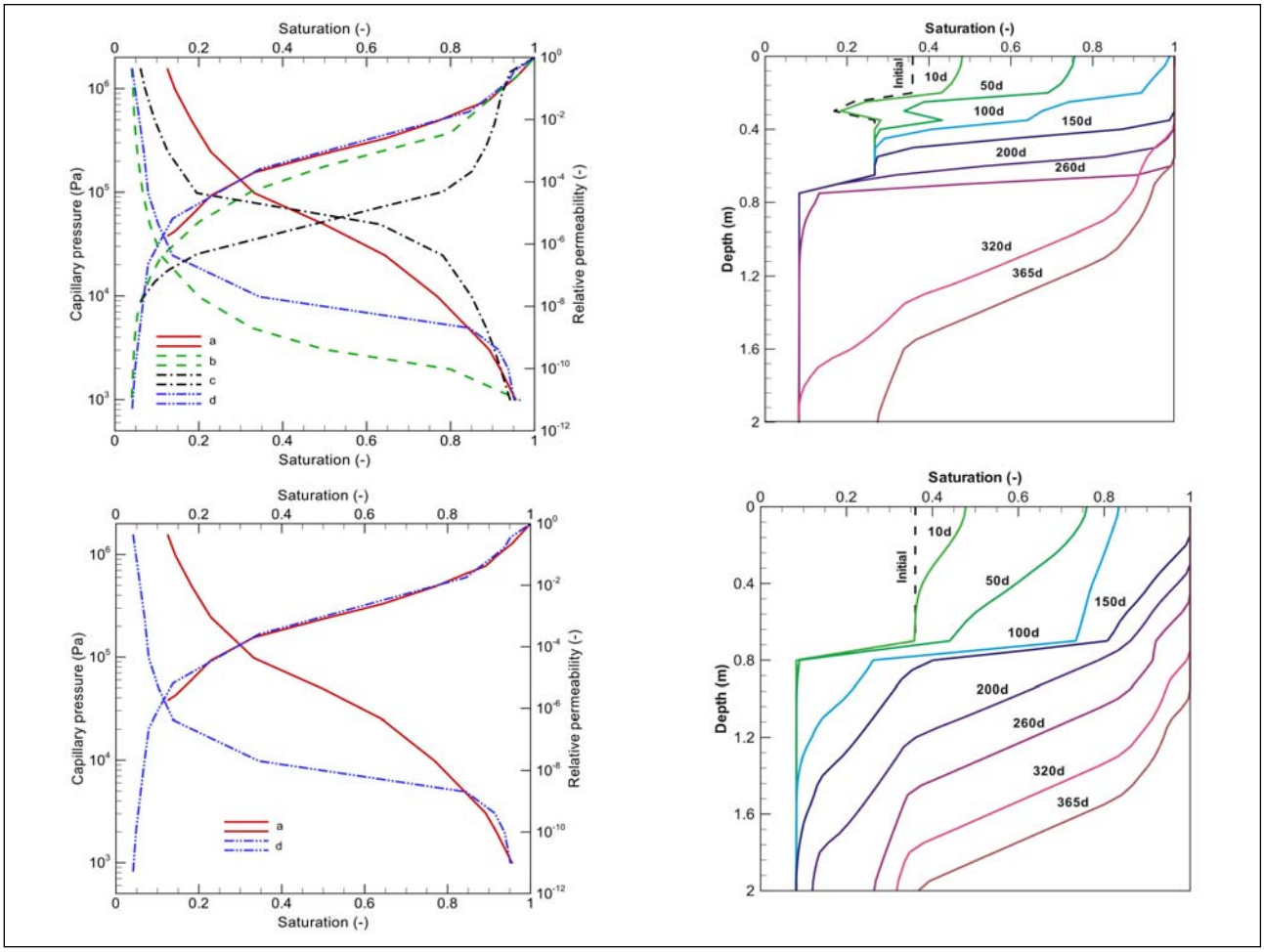

Figure 7. Soil water characteristic curves (SWCC) (left) and evolution of water saturation in selected soil columns (right). Top and bottom rows correspond to different sites of the basin. The time unit for the diagrams on the right is days [d].

Regional soil moisture patterns

The regional evolution of soil moisture patterns is shown in Figure 8 for day 30 and 60 of the year 2000. The influence of the lateral variation of soil profiles on the moisture transfer to the groundwater becomes quite evident, as the spatial variation of infiltration - even though existing - was found to be not so pronounced compared to the soil heterogeneity. Finally, the regional groundwater recharge distribution may be calculated from the bottom node soil water Darcy velocities, which were multiplied by the corresponding influence area for each soil profile.

Analysis of the computational performance

An important aspect of parallel computing is the efficient use of available computing resources. In this section we provide (parallel) computation times for an increasing number of processors and compare them to a serial run of the same problem size. Figure 9 depicts the graph of the functional relation between the measured computation time and the number of CPU's from one to eight and the resulting speed-up factors. It is important to note that the computation time includes also the data collection step at the end of each iteration.

A characteristic feature is that the speed-up factors level off, if more than four CPUs are used. This leveling off is believed to be due to the inherent broadcasting of results at the end of each parallel block. Even though all local Richards processes are set to the same model time period (one year) and number of time steps (366 days), the computation time for the solution of the individual non-linear Richards problems may vary. Considering that the Beerze-Reusel drainage basin consists of more than 12,000 influence areas and over 12,000 different transient boundary conditions, the estimation for the total computation time of individual Richards problems is not easily performed beforehand. This means that some processors may be idle while waiting for the

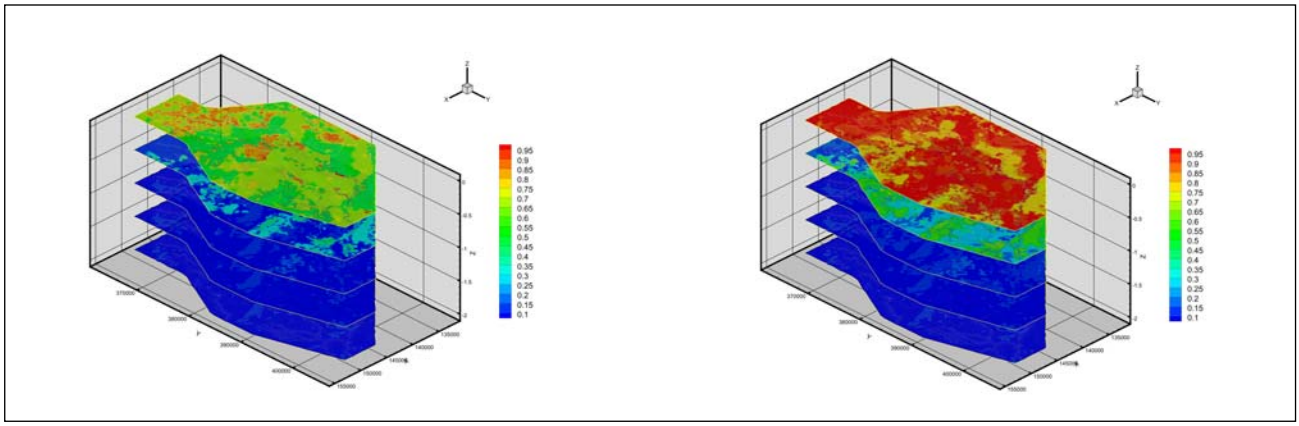

Figure 8. Regional water saturation distribution at days 30 and 60 (left and right, respectively).

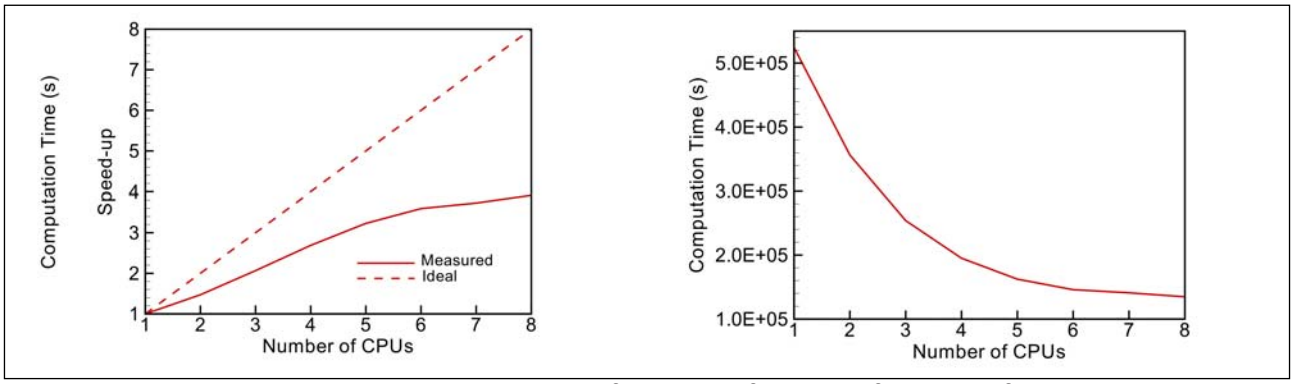

Figure 9. Execution times and resulting speed-up factors as a function of number of CPUs.

other processors to finish. As the parallel computation is only considered to be finished when results from all parallel processes are collected, it is this output aggregation that is believed to be the main cause of the reduction in computational performance. The key to optimize this parallel scheme could be the use of heuristic arguments (e.g. higher non-linearity of SWCC, higher heterogeneity of soil profiles, and higher expected computation times) to estimate computation times. Based on this estimation, the grouping of local Richards processes could be arranged in such a way that approximately the same computation time is necessary for each processor. Nevertheless, the optimal number of CPUs (i.e. four) for the parallel scheme used already reduced the computation time to almost 75% of the sequential (single processor) computation time.

SUMMARY AND CONCLUSIONS

The limitation of large-scale hydrological modeling stems from the requirement for small-scale discretization for accurate flow process representation on the one hand and the large areas to be covered on the other hand. Apart from the limitation in physical computer memory, it is the associated computation times that new computational approaches have to overcome. Within this framework, a RHSM combined with parallel computing techniques is proposed to tackle this problem. The key of the parallelized RHSM is to divide the massive computational demand into smaller computational units and achieve a parallel execution of these using the message passing interface. This study introduced the overall concept and the most important implementation details. A benchmark test showed the accuracy of the implementation by a direct comparison with MIN3P.

For a realistic test application, the Beerze-Reuzel drainage basin was selected for multi-scale hydrological modeling. Modeling this basin posed a challenge, as it covers an area of about 440 km2 of heterogeneous soil with strong lateral variation. Using an evaporation model, as well as daily air temperature, precipitation, and sunshine duration data, infiltration series were calculated to provide a realistic meteorological forcing for the RHSM. Interestingly, the object-oriented programming framework of GS/RF also provided for a flexible integration of the RHSM and the evaporation model. Finally it was possible for the parallelized RHSM to compute the spatio-temporal evolution of soil moisture patterns for this large-scale within reasonable computation times. As a matter of fact, the computation time was reduced by 75% compared to a sequential run using four CPUs on a Linux cluster. The speed-up curve was found to be sub-critical indicating room for better optimization. Although this also demonstrates a limitation of the current approach, the proposed framework does provide a foundation for solving large-scale problems in hydrological systems.

ACKNOWLEDGMENT

This work was funded by the European Union FP6 Integrated Project "AquaTerra"' (Project no. 505428) under the thematic priority "Sustainable development, global change and ecosystem". We are grateful to the Tübingen coordination team especially J. Barth, E. Frank and P. Grathwohl for their expert assistance. We would also like to thank L. Wang for proof reading the manuscript.

REFERENCES

Allen, R.G., L.S. Pereira, D. Raes, and M. Smith. 1998. Crop evapotranspiration: guidelines for computing crop water requirements. FAO Irrigation & Drainage Paper 56. FAO, Rome.

Aral, M.M., and O. Gunduz. 2003. Scale effects in large-scale watershed modeling. In: Yadava, V. P. S. R. N. (Ed.), In advances in Hydrology - Proceedings of the International Conference on Water and Environment: WE-2003. Allied Publishers Pvt. Limited, Bhopal, India, pp. 37-51.

Ashby, S.F., and R.D. Falgout. 1996. A parallel multigrid preconditioned conjugate gradient algorithms for groundwater flow simulations. Nuclear Science and Engineering, Vol. 124(1), pp. 145-59.

Buttner, K., and E. Sutter. 1935. Abkülungsgrößen in den Dunen, Rueckstrahlung verschiedener Bodenbedeckungen. Strahlentherapie, Vol. 54, pp. 156-173.

Clark, D., C. Taylor, and A. Thorpe. 2004. Feedback between the land surface and rainfall at convective length scales. Journal of Hydrometeorology, Vol. 5, pp. 625-639.

Dawson, C.N., H. Klie, M.F. Wheeler, and C.S. Woodward. 1997. A Parallel implicit cell-centred method for two-phase flow with a preconditioned Newton-Krylov solver, Computational Geosciences, Vol. 1, pp. 215-249.

Du, Y., C.M. Bürger, J.O. Delfs, O. Kolditz, B. van der Grift, and C. te Stroet. 2006. Development of a regional soil model for the Beerze-Reuzel area (Meuse). Tech. Rep. 2006-23, Centre for Applied Geoscience, University of Tübingen.

Garden, W.R. 1958. Some steady-state solutions of the unsaturated moisture flow equation with application to evaporation from water table. Soil Sci. Vol 85, pp 228-232.

Gedney, N., and P.M. Cox. 2003. The sensitivity of global climate model simulations to the representation of soil moisture heterogeneity. ASM 301, pp. 216-234.

Govindaraju, R.S., and C. Corradini. 2000. Infiltration over soils with spatially-correlated hydraulic properties. In: Joint Conference on Water Resource Engineering and Water Resources Planning and Management 2000. ASCECP.

Graser, E.A., and C.H.V. Bavel. 1982. The effect of soil moisture upon soil albedo. Agricultural Meteorology, Vol. 27, pp. 17-26.

Green, W.H., and G.A. Ampt. 1911. Studies in soil physics. I. the flow of air and water through soil. Journal of Agriculture Sci., Vol. 4, pp. 1-24.

Gunduz, O. 2004. Coupled flow and contaminant transport modeling in large watershed. PhD thesis, Georgia Institute of Technology, Atlanta.

Hardelauf, H., M. Javaux, M. Herbst, S. Gottschalk, R. Kasteel, J. Vanderborght, and H. Vereecken. 2007. PARSWMS: A parallelized model for simulating three-dimensional water flow and solute transport in variably saturated soils, Vadose Zone Journal, Vol. 6(2), pp. 255-259.

Hurk, V., M. Hirschi, C. Schar, G. Lenderink, and E.V. Meijgaard. 2004. Soil control on runoff response to climate change in regional climate model simulations. Journal of Climate, Vol. 17. pp. 3536-3551.

Jones J.E., and C.S. Woodward. 2001. Newton-krylov-multigrid solvers for large-scale, highly heterogeneous, variably saturated flow problems. Adv. in Water Res., Vol. 24, pp. 763-774.

Kavetski, D., P. Binning, and S.W. Sloan. 2001. Adaptive time stepping and error control in a mass conservative numerical solution of mixed form of Richards equation. Adv. in Water Res, Vol. 24, pp. 595-605.

Kollet, S.J., and R.M. Maxwell. 2006. Integrated surface-groundwater flow modeling: A free-surface overland flow boundary condition in a parallel groundwater flow model. Adv. in Water Res., Vol. 29(7), pp. 945-958.

Kollet, S.J., and R.M. Maxwell. 2008. Capturing the influence of groundwater dynamics on land surface processes using an integrated, distributed watershed model, Water Res. Res. Vol. 44: W02402.

Kolditz, O. 2002. Computational methods in environmental fluid mechanics. Springer.

Kolditz, O., and S. Bauer. 2004. A process-oriented approach to computing multi-field problems in porous media. Journal of Hydroinformatics, Vol. 6, pp. 225-244.

Kolditz, O., W. Wang, J. Hesser, Y. Du, and Shao, H. 2006. GeoSys/RockFlow Benchmarking. Centre for Applied Geoscience, University of Tübingen.

Kondrat'ev, K.Y. 1954. The radiant energy of the sun, Chapter 9, Albedo of the underlying surface and clouds. English summary by A. Kurlent and P. Larson. McGill University, Leningrad.

Levy, B.S., and P.F. German. 1988. Kinematic wave approximation to solute transport along preferred flow paths in soils. Journal of Contaminant Hydrology, Vol. 3, pp. 263-276.

Lighthill, M.J., and G.B. Whitham. 1955. On kinematic waves, I. flood movement in long rivers. In: Proc. Royal Soc. of London, Ser. A. pp. 281-316.

Makkink, G.F. 1957. Testing the Penman formula by means of lysimeters. International Journal of Water Engineering, Vol. 11, pp. 277-288.

Mayer, K.U., E.O. Frind, and D.W. Blowes. 2002. Multicomponent reactive transport modeling in variably saturated porous media using a generalized formulation for kinetically controlled reactions. Water Res. Res., Vol. 38, pp. 1174-1195.

Mein, R.G., and C.L. Larson. 1973. Modeling infiltration during a steady rain. Water Res. Res., Vol. 9, pp. 384-394.

Milly, P.C.D. 1988. Advances in modeling of water in the unsaturated zone. Transport in Porous Media 3, pp. 1573-1634.

Ogden, F.L., and B. Saghafian. 1997. Green and ampt infiltration with redistribution. Journal of Irrigation and Drainage Engineering, Vol.123, pp. 386-393.

Patton, E.G., P.P. Sullivan, and C.H. Moeng. 2005. The influence of idealized heterogeneity on wet and dry planetary boundary layers coupled to the land surface. Journal of Atmospheric Sci., Vol. 62, pp. 2078-2097.

Philip, J.R. 1968. Steady infiltration from buried point sources and spherical cavities. Water Res. Res., Vol. 4, pp. 1038-1047.

Philip, J.R. 1992. What happens near a quasi-linear point source? Water resources research, Vol. 28, pp. 47-52.

Prasad, S.N., and M.J.M. Romkens. 1982. An approximate integral solution of vertical infiltration under changing boundary conditions. Water Res. Res., Vol. 18, pp. 1022-1028.

Ren, L., and F. Yuan. 2005. The Xin'anjiang model on digital basin platform. Taylor and Francis.

Schaer, C., D. Luethi, and U. Beyerle. 1999. The soil-precipitation feedback: A process study with a regional climate model. Journal of Climate, Vol.12, pp. 772-741.

Schüze, N., G. Schmitz, and U. Petersohn. 2005. Self-organizing maps with multiple input-output options for modeling the Richards equation and its inverse solution. Water Res. Res., Vol. 41, W03022.

Segol, G. 1993. Classic groundwater simulations: Proving and improving numerical models. Prentice-Hall, Inc.

Singh, V.P. 1997. Kinematic Wave modelling in water resources, Environmental Hydrology. CRC, USA.

Smith, R.E. 1983. Approximate soil water movement by kinematic characteristics. Soil Science Society of America Journal, Vol. 47, pp. 3-8.

Srinivasan, R., and V. Lakshmi. 2005. Simulation of water and energy budgets using a macroscale hydrological model for the upper Mississippi river basin. Taylor and Francis.

Stamm, J.F., F.W. Eric, and P.L. Dennis. 1994. Sensitivity of a GCM simulation of global climate to the representation of land-surface hydrology. Journal of Climate, Vol. 7, pp. 1218-1239.

Troch, P., C. Paniconi, and E. van Loon. 2003. Hillslope-storage Boussinesq model for subsurface flow and variable source areas along complex hillslopes: 1. Formulation and characteristic response. Water Res. Res., Vol 39, pp. 1316-1329.

Troch, P., E. van Loon, and A. Hilberts. 2002. Analytical solutions to a hillslope storage kinematic wave equation for subsurface flow. Adv. Water Resource, Vol. 25, pp. 637-649.

van Genuchten, M.T. 1980. A closed-form equation for predicting the hydraulic conductivity of unsaturated soil. Soil Science Society of America Journal, Vol. 44, pp. 892-898.

van Kraalingen, D.W.G., and W. Stol. 1997. Evapotranspiration modules for crop growth simulation - implementation of the algorithms from Penman, Makkink and Priestley-Taylor. Quantitative Approaches in Systems Analysis 11.

Walker, J.P., and P.R. Houser. 2001. A methodology for initializing soil moisture in global climate model: Assimilation of near-surface soil moisture observations. Journal of Geophysical Research, Vol. 106, pp. 11761-

11774.

Wang, W., and O. Kolditz. 2007. Object-oriented finite element analysis of thermo-hydro-mechanical (THM) problems in porous media. International Journal of Numerical Methods in Engineering, Vol. 69, pp.162-201.

Wösten, J.H.M., G.J. Veerman, W.J.M. de Groot, and J. Stolte. 2001. Water retention and conductivity characteristics of upper en deeper soil layers in the Netherlands (in Dutch). Alterra report, pp.153.

Yeh, T.C., R.T. Wetherald, and S. Manabe. 1984. The effect of soil moisture on the short-term climate and hydrology change—a numerical experiment. Monthly Weather Review, Vol. 112(3), pp. 470-490.

ADDRESS FOR CORRESPONDENCE
Yanliang Du
School of Engineering
University of Plymouth
Drake Circus
Plymouth, PL48AA
UK

Email: yanliang.du@plymouth.ac.uk

Enclosed Publication

[EP4] C.-H. Park, **J.-O. Delfs** and O. Kolditz (2008): *Particle tracking of Cryptosporidium oocysts from surface to groundwater*, Groundwater quality 2007 proceedings, IAHS Publication 324, 47-54.

GQ07: Securing Groundwater Quality in Urban and Industrial Environments (Proc. 6th International Groundwater Quality Conference held in Fremantle, Western Australia, 2–7 December 2007). IAHS Publ. no. XXX, 2008.

Particle tracking of *Cryptosporidium* oocysts from surface to groundwater

C.-H. PARK[1], J.-O. DELFS[2] & O. KOLDITZ[1]

1 *Department of Environmental Informatics, Helmholtz Centre for Environmental Research – UFZ, Permoser str. 15, D-04318 Leipzig, Germany*
chanhee.park@ufz.de

2 *Center for Applied Geoscience, University of Tübingen, D-72076, Germany*

Abstract The fate and transport of *Cryptosporidium parvum* oocysts affecting groundwater involves processes at the surface and in the subsurface which are impacted by hydrological events and human and animal activities. In these coupled systems, numerical modelling is crucial to assess how oocysts deposited at the surface may influence the quality of groundwater. Describing the oocysts as microbial colloidal particles, we can obtain travel paths and the viability of oocysts using a random walk particle tracking (RWPT) method in a coupled flow system. The coupled flow system consists of overland flow and flow in variably saturated media. The interaction between two media is handled through coupling fluxes. For the given hydraulic and oocyst conditions, rapid oocyst transport is observed into groundwater, and oocysts traced remain viable for a long period in the aquifer.

Key words *Cryptosporidium parvum* oocysts; random walk particle tracking; Richard's flow; coupled hydrosystem; groundwater contamination

INTRODUCTION

Cryptosporidium parvum has been implicated in a number of waterborne disease outbreaks. The biggest outbreak occurred in Milwaukee in 1993 and infected more than 400 000 people. Because oocysts have a resilient wall that allows them to survive under various environmental stresses, *C. parvum* remains infective in both surface and groundwater (Schijven *et al.*, 2004). In river water it is reported to be viable for more than a month, even under severe winter conditions in Norway (Robertson & Gjerde, 2006). Depending on the surrounding environment, the viability of oocysts varies significantly. Given the relatively stable environment typical for groundwater, it is logical to expect that oocyst viability may be prolonged.

Transport of oocysts from the ground surface to deeper soil layers, and ultimately to the water table, is generally similar to the filtration process in water treatment plants. However, difficult source quantification (i.e. delineating deposition by live-stock), transport in variably-saturated porous media by infiltration (subject to hydrol-ogical events), and complex soil materials multiply the complexity of the transport process. In addition, the subsurface environment contains significant geometric and geochemical pore-scale heterogeneities. This heterogeneous environment impacts oocysts both physically and geochemically.

This paper describes the fate and transport of *C. parvum* oocysts from surface to subsurface in an hydrological-event-oriented manner. Treating oocysts as microbial

colloidal particles and using the particle tracking (PT) method, we demonstrate the detailed life of oocysts responding to hydrological events. The objective of the paper is to establish a new method of investigating waterborne pathogen behaviour in the hydrosystem, and apply it to understanding the physical and chemical processes affecting *C. parvum* oocysts in regional groundwater aquifers. A hypothetical scenario has been developed to assess the risk of groundwater contamination by waterborne pathogens subsequent to hydrological events.

THEORY

This study makes use of the coupled overland/soil flow model implemented in GeoSys/RockFlow code (Kolditz & Bauer, 2004). The model consists of a diffusive-wave overland flow model and Richards's soil water flow model for variably saturated subsurface flow. For coupling, a thin interface layer is assumed, and a coupling flux is calculated. The random walk particle tracking (RWPT) method is fully integrated into these models to describe fate and transport of oocysts.

Coupled overland/soil water flow model

Infiltration into the soil column is modelled by using a compartment where overland flow and Richards flow are coupled by exchange fluxes. The governing equation for overland flow runoff is the diffusive wave equation as follows:

$$\frac{\partial h^o}{\partial t} - \nabla \cdot \left(\mathbf{K^o} \nabla h^o \right) = R - I \tag{1}$$

where h^o is the water head in overland flow [L], $\mathbf{K^o}$ is the diffusive coefficient tensor [LT^{-1}], R is the rainfall rate [LT^{-1}], and I is the infiltration rate [LT^{-1}]. To represent wide shear flow (runoff), we used the Chezy equation:

$$V = C R_H^{\frac{1}{2}} S_o^{\frac{1}{2}} \text{ where } C = \sqrt{\frac{8g}{f}} \tag{2}$$

Here, V is the overland flow velocity [LT^{-1}], C is the Chezy coefficient [$L^{1/2}T^{-1}$], R_H is the hydraulic radius [L], S_o is the slope of runoff surface [-], g is the gravitational acceleration coefficient [LT^{-2}], and f is the Darcy-Weisbach friction factor [-]. Assuming that the momentum equation is applied to steady laminar uniform wide sheer flow, the hydraulic radius becomes the water depth for wide sheer flow. If this is the case, the diffusive coefficient can be derived as follows:

$$K^o = \frac{8g}{C_L \nu} H^3 \text{ where } C_L = 24 + 27.162 R^{0.407} \tag{3}$$

where $H = h - z - a$ is the water depth [L], z is the ground surface elevation [L], a is the interface layer thickness [L], C_L is the coefficient for the function of rainfall [-], and ν is the kinematic viscosity [L^2T^{-1}].

As for flow in variably saturated porous media, Richards's equation is solved with the van Genuchten model.

$$\phi \frac{\partial S}{\partial t} - \frac{\partial}{\partial z}\left[\frac{k k_r \rho}{\mu}\left(\frac{\partial h}{\partial z}\right)\right] = I \tag{4}$$

where ϕ is the porosity [-], S is the saturation ratio [-], k and k_r are the permeability and relative permeability of soil [L^2], respectively, and h is the hydraulic head. Using the saturation and residual saturation ratios, the effective saturation is given by:

$$S_e = \max\left(0, \frac{S - S_r}{1 - S_r}\right) = \left[\frac{1}{1 + \left(\alpha |h - z|\right)^n}\right]^m \tag{5}$$

where S_r is the residual saturation ratio [-], α is the parameter of a characteristic pore size [L^{-1}], n is the uniformity of the pores [-], and $m = 1 - 1/n$. The van Genuchten functional relationship for relative permeability as a function of the saturation ratio is given by:

$$k_r(S) = S_e^{\frac{1}{2}}\left[1 - \left(1 - S_e^{\frac{1}{m}}\right)^m\right]^2 \tag{6}$$

Coupling between overland and subsurface

To determine the infiltration rate in equation (1) from overland to subsurface, we assume a thin interface layer between overland and soil, and calculate a coupling flux as in VanderKwaak (1999):

$$I = -K_I \frac{\psi - H}{a} \tag{7}$$

where ψ is the capillary pressure head [L] and K_I is the relative coupling conductivity [LT^{-1}]. The coupling conductivity is given by:

$$K_I = S_I^{2(S_I - 1)} K \tag{8}$$

where $S_I = H/a$ is the ratio of the water depth to the interface layer thickness [-] and K is the soil conductivity. In this paper, we use the saturated soil conductivity to calculate the relative coupling conductivity. Richard's flow and overland flow elements that share the coupling term are solved iteratively until the water head in overland flow and the pressure in Richard's flow converge.

Transport model

One-dimensional transport of *C. parvum* oocysts for a colloid filtration model can be described using the following expression:

$$\frac{\partial c}{\partial t} + \frac{\rho_b}{\theta}\frac{\partial s}{\partial t} = v\alpha_L \frac{\partial^2 c}{\partial x^2} - v\left(\frac{\partial c}{\partial x} + \lambda c\right) \tag{9}$$

where c is the concentration of *C. parvum* oocysts in water, s is the concentration of the oocysts adsorbed on grain surfaces, ρ_b is the bulk density, θ is porosity, α_L is the hydrodynamic dispersivity coefficient, v is the advective pore velocity, and λ is the

colloid filtration coefficient. The filtration coefficient is determined by:

$$\lambda = \frac{3(1-\theta)}{2d_c}\alpha\eta \tag{10}$$

where d_c is the median grain size diameter, α is an empirical coefficient referred to as collision efficiency, and η is the single-collector efficiency.

The random walk particle tracking (RWPT) method

The stochastic differential equation equivalent to equation (1) in two dimensions can be written as (Hassan & Mohamed, 2003):

$$\begin{aligned} x_{t+\Delta t} &= x_t + \left(v_x(x_t, y_t) + \frac{\partial D_{xx}}{\partial x} + \frac{\partial D_{xy}}{\partial y} \right)\Delta t + \sqrt{2D_{xx}\Delta t}Z_1 + \sqrt{2D_{xy}\Delta t}Z_2 \\ y_{t+\Delta t} &= y_t + \left(v_y(x_t, y_t) + \frac{\partial D_{yx}}{\partial x} + \frac{\partial D_{yy}}{\partial y} \right)\Delta t + \sqrt{2D_{yx}\Delta t}Z_1 + \sqrt{2D_{yy}\Delta t}Z_2 \end{aligned} \tag{11}$$

where x and y are the coordinates of the particle location, Δt is the time step, and Z_i is a random number whose mean is zero and variance is one.

To add reversible attachment of oocysts to a sorption–desorption process that represents geochemical effects, the two-rate model from Johnson (1995) is used:

$$N/N_0 = Ae^{-k_1 t} + (1-A)e^{-k_2 t} \tag{12}$$

where N is the number of oocysts attached to soil media at time t, N_0 is the initial number of oocysts from the surface, k_1 and k_2 are the fast and slow sorption rate coefficients and A is a weighting factor. Only oocysts detached from the soil matrix are transported by groundwater. The rate constants and the weighting factor are the parameters determined empirically. These parameters represent the geochemical effects and water solution chemistry deeply analysed by Bradford *et al*. (2007). Although the two-rate model is used in this paper, various different detachment models can also be used. Note that we used the two-rate model for the fraction of oocysts bound to the soil matrix as a rate-limited sorption function. This produces asymmetry and tailing in the breakthrough curve as observed in Harter *et al.*'s experiment (Harter *et al*., 2000).

As for permanent removal, *C. parvum* removal in groundwater is conceptually different from permanent removal by filtration in water treatment plants. Subsurface media, such as river banks or aquifers, are thought to act as natural filters that capture *C. parvum* for a long time so that most oocysts that reach the well are no longer viable. This is based on the assumption that although oocysts are resistant to environmental stresses, they remain in subsurface media for long enough that they completely die off. Therefore, we used an exponential viability function to model the time-dependent die-off of oocysts. This function is applied to both adsorbed and desorbed oocysts in the medium. In addition to permanent filtering (trapping), as in the filtration model in a water treatment plant, the die-off rate model is incorporated as a first-order rate irreversible reaction that represents filtering and die-off simultaneously:

$$N/N_0 = e^{-\lambda_T t} \tag{13}$$

where $\lambda_T = \lambda + k_d$, λ_T is the combined removal rate coefficient, and k_d is the die-off rate coefficient. Note that the filtration coefficient in (9) is combined with the die-off coefficient in transport from surface to groundwater in the aquifer and is the only term that removes *C. parvum* oocysts permanently.

SENARIO DESCRIPTION

This scenario has been carefully prepared to generate hydrological-event-oriented flow and transport. The model domain represents a portion of an unconfined sand aquifer with dimensions of 10 m width, by 6 m depth from surface. The model initially has a 5-m deep groundwater table. The aquifer surface is subject to a severe continuous rainfall event at 0.36 m/h. This rainfall continues for the duration of the simulation, which ends at about when the water front from the surface meets the groundwater table rising from the bottom of the model domain. To allow modelling of the movement of both water fronts due to infiltration, no fixed pressure head boundary conditions are used. Instead, infiltration is coupled between overland flow and Richards flow and assessed as a source term as described previously. A schematic of the modelling scenario is given in Fig. 1.

One important modelling parameter that changes *C. parvum* transport behaviour significantly, is the dispersivity of the aquifer. To exclude the effects of the dispersivity, we intentionally set dispersivity low to minimise its effect on transport. This allows us to focus on other factors that affect the behaviour of *C. parvum* transport. Despite defining a very low dispersivity, it is not necessary to define an extremely fine grid to avoid problems of numerical dispersion and instability. This is one of the advantages of the RWPT method.

Setting the dispersivity aside, we focus on geochemical, geometrical, and microbio logical parameters and their impact on viable oocysts. The geochemical effects are represented by the rate-limited sorption–desorption process. Geometrical (filtering) and die-off effects are represented by the combined irreversible removal rate model. Note that

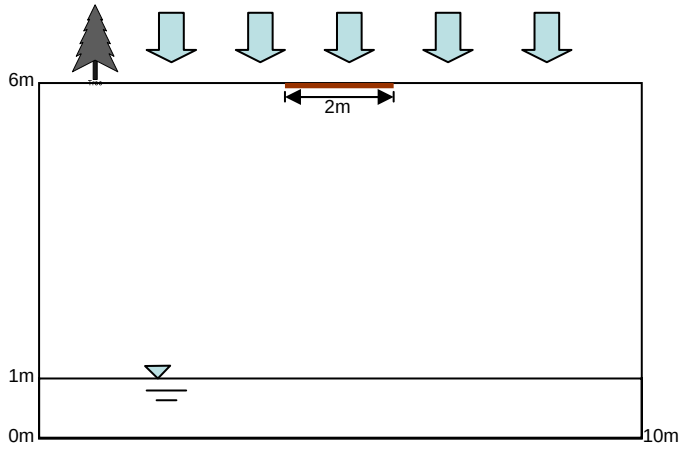

Fig. 1 Simplified diagram for Hortonian coupled flow and oocyst transport.

the overall history of travel experience by individual particles can be obtained fully by the RWPT method. The modelling parameters for flow and transport are summarized in Table 1.

Table 1 Modelling parameters for flow and transport.

Subsurface soil parameters:		Sorption-desorption parameters	
α	5.6 m^{-1}	A	0.99 [-]
n	0.316 [-]	k_1	0.1 min^{-1}
S_r	0.051 [-]	k_2	0.001 min^{-1}
θ	0.43 [-]	Oocyst parameters	
k	5.04×10^{-12} m^2	Number of particles	10 000 [-]
α_L	2.0×10^{-4} m	k_d	8.334×10^{-6} min^{-1}*
α_T	2.0×10^{-5} m	λ	5.92×10^{-4} min^{-1}

* The value is taken from Robertson (1992).

COUPLED FLOW AND OOCYST TRANSPORT

When the infiltration rate falls below the precipitation rate, ponding occurs. Initially, the soil pressure term is high in the coupling flux calculation and the relative coupling conductivity keeps the infiltration rate slightly below the precipitation rate. Soil moisture increases rapidly and water accumulates slowly on the surface. In addition to the downward progression of this wetting front, the water table also rises slowly. The movement rates of these two water fronts are different. In the given set of hydraulic conditions, we observe that the movement of the surface water front is faster than the groundwater table rise. The resulting time-dependent pressure and saturation development in the vertical direction is depicted in Fig. 2.

Figure 2 shows the aquifer becoming saturated from the top down and the bottom up, with an ever-decreasing unsaturated area in-between. This unsaturated zone is still under negative pressure head that generates capillary suction. As infiltration continues, the unsaturated zone diminishes until the two water fronts finally meet.

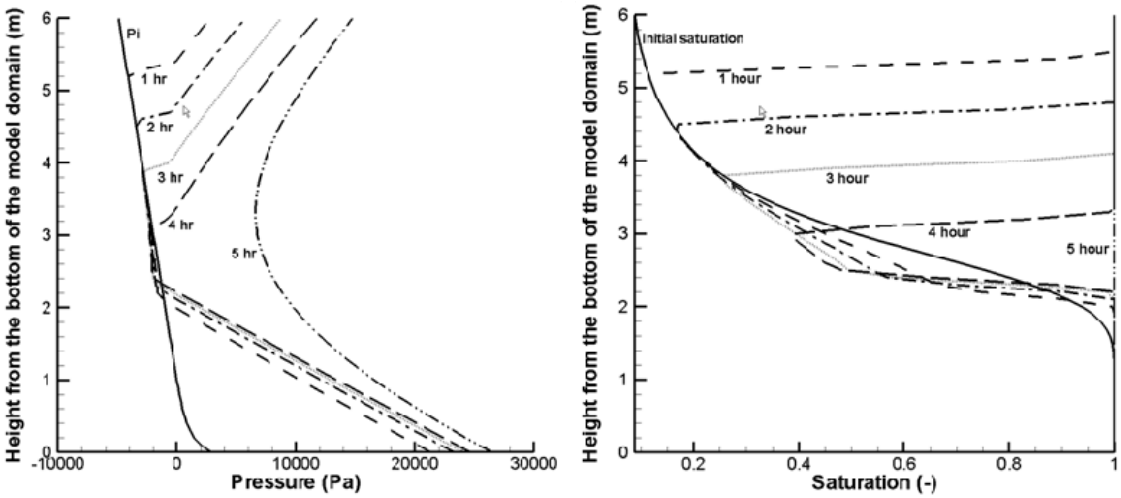

Fig. 2 Pressure and saturation development in response to Hortonian flow.

C. parvum oocysts are initially placed at a depth of 5 cm in the soil so as not to be washed away by the overland flow generated during the rainfall event. As soon as rainfall generates infiltration, these oocysts (represented as particles) are transported and experience sorption and desorption, trapping (filtration), and die-off processes at the pore scale. The sorption–desorption process is time-convoluted with transport such that anomalous transport occurs. This retardation is governed by the two-rate model equation (12). Since the two-rate model is a function of residence time with three fitting parameters, these parameters should be determined by field measurement.

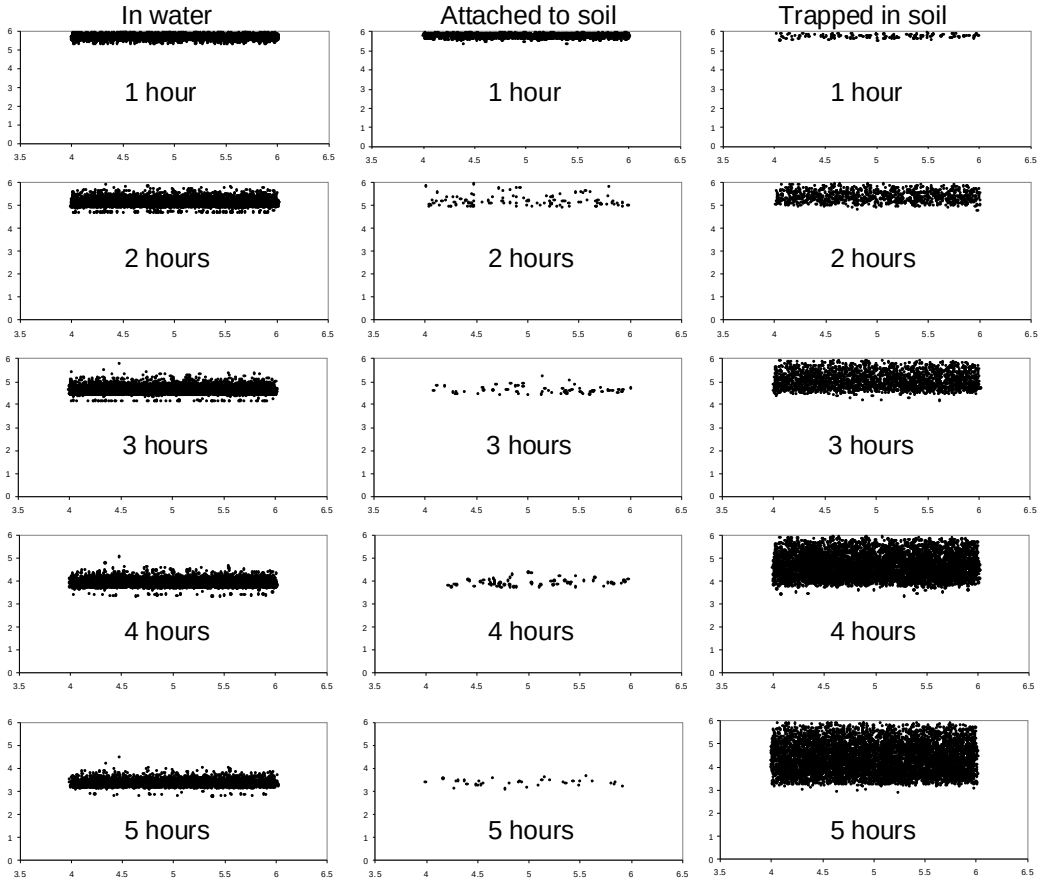

Fig. 3 Hourly oocyst distributions at various states: oocysts in water, oocysts temporarily attached to the soil matrix, and oocysts trapped in micro pores or inactivated by die-off.

Those oocysts trapped in micro pores or inactivated by die-off are interpreted as permanently removed. Due to the longevity of oocyst viability, none of oocysts died within the given simulation time. Instead, they were mostly trapped or filtered out as in water plant filtration. The proportion of trapped oocysts increased with increasing travel distance. Therefore, river banks may be one of the natural barriers preventing oocysts from reaching water courses. Nevertheless, these trapped oocysts can be reversed back to travel if flow conditions are changed (i.e. water flow direction change). For instance, if pumping is practised near trapped oocysts, viable oocysts can easily be pumped out by increasing the pumping rate and the resulting shear forces. Oocysts are also known to be flexible enough to pass through pores smaller than the size of oocysts (Park & Huck, 2003). Therefore, filtration in the aquifer is not truly a

permanent removal process, unlike in water plant filtration. However, die-off is still a true permanent removal process. Figure 3 shows five hourly snapshots of oocysts in various states. These states are oocysts in water, attached to the soil matrix temporarily and permanently trapped or dead.

CONCLUSIONS

The objective of this simulation work was to investigate the fate and transport of *C. parvum* oocysts in a hydrosystem in which there is coupling between surface and subsurface flow systems. The results indicate that transport of oocysts through the unsaturated zone to the groundwater table can be very rapid. Indeed, in the selected hypothetical case study it takes less than five hours for a significant proportion of oocysts to reach the aquifer. Due to geochemical and geometrical interactions between the soil matrix and oocyst particles at the pore scale, anomalous transport is observed in the homogeneous sand aquifer even with relatively low dispersivities set in the model. Given the chosen hydrological event, all the oocysts from the surface were transported to the subsurface system. A significant proportion of oocysts were trapped along the transport paths, but no oocysts died within the time frame of the hydrological event. Thus, the oocysts trapped in the soil still remain viable and impose a potential long-term threat to groundwater and ultimately drinking water quality.

Acknowledgements The authors gratefully acknowledge the support of the European Union Integrated Project "AquaTerra" and constructive comments offered by Robert Walsh at the University of Tübingen.

REFERENCES

Bradford, S. A., Torkzaban S. & Walker S. L. (2007) Coupling of physical and chemical mechanisms of colloid straining in saturated porous media. *Water Res.* **41**(13), 3012–3024.

Harter, T., Wagner, S. & Atwill, E. R. (2000) Colloid transport and filtration of *Cryptosporidium parvum* in sandy soils and aquifer sediments. *Environ. Sci. Technol.* **34**(1), 62–70.

Hassan, A. E. & Mohamed, M. M. (2003) On using particle tracking methods to simulate transport in single-continuum and dual continua porous media. *J. Hydrol.* **275**(3-4), 242–260.

Johnson, W. P., Blue, K. A. & Logan, B. E. (1995) Modeling bacterial detachment during transport through porous media as a residence-time-dependent process. *Water Resour. Res.* **31**(11), 2649–2658.

Kolditz, O. & Bauer, S. (2004) A process-oriented approach to computing multi-field problems in porous media. *J. Hydroinfo.* **6**(3), 225–244.

Park, C.-H. & Huck, P. M. (2003) A conceptual model for *Cryptosporidium* transport in watersheds. *Water Qual. Res. J. Can.* **38**(1), 77–113.

Robertson, L. J., Campbell, A. T. & Smith, H. V. (1992) Survival of *Cryptosporidium-Parvum* oocysts under various environmental pressures. *Appl. Environ. Microbiol.* **58**(11), 3494–3500.

Robertson, L. J. & Gjerde, B. K. (2006) Fate of *Cryptosporidium* oocysts and *Giardia* cysts in the Norwegian aquatic environment over winter. *Microbial Ecol.* **52**(4), 597–602.

Schijven, J. F., Bradford, S. A. & Yang, S. H. (2004) Release of *Cryptosporidium* and *Giardia* from dairy cattle manure: Physical factors. *J. Environ. Qual.* **33**(4), 1499–1508.

VanderKwaak, J. E. (1999) Numerical simulation of flow and chemical transport in integrated surface–subsurface hydrologic systems. Ph D Thesis, University of Waterloo Dept. of Earth Sciences, Waterloo, Canada.

Enclosed Publication

[EP5] O. Kolditz, Y. Du, C. M. Bürger, **J.-O. Delfs**, D. Kunz, M. Beinhorn, M. Hess, W. Wang, B. van der Grift and C. te Stroet (2007): *Development of a regional hydrologic soil model and application to the Beerze-Reusel drainage basin*, Journal of Environmental Pollution 148(3), 855-866.

Available online at www.sciencedirect.com
ScienceDirect
Environmental Pollution 148 (2007) 855–866
ENVIRONMENTAL POLLUTION
www.elsevier.com/locate/envpol

Development of a regional hydrologic soil model and application to the Beerze–Reusel drainage basin

O. Kolditz [a,*], Y. Du [a], C. Bürger [a], J. Delfs [a], D. Kuntz [a], M. Beinhorn [a], M. Hess [a], W. Wang [a], B. van der Grift [b], C. te Stroet [b]

[a] *GeoSystemsResearch, Center for Applied Geosciences, Geohydrology–Hydroinformatics, University of Tübingen, Sigwartstrasse 10, D-72076 Tubingen, Germany*
[b] *Netherlands Institute of Applied Geosciences TNO – National Geological Survey, Utrecht, The Netherlands*

Received 30 January 2007; accepted 31 January 2007

A real case application of concept of regional hydrologic soil modelling is presented.

Abstract

The soil compartment is an important interface between the atmosphere and the subsurface hydrosphere. In this paper a conceptual approach for regional hydrologic soil modelling (RHSM) is presented, which provides two important qualities for modelling. First, the soil compartment is directly coupled to the atmosphere via the land surface and to the aquifers. Second, extremely fine (5 cm vertical) resolutions of the soil system can be realized at regional scales (several hundreds of km^2). This high-resolution modelling could be achieved by parallel computation techniques. The RHSM approach is applied to the Beerze–Reusel drainage basin, which belongs to the Meuse River basin. Moisture transport in the soil system was calculated with extremely high vertical resolution at a regional scale based on rainfall–evaporation data for the year 2000. As a result, highly resolved regional groundwater recharge pattern addressing the heterogeneity of soil systems could be determined.

Keywords: Regional hydrologic soil model; Compartment approach; Numerical hydrosystem modelling; Meuse River basin; Beerze–Reusel drainage basin; High performance computing; AquaTerra EU project

1. Introduction

Hydrosystems belong to the most complex, dynamic and fragile environmental compartments on the earth affected by both natural and human pressures. Hydrological processes encompass not only the hydro- and geosphere, but also bio- and atmosphere partitions. An integrated process understanding is required in order to assess the impact of anthropogenic interventions concerning environmental pollution and to evaluate the evolution of hydrosystems.

The hydrosphere can be subdivided roughly into surface water, soil water and aquifer compartments (Fig. 1). The corresponding hydrological processes on the surface are lake, river and overland flow and in the subsurface unsaturated soil flow as well as groundwater flow in porous and fractured media. Water exchange with the atmosphere occurs via evaporation and precipitation whereas root water uptake and transpiration represent links to the biosphere. In the framework of continuum mechanics, physically and chemically based mass, momentum and energy conservation laws expressed by partial differential equations can be applied to describe those processes in surface and subsurface compartments as well as their interactions (Abbott et al., 2001).

Hydrological analysis requires a complete model representation of the hydrological systems. Abbott et al. (2001) recognized scaling, parameter uncertainty, process coupling, processing and visualisation of large data, software design

* Corresponding author. Tel.: +49 7071 29 73170.
E-mail address: kolditz@uni-tuebingen.de (O. Kolditz).

0269-7491/$ - see front matter © 2007 Elsevier Ltd. All rights reserved.
doi:10.1016/j.envpol.2007.01.046

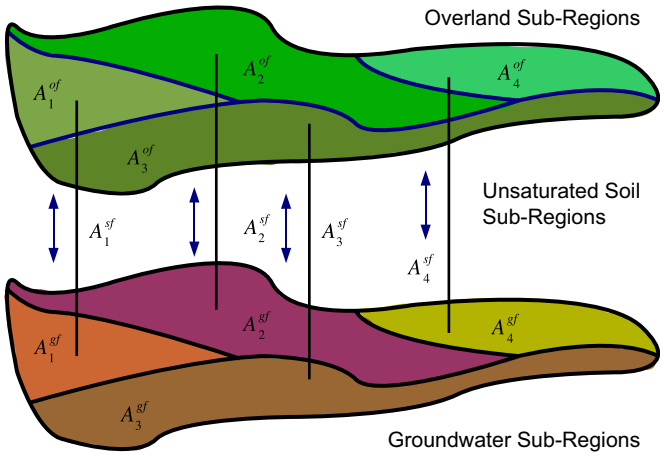

Fig. 1. Compartment approach for hydrosystem analysis (Kolditz et al., submitted for publication).

and efficiency of computational methods as key difficulties in hydrological analysis. An increasing realistic representation of hydrological processes by numerical modelling has been successively achieved during the last 30 years as the accuracy of numerical algorithms and the feasible spatial and temporal discretizations due to increasing computation power has continuously improved (Singh and Frevert, 2005).

A general overview of physically based surface and watershed hydrologic modelling can be found in Anderson and Burt (1985), Abbott et al. (1986a) and Singh and Frevert (2005). In subsurface hydrology some existing models are established for both saturated and variably saturated flow in porous media (Harbaugh et al., 2000; Šimůnek et al., 2005) and for multi-continua approaches (Pruess et al., 1990; Vogel et al., 2001). Coupled surface–subsurface models have been developed since they were first outlined by Freeze and Harlan (1969). Existing numerical codes for hydrosystem analysis are for instance MODFLOW2000 (Harbaugh et al., 2000), TOPMODEL (physically based run-ff production model, Bertoldi et al., 2004), Feflow-MIKE (Wasy Software, 2004), MIKE-SHE (Abbott et al., 1986b), Hydrogeosphere (Sudicky et al., 2000; Hydrosphere, 2004), SWAT (Arnold et al., 1998), and HSPF (Donigian and Imhoff, 2006; Gunduz and Aral, 2005). These models treat and couple different processes using a variety of simple to complex process descriptions, solution strategies and software concepts – from simple file interfaces to flexible interface manager.

The recognition of the importance of integrated approaches also spawned object-oriented modelling software aimed at code integration on a higher level. Within the field of computational hydrology, e.g. the CUASHI Hydrologic Information System (CUASHI, 2006), Tarsier (Watson and Rahman, 2004), OpenMI (Gijsberg et al., 2004) and DANUBIA (Barth et al., 2004; Mauser, 2006) provide generic modelling frameworks that allow communication and data exchange between different hydrological simulation models. Additionally, they offer GIS, visualisation or data analysis tools. A common strategy of these approaches appears to be the flexible combination of existing model applications and software tools. As a consequence, modern software concepts have to be very general to avoid computational bottlenecks and limitations.

Current efforts in the development of a new scientific software concepts for integrated hydrological analysis is aimed at following challenges – coupling of processes within hydrosystems and to the atmosphere as well as the modelling of multi-scale processes in those environmental systems:

- Coupling of processes in hydrosystems: A central question in hydrosystem analysis is the coupling concept for the individual compartments. Generally, different processes are coupled at their common interfaces such as the ground surface, capillary fringe, water table, aquifer boundaries or fractures. A popular approach for inter compartment transfer is to establish first order flux relationships at the compartment boundaries with source terms (VanderKwaak, 1999; Hydrosphere, 2004). Alternatively continuity assumptions can be used with boundary value iteration. This is established for instance by Miglio (2000) for a coupled ground and surface water model capable to describe short ocean waves. A comparison of both approaches is given in VanderKwaak (1999).
- Multi-scale processes in hydrosystems: A fundamental challenge of hydrological analysis remains the multi-scale nature of its processes: River basins can easily occupy thousands of square kilometres whereas soil structures range in the order of millimetres. Moreover, the non-linearity of hydrologic processes in combination with the heterogeneity of hydrologic systems interdicts a simple averaging of governing continuity equations to obtain large-scale descriptions (Das and Hassanizadeh, 2005). Even if it was possible to develop a unifying scaling theory – i.e. the definition of larger scale equations and their corresponding large-scale parameters on the basis of smaller scale parameter values – the resulting large-scale models would be of limited practical value since the small-scale parameters are commonly unknown in surface and subsurface hydrology (Dagan, 1986; Tayfur and Kavvas, 1998).
- Hydrosphere–atmosphere coupling: The soil compartment in its regional extent plays an exposed position in this coupling process as it is the interface between both. Estimation of regional scale soil characteristics in unsaturated zone is relied on the response of meteorologic factors such as precipitation and evapotranspiration. Existing models (e.g. Pan et al., 2001) focus on the impact of climate variabilities to the vadose zone and in return, how the soil zone can influence the climate system at a local scale. Hurk et al. (2004), Schär et al. (1998) developed a regional model for coupling soil hydrology with climate effects. An integrated modelling concept for the atmospheric deposition of heavy metal pollutions (cadmium and zinc) and corresponding transport through soil and groundwater in the South of the Netherlands is presented by van der Grift et al. (2006).

The present work is related to the latter topic concerning the coupling of hydrosphere and atmosphere. In this paper

a regional hydrologic soil model (RHSM) is developed and applied to the Beerze–Reusel drainage basin in the Netherlands. The concept of RHSM allows the evaluation of groundwater recharge pattern at a regional scale addressing the small-scale heterogeneity of the soil system as well as atmospheric rainfall–evaporation scenarios. The scientific software is developed according to object-oriented principles allowing the utilization of high performance computation techniques.

The complete development of a numerical hydrosystem model includes the conceptual model (Section 2.1), mathematical description of the set of balance equations (Section 2.2), their numerical discretizations (Section 3.1), software implementation (Section 3.2), and benchmark tests for verification purposes (Section 3.3) before the model is eligible for application studies (Section 4).

2. Model development

2.1. Conceptual model

The regional hydrologic soil model for the Beerze–Reusel drainage basin was developed in the framework of the compartment approach (Fig. 1), which was already successfully applied to a Borden aquifer field study (Kolditz et al., submitted for publication).

With the compartment approach the individual processes (overland, soil and groundwater flows) are solved independently in a partitioned algorithm and are coupled at relevant time scales at the compartment interfaces by exchange fluxes (A_i^{of}, A_i^{sf}, $A_i^{gf} - i$ is the number of compartment sub-regions; Fig. 1). This procedure offers superior flexibility concerning time and space discretizations as well as selection of an optimal numerical method for the solution of the groundwater, unsaturated and overland flow equations, respectively. An important prerequisite for this conceptual compartment approach was the development of an object-oriented software framework (Section 3.2).

2.2. Model equations

The complete set of model equations for a hydrosystem compartment is derived from the fluid mass balance equations for the surface, soil, and groundwater compartments, which are coupled by flux-exchange terms. The model equations for the hydrosystem compartment approach can be formulated in terms of a generalized non-linear diffusion equation (Section 2.2.2). Multiple one-dimensional vertical Richards' models (Richards, 1931) are used for the regional hydrologic soil model in order to describe the regional water flow in the unsaturated zone. The RHSM must be able to represent the heterogeneity of the real soil system (Section 4.1) and to address regionally distributed infiltration pattern (Section 4.2).

2.2.1. Soil water flow: Richards' equation

The Richards' model assumes that the air phase pressure is constant and makes use of a generalized form of the Darcy equation of groundwater flow. It is based on empirical capillary pressure-saturation and relative permeability-saturation functions (soil–water-characteristic-curves) given by van Genuchten (1980). Furthermore, it is assumed that the fluid is incompressible and the porous matrix non-deformable. Therefore the pressure-based Richards' equation reads:

$$n\frac{\partial S}{\partial t}+\frac{\partial q}{\partial z}=q_s, \tag{2.1}$$

where n is soil porosity, S is soil saturation, q_s is a source/sink term. The flux q is given by the Darcy law:

$$q=-\frac{k_{rel}k}{\mu}\left(\frac{\partial p}{\partial z}+\rho g\right), \tag{2.2}$$

where p, soil water pressure, is the primary variable of unsaturated flow, k_{rel} denotes relative permeability, k the saturated soil permeability, μ the water viscosity, ρ the water density and g the gravitational acceleration. Two material dependent constitutive relationships for saturation and permeability are required to close the fluid mass balance equation. The van Genuchten functional relationships $p(S)$ and $k_{rel}(S)$ are used neglecting hysteresis. With the effective saturation:

$$S_{eff}=\max\left(0,\frac{S-S_{res}}{1-S_{res}}\right), \tag{2.3}$$

where S_{res} is the residual saturation and the empirical functions for capillary pressure head and relative permeability are:

$$p=\frac{\rho g}{\alpha}\left(S_{eff}^{1/m}-1\right)^{1-m}, \tag{2.4}$$

$$k_{rel}(S)=S_{eff}^{1/2}\left[1-\left(1-S_{eff}^{1/m}\right)^{m}\right]^2, \tag{2.5}$$

where α and m are the so-called van Genuchten parameters characterizing the hydraulic soil behavior.

2.2.2. Non-linear diffusion equation

The governing equations for hydrosystem compartments, i.e. for groundwater, soil, and overland flow, belong to the general class of (non-linear) diffusion-type partial differential equations, which can be expressed as:

$$A(u)\frac{\partial u}{\partial t}-\nabla\cdot B(u)\nabla u=Q(u), \tag{2.6}$$

where u is the unknown field function (primary variable), A is a capacitance matrix (representing time dependencies), B is a conductivity matrix (representing space dependencies), Q is a source/sink term. In general A, B and Q are dependent on the unknown field function u, which results in non-linearities.

The introduction of the generalized non-linear diffusion-type Eq. (2.6) is important for the general numerical treatment of the partial differential equations (Section 3.1) and the object-oriented implementation of the numerical solution procedure (Section 3.2).

3. Code development

3.1. Numerical model

In general, a variety of finite difference, finite element and finite volume methods are available to solve the partial differential equations for fluid flow in hydrosystem compartments, e.g. (Weiyan, 1992; Segol, 1993; Vreugdenhil, 1994; Starke, 2000, 2005; LeVeque, 2002; Kolditz, 2002; Delfs, 2005). Within the framework of compartment approach different types of finite element methods (FEM) to solve the generalized diffusion Eq. (2.6) are applicable for the shallow water equations, the Richards' equation and the groundwater flow equation, respectively (Kolditz et al., submitted for publication). In general, either of these numerical methods leads to a non-linear algebraic system of equations, which can be resolved by use of iteration schemes. For time discretization of the generalized diffusion-type partial differential Eq. (2.6) an automatic time stepping scheme is used.

3.1.1. Finite element method for the generalized non-linear diffusion equation

Details of the specific finite element methods for the different hydrosystem compartments can be found in Beinhorn (2005) and Delfs (2005). They are based on weak formulations of the partial differential equations, which allow the search for generalized solutions. In order to obtain the weak formulation of the general diffusion equation, the Eq. (2.6) is multiplied with test functions v and integrated over the domain Ω giving:

$$\int_{\Omega} v\left(A\frac{\partial u}{\partial t}-\nabla\cdot B\nabla u\right)\mathrm{d}\Omega=\int_{\Omega} vQ\mathrm{d}\Omega, \tag{3.1}$$

Conducting the following steps: Application of Green's formula in order to reduce second order derivatives, introduction of piecewise polynomial functions ϕ_s, ψ_r at element level forming the *ne*-dimensional basis of an approximated solution and test function space (shape functions), use of an Euler finite difference scheme for time derivatives, we derive the following system of algebraic equations:

$$\sum_{s=1}^{ne}\left(\frac{A^e_{rs}}{\Delta t}+\theta B^e_{rs}\right)u^{n+1}_s=g^e_r+s^e_r+r^e_r+\sum_{s=1}^{ne}\left(\frac{A^e_{rs}}{\Delta t}-(1-\theta)B^e_{rs}\right)u^n_s,\quad r=1,\ldots,ne, \tag{3.2}$$

where A^e_{rs} is the capacitance matrix, B^e_{rs} the conductivity matrix, g^e_r accounts for the gravity term, which is only present in Richard's flow, s^e_r for the source terms and r^e_r for the boundary fluxes. The integrals are calculated with Gauss integration yielding for the capacitance matrix entries:

$$A^e_{rs}=\int_{\Omega^e}\psi_r A\phi_s\mathrm{d}\Omega=\int_{\widehat{\Omega}}\widehat{\psi}_r\widehat{A}\widehat{\phi}_s\det\mathbf{J}\,\mathrm{d}\widehat{\Omega}$$

$$=\sum_{k=1}^{gp}W_k\left(\widehat{x}_k\right)\widehat{\psi}_r\left(\widehat{x}_k\right)\widehat{A}\left(\widehat{x}_k\right)\widehat{\phi}_s\left(\widehat{x}_k\right)\det\mathbf{J}\left(\widehat{x}_k\right), \tag{3.3}$$

with the Jacobian matrix $\mathbf{J}$ of the coordinate transformation from the basis element domain $\widehat{\Omega}$ to the element domain $\widehat{\Omega}^e$ and the Gauss weights W_k at the Gauss points $\widehat{x}_k$. Entries of conductance matrix B^e_{rs} as well as of gravity g^e_r, source s^e_r and boundary flux vector r^e_r are calculated accordingly.

3.1.2. Finite element matrices and vectors for Richards' flow

For flow in the unsaturated zone according to Eq. (2.1), the capacitance and conductance matrices as well as gravity, source and boundary flux vectors of the general algebraic Eq. (3.2) are given by:

$$A^e_{rs}=\int_{\Omega^e}\psi_r n\frac{\partial S}{\partial p}\phi_s\mathrm{d}\Omega, \tag{3.4}$$

$$B^e_{rs}=\int_{\Omega^e}\nabla\psi_r\frac{k_{\mathrm{rel}}k}{\mu}\nabla\phi_s\mathrm{d}\Omega, \tag{3.5}$$

$$g^e_r=-\int_{\Omega^e}\nabla\psi_r\frac{k_{\mathrm{rel}}k}{\mu}\rho g\mathrm{d}\Omega, \tag{3.6}$$

$$s^e_r=\int_{\Omega^e}\psi_r q\mathrm{d}\Omega, \tag{3.7}$$

$$r^e_r=\int_{\Gamma^e}\psi_r q_n\mathrm{d}\Gamma, \tag{3.8}$$

respectively, where q_{n} is the soil water flux vector normal to the element boundary Γ^e.

3.2. Software implementation

The most important concepts of the present software implementation are object-orientation for flexibility in the code development (Section 3.2.1) and code parallelization for computational efficiency (Section 3.2.2).

3.2.1. Object-orientation

The general idea of object-oriented programming (OOP) is the projection of the domain of problems (i.e. solution of partial differential equations) to a hierarchic class concept. The basic feature of OOP is the inheritance of class properties. The present object-oriented concept is designed for the solution of multi-field problems in the framework of continuum

mechanics. It has already been successfully applied in several areas of porous media mechanics, e.g. thermo-hydraulic (TH) (Kolditz and Bauer, 2004) and thermo-hydro-mechanical (THM) problems (Wang and Kolditz, 2007). Recently, this software concept was extended to coupled multi-scale hydrosystems (Kolditz et al., submitted for publication). This requires the solution of partial differential equations on completely different time and space discretizations and appropriate coupling concepts of the separate compartments at their common interfaces.

In this work, this software concept, in particular the inheritance of process (PCS) classes, is adopted for the regional hydrologic soil model. The RHSM for the Beerze–Reusel basin (Section 4.1) consists of 12.210 local Richards processes for each influence area. Local Richards processes are easily derived from the regional Richards (master) process. All properties are inherited from the master process except of finite element geometry, material properties (soil profile codes) and infiltration boundary conditions, which are the only differences of each local process.

3.2.2. Parallelization

The computation of the RHSM for the Beerze–Reusel basin (Section 4.3) is extremely time consuming. For a 1-year simulation period about 50.000 time steps have to be calculated for 12.210 local (non-linear) Richards problems consisting of 40 line elements. The required computation time on a high-end PC is about 2 weeks for a single realization. The RHSM can be perfectly parallelized, i.e. a nearly perfect speed-up can be achieved, because there is no direct communication between the local Richards problems. The parallelized RHSM is running on Linux clusters and Linux supported symmetric multiprocessing computers with MPI (multiple processor instruction) environment (Wang et al., 2006). The computation time for the RHSM could be perfectly reduced according to the cluster size (tested on a 8-node cluster so far).

3.3. Benchmarking

Basically, two methods are available for numerical model verification, i.e. comparison to analytical solutions and/or to well designed experiments. Testing the accuracy of numerical solutions for non-linear problems, such as the Richards problem, with sophisticated boundary conditions is complicated because of the absence of exact solutions (Segol, 1993). In particular for multi-physics problems, such as coupled overland–soil–groundwater flow and thermo-hydro-mechanical (THM) coupled processes, where only a few experimental data exist, the benchmarking procedure has to rely on intercomparison of different numerical simulators (Rutqvist et al., submitted for publication). The following Table 1 provides some classic benchmark tests for unsaturated flow and infiltration models, which have been used for model verification of GeoSys/RockFlow (GS/RF) (Kolditz et al., 2006).

Hortonian flow is coupled overland/soil water flow. Smith and Woolhiser (1971) presented results for a laboratory experiment concerning infiltration of light oil into unsaturated soil. Abdul (1985) conducted field experiments in the Borden aquifer in order to evaluate the interaction of precipitation, surface run-off and groundwater recharge. Both data sets are part of the benchmarking procedure for GS/RF concerning coupled hydrosystem analysis (Delfs et al., submitted for publication). For testing the accuracy of the RHSM we concentrated on unsaturated flow problems with transient boundary conditions. The results obtained by GS/RF for this type of problems have been compared with findings by MIN3P (Mayer et al., 1999), HYDRUS (Šimůnek et al., 2005) and Hydrogeosphere Hydrosphere (2004). The results are in good agreement as reported in Kolditz et al. (2006).

Table 1
Benchmarks for unsaturated flow and infiltration models (Kolditz et al., 2006)

Processes	Specifics	Reference
Infiltration	Homogeneous soil	Forsyth et al. (1995)
Infiltration	Heterogenous soil	HYDRUS inter-comparison, Šimůnek et al. (2005)
Infiltration	Dirichlet boundary conditions	Celia et al. (1990)
Infiltration	Neumann boundary conditions	Abeele et al. (1981)
Infiltration	Transient boundary conditions	MIN3P inter-comparison, Mayer et al. (1999)
Infiltration	Dual continua	TOUGH2 inter-comparison
Hortonian flow	Homogeneous soil	Abdul (1985), Hydrosphere (2004)
Hortonian flow	Heterogenous soil	Smith and Woolhiser (1971)
Consolidation	Homogeneous soil	Liakopoulos (1965)
Tracer transport	Homogeneous soil	Warrick and Nielsen (1971)

4. Regional soil model of the Beerze–Reusel drainage basin

In this section the development of a regional soil model for the Beerze–Reusel drainage basin is described. Data import and conversion tools have been developed in order to use the comprehensive soil database of the Geological Survey of the Netherlands (TNO) (Section 4.1.1) and generate a high-resolution numerical model (Section 4.1). In addition to the detailed soil model, the RHSM uses generic infiltration time series (Section 4.2) to simulate the regional moisture evolution during the year 2000 (Section 4.3).

4.1. Site description

The study region is located in the Province of North Brabant in the southern half of the Netherlands. An overview of the Beerze–Reusel drainage basin itself is given in Fig. 2. The subsoil mainly consists of sandy deposits formed in the Pleistocene. The flat region gently slopes in a north to northeast direction, from an altitude of 45 m + NAP (m above Mean Sea Level) down to 3.7 m + NAP. There are several aeolian sand ridges up to a few meters in height that are orientated in a west to east direction. These ridges have a large impact on the geomorphology of the stream valleys, as they are situated transversely to the general slope and drainage pattern

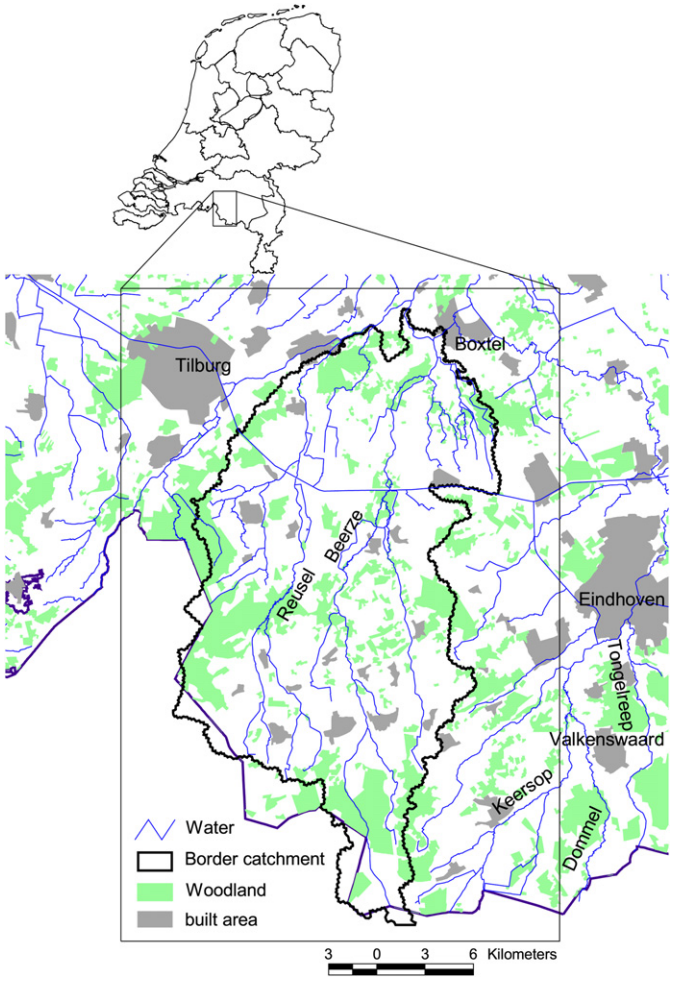

Fig. 2. Beerze–Reusel study area in the Meuse basin (vertical direction is North, geographic data: Tilburg (51°33′N, 5°5′E), Boxtel (51°35′N, 5°19′E), Eindhoven (51°27′N, 5°27′E).

of the area. In the plains between the ridges the valleys are much wider. In the valleys alluvial soils have been formed consisting of redeposited sand, loam and peat. Because of the intensive agricultural drainage of the areas these peaty soils are strongly oxidized and have often become very shallow. Agriculture is the dominant land use in the region – grassland and maize being most frequent.

4.1.1. Data concept

A comprehensive database for soil and aquifer properties of the Beerze–Reusel basin is available (Wösten et al., 2001). The database for the soil compartment contains following information: hydraulic properties of soil types (van Genuchten curves), structure of soil columns consisting of different soil types (soil profiles) and, area distribution of soil profiles (influence areas).

The data are organized in following GIS projects and databases:

- GIS (shape) files with polygons of influence areas, describing the area distribution of soil profiles in the basin.
- Data file linking the influence area number with a soil profile code.
- Data file linking the profile codes with a soil profile of soil types.
- Data file with the soil types and their parameters.

The relationships between these database parts are illustrated in Fig. 3. The investigation site consists of more than 12,000 influence areas described as GIS polygons. They represent the horizontal distribution of soil profiles (Fig. 3, left). A first data table gives the relation between influence area and soil profile number (profile code) (Fig. 3, right, upper). A second data table describes the soil structure (Fig. 3, right, middle) (vertical distribution, depth). The soil profiles consist of several soil types, which are coded for instance as H03, H07 and H20. A third data table gives the van Genuchten curves, i.e. soil water characteristics concerning capillary pressures and relative permeabilities, for each soil type (Fig. 3, right, lower).

4.1.2. Data processing

In the following the processing of the GIS based data set is described in order to set up a numerical model for the RSM simulations (Section 4.3). For an efficient, accurate and robust data processing several interface tools for GIS (shape files) and EXCEL data tables have been developed (Chen, 2006; Gronewold, 2006).

4.1.3. Influence areas

The first step of data processing is the import and the conversion of geometric GIS data, which consists of points and polygons. These data are converted to GEO data and can be displayed in the graphical user interface (GUI). Visual control, in particular for large, complex data sets, is a very important scientific tool for model development (Kalbacher, 2006).

4.1.4. Soil profiles

Second, import and conversion of soil profile data is conducted. Data table DT1, containing the references between influence areas and soil profiles (horizontal distribution), and data table DT2, comprising the vertical distribution of soil types within a profile, can be combined interactively. As a result, the relations: influence area (GIS-ID), soil profile code, and soil types of each profile (sections) are determined and stored in corresponding data constructs.

4.1.5. Soil types

The soil system of the Beerze–Reusel drainage basin is subdivided into 56 different soil types representing sand, loam, and peat soils formed during the Pleistocene. For each soil code type a corresponding set of soil water characteristic curves (SWCC) is given according to Eq. (2.5). Examples of SWCCs, i.e. capillary pressure- and relative permeability-saturation relationships, typical for the study area are displayed in Fig. 5 (left). The complete set of SSWCs for the investigation area can be found in (Du et al., 2006).

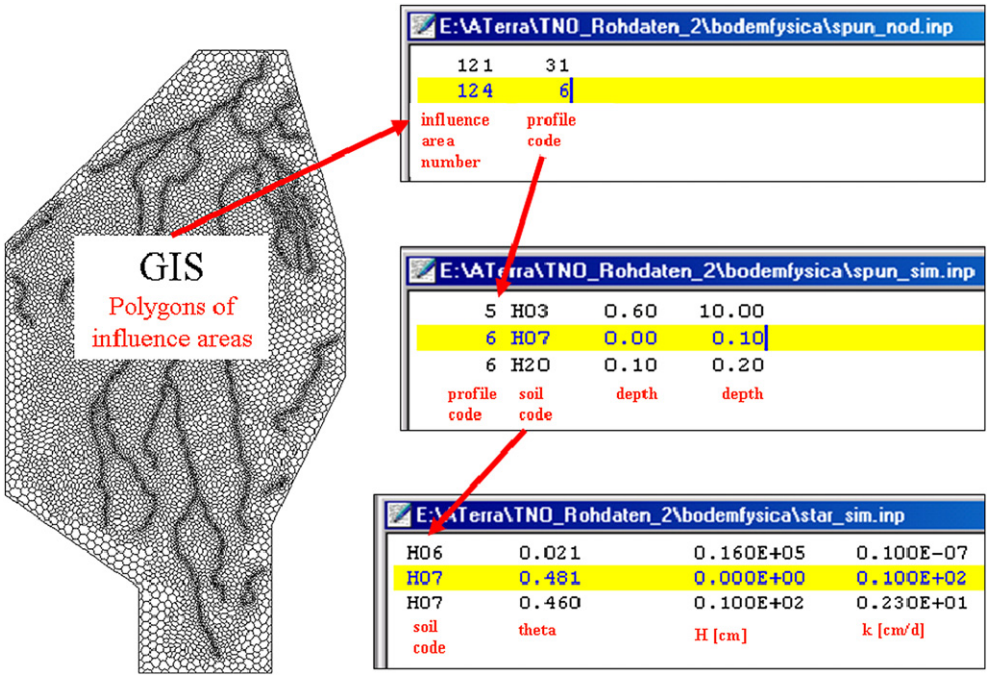

Fig. 3. GIS based soil data concept of the TNO.

4.1.6. Mesh generation and assignment of material properties

After the construction of the soil structure model, the corresponding finite element mesh for the regional soil model is generated. The first step of mesh generation is the analysis of the entire soil structure in order to determine an optimum discretization. The soil systems of 62 different soil profiles. In order to represent most changes in the soil types an element length of 5 cm was used. According to the optimum discretization as described above, for each influence area a column of line elements is created for each soil profile. The second step is the assignment of soil properties to the finite elements, which is done by the combination of geometric influence area, soil structure and material soil type data.

4.2. Meteorologic input data

As a time-dependent boundary condition to the regional soil model precipitation and evaporation time series are used. The raw data of time series were obtained from ECA&C (2006). For the model application minimum and maximum temperature, sunshine duration, and precipitation from the stations De Bilt, Twenthe, Vlissingen, Eindhoven, and Maastricht are used to compute daily infiltration series, i.e. precipitation P minus potential evaporation E, where $P > E$ and $P = 0$ else. As an example Fig. 4 shows the calculated meteorologic data for Eindhoven in the year 2000.

Potential evaporation E_{MK} is computed by the Makkink method (Makkink, 1957), which uses only temperature and net shortwave radiation R_S as an input (based on the assumption of a constant ratio between net radiation and net shortwave radiation)

$$E_{MK} = C_{MK}\frac{1}{\lambda}\frac{R_S s}{s+\gamma}, \tag{4.1}$$

where λ is the latent heat of water evaporation, γ is the psychrometric constant and s is the slope of saturated vapour pressure curve (a function of temperature). The Makkink parameter $C_{MK} = 0.63$ was chosen according to the findings of van Kraalingen and Stol (1997) for the Netherlands. Daily net shortwave radiation and R_S values are calculated based on the equations and recommendations given in Allen et al. (1998). A general albedo parameter of 0.23 is assumed to be

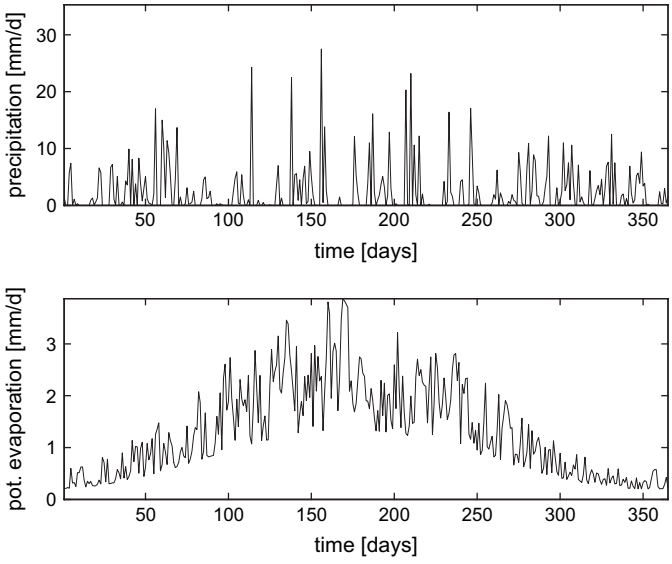

Fig. 4. Precipitation and potential evaporation for station Eindhoven (year 2000).

representative for wet sand (Buttner and Sutter, 1935; Graser and Bavel, 1982) or dry grey soil (Kondrat'ev, 1954). For this first RSM application (Section 4.3), infiltration series are generated for each climate station individually and then transferred to each influence area by daily inverse distance squared interpolation. However, the calculation of E_{MK} could be carried out for each soil column individually, which makes sense once a denser climate station network becomes available.

4.3. Soil hydrology simulations for the Beerze–Reusel basin

After the expending preprocessing steps including database import, data conversion, soil structure model, mesh generation, assignment of material properties, generation of driving boundary conditions (meteorologic infiltration data), the remaining data for the processing step of the numerical model have to be specified.

4.3.1. Soil profiles

The RSM of the Beerze–Reusel drainage basin consists of 12,210 individual soil colums, which can be categorized into 61 different kinds of soil profiles composed of 56 soil types. For each soil type a corresponding set of soil water characteristic curves (SWCC), i.e. capillary pressure- and relative permeability-saturation relationships, are defined.

For some detailed information of results of RSM, several typical soil profiles, which are located at different parts in the region, are selected. The typical soil profiles are composed by 4, 2 and 3 different soil layers, and the specific soil profile codes are defined as 16, 14 and 46, respectively. Each soil column with the corresponding daily precipitation series is simulated for the whole 2000-year period. Soil properties (SWCC) and temporal water saturations are shown in Figs. 5 and 6, respectively. Due to the soil heterogeneity a very different evolution of moisture occurs with locally varying infiltration into the groundwater compartment (van der Grift et al., 2006).

4.3.2. Regional hydrologic soil model

The regional evolution of the soil water distribution is presented in Fig. 7 for day 25, 50, and 100 of the year 2000. It can be seen that the infiltration process into the soil compartment is very heterogenous. As the meteorological precipitation–evaporation conditions are rather homogeneously distributed in the region (Section 4.2), the pronounced differential moisture propagation in the region is caused by the local variation of hydraulic soil properties. The regional groundwater recharge distribution is calculated from the soil water Darcy velocities multiplied by the corresponding influence area of each soil profile (Section 4.1.2).

5. Conclusions and future work

In this paper a regional hydrologic soil model (RHSM) is developed and applied successfully to the Beerze–Reusel drainage basin. The underlying concept of a compartment approach (Kolditz et al., submitted for publication) allows accurate numerical multi-scale simulations. The regional heterogeneity of the soil system of the Beerze–Reusel drainage basin has been represented at a new quality level. Extremely fine (centimeters) resolutions of the soil could be used at regional scales (several hundreds of km^2). This is, on the one hand, a significant improvement of numerical accuracy in hydrological modeling, which could be achieved by high performance computing (HPC) methods. On the other hand, regional groundwater recharge pattern are derived by a combination of large-scale meteorological data (rainfall–evaporation time series) and small-scale soil structure data representing the regional heterogeneity of the Beerze–Reusel soil system.

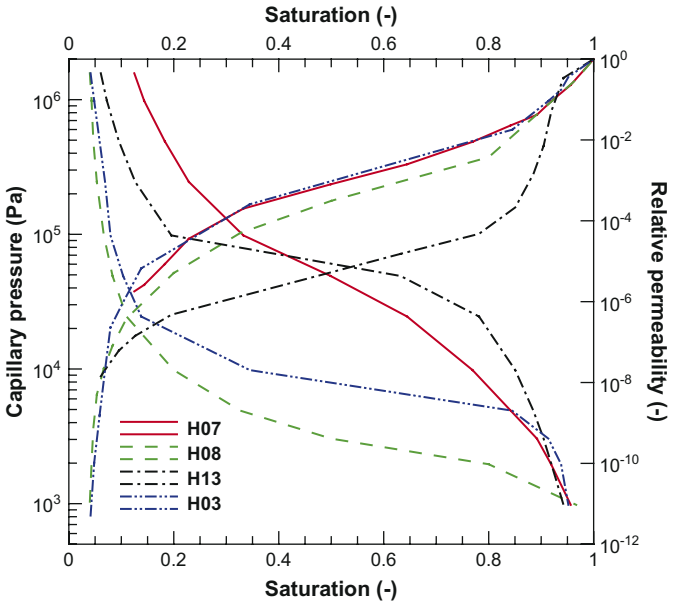

Fig. 5. Soil water characteristic curves (SWCC) in a selected soil column.

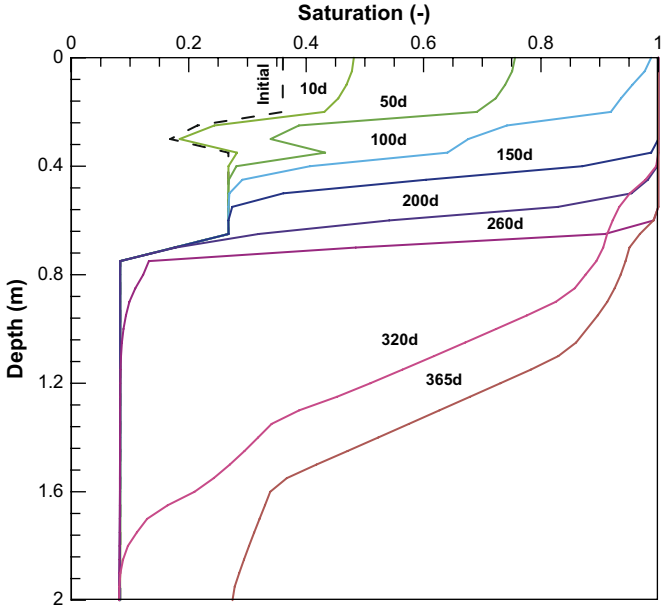

Fig. 6. Time evolution of water saturation in a selected soil column.

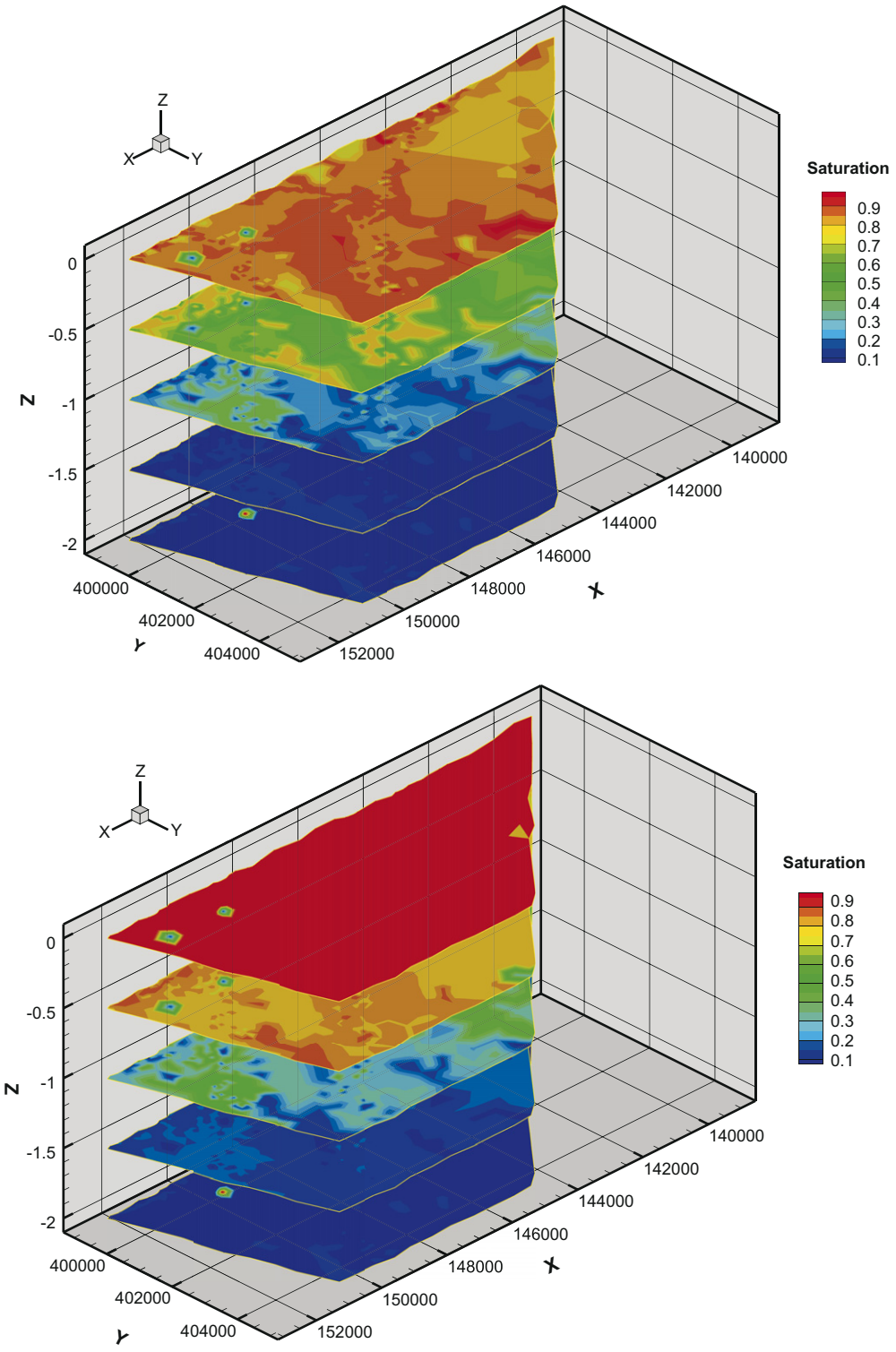

Fig. 7. Regional water saturation distribution at days 100 (top) and 150 (bottom).

5.1. Achievements of the RHSM concept

The more specific achievements of this work are outlined below.

- The physical infiltration model of the RHSM concept is verified against classic and new test cases (Section 3.3) based on experimental data as well as inter-comparisons to other numerical codes, i.e. MIN3P, HYDRUS and Hydrogeosphere. The new test cases address in particular (1) time-dependent boundary conditions arising from typical periods of precipitation events in combination (2) with typical soil heterogeneity.
- The RHSM approach is successfully applied to the Beerze–Reusel drainage basin. For this area exists a comprehensive,

unique database for the soil and aquifer system. Efficient software methods and tools, including GIS, database management systems as well as the required interfaces for numerical simulations, have been developed for processing the large data amounts in order to set up a realistic regional soil model (Section 4.1). These general tools can be easily adopted and applied to other river basins.

- The RHSM concept allows the realization of high-resolution soil models (5 cm vertical discretization) for large catchment areas (ca. 440 km^2 for Beerze–Reusel drainage basin, about 100 m horizontal resolution). Therefore, accurate images of soil heterogeneity can be used for hydrological analysis.
- In addition to a detailed soil structure model, a daily-resolution meteorological model has been used for the calculation of infiltration distributions in the Beerze–Reusel area (Section 4.2). The model takes temperature, sunshine duration, and precipitation from several stations De Bilt, Twenthe, Vlissingen, Eindhoven, and Maastricht into account.
- Based on the RHSM approach, groundwater recharge pattern can be determined combining high-resolution meteorological data (time series of precipitation–evapotranspiration data) and high-resolution soil structure data.
- The application of high performance computation (HPC) methods is a key technology for the accomplishment of realistic, high-resolution hydrological models.

5.2. Deficiencies and future options of the RHSM concept

Despite the achievements, the current RHSM approach has to be improved in future work concerning the following subjects.

- A weak point of the current RHSM implementation using column elements for the regional soil model is that lateral flow in the soil compartment is neglected. This assumption holds for flat ground surface areas and a relatively homogeneous infiltration process as may be assumed for the Beerze–Reusel basin. Based on the (Smith and Woolhiser, 1971) problem for coupled overland/soil water flow, it could be shown, that for flat ground surfaces the horizontal flow in the soil can be neglected (Delfs et al., submitted for publication). However, if significant lateral pressure or moisture gradients, even in flat areas, exist, horizontal flow components in the soil layer have to be taken into account. This shortcoming will be solved in the numerical model by the use of connecting triangle or prism elements for the soil layer discretization.
- The determination of realistic initial field conditions for hydraulic soil models is complicated (Delfs et al., submitted for publication). In laboratory experiments well defined drained or fully wetted conditions can be produced (Smith and Woolhiser, 1971), which is not realistic in the field. A more realistic initial status can be obtained if steady-state models based on the equilibrium between capillary and gravity forces are used (i.e. field capacity as initial saturation).
- Temperature effects are taken into account by the meteorological model for the generation of infiltration pattern, however, are neglected in the soil model. Non-isothermal effects as well as water uptake by plant roots have to be considered in future work for improving the physical soil model.
- As the concept of RHSM allows the consideration of small-scale soil heterogeneity at catchment size, resulting dispersion phenomena as well as local pollution effects (point sources) can be taken into account even at large scales. Precise hydrological models are prerequisites to pollutant transport simulation.
- Moreover, as the RHSM approach permits the establishment of high-resolution numerical hydrologic models, the integration of adequate high-resolution data from digital elevation models (DEM) as well as remote sensing becomes feasible.

Acknowledgements

This work was funded by the European Union FP6 Integrated Project ‘‘AquaTerra’’ (Project no. 505428) under the thematic priority ‘‘Sustainable development, global change and ecosystems’’. We are grateful to the Tübingen coordination team J. Barth, E. Frank and P. Grathwohl for saving us lots of time for research. The important comments and suggestions of the reviewers are greatly acknowledged. We would also like to thank Robert Walsh and Chris McDermott for improving the manuscript.

References

Abbott, M.B., Babovic, V.M., Cunge, J.A., 2001. Towards the hydraulics of the hydroinformatics era. Journal of Hydraulic Research 39 (4), 339–349.

Abbott, M.B., Bathurst, J.C., Cunge, J.A., O’Connell, P.E., Rasmussen, J., 1986a. An introduction to the European hydrological system – Système Hydrologique Européen, ‘SHE’, 1: history and philosophy of a physically-based, distributed modelling system. Journal of Hydrology 87 (1), 45–59.

Abbott, M.B., Bathurst, J.C., Cunge, J.A., O’Connell, P.E., Rasmussen, J., 1986b. An introduction to the European hydrological system – Système Hydrologique Européen, ‘SHE’, 2: structure of a physically-based, distributed modelling system. Journal of Hydrology 87 (2), 61–77.

Abdul, A.S., 1985. Experimental and Numerical Studies of the Effect of the Capillary Fringe on Streamflow Generation. Ph.D. thesis, Department of Earth Sciences, University of Waterloo.

Abeele, W.V., Wheeler, M.L., Burton, B.W., 1981. Geohydrology of Bandelier Tuff. Technical Report LA-8962, Los Alamos National Laboratory Report.

Allen, R.G., Pereira, L.S., Raes, D., Smith, M., 1998. Crop Evapotranspiration: Guidelines for Computing Crop Water Requirements. FAO, Rome. FAO Irrigation & Drainage Paper 56.

Anderson, M.G., Burt, P.T., 1985. Hydrological Forecasting. Wiley Publisher, Berlin.

Arnold, J.G., Sirinivasan, R., Muttiah, R.S., Williams, J.R., 1998. Large area hydrologic modeling and assessment, part 1-model development. Journal of American Water Resources Association 34 (1), 73–89.

Barth, M., Hennicker, R., Kraus, A., Ludwig, M., 2004. DANUBIA: an integrative simulation system for global change research in the upper danube basin. Cybernetics and Systems 35 (7–8), 639–666.

Beinhorn, M., 2005. Non-linear Flow Processes in Subsurface and Surface Hydrosystems. Ph.D. thesis, Center for Applied Geoscience, University of Tübingen.

Bertoldi, G., Tamanini, D., Zanotti, F., Rigon, R., 2004. GEOtop, A Hydrological Balance Model, Technical Description and Programs Guide (V0.875). Department of Civil and Environmental Engineering, University of Trento.

Buttner, K., Sutter, E., 1935. Abkülungsgrößen in den Dünen, Rückstrahlung verschiedener Bodenbedeckungen. Strahlentherapie 54, 156–173.

Celia, M.A., Boulouton, E.T., Zarba, R.L., 1990. A general mass conservation numerical solution for the unsaturated flow equation. Water Resources Research 26, 1483–1496.

Chen, C., 2006. Integrating GIS Methods for the Analysis of GeoSystems. Ph.D. thesis, Center for Applied Geoscience, University of Tübingen.

CUASHI, 2006. Available from: <http://river.sdsc.edu/HDAS/>.

Dagan, G., 1986. Statistical theory of groundwater flow and transport: pore to laboratory, laboratory to formation and formation to regional scale. Water Resources Research 22, 121–135.

Das, D.B., Hassanizadeh, S.M., 2005. Upscaling Multiphase Flow in Porous Media – From Pore to Core and Beyond. Springer, Dordrecht.

Delfs, J.-O., 2005. Methods for the Simulation of Surface Runoff. Diploma thesis, Institute of Astronomy and Astrophysics, Center for Applied Geoscience, University of Tübingen.

Delfs, J.O., Du, Y., Burger, C., Kolditz, O. Re-analysis of the Laboratory Experiments by Smith and Woolhiser (1971) for Coupled Overland/Soil Water Flow. Water Resources Research, submitted for publication.

Donigian, A.S., Imhoff, J., 2006. History and evolution of watershed modeling derived from the Stanford Watershed Model. In: Singh, V.P., Frevert, D. (Eds.), Watershed Models. CRC Press, Boca Raton.

Du, Y., Bürger, C.M., Delfs, J.O., Kolditz, O., van der Grift, B., te Stroet, C., 2006. Development of a Regional Soil Model for the Beerze–Reuzel Area (Meuse). Technical Report 2006-23. Center for Applied Geoscience, University of Tübingen.

ECA&C, 2006. Available from: <http://eca.knmi.nl/dailydata/index.php>.

Forsyth, P.A., Wu, Y.S., Pruess, K., 1995. Robust numerical methods for saturated–unsaturated flow with dry initial conditions in heterogeneous media. Advances in Water Resources 18, 25–38.

Freeze, R.A., Harlan, R.L., 1969. Blueprint for a physically based, digitally-simulated hydrological response model. Journal of Hydrology 9, 237–258.

van Genuchten, M.T., 1980. A closed-form equation for predicting the hydraulic conductivity of unsaturated soil. Soil Science Society of America Journal 44, 892–898.

Gijsberg, P., Brakkee, E., Gregersen, J.B., Hummel, S., Westen, S.2004. Part C- the org.OpenMI.Standard interface specification. HarmonIT Document Series, EU-Project HarmonIT, Contract EVK1-CT-2001-00090.

Graser, E.A., Bavel, C.H.V., 1982. The effect of soil moisture upon soil albedo. Agricultural Meteorology 27, 17–26.

van der Grift, B., Passier, H., Rozemeijer, J., Griffioen, J., Smidt, E., 2006. Integrated Modeling of Cadmium and Zinc Contamination in Groundwater and Surface Water of the Kempen Region, the Netherlands. Tech. rep. Netherlands Institute of Applied Geoscience TNO – National Geological Survey.

Gronewold, J., 2006. Development of an Internet Information System for Modelling Natural Attenuation Processes in Groundwater. Ph.D. thesis, Center for Applied Geoscience, University of Tübingen.

Gunduz, O., Aral, M.M., 2005. River networks and groundwater flow: simultaneous solution of a coupled system. Journa of Hydrology 301 (1-4), 216–234.

Harbaugh, A.W., Banta, E.R., Hill, M.C., McDonald, M.G., 2000. MODFLOW-2000, the U.S. Geological Survey Modular Ground-water Model – User Guide to Modularization Concepts and the Groundwater Flow Process. Tech. Rep. 00-92. U.S. Geological Survey. Open-File Report.

Hurk, V., Hirschi, M., Schar, C., Lenderink, G., Meijgaard, E.V., 2004. Soil control on runoff response to climate change in regional climate model simulations. Journal of Climate 17.

Hydrosphere, 2004. Available from: <http://sciborg.uwaterloo.ca/mclaren/public/> or <http://www.modhms.com/software/hydrosphere.html>.

Kalbacher, T., 2006. Geometric Modelling and 3D-Visualisation of Hydrogeological Systems: Software Design and Application. Ph.D. thesis, Center for Applied Geoscience, University of Tübingen.

Kolditz, O., 2002. Computational Methods in Environmental Fluid Mechanics. Springer Publisher, Berlin.

Kolditz, O., Bauer, S., 2004. A process-orientated approach to compute multi-field problems in porous media. International Journal of Hydroinformatics 6, 225–244.

Kolditz, O., Delfs, J.-O., Beinhorn, M., Bürger, C. A compartment approach for hydrosystem analysis based on object-oriented principles. Journal of Hydroinformatics, submitted for publication.

Kolditz, O., Wang, W., Hesser, J., Du, Y., Shao, H., 2006. GeoSys/RockFlow Benchmarking. Tech. rep.. Center for Applied Geoscience, University of Tübingen. GeoSys-Preprint.

Kondrat'ev, K.Y., 1954. The Radiant Energy of the Sun, Chapter 9, Albedo of the underlying surface and clouds, English Summary by A. Kurlent and P. Larson. McGill University, Leningrad.

van Kraalingen, D.W.G., Stol, W., 1997. Evapotranspiration modules for crop growth simulation – implementation of the algorithms from Penman, Makkink and Priestley-Taylor. Quantitative Approaches in Systems Analysis 11.

LeVeque, R.J., 2002. Finite Volume Methods for Hyperbolic Problems. Cambridge University Press, Cambridge.

Liakopoulos, A., 1965. Retention and distribution of moisture in soils after infiltration has ceased. Bulletin of the International Association for scientific hydrology 10, 58–69.

Makkink, G.F., 1957. Testing the Penman formula by means of lysimeters. International Journal of Water Engineering 11, 277–288.

Mauser, W., 2006. Global Change Atlas, Einzugsgebiet Obere Donau (in german). GLOWA-Danube-Projekt. LMU Munich, Department of Geo- and Environmental Sciences.

Mayer, K.U., Benner, S.G., Blowes, D.W., Frind, E.O., 1999. The reactive transport model MIN3P: Application to acid mine drainage generation and treatment – Nickel Rim Mine Site, Sudbury. Vol. 1. Ch. In: Conference on Mining and the Environment, pp. 145–154.

Miglio, E., 2000. Mathematical and Numerical Modeling for Environmental Applications. Ph.D. thesis, Modeling and Scientific Computation Laboratory, Polytecnic University of Milan.

Pan, Z., Arritt, R., Gutowski, W., Takle, E., 2001. Soil moisture in regional climate models: simulation and projection. Geophysical Research Letters 28, 2947–2950.

Pruess, K., Wang, J.S.Y., Tsang, Y.W., 1990. On thermohydrologic conditions near high-level nuclear wastes emplaced in partially saturated fractured tuff – part 1: simulation studies with explicit consideration for fracture effects. Water Resource Research 26, 1235–1248.

Richards, L.A., 1931. Capillary conduction of liquids through porous mediums. Physics 1, 318–333.

Rutqvist, J., Barr, D., Birkholzer, J.T., Chijimatsu, M., Kolditz, O., Liu, Q., Oda, Y., Wang, W., Zhang, C. Results from an international simulation study on coupled thermal, hydrological, and mechanical (THM) processes near geological nuclear waste repositories. Journal of Nuclear Technologies, submitted for publication.

Schär, C., Lthi, D., Beyerle, U., 1998. The soil-precipitation feedback: a process study with a regional climate model. Journal of Climate 12, 722–741.

Segol, G., 1993. Classic Groundwater Simulations – Proving and Improving Numerical Models. Prentice-Hall Inc.

Šimůnek, J., van Genuchten, M.T., Šejna, M., 2005. The Hydrus-1d Software Package for Simulating the One-dimensional Movement of Water, Heat, and Multiple Solutes in Variably-Saturated Media, Version 3.0. Technical Report. Department of Environmental Sciences, University of California Riverside.

Singh, V.P., Frevert, D.K., 2005. Watershed Models. CRC, USA.

Smith, R.E., Woolhiser, D.A., 1971. Overland flow on an infiltrating surface. Water Resources Research 7 (4), 899–913.

Starke, G., 2000. Gauss–Newton multilevel methods for least-squares finite element computations of variably saturated subsurface flow. Computing 64, 323–338.

Starke, G., 2005. A first-order system least-squares finite element method for the shallow water equations. SIAM Journal on Numerical Analysis 42, 2387–2407.

Sudicky, E.A., Jones, J.P., McLaren, R.G., Brunner, D.S., VanderKwaak, J.E., 2000. A fully-coupled model of surface and subsurface water flow: model

overview and application to the laurel creek watershed. In: Balkema, A.A. (Ed.), Computational Methods in Water Resources. No. 2, pp. 1093–1099.

Tayfur, G., Kavvas, M.L., 1998. Areally-averaged overland flow equations at hillslope scale. Hydrological Sciences Journal 43, 361–378.

VanderKwaak, J.E., 1999. Numerical Simulation of Flow and Chemical Transport in Integrated Surface-Subsurface Hydrologic Systems. Ph.D. thesis, Department of Earth Sciences, University of Waterloo.

Vogel, T., van Genuchten, M.T., Cislerova, M., 2001. Effect of the shape of the soil hydraulic functions near saturation on variably-saturated flow predictions. Advances in Water Resources 24, 133–144.

Vreugdenhil, C.B., 1994. Numerical Methods for Shallow-Water Flow. Kluwer Academic Publishers, Dordrecht.

Wang, W., Hess, M., Kolditz, O., 2006. MPI-Parallelization of GeoSys/RockFlow. Technical Report 2006-24. Center for Applied Geoscience, University of Tübingen.

Wang, W., Kolditz, O., 2007. Object-oriented finite element analysis of thermo-hydro-mechanical (THM) problems in porous media. International Journal of Numerical Methods in Engineering 69 (1), 162–201.

Warrick, W.B., Nielsen, D., 1971. Simultaneous solute and water transfer for an unsaturated soil. Water Resource Research 7, 1216–1225.

Wasy Software, 2004. IFMMIKE11 1.1, User Manual. Wasy GmbH, Institute for Water Resources Planning and System Research.

Watson, F.G.R., Rahman, J.M., 2004. Tarsier: a practical software framework for model development, testing and deployment. Environmental Modelling and Software 19 (3), 245–260.

Weiyan, T., 1992. Shallow Water Hydrodynamics. Water & Power Press, Hong Kong.

Wösten, J.H.M., Veerman, G.J., de Groot, W.J.M., Stolte, J., 2001. Water retention and conductivity characteristics of upper en deeper soil layers in the Netherlands (in dutch). Alterra report 153.

Enclosed Publication

[EP6] O. Kolditz, **J.-O. Delfs**, C. M. Bürger, M. Beinhorn, C.-H. Park (2007): *Numerical analysis of coupled hydrosystems based on an object-oriented compartment approach*. Journal of Hydroinformatics 10(3), 227-244.

Numerical analysis of coupled hydrosystems based on an object-oriented compartment approach

Olaf Kolditz, Jens-Olaf Delfs, Claudius Bürger, Martin Beinhorn and Chan-Hee Park

ABSTRACT

In this paper we present an object-oriented concept for numerical simulation of multi-field problems for coupled hydrosystem analysis. Individual (flow) processes modelled by a particular partial differential equation, i.e. overland flow by the shallow water equation, variably saturated flow by the Richards equation and saturated flow by the groundwater flow equation, are identified with their corresponding hydrologic compartments such as land surface, vadose zone and aquifers, respectively. The object-oriented framework of the compartment approach allows an uncomplicated coupling of these existing flow models. After a brief outline of the underlying mathematical models we focus on the numerical modelling and coupling of overland flow, variably saturated and groundwater flows via exchange flux terms. As each process object is associated with its own spatial discretisation mesh, temporal time-stepping scheme and appropriate numerical solution procedure. Flow processes in hydrosystems are coupled via their compartment (or process domain) boundaries without giving up the computational necessities and optimisations for the numerical solution of each individual process. However, the coupling requires a bridging of different temporal and spatial scales, which is solved here by the integration of fluxes (spatially and temporally). In closing we present three application examples: a benchmark test for overland flow on an infiltrating surface and two case studies – at the Borden site in Canada and the Beerze–Reusel drainage basin in the Netherlands.

Key words | Borden aquifer, control-volume finite element method, coupled hydrosystem modelling, Meuse river basin, nonlinear diffusion equation, object-oriented programming

Olaf Kolditz (corresponding author)
Jens-Olaf Delfs
Geohydrology and Hydroinformatics,
Center for Applied Geoscience,
University of Tübingen,
Tübingen D-72076,
Germany
and Environmental Informatics,
Helmholtz Center for Environmental Research - UFZ,
04318 Leipzig,
Germany
E-mail: *olaf.kolditz@ufz.de*

Claudius Bürger
Martin Beinhorn
Geohydrology and Hydroinformatics,
Center for Applied Geoscience,
University of Tübingen,
Tübingen D-72076,
Germany

Chan-Hee Park
Environmental Informatics Helmholtz,
Center for Environmental Research - UFZ,
04318 Leipzig,
Germany

INTRODUCTION

Hydrological systems belong to the most complex, dynamic and fragile environmental systems affected by both natural and human pressures. Hydrological systems encompass not only hydro- and geosphere partitions, but are affected by the bio- and atmosphere as well. An integrated process understanding is required in order to evaluate the impact of anthropogenic influences and the evolution of hydrosystems (Chen *et al.* 2006).

The hydrosphere can be subdivided roughly into surface water, vadose zone and aquifer compartments (Figure 1). The unsaturated zone is denoted as soil compartment hereafter. The corresponding hydrological processes on the surface are related to lakes as well as rivers and overland flow. In the subsurface, unsaturated flow in soils and groundwater flow in porous as well as fractured aquifers occurs. The hydrosphere directly interacts with the biosphere and the atmosphere. Water exchange with the atmosphere occurs via evaporation and precipitation whereas root water uptake and transpiration represent links to the biosphere. The transport of contaminants in the hydrosystems strongly depends on the water movement through the compartments. The same physical principles

doi: 10.2166/hydro.2008.003

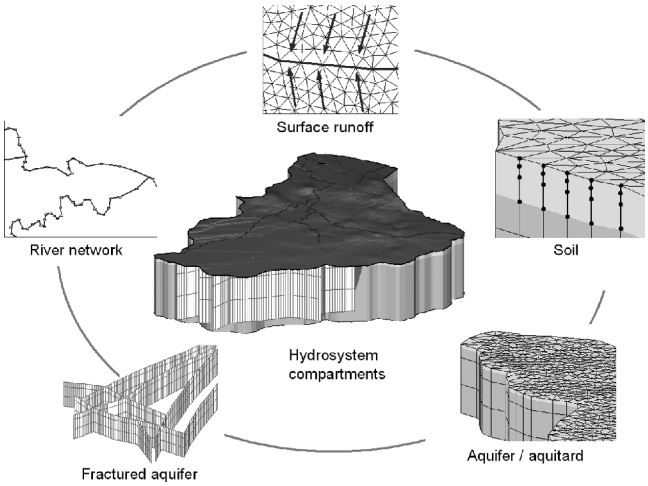

Figure 1 | Compartments of environmental hydrosystems.

apply to water movement and contaminant transport in surface and subsurface hydrosystems. Thus, physically and chemically based mass, momentum and energy conservation laws expressed by partial differential equations are used to describe the processes and their interactions (Lees 2000; Abbott *et al.* 2001).

Hydrological analysis requires a complete model representation of the hydrological systems. Abbott *et al.* (2001) identified scaling, parameter uncertainty, process coupling, processing and visualisation of large datasets, software design and efficiency of computational methods as key challenges in hydrological analysis. A more and more realistic representation of hydrological processes has been achieved during the last thirty years as the accuracy of numerical algorithms and the feasible spatial and temporal discretisation has continuously improved. Computational modelling is a tool rapidly developed in hydrological analysis. In particular, advances in numerical mathematics and computer science have tremendously enlarged the variety and the nature of problems addressed by environmental scientists and engineers. It is certainly true that for each hydro-compartment (Figure 1) there exist many excellent simulation codes, but traditionally the development has been isolated within the specific disciplines. As a result, surface water models commonly lack rigorous representations of flow and transport in complex geological formations. On the other hand, groundwater models typically ignore the dynamics of overland flow and surface water quality issues. There is a clear need to establish an integrative framework for the robust and sound analysis of terrestrial hydrological systems. Comprehensive overviews of physically based surface water and watershed hydrologic modelling can be found in (Anderson & Burt 1985; Abbott *et al.* 1986*a*; Singh & Frevert 2005). In subsurface hydrology well-established models exist for both saturated and variably saturated flow in porous media (Huyakorn & Pinder 1983; Simunek *et al.* 1999) and in dual-continua porous media (Vogel *et al.* 2001).

Coupled surface–subsurface flow models have been developed since they were first outlined in (Freeze & Harlan 1969). Examples of existing conceptual models and numerical codes include MODFLOW2000 (MODular three finite-difference ground-water FLOW model (Harbaugh *et al.* 2000)), TOPMODEL (physically based runoff production model (Bertoldi *et al.* 2004)), Feflow (Wasy Software (2004)), MIKE-SHE (Système Hydrologique Européen (Abbott *et al.* 1986*b*)), Hydrosphere (Sudicky *et al.* 2000) (see also http://sciborg.uwaterloo.ca/ ~mclaren/public/ or http://www.modhms.com/software/hydrosphere.html), SWAT (Arnold *et al.* 1998), HSPF (Gunduz & Aral 2005; Donigian & Imhoff 2006) and ParFlow (Kollett & Maxwell 2006), to name just a few. These finite difference, element and volume implementations include a variety of monolithic and partitioned coupling schemes which rely on combinations of continuity assumptions and exchange flux calculations.

Object-oriented programming (OOP) has proven to be a key concept in developing complex software not only in engineering computation (e.g. Forde *et al.* 1990) but also in hydrogeology (Desitter *et al.* 2000; Wang & Kolditz 2007). Its advantages become particularly visible in the context of large developer teams and for the reuse, maintenance and extension of codes. In the field of water resources and hydrology, recent object-oriented software developments include models for flood analysis (Alfredsen & Saether 2000), topographically based watershed analysis (Wang *et al.* 2005), surface water quality (Elshorbagy & Ormsbee 2006) and pollutant transport in mine spoil heaps (Gandy & Younger 2007). The approval of integrated approaches also spawned object-oriented modelling software aimed at integration on a higher level. Within the hydrology community the CUAHSI (2007) Hydrologic Information System (http://river.sdsc.edu/HDAS/) is dedicated to the linkage,

visualisation and dissemination of numerous sources of hydrologic data. OpenMI (Gregersen *et al.* 2006) defines a generic modelling framework that allows communication and data exchange between different hydrological simulation models that are compatible with the according framework interface, JUPITER (Banta *et al.* 2006) describes an API (application programming interface) for hydrologic model analysis in terms of parameter identification and reliability. Finally, DANUBIA (Barth *et al.* 2004) provides an internet-based platform integrating the distributed simulation models of socio-economic and natural science disciplines taking part in the GLOWA-Danube project. The common idea to all of these initiatives is a flexible combination of existing models and software tools. An important backbone of hydroinformatics remains the existence and further development of open source software (Harvey & Han 2002; Abbott 2003; Khatibi *et al.* 2004).

Compartment approach

Two of the most difficult and challenging topics in hydrosystem analysis are scale bridging and process coupling. To overcome these difficulties, we propose a compartment approach. The hydrologic compartments individually host the different flow and transport processes, which are coupled at their common compartment interfaces by exchange flux terms. This concept allows the consideration of each process appropriately at its specific time and space scale. To keep flexibility in the spatial resolution, each process is solved with a mesh optimized for its geological and hydrological structures, and numerical constraints. Together with the object-oriented method, this allows a use of multiple meshes tailor-made for each process (Figure 5), and leads to flexibility of the compartment approach. The central idea behind the multi-mesh concept is that the partial differential equation of each compartment can be solved numerically with the most suitable spatial discretisation. In addition, flexibility can also be achieved with sub-time steps for each individual process for the time discretisation. Thus, the time steps can be chosen according to the stability requirements of the process-specific numerical scheme (see Time-stepping synchronisation). Moreover, the compartment approach allows the combination of different numerical schemes, such as a Galerkin finite element method (G-FEM) and a control-volume finite element method (CV-FEM) (see Numerical methods). This separation of methods via the compartment is particularly powerful when the nonlinearity of each process does prefer certain numerical methods. Solution techniques for the coupled problem can be handled in the following two ways: partitioned coupling schemes and monolithic schemes to account for strongly coupled processes. In this paper, partitioned coupling is of interest. To harbor the flexibility over each process separable in the numerical scheme of the compartment approach, object-oriented programming was our choice for code implementation. In particular, the implementation of the multi-process concept (Kolditz & Bauer 2004) benefits from object orientation as the main steps of the numerical solution procedure for the partial differential equations are independent of the specific problem, i.e. calculation of element contributions, assembly of algebraic equation systems (including treatment of boundary conditions and source terms), solution of the algebraic equation systems and calculation of secondary variables.

This paper is structured as follows. After a brief overview of the governing equations for overland, soil water and groundwater flow used for the compartment approach we expand on the applied numerical solution methods. A comprehensive description of the coupling concept finishes the theoretical part of this paper. Subsequently we present three example applications of the compartment approach: a benchmark test based on the classic experiment by (Smith & Woolhiser 1971) and two case studies, the Borden site in Canada (Abdul 1985) and the Beerze–Reusel drainage basin in the Netherlands.

GOVERNING EQUATIONS

In this section we briefly summarise the governing equations of the compartment approach for three-dimensional groundwater flow (first subsection), one-dimensional flow in the unsaturated zone (second subsection) as well as a two-dimensional overland flow (third subsection). Each equation is based on mass conservation and a flux–primary variable relationship resulting in a parabolic equation that is linear for groundwater and nonlinear for soil and overland flow.

Groundwater flow: Darcy equation

The groundwater flow is described by a three-dimensional fluid mass balance equation with fluxes given by Darcy's law which is restricted to laminar flow (Bear 1988).

Therefore the flow equation is

$$n^{\mathrm{gf}} S_0^{\mathrm{gf}} \frac{\partial h^{\mathrm{gf}}}{\partial t} + \nabla \cdot \mathbf{q}^{\mathrm{gf}} = q_{\mathrm{s}}^{\mathrm{gf}} \tag{1}$$

where h^{gf}, the hydraulic head, is the primary variable of the groundwater flow equation, n^{gf} is the aquifer porosity, S_0^{gf} is the aquifer storativity which accounts for the porous medium matrix and the fluid compression, ∇ is the three-dimensional nabla operator and $q_{\mathrm{s}}^{\mathrm{gf}}$ is a source/-sink term. The groundwater flux $\mathbf{q}^{\mathrm{gf}}$ is given according to Darcy's law by

$$\mathbf{q}^{\mathrm{gf}} = -\mathbf{K}^{\mathrm{gf}} \nabla h^{\mathrm{gf}} \tag{2}$$

where $\mathbf{K}^{\mathrm{gf}}$ is the aquifer hydraulic conductivity tensor.

Flow in the unsaturated zone: Richards' equation

A series of one-dimensional vertical Richards models are used in order to describe water flow in the unsaturated zone. The Richards model assumes that the air phase pressure is constant and makes use of a generalised form of Darcy's equation used in the groundwater model presented above. It is based on empirical capillary pressure–saturation and relative permeability–saturation functions given by (van Genuchten 1980). Furthermore we assume that the fluid is incompressible and the porous matrix is non-deformable. Therefore the pressure-based Richards equation is

$$n^{\mathrm{sf}} \frac{\partial S^{\mathrm{sf}}}{\partial t} + \frac{\partial q^{\mathrm{sf}}}{\partial z} = q_{\mathrm{s}}^{\mathrm{sf}} \tag{3}$$

where n^{sf} is soil porosity, S^{sf} is soil water saturation and q_s^{sf} is a source/sink term. The flux q^{sf} is given by Darcy's law:

$$q^{\mathrm{sf}} = -k_{\mathrm{rel}}^{\mathrm{sf}} \frac{\rho g}{\mu} k^{\mathrm{sf}} \left(\frac{\partial h^{\mathrm{sf}}}{\partial z} - 1 \right) \tag{4}$$

where h^{sf}, the soil water pressure head, is the primary variable of unsaturated flow, $k_{\mathrm{rel}}^{\mathrm{sf}}$ denotes relative permeability, k^{sf} the saturated soil permeability, μ the water viscosity, ρ the water density and g the gravitational acceleration. Two material-dependent constitutive relationships for saturation and permeability are required to close the fluid mass balance equation. The van Genuchten functional relationships $h^{\mathrm{sf}}(S^{\mathrm{sf}})$ and $k_{\mathrm{rel}}^{\mathrm{sf}}(S^{\mathrm{sf}})$ are used neglecting hysteresis. With the effective saturation

$$S_{\mathrm{eff}} = \max\left(0, \frac{S^{\mathrm{sf}} - S_{\mathrm{res}}}{1 - S_{\mathrm{res}}}\right) \tag{5}$$

where S_{res} is the residual saturation, the empirical functions for capillary pressure and relative permeability are

$$h_{\mathrm{cap}} = -h^{\mathrm{sf}} = \frac{1}{\alpha}\left(S_{\mathrm{eff}}^{1/m} - 1\right)^{1-m} \tag{6}$$

$$k_{\mathrm{rel}}^{\mathrm{sf}}(S^{\mathrm{sf}}) = S_{\mathrm{eff}}^{1/2}\left[1 - \left(1 - S_{\mathrm{eff}}^{1/m}\right)^{m}\right]^2 \tag{7}$$

where α and m are soil material parameters.

Overland flow: diffusive wave shallow water equation

For the simulation of overland flow a two-dimensional diffusive wave approximation of the Saint-Venant equations is used. The Saint-Venant equations are derived by depth integration of the Reynolds averaged Navier–Stokes equations with the main assumptions of a hydrostatic pressure distribution, small morphology variations and empirical flow resistance distributions (Vreugdenhil 1994; Gerbeau & Perthame 2001). These equations are hyperbolic and capable of handling extreme conditions such as dam breaks (LeVeque 2002). The diffusive wave approximation of the Saint-Venant equations is parabolic and is derived by neglecting the inertial terms such that they are restricted to subcritical flow conditions (Beinhorn 2005). For runoff simulations they have proven their reliability (VanderKwaak 1999). Criteria for the applicability of this equation as well as the kinematic wave equation are given in Ponce *et al.* (1977) and Singh (1994).

The diffusive wave shallow water equation is given by

$$\frac{\partial h^{\mathrm{of}}}{\partial t} + \nabla \cdot \mathbf{q}^{\mathrm{of}} = q_{\mathrm{s}}^{\mathrm{of}} \tag{8}$$

where $h^{\mathrm{of}} = H + z$, the hydraulic head, is the primary variable of surface water flow, H is surface water depth, z is

the elevation, ∇ is the two-dimensional nabla operator and q_s^{of} is a source/sink term for surface water. The use of Manning's resistance to flow distribution, as well as neglecting the inertia terms in the Saint-Venant equations, gives the flux $\mathbf{q}^{of}$:

$$\mathbf{q}^{of} = -k_{rel}^{of} K^{of} \nabla h^{of}. \tag{9}$$

The conductivity terms k_{rel}^{of} and K^{of} are given by

$$k_{rel}^{of} = H^{5/3} \tag{10}$$

$$K^{of} = \frac{1}{n^{of} S_s^{1/2}} \tag{11}$$

where n^{of} is the Manning coefficient and S_s is the friction slope coefficient given by

$$S_s = \left[\left(\frac{\partial h^{of}}{\partial x} \right)^2 + \left(\frac{\partial h^{of}}{\partial v} \right)^2 \right]^{1/2}. \tag{12}$$

Nonlinear diffusion equation

The previously introduced governing equations for groundwater, soil and overland flow belong to the general class of (nonlinear) diffusion type partial differential equations which can be written as

$$A(u) \frac{\partial u}{\partial t} - \nabla \cdot B(u) \nabla u = Q(u) \tag{13}$$

where U is the unknown field function (primary variable), A is a capacitance matrix (representing time dependences), B is a conductivity matrix (representing space dependences) and Q is a source/sink term. In general A, B and Q are dependent on the unknown field function U which results in nonlinearities. The object-oriented numerical solution of different types of partial differential equations is described in (Wang & Kolditz 2007).

NUMERICAL METHODS

A variety of finite difference, finite element and finite volume methods are available to solve the partial differential equations appearing in hydrosystems (Weiyan 1992; Vreugdenhil 1994; LeVeque 2002; Starke 2005). In general, either of these methods leads to a (nonlinear) algebraic system of equations. In order to resolve nonlinearities in the governing equations, Picard and Newton–Raphson iteration schemes are used. For a comparison of both see, for instance, Paniconi *et al.* (1991). For the demonstration examples (see Examples) we use finite element methods, more specifically the Galerkin and the control volume finite element method with Picard and Newton–Raphson iteration, respectively, to solve the governing equations of the form (13) as these are well suited for problems with complex geometries. For time discretisation a weighting parameter enables the choice between fully explicit and implicit Euler stepping schemes. Usually time stepping for parabolic equations is chosen in accordance with the Neumann criterion (36).

Finite element method

The finite element method is based on the weak formulation of a partial differential equation, which allows the search for generalised solutions in Sobolev spaces. These contain discontinuous solutions and allow the assignment of discontinuous functions for material properties. The model domain is subdivided into small subdomains, the finite elements. The division can be performed according to geological structures, hydrological structures or other requirements. Calculations for these finite elements are performed after a transformation to a basis element. On each element the solution is locally approximated with piecewise polynomial functions forming the basis of an approximated solution space. The equation system for the solution of the unknown field function u is assembled from all element contributions.

Galerkin finite element method

The standard Galerkin finite element method is used for the subsurface compartments (soil and groundwater) because of the slow water movement. In order to obtain the weak formulation of the general diffusion equation, the expression (13) is multiplied by test functions v and

integrated over the domain Ω, giving

$$\int_\Omega v\left(A\frac{\partial u}{\partial t} - \nabla\cdot B\nabla u\right)\mathrm{d}\Omega = \int_\Omega vQ\,\mathrm{d}\Omega. \tag{14}$$

Applying Green's formula gives

$$\int_\Omega vA\frac{\partial u}{\partial t}\,\mathrm{d}\Omega + \int_\Omega \nabla v\cdot B\nabla u\,\mathrm{d}\Omega = \int_\Gamma v(B\nabla u)\cdot\mathbf{n}\,\mathrm{d}\Gamma + \int_\Omega vQ\,\mathrm{d}\Omega \tag{15}$$

where $\Gamma = \partial\Omega$ is the domain boundary. These equations are valid for all test functions v in the Sobolev space $H^1(\Omega)$. In the Galerkin and the control volume finite element method (see the next subsection) the unknown field functions U as well as test functions v belong to the same Sobolev space. For the numerical solution u is replaced by a finite-dimensional subspace spanned by polynomial basis functions. This is

$$u(t,x,y,z) \approx \hat{u}(t,x,y,z) = \sum_{j=1}^{\mathrm{ng}} \phi_j(x,y,z)u_j(t) = \sum_{j=1}^{\mathrm{ng}} \phi_j u_j \tag{16}$$

$$v(t,x,y,z) \approx \hat{v}(t,x,y,z) = \sum_{i=1}^{\mathrm{ng}} \phi_i(x,y,z)v_i(t) = \sum_{i=1}^{\mathrm{ng}} \phi_i v_i \tag{17}$$

where $\hat{u}$ and $\hat{v}$ are the approximate solutions, ϕ_i are the basis functions and ng the dimension of the subspace which is equal to the number of grid nodes in the finite element discretisation.

Therefore, Equation (15) is transformed into an algebraic equation system

$$\sum_{j=1}^{\mathrm{ng}}\left(\left[\int_\Omega \phi_i A\phi_j\mathrm{d}\Omega\right]\frac{\mathrm{d}u_j}{\mathrm{d}t} + \left[\int_\Omega \nabla\phi_i\cdot B\nabla\phi_j\mathrm{d}\Omega\right]u_j\right) = \int_{\partial\Omega}\phi_i(B\nabla u)\cdot\mathbf{n}\,\mathrm{d}\Gamma + \int_\Omega \phi_i Q\,\mathrm{d}\Omega \quad i = 1,\ldots\mathrm{ng}. \tag{18}$$

The basis functions are subdivided into local basis functions for each element e with the domain Ω^e giving

$$\sum_{s=1}^{ne}\left(\left[\int_{\Omega^e}\phi_r A\phi_s\mathrm{d}\Omega\right]\frac{\mathrm{d}u_s}{\mathrm{d}t} + \left[\int_{\Omega^e}\nabla\phi_r\cdot B\nabla\phi_s\mathrm{d}\Omega\right]u_s\right) = \int_{\partial\Omega^e}\phi_r(B\nabla u)\cdot\mathbf{n}\,\mathrm{d}\Gamma + \int_{\Omega^e}\phi_r Q\,\mathrm{d}\Omega \quad r = 1,\ldots,ne \tag{19}$$

where ne is the number of element nodes. Equation (19) can be written as

$$\sum_{s=1}^{ne}\left(A_{rs}^e\frac{\mathrm{d}u_s}{\mathrm{d}t} + B_{rs}^e u_s\right) = g_r^e + s_r^e + r_r^e \quad r = 1,\ldots,ne \tag{20}$$

where A_{rs}^e is the capacitance matrix, B_{rs}^e is the conductance matrix, g_r^e accounts for the gravity term, s_r^e for the source terms and r_r^e for the boundary fluxes. The integrals are calculated with the Gaussian integration scheme, yielding for the capacitance matrix entries

$$A_{rs}^e = \int_{\Omega^e}\phi_r A\phi_s\,\mathrm{d}\Omega = \int_{\hat{\Omega}^e}\hat{\phi}_r\hat{A}\hat{\phi}_s\det\mathbf{J}\,\mathrm{d}\hat{\Omega} = \sum_{k=1}^{gp} W_k(\hat{x}_k)\hat{\phi}_r(\hat{x}_k)\hat{A}(\hat{x}_k)\hat{\phi}_s(\hat{x}_k)\det\mathbf{J}(\hat{x}_k) \tag{21}$$

with the Jacobian matrix $\mathbf{J}$ of the coordinate transformation from the basis element domain $\hat{\Omega}$ to the element domain $\hat{\Omega}_e$ and the Gauss weights W_k. Entries of the capacitance matrix as well as of gravity, source and boundary flux vector are calculated accordingly. Applying an Euler finite difference scheme to Equation (20) for the approximation of the time derivative yields

$$\sum_{s=1}^{ne}\left(\frac{A_{rs}^e}{\Delta t} + \theta B_{rs}^e\right)u_s^{n+1} = g_r^e + s_r^e + r_r^e + \sum_{s=1}^{ne}\left(\frac{A_{rs}^e}{\Delta t} - (1-\theta)B_{rs}^e\right)u_s^n \quad r = 1,\ldots,ne \tag{22}$$

where θ is an implicit-explicit weighting parameter. Frequently mass lumping schemes are employed in order to stabilise the numerical method. Defining

$$M_r^e = \int_{\Omega^e} A\phi_r\,\mathrm{d}\Omega \tag{23}$$

the mass matrix lumped form of Equation (20) is

$$M_r^e\frac{\mathrm{d}u_r}{\mathrm{d}t} + \sum_{s=1}^{ne} B_{rs}^e u_s = g_r^e + s_r^e + r_r^e \quad r = 1,\ldots,ne \tag{24}$$

After the derivation of a general finite element scheme for the nonlinear diffusion Equation (13), the resulting finite element matrices are specified for the corresponding flow processes.

Control volume finite element method for overland flow

The traditional finite element methods such as the Galerkin and Petrov–Galerkin schemes tend to show non-physical oscillations for overland flow simulations (Giammarco *et al.* 1996; Beinhorn 2005). On the other hand, finite volume methods have shown how to handle these difficulties (LeVeque 2002). Giammarco *et al.* (1996) suggested the control volume finite element method which effectively combines the finite element with the finite volume method. It avoids oscillations by mass matrix lumping as well as conductivity term upwinding (Forsyth & Kropinski 1997) and guarantees local mass conservation. Using Lagrange polynomial basis functions ϕ_r where $\sum \phi_r = 1$, for the numerical approximation of the solution u and for the test function v, we have

$$\nabla \sum_{s=1}^{ne} u_s \phi_s = \nabla \sum_{s \neq r} \phi_s (u_s - u_r). \tag{25}$$

This allows usto express the diffusion term in Equation (19) as a function of the primary variable difference between node r and its neighbours. Using this scheme, the lumped mass matrix Equation (24) becomes

$$V_r^e \frac{\mathrm{d}u_r}{\mathrm{d}t} + \sum_{s \neq r} B_{rs}^e (u_s - u_r) = s_r^e + r_r^e \quad r = 1, \ldots, ne \tag{26}$$

where

$$V_r^e = \int_{\Omega^e} \phi_r \, \mathrm{d}\Omega. \tag{27}$$

The conductance term can be written as $B = k_{\mathrm{rel}}\ \mathbf{K}$, where $k_{\mathrm{rel}}(u)$, $\mathbf{K}$ represent primary variable dependent and independent parts, respectively. They are given for overland flow by Equations (10) and (11), respectively. Therefore, Equation (26) becomes

$$V_r^e \frac{\mathrm{d}u_r}{\mathrm{d}t} = \sum_{s \neq r} \lambda_{rs+1/2} \gamma_{rs}^e (u_s - u_r) + s_r^e + r_r^e \quad r = 1, \ldots, ne \tag{28}$$

where

$$\gamma_{rs}^e = \int_{\Omega^e} \nabla \phi_r \mathbf{K} \nabla \phi_s \, \mathrm{d}\Omega = \int_{\Omega^e} \hat{\nabla} \hat{\phi}_r \hat{\mathbf{K}} \hat{\phi}_s \det \mathbf{J} \, \mathrm{d}\hat{\Omega}$$
$$= \sum_{k=1}^{\mathrm{gp}} W_k(\hat{x}_k) \hat{\nabla} \hat{\phi}_r(\hat{x}_k) \hat{\mathbf{K}}(\hat{x}_k) \hat{\nabla} \hat{\phi}_s(\hat{x}_k) \det \mathbf{J}(\hat{x}_k) \tag{29}$$

and upwinding is implemented by

$$\lambda_{rs+1/2} = \begin{cases} k_{\mathrm{rel}\,s}; \text{ if } \gamma_{rs}(u_s - u_r) > 0 \\ k_{\mathrm{rel}\,r} \text{ if } \gamma_{rs}(u_s - u_r) < 0 \end{cases} \tag{30}$$

such that k_{rel} represents a weighted conductivity. The right-hand-side terms s_r^e, r_r^e are coupling terms to the soil compartment. The Euler time stepping scheme gives

$$\frac{V_r^e}{\Delta t} u_r^{n+1} + \theta \sum_{s \neq r} \lambda_{rs+1/2}^{n+1} \gamma_{rs}^e \left(u_s^{n+1} - u_r^{n+1} \right)$$
$$= s_r^e + r_r^e - \frac{V_{rs}^e}{\Delta t} u_s^n - (1 - \theta) \sum_{s \neq r} \lambda_{rs+1/2}^n \gamma_{rs}^e (u_s^n - u_r^n) \tag{31}$$
$$r = 1, \ldots, ne$$

with the implicit-explicit weighting parameter θ. For linearisation a Newton–Raphson scheme is applied. The Jacobian matrix in this iteration is approximated by a numerical derivative, which provides an effective matrix assembly method (Forsyth *et al.* 1995).

Object orientation

Object-oriented programming regards a software programme as a collection of objects and their defined interactions. Hereby, objects are instances of (abstractly) defined classes that contain both data (also called properties) and functions (also called methods) to manipulate this data. Thus the so-called encapsulation is achieved, as an object's (protected) properties can only be accessed by its own methods. Defined interaction between objects (also of objects belonging to different classes) is achieved by one object calling the other object's methods and vice versa. Another fundamental concept is inheritance, where new classes may be defined by inheriting properties and methods from already existing classes. If properly designed, these concepts achieve two of the big advantages of object

orientation: easy extendability of the software's functionality and code reuse.

In the scientific software environment GeoSys/RockFlow a central unit is the top-level process class (PCS). All numerical processes described above are instances of this base class. Each PCS object contains its relevant PDE solution procedure objects: FEM (for finite element method), TIM (for time discretisation), EQS (equation system including solver) as well as process-related material properties (MAT), boundary condition (BC), initial condition (IC) and source term objects (ST) (Kolditz & Bauer 2004) as well as a computational mesh object (MSH). The development and implementation of the MSH class for instantiation of meshes for the different hydrological compartments is the novel part of the GS/RF code development in this work.

Geometries are defined process-independent by geometrical objects such as points, polygons, surfaces and volumes (GEO). These can be used for a computationally efficient visualisation of overall geometries as well as for initialisation of MSH objects, e.g. for the initial definition of the individual compartments. However, depending on the flow process and/or the coupling of processes the MSH object itself is allowed to adapt in accordance with the temporal and/or spatial evolution of the process(es). Thereby, (adjacent) MSH objects of coupled processes are required to be topologically consistent at their mutual interface. The latter means that each coupling boundary element of a MSH object always has a defined neighbouring element belonging to a coupled MSH object. Based on these topological mesh relations the assignment of correct coupling fluxes is facilitated.

COUPLING CONCEPT

In general, two concepts exist for equation coupling: monolithic schemes for strongly coupled systems (e.g. Wang & Kolditz 2007) and partitioned (or staggered) techniques for weakly connected systems. If we focus on hydrological systems, distinct and separate compartments such as surface, soil (vadose zone) and aquifers can be recognised. In fact, compartment interactions take place only at their combined interfaces, such as the ground surface, capillary fringe and water table. Moreover, the time and space scales of hydraulic processes in different compartments typically differ substantially. Time scales of flow processes can easily range from seconds (e.g. overland flow) to years (e.g. flow in low-permeability aquitards). Therefore, we have adopted a partitioned coupling scheme for hydrosystems modelling. For the surface/soil/groundwater hydrosystem the equation system becomes

$$\begin{aligned}[P^{\mathrm{of}}][u^{\mathrm{of}}] &= [r^{\mathrm{of}} + r^{\mathrm{of/sf}}] \\ [P^{\mathrm{sf}}][u^{\mathrm{sf}}] &= [r^{\mathrm{sf}} + r^{\mathrm{sf/of}} + r^{\mathrm{sf/gf}}] \\ [P^{\mathrm{gf}}][u^{\mathrm{gf}}] &= [r^{\mathrm{gf}} + r^{\mathrm{gf/sf}}]\end{aligned} \tag{32}$$

where P^*, u^*, r^* are system matrix, solution vector and RHS vector for overland, soil and groundwater flow, respectively, the exponents of, sf, gf indicate overland flow, soil and groundwater flow, respectively, and $r^{\mathrm{of/sf}}$, $r^{\mathrm{sf/of}}$, $r^{\mathrm{sf/gf}}$ denote compartment exchange terms. In the partitioned scheme the computation of the individual processes can be conducted at completely different temporal and spatial discretisations using different numerical methods. The computational advantage is that the numerical schemes for each process can be optimised despite the differences in their corresponding physical scales.

Flux coupling

The coupling concept is based on first-order flux exchange relationships at the compartment interfaces (Figure 2). Depending on hydrological/hydrogeological considerations, each compartment may be subdivided into subdomains ($A_i^{\mathrm{of}}, A_j^{\mathrm{sf}}, A_k^{\mathrm{gf}}$). An important requirement for flux coupling is topological consistency, specifically, the inter-

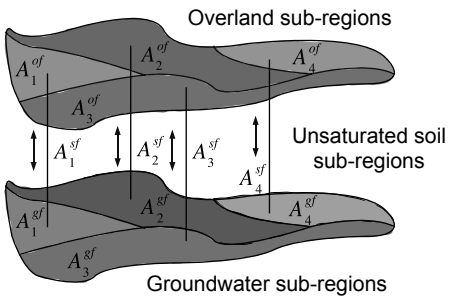

Figure 2 | Flux-oriented coupling approach.

face area between coupled compartments has to be the same for both.

If we consider the coupling between overland flow and unsaturated flow in soils, the vertical fluxes of the former are collected and passed to the latter process within hydraulically relevant time periods. This means integrating fluxes on certain compartment elements over proper time intervals, yielding source terms. The overland and soil process coupling is

$$Q_i^{\mathrm{of}}\Delta t = -Q_i^{\mathrm{sf}}\Delta t = \int_{\Delta t^{\mathrm{sf}}}\int_{A_i^{\mathrm{sf}}} q^{\mathrm{of/sf}} \times \left(\Lambda^{\mathrm{of/sf}}(x,y,t), u^{\mathrm{of}}(x,y,t), u^{\mathrm{sf}}(x,y,t)\right)\mathrm{d}\Omega\,\mathrm{d}t \tag{33}$$

where the exchange flux $q^{\mathrm{of/sf}}$ depends on both an exchange coefficient $\Lambda^{\mathrm{of/sf}}$ and the hydraulic heads of both processes. For first-order coupling it is

$$q^{\mathrm{of/sf}} = \Lambda^{\mathrm{of/sf}}(u^{\mathrm{sf}} - u^{\mathrm{of}}). \tag{34}$$

As an example we provide the coupling equation for the surface and soil compartments which is based on an interface layer concept (Delfs *et al.* 2007, 2008). The interface layer allows the definition of a discrete exchange flux to couple the flow processes in both compartments mutually. The description of the interface flux is motivated by a Darcy approach (VanderKwaak 1999):

$$q^{\mathrm{of/sf}} = -k_r^{\mathrm{c}} K^{\mathrm{c}} \frac{h^{\mathrm{of}} - h^{\mathrm{sf}}}{a} \tag{35}$$

where $k_r^{\mathrm{c}} \in [0,1]$ is a infiltration capacity, K^{c} is the interface layer conductivity and a is the interface layer thickness. The infiltration capacity is given by $k_r^{\mathrm{c}} = \min((\theta^{\mathrm{sf}})^{2(1-S)}, 1)$, where $\theta = h^{\mathrm{of}}/a$.

Technically, during the source/sink term calculations, node and element contributions from corresponding areas (e.g. A_1^{of} for A_1^{sf}) are exchanged. The same technique is used for the soil/groundwater interface.

Time stepping synchronisation

Besides spatial discretisation, time stepping schemes need to meet process-specific requirements. This is critical for numerical stability as each individual flow process may require completely different time steps. This is underlined by the Neumann criteria for maximum time steps in diffusion type partial differential Equations (13):

$$\Delta t = \frac{1}{2}\frac{\Delta l^2}{D} \tag{36}$$

where Δl is a characteristic length scale of the spatial discretisation and D is a process-related diffusivity coefficient.

The time stepping for all processes was synchronised in order to calculate exchange terms according to Equation (33). Table 1 illustrates the implementation of the synchronisation scheme between the different processes. In the Borden site demonstration example (see Rainfall–runoff experiment) we use fully implicit time stepping with the following intervals: $\Delta t = 10^2$ s for overland flow, $\Delta t \sim 10^3$ s (adaptive) for soil flow and $\Delta t = 10^4$ s for groundwater flow.

Ultimately, the above illustrates the central feature of the compartment approach: each individual flow and transport process can have its own discretisation in space and in time (Figure 1).

EXAMPLES

In this section three examples are provided in order to verify the compartment approach and to demonstrate the applicability of this concept to field data.

The verification of the present numerical code for the individual processes is given, for example, in Kolditz *et al.* (1998) and Beinhorn (2005). Despite abundant test cases for flow in saturated and unsaturated porous media (e.g. Segol 1993) or overland flow (e.g. van Rijn 1986) only a few

Table 1 | Coupling scheme for time discretisation

Δt	Overland (OF)	Soil (SF)	Groundwater (GF)	Coupling
1	Δt_1^{of}			
⋮	⋮			
i	Δt_i^{of}	Δt_1^{sf}		OF/SF
⋮	⋮	⋮		
j	Δt_j^{of}	Δt_k^{sf}	Δt_1^{gf}	OF/SF/GF
⋮	⋮	⋮	⋮	

examples are available for testing numerical models for coupled surface–subsurface systems. In order to prove the correct coupling between overland and soil water flow, the Smith & Woolhiser (1971) problem is considered (see the next subsection). In this laboratory experiment the soil conditions were found to dominate the coupled hydrosystem behaviour. In addition, an example in the Borden aquifer with the focus on coupling of the overland, soil and groundwater processes across temporal and spatial scales is demonstrated (see Rainfall–runoff experiment). Finally, through a field application to the Beerze–Reusel catchment in the Meuse river basin (see Beerze–Reusel drainage basin), a high resolution of the infiltration dynamics could be achieved with the compartment approach.

Smith & Woolhiser laboratory experiment

A well-known problem in process coupling is that, even if numerical models for the individual processes are implemented correctly, their combination can fail if the coupling scheme is not appropriate. Therefore, the compartment approach was tested against experimental data. Delfs *et al.* (2007) provided a detailed analysis of the classic experiment by Smith & Woolhiser (1971) on infiltration excess (Hortonian) overland flow. The Smith & Woolhiser problem is one of the few experimental datasets available for the analysis of coupled surface/subsurface flow systems and was used for a code intercomparison study (Figure 3).

The study by Delfs *et al.* (2007) was focused on (i) a comparison of different conceptual models and (ii) a parameter sensitivity study. Therein, different conceptual approaches were compared for overland flow (i.e. Saint-Venant vs kinematic and diffusive wave approximations), soil water movement (Richards vs Green–Ampt models) and, in particular, their coupling. It could be shown that a flux-based coupling concept using an interface layer reproduces the experimental results appropriately. Moreover, further reduction in model complexity was achieved as the Green–Ampt model could successfully reproduce water flow in the unsaturated zone. As an example Figure 3 shows a comparison of computed hydrographs for the overland flow of the GS/RF code and those obtained from several studies on the Smith & Woolhiser experiment.

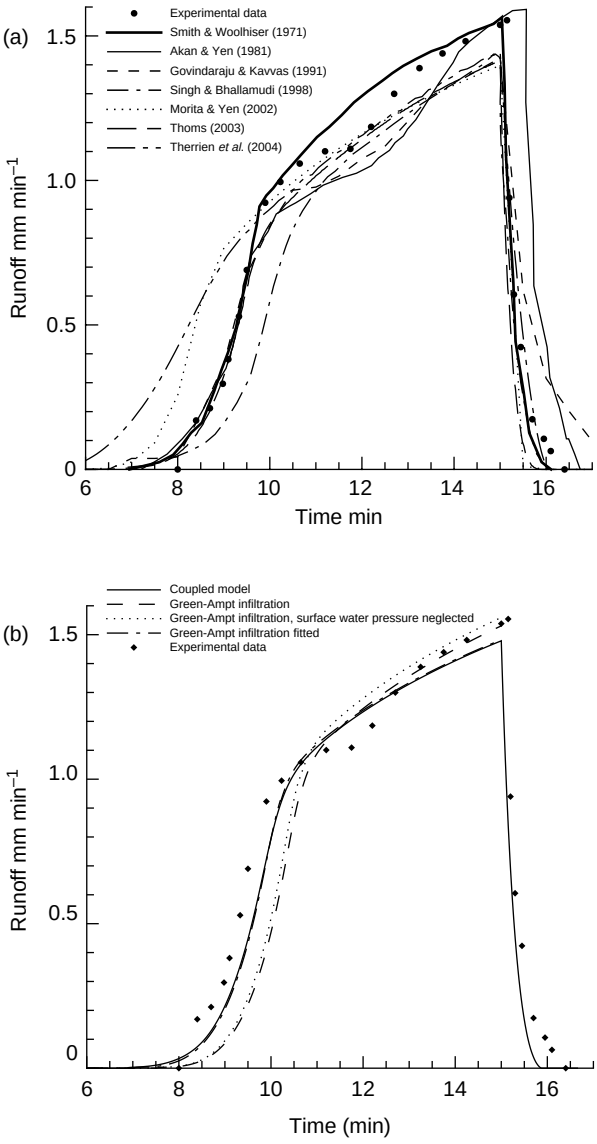

Figure 3 | Hydrograph results for the Smith & Woolhiser problem. Left: existing studies, right: GS/RF present results (interface layer/compartment approach).

Rainfall–runoff experiment at the Borden aquifer

The second example is based on a field-scale rainfall–runoff experiment at the Canadian Forces Base, Borden, Ontario. The experimental set-up and evaluation are described in Abdul (1985) and Abdul & Gilham (1989). A comprehensive documentation of site details, flow characteristics and results can be found in VanderKwaak (1999) and Hydrosphere (2004). In order to apply the presented compartment approach for the coupling of overland, soil water and

groundwater flow, we modified the description of the subsurface zone. We introduced two separate compartments, one for an unsaturated and one for a groundwater domain of two and ten meters thickness, respectively.

Figure 4 shows the elevation of the land surface with the stream bed in the middle. It consists of a man-made channel surrounded by grass-covered land and has a depth of approximately 1.2 m. Prior to the beginning of the experiment the channel is dry. Then uniform artificial recharge is applied at a rate of $0.02\,\mathrm{m\,h^{-1}}$ over the entire area for 50 min. The rainfall intensity is the same over the entire area. The total experiment lasts 24 h. The following hydrologic processes were recognised to govern the field experiment (Abdul 1985; Abdul & Gilham 1989): water infiltration in upland region, discharge into lower areas and surface runoff.

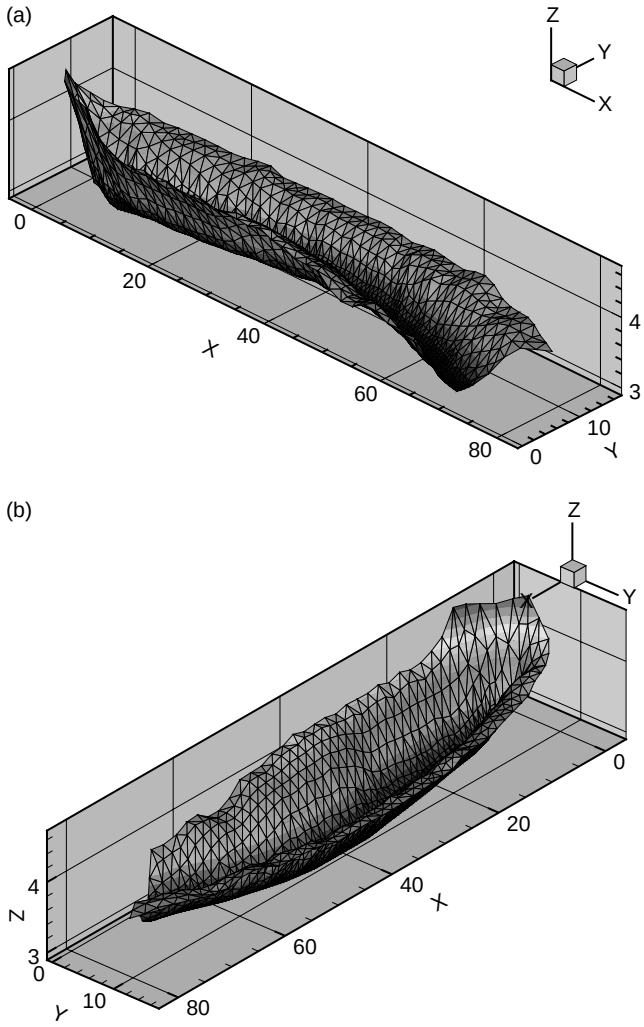

Figure 4 | Channel geometry of the field-scale rainfall–runoff experiment.

The parameter values for overland, Richards, and Darcy flows in this model set-up are provided in Table 2.

Figure 5 depicts the discretisation of the multi-mesh system for the Borden study. Three topologically coupled meshes are used for the surface, soil and groundwater compartments. The multi-mesh system consists of the following numbers and types of elements: 2,651 triangles for the surface, 106,040 line elements for the soil and 26,510 prisms for the aquifer. Each soil column has 40 line elements and the groundwater compartment is split into 10 element layers. The governing equations are solved fully implicitly with fixed time steps of $\Delta t = 10^2\,\mathrm{s}$ and $\Delta t = 10^4\,\mathrm{s}$ for overland flow and groundwater flow, respectively. For soil water flow a self-adaptive time stepping is applied, resulting in time steps of the order of $\Delta t = 10^3\,\mathrm{s}$.

The results of the coupled flow modelling are depicted in Figures 6–8. The surface water level within the stream channel is shown in Figure 6 for the first hour. The water level rise is a result of the uniform recharge applied during the first 50 min. The water flows rapidly into the topographically lowest part of the channel in the middle of the domain and follows its course to the outlet at $x = 80\,\mathrm{m}$ (lower domain boundary). After precipitation has stopped, the water level in the channel commences to decline.

Figure 7 illustrates the infiltration process resulting from overland flow. The water saturation is shown for different times at a soil depth of 1 m. With increasing simulation time the

Table 2 | Properties of the coupled hydrosystem

Parameter	Symbol	Value	Unit
Manning coefficient	n^{of}	0.15	$\mathrm{s\,m^{-1/3}}$
Soil porosity	n^{sf}	0.37	–
Soil permeability	k^{sf}	2.95×10^{-13}	$\mathrm{m^2}$
Residual saturation	S_{res}	0	–
van Genuchten parameter	α	1.43	$\mathrm{m^{-1}}$
van Genuchten parameter	M	0.336	–
Aquifer porosity	n^{gf}	0.33	–
Aquifer storage coefficient	S_0^{gf}	1.2×10^{-7}	$\mathrm{m^{-1}}$
Aquifer hydraulic conductivity	$\mathbf{K}^{\mathrm{gf}}$	10^{-5}	$\mathrm{m\,s^{-1}}$

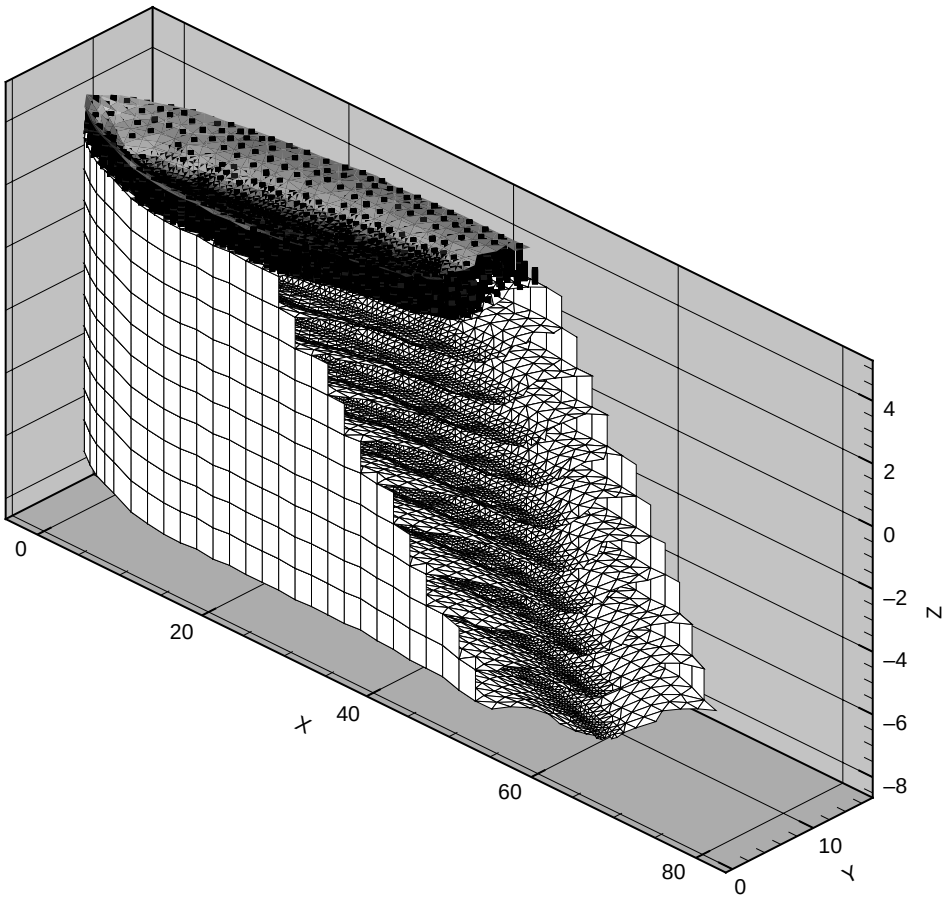

Figure 5 | MultiMSH discretisation of the test catchment consisting of triangle elements for overland flow, line elements for soil water movement, and prism elements for groundwater flow.

water saturation keeps increasing – even after the artificial recharge was stopped. An overland/soil coupling flux is used which depends solely on the hydrostatic surface water pressure, leading to a large contrast in overland and soil velocities and spatially distinctive head profiles. As the surface water depth drives the infiltration rate, the largest increase in water saturation is found in the middle of the channel.

The hydraulic head distribution in the groundwater compartment is shown in Figure 8. Due to the buffering effect of the increasing soil moisture content, no significant hydraulic reaction of the aquifer is observed at the beginning of the rainfall event. After 12 h the infiltrated rainfall water reaches the aquifer top and causes a local increase in hydraulic head along the channel bottom. This leads to a small deformation of the flow pattern, resulting in some lateral flow towards the left and right domain boundaries. This effect slowly decreases as less water reaches the groundwater table at the end of the simulation time period. These results are in good qualitative agreement with the expected system response. This example demonstrates the ability of the compartment approach to couple surface and subsurface processes across distinct temporal and spatial scales.

Beerze–Reuzel drainage basin

In this subsection we present a real-world application of the compartment approach. The study region is located in the Province of North Brabant in the southern half of the Netherlands. The size of the Beerze–Reusel drainage basin is about 440 km^2 large (Figure 9 (left)). The subsoil mainly consists of sandy deposits formed in the Pleistocene. The generally flat region gently slopes in a north to northeast direction. There are several aeolian sand ridges up to a few

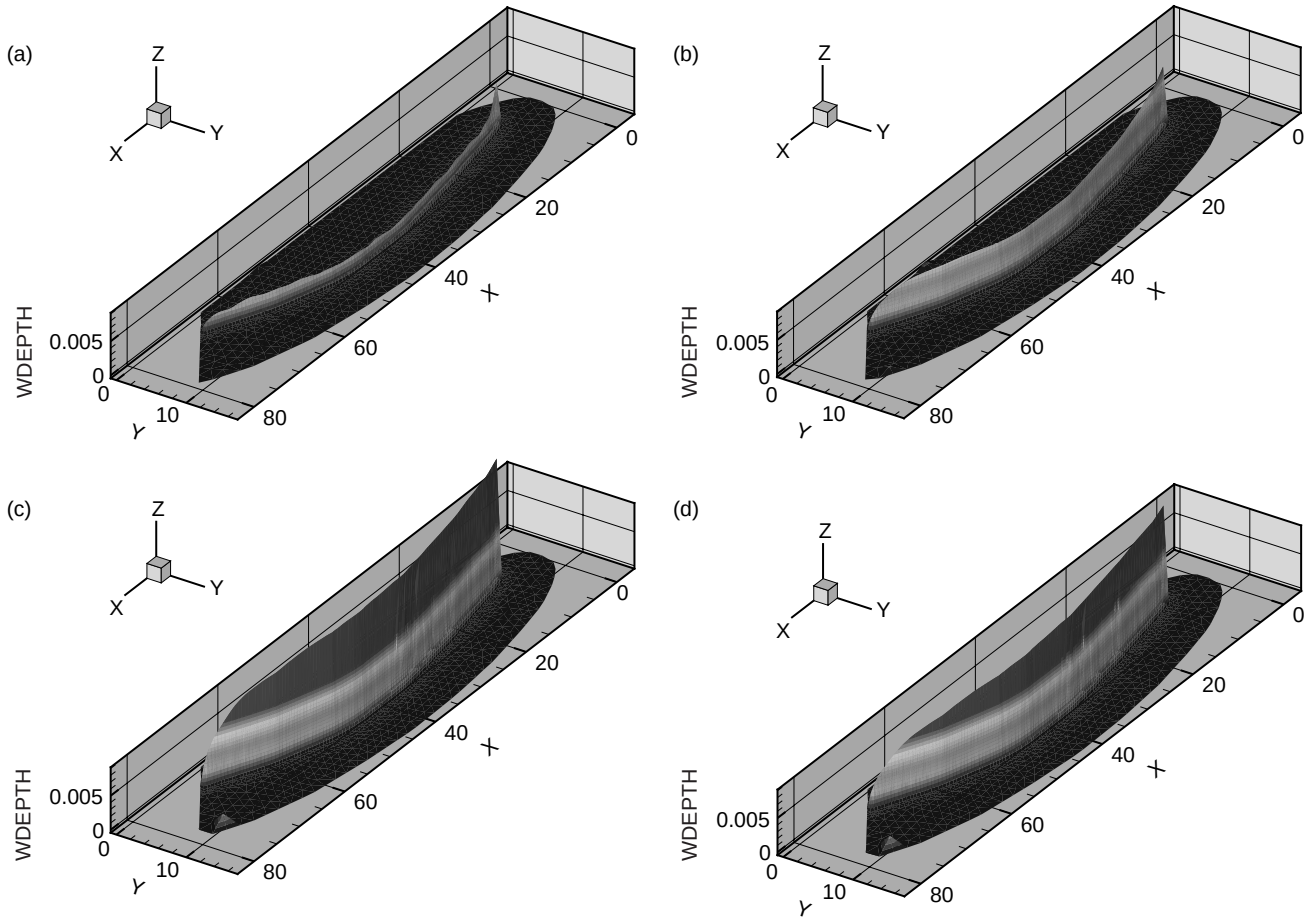

Figure 6 | Water depth in the channel after 10, 20, 50 min and 1 h ((a)–(d)), respectively.

metres in height that are oriented in a west to east direction. In the valleys alluvial soils have been formed consisting of redeposited sand, loam and peat. Because of the intensive agricultural drainage of the areas these peaty soils are strongly oxidized and have often become very shallow. Agriculture is the dominant land use in the region – grassland and maize being the most frequently used crops. Hence, the movement of soil moisture appears very important to assess the nitrate transport into the groundwater system.

The objective of the case study is, at first, to develop a hydrologic soil model for the Beerze–Reusel drainage basin at a regional size in order to evaluate the nitrate cycle at the catchment scale later on.

A comprehensive soil database was made available from the Geological Survey of the Netherlands for this study. The database represents the result of a soil classification survey where more than 12,000 influence areas were identified that represent the lateral extent of distinct soil profiles (van der Grift *et al.* 2006). These influence areas are outlined by polygons as shown in Figure 9 (right). The more densely arranged polygones follow the river sediments indicate the flow network of the Beerze–Reusel catchment. For each of these influence areas the vertical stratification of soil types, as well as the corresponding hydraulic (van Genuchten) parameter, is given. Based on this unique dataset the concept of a regional hydrological soil model (RHSM) for the entire drainage basin (440 km^2) was developed. It allows us to keep a high vertical resolution (here 5 cm) of the soil compartment for the solution of the Richards' equation over a large lateral extent. The time step was made adaptive for numerical reasons. The high resolution of the soil compartment is indispensable in order to represent the unsaturated flow through the heterogeneous soil properly by a numerical Richards' model.

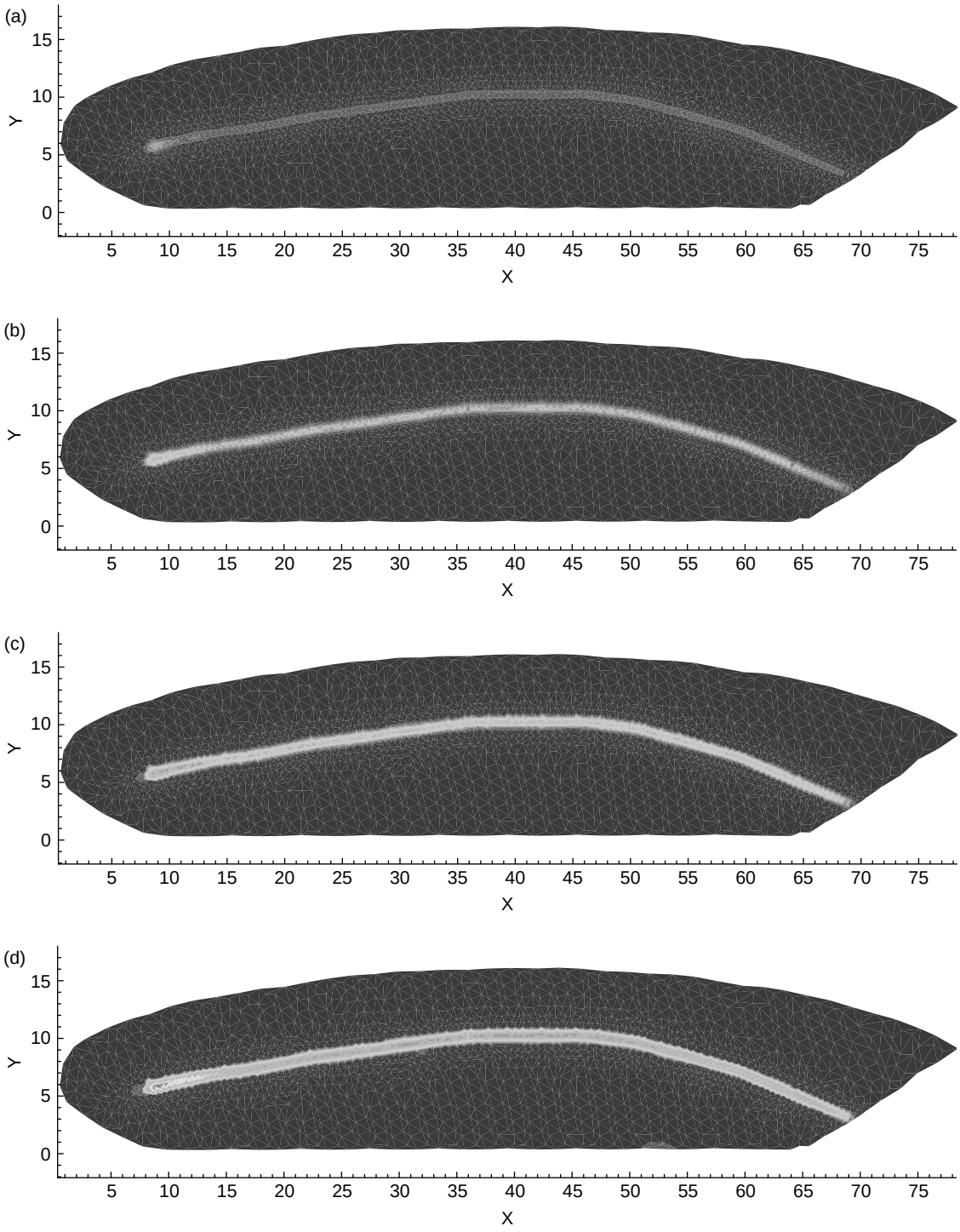

Figure 7 | Water saturation in the soil compartment at 1, 3, 6 and 12 h ((a)–(d)), respectively.

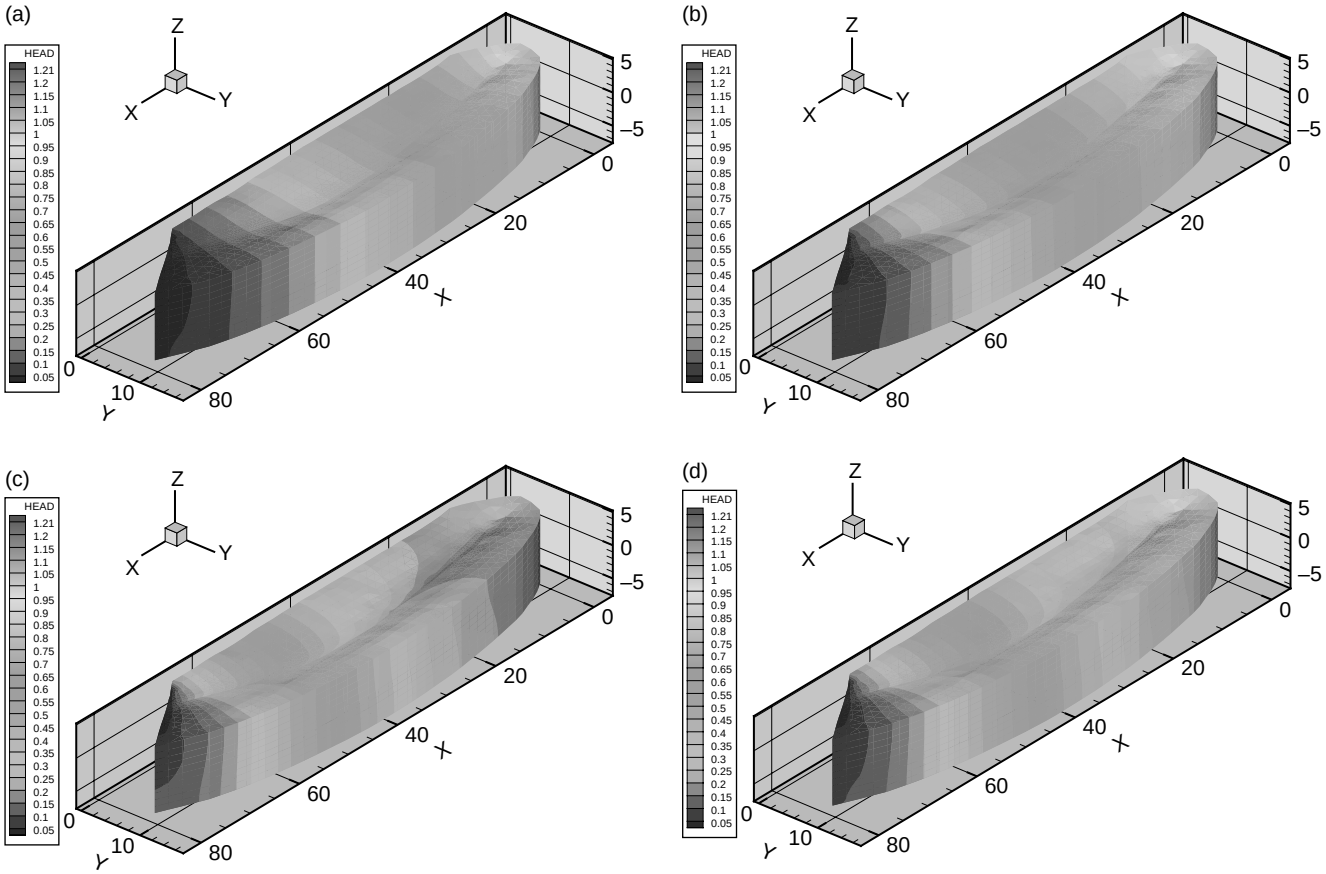

Figure 8 | Hydraulic head in the groundwater compartment at 1, 3, 12 and 24 h ((a)–(d)), respectively.

Figure 10 (right) shows calculated moisture profiles for an example influence area. Figure 10 (left) illustrates the regional moisture pattern which is assembled from all influence areas. As within the modelled time span the precipitation–evaporation conditions were rather homogeneous in the region, the pronounced differential moisture propagation is interpreted as being primarily due to the local variation of hydraulic soil properties. The regional groundwater recharge distribution is calculated from the soil water Darcy velocities multiplied by the corresponding influence area of each soil profile. More details including software development, data import and conversion tools are described in Kolditz *et al.* (2007).

Due to the still enormous number of finite elements for the RHSM of the Beerze–Reusel drainage basin, computation times are very expensive (about one month CPU time for a one-year simulation). Therefore, RHSM

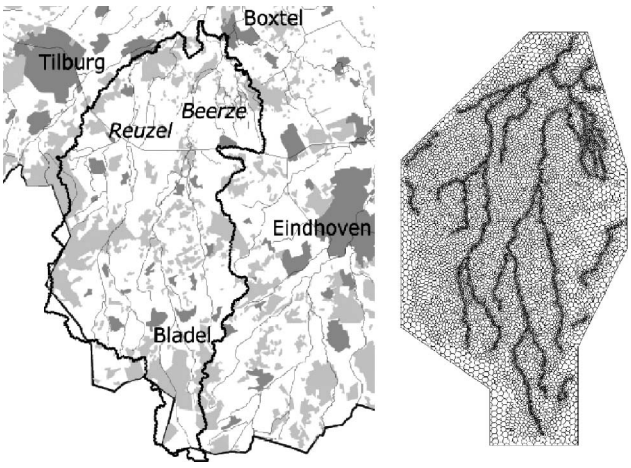

Figure 9 | Beerze–Reusel study area in the Meuse basin (left), identified influence areas for soil type characterization (right).

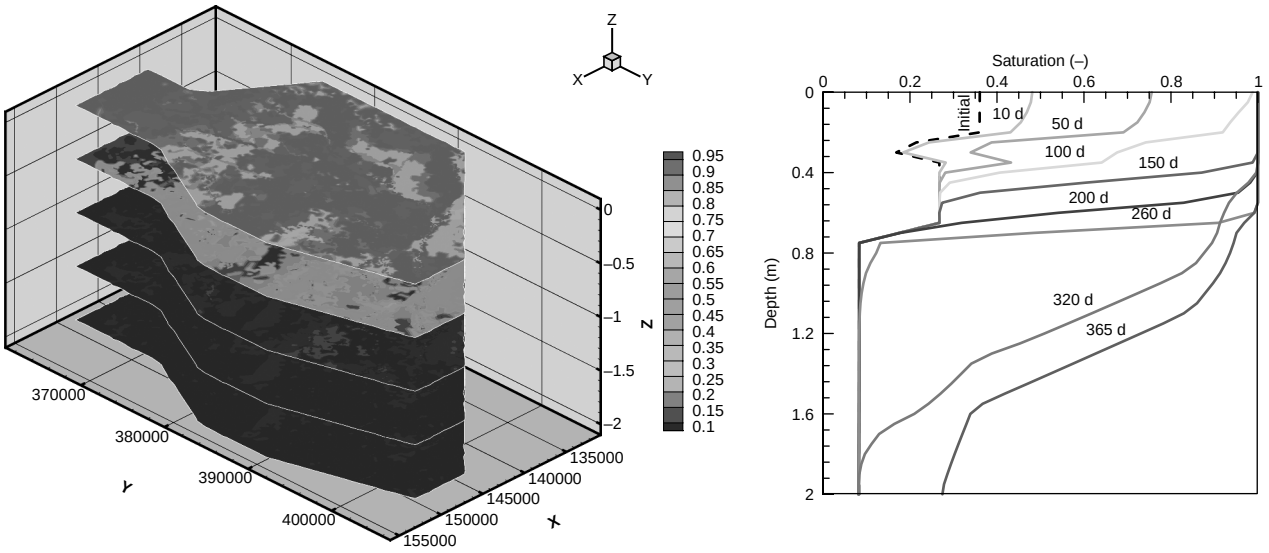

Figure 10 | Snapshot of the regionally heterogeneous moisture distribution (left), evolution of vertical moisture profiles in a selected influence area (right).

parallelisation became necessary for computation of this type of real-world applications.

CONCLUSIONS AND FUTURE WORK

In this paper we presented a compartment approach for the numerical simulation of coupled processes in hydrosystems comprising of overland, unsaturated and groundwater flows. We demonstrated the applicability and limitations of this approach in three example studies spanning from laboratory to catchment scale:

- The classic laboratory experiment by Smith & Woolhiser (1971) on infiltration excess (Hortonian) overland flow (1–10 m scale),
- a (small) field-scale experiment at the Borden site by Abdul & Gilham (1989) (10–100 m scale), and
- a field-scale study on regional infiltration in the Beerze–Reuzel drainage basin (about 440 km^2 catchment size).

The case studies show that the underlying (nonlinear) diffusion-type Equations (13) can be solved efficiently utilising the compartment approach's inherent flexibility for combining different numerical methods (G-FEM and CV-FEM) with accordingly adapted spatial and temporal discretisations. The object-oriented software concept, which was originally developed for hydrogeological problems (Kolditz & Bauer 2004), can be identified as a key component for this achievement. Based on the earlier work only two basic features had to be developed in a new mesh class to extend the GeoSys/RockFlow (GS/RF) scientific software environment for a hydrological compartment approach: (1) mesh instances are used for distinct compartment discretisations and (2) coupling terms are located based on topological mesh relations.

Using the regional hydrologic soil model (RHSM) concept (see Beerze–Reuzel drainage basin), comparatively thin soil layers can be incorporated into large catchment areas and coupled to overland and groundwater flow. A potential application of the RHSM could be hydrological upscaling analysis, e.g. for the calculation of groundwater recharge from precipitation without losing accuracy due to restrictions on the vertical soil resolution.

Although the presented work shows the flexibility and potential of the compartment approach for numerical analysis of hydrosystems at different scales, future work is needed, for example in the following directions:

- The development of qualified benchmarks for quantitative verification of fully coupled surface/soil/groundwater hydrosystems: a major focus hereby is the evaluation of numerical coupling errors. These are expected to be dominated by the consideration of the influence of the exchange terms on the stability in

the numerical scheme, which limits the compartments individuality. The Neumann criterion given by Equation (36) ignores flux terms such that its application as a guideline is restricted in coupled hydrosystem models.

- The evaluation of lateral flow effects in the soil compartment: Using column elements for the RHSM we neglect lateral flows in the soil. This assumption holds for flat ground surface areas and a relatively homogeneous infiltration process. If significant lateral pressure or moisture gradients, even in flat areas, should exist, horizontal flow components in the soil layer have to be considered. This shortcoming can be solved by the use of prism instead of line elements for the soil layer discretisation.

ACKNOWLEDGEMENTS

This work was funded by the European Union FP6 Integrated Project "AquaTerra" (project no. 505428) under the thematic priority "Sustainable development, global change and ecosystems". We thank the anonymous reviewers for their careful reviews based on which the manuscript was substantially improved. We are grateful to the Tübingen coordination team (J. Barth, E. Frank and P. Grathwohl) for saving us lots of time for research. We would also like to thank C. Chen, Y. Du, M. Hess, C. McDermott, R. Walsh, W. Wang and M. Xie for commenting on the manuscript.

REFERENCES

Abbott, M. B. 2003 Discussion of "the relevance of open source to hydroinformatics" by Harvey & Han (2002). *J. Hydroinf.* **5** (3), 203–206.

Abbott, M. B., Babovic, V. M. & Cunge, J. A. 2001 Towards the hydraulics of the hydroinformatics era. *J. Hydraul. Res.* **39** (4), 339–349.

Abbott, M. B., Bathurst, J. C., Cunge, J. A., O'Connell, P. E. & Rasmussen, J. 1986 An introduction to the European hydrological system–Système Hydrologique Européen (SHE), 1: history and philosophy of a physically-based, distributed modelling system. *J. Hydrol.* **87** (1), 45–59.

Abbott, M. B., Bathurst, J. C., Cunge, J. A., O'Connell, P. E. & Rasmussen, J. 1986 An introduction to the European hydrological system–Système Hydrologique Européen (SHE), 2: structure of a physically-based, distributed modelling system. *J. Hydrol.* **87** (2), 61–77.

Abdul, A. S. 1985 *Experimental and Numerical Studies of the Effect of the Capillary Fringe on Streamflow Generation*. Department of Earth Sciences, University of Waterloo. Ontario.

Abdul, A. S. & Gilham, R. W. 1989 Field studies of the effects of the capillary fringe on streamflow generation. *J. Hydrol.* **112**, 1–18.

Alfredsen, K. & Saether, B. 2000 An object-oriented application framework for building water resource information and planning tools applied to the design of a flood analysis system. *Environ. Modell. Software* **15** (3), 215–224.

Anderson, M. G. & Burt, P. T. 1985 *Hydrological Forecasting*. Wiley. New York.

Arnold, J. G., Sirinivasan, R., Muttiah, R. S. & Williams, J. R. 1998 Large area hydrologic modeling and assessment. Part 1 - model development. *J. AWRA* **34** (1), 73–89.

Banta, E. R., Poeter, E. P., Doherty, J. E. & Hill, M. C. 2006 *JUPITER: Joint Universal Parameter IdenTification and Evaluation of Reliability–An Application Programming Interface (API) for Model Analysis.* USGS Techniques and Methods, 06-E1, US Geological Survey. Available at: http://water.usgs.gov/nrp/gwsoftware/jupiter/jupiter_api.html

Barth, M., Hennicker, R., Kraus, A. & Ludwig, M. 2004 DANUBIA: an integrative simulation system for global change research in the Upper Danube Basin. *Cybern. Syst.* **35** (7–8), 639–666.

Bear, J. 1988 *Dynamics of Fluids in Porous Media*, 2nd edition. Dover Publications. New York.

Beinhorn, M. 2005 *Non-linear Flow Processes in Subsurface and Surface Hydrosystems.* PhD Thesis, Center of Applied Geoscience, University of Tübingen.

Bertoldi, G., Tamanini, D., Zanotti, F. & Rigon, R. 2004 *GEOtop, A Hydrological Balance Model, Technical Description and Programs Guide (version 0.875).* Department of Civil and Environmental Engineering, University of Trento.

Chen, Q., Morales-Chaves, Y., Li, H. & Mynett, A. E. 2006 Hydroinformatics techniques in eco-environmental modelling and management. *J. Hydroinf.* **8** (4), 297–316.

CUASHI 2007 Available at: http://river.sdsc.edu/HDAS

Delfs, J. O., Du, Y., Burger, C. M., Kolditz, O. 2007 *Re-analysis of the Laboratory Experiments by Smith and Woolhiser (1971) for Coupled Overland/Soil Water Flow.* Technical Report, Center of Applied Geosciences, University of Tübingen.

Delfs, J. O., Park, C.-H. & Kolditz, O. 2008 *Sensitivity Analysis for Validation of an Interface Concept for Coupled Overland and Soil Water Flow.* ENVIN-Report, 07/2008, Helmholtz Center for Environmental Research, UFZ, Leipzig.

Desitter, A., Bates, P. D., Anderson, M. G. & Hervouet, J.-M. 2000 Development of one, two, and three-dimensional finite element groundwater models within a generalized object-oriented framework. *Hydrol. Process.* **14** (13), 2245–2259.

Donigian, A. S. & Imhoff, J. 2006 History and evolution of watershed modeling derived from the stanford watershed model. In *Watershed Models* (Singh V. P. & Frevert D (Eds.)), CRC Press. Boca Raton, FL, pp. 21–46.

Elshorbagy, A. & Ormsbee, L. 2006 Object-oriented modeling approach to surface water quality management. *Environ. Modell. Softw.* **21** (5), 689–698.

Forde, B. W. R., Foschi, R. O. & Stiemer, S. F. 1990 Object-oriented finite element analysis. *Comput. Struct.* **34** (3), 355–374.

Forsyth, P. A. & Kropinski, M. C. 1997 Monotonicity considerations for saturated-unsaturated subsurface flow. *SIAM J. Sci. Comput.* **18**, 1328–1354.

Forsyth, P. A., Wu, Y. S. & Pruess, K. 1995 Robust numerical methods for saturated-unsaturated flow with dry initial conditions in heterogeneous media. *Adv. Water Res.* **18**, 25–38.

Freeze, R. A. & Harlan, R. L. 1969 Blueprint for a physically based, digitally-simulated hydrological response model. *J. Hydrol.* **9**, 237–258.

Gandy, C. J. & Younger, P. L. 2007 An object-oriented particle tracking code for pyrite oxidation and pollutant transport in mine spoil heaps. *J. Hydroinf.* **9** (4), 293–304.

Gerbeau, J.-F. & Perthame, B. 2001 Derivation of viscous Saint-Venant system for laminar shallow water: numerical validation. *Discr. Cont. Dyn. Syst. Ser.* **B1**, 89–102.

Giammarco, P. D., Todini, P. E. & Lamberti, P. 1996 A conservative finite elements approach to overland flow: the control volume finite element formulation. *J. Hydrol.* **175**, 267–291.

Gregersen, J. B., Gijsbers, P. J. A. & Westen, S. J. P. 2006 Open MI: open modelling interface. *J. Hydroinf.* **9** (3), 175–191.

Gunduz, O. & Aral, M. M. 2005 River networks and groundwater flow: simultaneous solution of a coupled system. *J. Hydrol.* **301** (1–4), 216–234.

Harbaugh, A. W., Banta, E. R., Hill, M. C. & McDonald, M. G. 2000 *MODFLOW-2000: The US Geological Survey Modular Ground-water Model. User Guide to Modularization Concepts and the Groundwater Flow Process.* Open-File Report 00-92, US Geological Survey, Denver, CO.

Harvey, H. & Han, D. 2002 The relevance of open source to hydroinformatics. *J. Hydroinf.* **4** (4), 219–234.

Huyakorn, P. & Pinder, G. 1983 *Computational Methods in Subsurface Flow*. Academic. New York.

Hydrosphere 2004 Available at: http://sciborg.uwaterloo.ca/~mclaren/public/ or http://www.modhms.com/software/hydrosphere.html

Khatibi, R., Jackson, D., Curtin, J., Whitlow, Ch., Verwey, A. & Samuels, P. 2004 Vision statement on open architecture for hydraulic modelling software tools. *J. Hydroinf.* **6** (1), 57–74.

Kolditz, O. & Bauer, S. A. 2004 A process-orientated approach to compute multi-field problems in porous media. *Int. J. Hydroinf.* **6**, 225–244.

Kolditz, O., Du, Y., Burger, C. M., Delfs, J. O., Hess, M., Wang, W., van der Grift, B. & Te Stroet, C. 2007 Development and application of a compartment approach for hydro-system analysis to the Beerze-Reuzel catchment (Meuse basin). *J. Environ. Pollut.* **148** (3), 855–866.

Kolditz, O., Ratke, R., Diersch, H. J. & Zielke, W. 1998 Coupled groundwater flow and transport: 1. Verification of variable density flow and transport models. *Adv. Water Res.* **21** (1), 27–46.

Kollet, S. J. & Maxwell, R. M. 2006 Integrated surface–groundwater flow modeling: a free-surface overland flow boundary condition in a parallel groundwater flow model. *Adv. Water Res.* **29** (7), 945–958.

Lees, M. J. 2000 Data-based mechanistic modelling and forecasting of hydrological systems. *J. Hydroinf.* **2** (1), 15–34.

LeVeque, R. J. 2002 *Finite Volume Methods for Hyperbolic Problems*. Cambridge University Press. Cambridge.

Paniconi, C., Aldama, A. A. & Wood, E. 1991 Numerical evaluation of iterative and noniterative methods for the solution of nonlinear Richards equation. *Water Resour. Res.* **27**, 1147–1163.

Ponce, V. M., Ruh-Ming, Li. & Simmons, D. B. 1977 Applicability of kinematic and diffusion models. *J. Hydraul. Div. ASCE* **104**, 353–360.

Segol, G. 1993 *Classic Groundwater Simulations–Proving and Improving Numerical Models*. Prentice-Hall. Englewood Cliffs, NJ.

Simunek, J., Sejna, M. & van Genuchten, M. Th. 1999 *The Hydrus-2D Software Package for Simulating Two-dimensional Movement of Water, Head and Multiple Solutes in Variably Saturated Media, Version 2.0.* IGWMC-TPS-53, International Ground Water Modeling Center, Colorado School of Mines, Golden, CO.

Singh, V. P. 1994 Derivation of errors of kinematic-wave and diffusion-wave approximations for space-independent flows. *Water Res. Manage.* **8**, 57–82.

Singh, V. P. & Frevert, D. K. 2005 *Watershed Models*. CRC Press. Boca Raton, FL.

Smith, R. E. & Woolhiser, D. A. 1971 Overland flow on an infiltrating surface. *Water Resour. Res.* **7** (4), 899–913.

Starke, G. 2005 A first-order system least-squares finite element method for the shallow water equations. *SIAM J. Numer. Anal.* **42**, 2387–2407.

Sudicky, E. A., Jones, J. P., McLaren, R. G., Brunner, D. S. & VanderKwaak, J. E. 2000 A fully-coupled model of surface and subsurface water flow: model overview and application to the Laurel Creek Watershed. In *Proc. 14th Int. Conf. Comput. Meth. Water Res.*, **2**, pp. 1093–1099. Kluwer Publisher. Dordrecht.

van der Grift, B., Passier, H., Rozemeijer, J., Griffioen, J. & Smidt, E. 2006 *Integrated Modeling of Cadmium and Zinc Contamination in Groundwater and SurfaceWater of the Kempen Region, The Netherlands.* Technical Report, Institute of Applied Geoscience TNO, National Geological Survey, Utrecht, The Netherlands.

van Genuchten, M. T. 1980 A closed-form equation for predicting the hydraulic conductivity of unsaturated soil. *Soil Sci. Soc. Am. J.* **44**, 892–898.

van Rijn, L. C. 1986 *Principles of Fluid Flow and Surface Waves in Rivers, Estuaries, Seas and Oceans*. Aqua Publications. Blokzijl, The Netherlands.

VanderKwaak, J. E. 1999 *Numerical Simulation of Flow and Chemical Transport in Integrated Surface-Subsurface Hydrologic Systems*. Department of Earth Sciences, University of Waterloo. Ontario.

Vogel, T., van Genuchten, T. & Cislerova, M. 2001 Effect of the shape of the soil hydraulic functions near saturation on variably-saturated flow predictions. *Adv. Water Res.* **24**, 133–144.

Vreugdenhil, C. B. 1994 *Numerical Methods for Shallow-Water Flow*. Kluwer. Dordrecht.

Wang, J., Endreny, T. A. & Hassett, J. M. 2005 A flexible modeling package for topographically based watershed hydrology. *J. Hydrol.* **314** (1–4), 78–91.

Wang, W. & Kolditz, O. 2007 Object-oriented finite element analysis of thermo-hydro-mechanical (THM) problems in porous media. *Int. J. Numer. Meth. Eng.* **69** (1), 162–201.

Wasy Software 2004 *IFMMIKE11 1.1 User Manual*. Wasy GmbH, Institute for Water Resources Planning and System Research, Berlin.

Weiyan, T. 1992 *Shallow Water Hydrodynamics*. Water, Power Press. Hong Kong.

Enclosed Publication

[EP7] C. Schneider, S. Attinger, **J.-O. Delfs** and A. Hildebrandt (2010): *Implementing small scale processes at the soil-plant interface - the role of root architectures for calculating root water uptake profiles*, Hydrology and Earth System Sciences 14(2), 279-289. The original article is available on http://www.hydrol-earth-syst-sci.net/.

Hydrol. Earth Syst. Sci., 14, 279–289, 2010
www.hydrol-earth-syst-sci.net/14/279/2010/

Hydrology and Earth System Sciences

Implementing small scale processes at the soil-plant interface – the role of root architectures for calculating root water uptake profiles

C. L. Schneider[1], **S. Attinger**[1,2], **J.-O. Delfs**[3], **and A. Hildebrandt**[1]

[1]Helmholtz Centre for Environmental Research – UFZ, Department of Computational Hydrosystems, Leipzig, Germany
[2]Institute for Geosciences, University of Jena, Jena, Germany
[3]Helmholtz Centre for Environmental Research – UFZ, Department of Environmental Informatics, Leipzig, Germany

Received: 19 May 2009 – Published in Hydrol. Earth Syst. Sci. Discuss.: 12 June 2009
Revised: 20 January 2010 – Accepted: 24 January 2010 – Published: 12 February 2010

Abstract. In this paper, we present a stand alone root water uptake model called aRoot, which calculates the sink term for any bulk soil water flow model taking into account water flow within and around a root network. The boundary conditions for the model are the atmospheric water demand and the bulk soil water content. The variable determining the plant regulation for water uptake is the soil water potential at the soil-root interface. In the current version, we present an implementation of aRoot coupled to a 3-D Richards model. The coupled model is applied to investigate the role of root architecture on the spatial distribution of root water uptake. For this, we modeled root water uptake for an ensemble (50 realizations) of root systems generated for the same species (one month old Sorghum). The investigation was divided into two Scenarios for aRoot, one with comparatively high (A) and one with low (B) root radial resistance. We compared the results of both aRoot Scenarios with root water uptake calculated using the traditional Feddes model. The vertical rooting density profiles of the generated root systems were similar. In contrast the vertical water uptake profiles differed considerably between individuals, and more so for Scenario B than A. Also, limitation of water uptake occurred at different bulk soil moisture for different modeled individuals, in particular for Scenario A. Moreover, the aRoot model simulations show a redistribution of water uptake from more densely to less densely rooted layers with time. This behavior is in agreement with observation, but was not reproduced by the Feddes model.

Correspondence to: C. L. Schneider
(christoph.schneider@ufz.de)

1 Introduction

The global water and carbon cycles are key issues in climate and global change research. Within these complex systems, plants are the central interface between the atmosphere and hydrosphere. Transpiration plays a crucial role for the surface energy balance as well as for the water cycle. It is also linked to the carbon cycle through its close connection with photosynthesis. Hydrological as well as climate models will benefit from an improved understanding of the process of water flow through plants, in particular because they are sensitive to root water uptake parameters (Desborough, 1997; Zeng et al., 1998). Also, great uncertainty in modeling transpiration stems from lack of knowledge about how much water is available to plant roots (Lai and Katul, 2000; Feddes et al., 2001).

Plant water uptake responds to soil moisture limitation at different time and space scales. At the seasonal time scale, plants may adapt their rooting system by root growth, in order to reach moister soil areas (Wan et al., 2002). But also at smaller time scales (like hours to days), plants have been observed to change their uptake zone, and without altering their root system (Sharp and Davies, 1985; Green and Clothier, 1995; Garrigues et al., 2006).

However, models for describing water flow at the soil-plant-atmosphere-interface (SVAT-schemes) include these processes only partially. These schemes use a heuristic parametrization for root water uptake that is applied as a sink in the one-dimensional Richards Equation. Commonly, vertical root water uptake profiles are related to the product of a water stress function and the vertical rooting density distribution (like in Feddes et al., 1976). However, this parametrization leads to early predictions of limited transpiration, when densely rooted soil layers dry out (Feddes et al., 2001) and thus neglects the plants adaptive response to water stress.

Published by Copernicus Publications on behalf of the European Geosciences Union.

In order to deal with these shortcomings, several algorithms have been developed to allow for a longer period of transpiration in a SVAT context. Li et al. (2001) and Teuling et al. (2006) presented models that compensate water stress in one part of the root zone by increased uptake from other soil areas without altering rooting density profiles. Šimůnek and Hopmans (2009) followed a similar approach. They proposed a root water uptake compensation mechanism for HYDRUS (Šimůnek et al., 2006, 2008), which allows for parallel consideration of compensated water and nutrient uptake in three dimensions. Also, besides compensation effects, another mechanism sustaining transpiration in dry soil, is hydraulic redistribution. It is defined as water transfer from wetter into drier soil areas, via flow through the root system. Recently, Siqueira et al. (2008) and Amenu and Kumar (2008) investigated this effect for delayed onset of water stress in a root water uptake model, again based on rooting density profiles.

The above models treat uptake and adaptation in a lumped way, and therefore do not consider the mechanisms at the scale at which they take place. Models which include more detail could be used to gain the necessary process understanding, in order to transfer it to the SVAT scale. Small scale processes of root water uptake have already been implemented in models of varying levels of complexity.

First level models distribute the transpirational demand on the soil domain simply by the spatial distribution of roots either in one (as SVAT models do), two or three dimensions (Vrugt et al., 2001; Clausnitzer and Hopmans, 1994).

Second level models include a description of microscopic water flow along the potential gradient between the soil and the root, either using an effective resistance along this gradient like Gardner (1960, 1964) or more realistic radial dependent soil hydraulic properties (Tuzet et al., 2003; de Jong van Lier et al., 2006). The latter cover the nonlinear behavior of unsaturated water flow. This is an important mechanism in drying soils (Schröder et al., 2008), because steep potential gradients develop around the roots. These models can be extended to include root radial resistance additionally to soil resistance (Siqueira et al., 2008; Schymanski et al., 2008). For example Levin et al. (2007) showed with such a combined model that vertical uptake profiles changed depending on the assumed radial resistance. Schymanski et al. (2008) applied such a model to modify root distribution within biological constraints according to soil water availability.

The approaches above imply that the potential on the side of the root is constant throughout the root system. However, Zwieniecki et al. (2003) suggested in a combined measurement and model study that internal gradients along the root xylem exist. Depending on the ratio between the roots radial and axial resistance, the active uptake region could extend over the entire root or just part of it. This research was conducted only for a single root, but might also be relevant for uptake along the entire root system.

Third level models combine a variable xylem potential distribution along the root structure with the flow processes in the soil domain. One such model was introduced by Doussan et al. (1998). Such root water uptake models can be coupled to three dimensional soil water flow models as done in Doussan et al. (2006) or Javaux et al. (2008). Simulations with these detailed models show that the region of water uptake moves with time to deeper and moister layers, when top layers dry out. The coupling of soil and root water flow in the vicinity of the root segments was first based on an averaging approach. A finer spatial discretization of the numerical soil grid around the roots (as shown in Schröder et al., 2009) can represent the local gradients in soil water potential but at the cost of increased computational burden.

In summary, previous research using small scale models for water uptake indicates that both water flow in the soil near the root, but also within the root system itself shape the uptake behavior of the plant. Plant root systems vary greatly in form and morphology, not only between species, but also between individuals of the same species. This chapter contributes to answer the question, how does this variety influence the expected uptake pattern. Therefore, we propose a simplified third level model called aRoot and apply it to simulate the water uptake of an ensemble of root systems of the same species and age. Our model results suggest that water uptake profiles vary significantly between individuals.

2 Models and methods

The major assumption for this study is that the process of plant water uptake is gradient driven by the difference between soil water potential and atmospheric demand. In real plants, this leads to a distribution of water potentials from the leaves (stomata control) over the trunks to the stem and finally to the root system. Hence, the outer boundaries of the plants water uptake system are the atmospheric water deficit and the soil water potential. In this model exercise, we only consider the part from the soil up to the root collar. Within this study we make a comparison between two model approaches for root water uptake. One approach uses a full 3-D Richards Equation (see Sect. 2.1) coupled to the Feddes reduction function (Sect. 2.4) to simulate soil water stress effects on root water uptake. The other approach again uses the 3-D Richards Equation to model the bulk soil water flow combined with a smaller scale water uptake model called "aRoot" (Sect. 2.2). This "aRoot" model was divided into two scenarios of different root hydraulic parameterizations.

2.1 Bulk water flow in the unsaturated zone

The Richards' equation describing the water movement in the soil system is known as

$$\frac{\partial \theta}{\partial t} = \nabla[K \nabla(\psi_{\text{soil}} + z)] - \varrho(x, y, z, t)\,, \tag{1}$$

where $\theta\,[\mathrm{m^3\,m^{-3}}]$ is the volumetric soil water content, $\varrho\,[\mathrm{m^3\,m^{-3}\,s^{-1}}]$ is the sink term rate delivered by the root water uptake model (see Eq. 22) for the aRoot approach of volumetric flow rates) and t [s] is time. The numerical solution of the Richards Equation for bulk soil water flow is provided by GeoSys (Kolditz et al., 2008).

Volumetric soil water saturation θ is defined as a function of the soil water potential $\psi_{\mathrm{soil}}\,[\mathrm{m}]$ and can be expressed by the Mualem-van-Genuchten parametrization (van Genuchten, 1980) as

$$\frac{\theta-\theta_{\mathrm{r}}}{\phi-\theta_{\mathrm{r}}}=\Theta=\left[\frac{1}{1+|\alpha_{\mathrm{G}}\psi_{\mathrm{soil}}|^{n_{\mathrm{G}}}}\right]^{m_{\mathrm{G}}}, \tag{2}$$

where Θ is the normalized (or relative) water content, ϕ is the porosity of the soil and θ_{r} the residual volumetric water content (at so-called permanent wilting point), where α_{G}, n_{G} and m_{G} are soil specific parameters (see Table 1). $K\,[\mathrm{m\,s^{-1}}]$ in terms of normalized (or relative) water content Θ is then given by

$$K(\Theta)=K_{\mathrm{s}}k(\Theta)=K_{\mathrm{s}}\Theta^{\lambda_{\mathrm{G}}}\left(1-\left(1-\Theta^{\frac{1}{m_{\mathrm{G}}}}\right)^{m_{\mathrm{G}}}\right)^2, \tag{3}$$

where Θ can be replaced by ψ_{soil} using Eq.(2). The saturated hydraulic conductivity K_{s} as well as the bulk soil porosity ϕ are given in Table 1. Accounting for the effect of root segments exploring a certain soil volume, within our model the porosity ϕ of all soil grid cells is decreased by the corresponding fraction of volumetric root content. This is motivated by the fact that as root volume increases in a certain soil volume, the soils pore space gets less and hence less water can be hold in this soil volume.

Table 1. Model parameters.

Root properties				
Segm. Order	r_0 [m]	ζ_p [s] Scenario A	Scenario B	$\mathcal{R}_l\,[\mathrm{s\,m^{-3}}]$ Scenario A/B
0	0.006–0.004	5×10^{10}	5×10^{10}	1×10^{9}
1	0.004–0.003	1.5×10^{10}	1.5×10^{10}	2×10^{9}
2	0.003–0.002	7×10^{9}	9×10^{8}	6×10^{9}
3	0.002–0.001	3×10^{9}	5×10^{8}	8×10^{10}
4 ($\geqq$)	0.001–0.0005	1×10^{9}	1×10^{8}	1×10^{12}
Soil properties				
$\theta_{\mathrm{soil}}^{\mathrm{init}}$	0.4	initial soil water status [–]		
$\theta_{\mathrm{soil}}^{\mathrm{PWP}}$	0.08	permanent wilting point saturation [–]		
van Genuchten parameters for sandy soil				
K_{s}	1.785	saturated soil water conductivity [$\mu\mathrm{m\,s^{-1}}$]		
ϕ	0.46	soil porosity [–]		
α_{G}	1.44	[1 m]		
λ_{G}	−0.215	[–]		
β_{G}	0.534	[–]		
m_{G}	0.348	$=\beta_{\mathrm{G}}/(1+\beta_{\mathrm{G}})$		
n_{G}	1.534	$=\beta_{\mathrm{G}}+1$		
Feddes model: water stress function β_{rw} for sandy soil				
ψ_1	−1	[m]		
ψ_2	−2	[m]		
ψ_3	−100	[m]		
ψ_4	−150	[m]		
Boundary conditions				
T_{Pot}	−0.8	potential transpiration rate [$\mathrm{mm^3\,s^{-1}}$]		
$\psi_{\mathrm{xylem}}^{\mathrm{crit}}$	−150	critical xylem water potential [m]		

2.2 The hydraulic root water uptake model "aRoot"

In the following, we present a stand alone root water uptake model called aRoot, which calculates the sink term for the bulk soil water flow model. Since we apply an analytical expression for the radial water flow towards the root, our model concept does not require intense iteration between the bulk water flow model and aRoot for each time step.

2.2.1 Water flow within the root system

Water flow within the plants takes place as a flow from root surface to the inner root xylem (radial) and along the xylem tubes (axial). The hydraulic uptake model applied to the root system is spatially explicit consisting of a network of root segments. Each individual root segment is modeled as a series of axial and radial resistances similar to Doussan et al. (1998). These root resistances operate as an effective value for the underlying processes, like xylem development for the axial pathway and radial connectivity within the root cortex and epidermis (as described in Steudle and Peterson (1998) as the apoplastic, symplastic and transcellular pathways).

Root hydraulic properties are assigned to each root segment according to their root order given by RootTyp (see Sect. 2.3 and Table 1). The axial resistance R_{ax} is calculated by multiplying the axial resistivity per length with the corresponding root length l_{r}, while the radial resistance R_{r} is estimated by dividing the specific radial resistivity (material property of each root segment) by root surface area.

The influence of osmotic potential differences are neglected as well as the effect of aquaporins changing the specific radial resistivity per root segment (Steudle, 2000) or the effect of cavitation on xylem vulnerability increasing the axial resistance (Sperry et al., 2003).

For each root segment n the axial flux is implemented by the formula

$$J_{\mathrm{ax}}^{n}=\frac{1}{R_{\mathrm{ax}}^{n}}\left(\Delta\psi_{\mathrm{xylem}}^{n}+\Delta z^{n}\right), \tag{4}$$

where Δ is the potential gradient along the root xylem axis between two root nodes. The radial flux, which is the inflow

from the soil to the root segment n is given by

$$J_{\mathrm{rad}}^{n} = \frac{1}{R_{\mathrm{r}}^{n}}(\psi_{\mathrm{xylem}}^{n} - \psi_{\mathrm{soil}}^{n}(r_0)) , \tag{5}$$

with $\psi_{\mathrm{xylem}}^{n}$ denoting the xylem water potential within root segment n and $\psi_{\mathrm{soil}}^{n}(r_0)$ the soil water potential at the root surface of the corresponding soil disc n.

By applying the Kirchhoff's Law for summing up all in- and outflows at a root node, we receive a system of equations describing the water fluxes of the root network that can be best described in matrix notation such as

$$\mathbf{A}\,\psi_{\mathrm{xylem}} = \mathbf{B}\,\psi_{\mathrm{soil}}(r_0) + \boldsymbol{c} , \tag{6}$$

where $\mathbf{A}$ is the system matrix (regarding radial and axial root resistances) coupling root xylem pressure for interlinked root nodes, $\mathbf{B}$ is the input matrix connecting xylem potential to corresponding soil potentials and $\boldsymbol{c}$ is the offset vector accounting for gravitation (lifting water up over the vertical axis) and the upper boundary condition (flux or potential boundary at root collar). The boundary condition at the root collar is initially fixed to a given flux T_{Pot}. If the corresponding variable collar potential drops below a critical value $\psi_{\mathrm{xylem}}^{\mathrm{crit}}$, then boundary switches to a potential condition and transpirational flux becomes variant.

Rearranging Eq. (6) gives

$$\psi_{\mathrm{xylem}} = \mathbf{A}^{-1}\mathbf{B}\,\psi_{\mathrm{soil}}(r_0) + \mathbf{A}^{-1}\boldsymbol{c} . \tag{7}$$

By rewriting Eq. (5) for all root segments N and introducing the conductance matrix $\boldsymbol{\kappa}_{\mathrm{r}}$ (main diagonal matrix containing the inverse of the radial resistances $\boldsymbol{\kappa}_{\mathrm{r}} = \mathrm{diag}\left[1/R_{\mathrm{r}}^{0}, ..., 1/R_{\mathrm{r}}^{n}, ..., 1/R_{\mathrm{r}}^{N}\right]$) as well as new notations $\mathbf{E} = \mathbf{A}^{-1}\mathbf{B}$ and $\mathbf{d} = \mathbf{A}^{-1}\boldsymbol{c}$ leads to a system of equations for the overall radial fluxes in the root system, namely

$$J_{\mathrm{rad}} = \boldsymbol{\kappa}_{\mathrm{r}}[(\mathbf{E} - \mathbf{I})\,\psi_{\mathrm{soil}}(r_0) + \mathbf{d}] , \tag{8}$$

where $\mathbf{I}$ is the identity matrix of dimension N, the overall number of root nodes. This system can be simplified to

$$J_{\mathrm{rad}} = \mathbf{W}\psi_{\mathrm{soil}}(r_0) + \omega , \tag{9}$$

where $\mathbf{W} = \boldsymbol{\kappa}_{\mathrm{r}}(\mathbf{E} - \mathbf{I})$ and $\omega = \boldsymbol{\kappa}_{\mathrm{r}}\mathbf{d}$.

2.2.2 The microscopic radial water flow within the soil

The microscopic flow towards the root is assumed to be only one dimensional in radial direction towards the root, where the soil domain is modeled as a cylinder of radius r_{disc} and height l_r. Local hydraulic gradients in soil water potential towards the root can be obtained with an approximated analytical solution of the Richards equation (steady rate assumption after Jacobsen (1974) and De Willigen and van Noordwijk (1987) where the temporal change in water content is assumed to be r independent)

$$\frac{\partial \theta_{\mathrm{soil}}}{\partial t} = \frac{1}{r}\frac{\partial}{\partial r}\left[K(\psi_{\mathrm{soil}})\,r\,\frac{\partial \psi_{\mathrm{soil}}}{\partial r}\right] = \mathrm{const.} \tag{10}$$

In matric flux potential notation, this equation becomes an ODE as

$$\frac{1}{r}\frac{\partial \Phi_{\mathrm{soil}}}{\partial r} + \frac{\partial^2 \Phi_{\mathrm{soil}}}{\partial r^2} = \mathrm{const.} , \tag{11}$$

with the following solution

$$\Phi_{\mathrm{soil}}(r) = \frac{\tau_3}{4}r^2 + \tau_2 \log(r) + \tau_1 , \tag{12}$$

where τ_p are integration constants set by boundary/initial conditions.

The matric flux potential $\Phi_{\mathrm{soil}}\,[\mathrm{m^2\,s^{-1}}]$ is defined as a function of soil water potential ψ_{soil} by

$$\Phi_{\mathrm{soil}}(\psi_{\mathrm{soil}}) - \Phi_{\mathrm{soil}}^{\mathrm{ref}} = \int_{\psi_{\mathrm{soil}}^{\mathrm{ref}}}^{\psi_{\mathrm{soil}}} K(h'_{\mathrm{soil}})\,dh'_{\mathrm{soil}} , \tag{13}$$

where $\Phi_{\mathrm{soil}}^{\mathrm{ref}}$ and $\psi_{\mathrm{soil}}^{\mathrm{ref}}$ are reference states of the system. For $\psi_{\mathrm{soil}}^{\mathrm{ref}} \to -\infty$, the reference matric flux potential tends to $\Phi_{\mathrm{soil}}^{\mathrm{ref}} \to 0$, so

$$\Phi_{\mathrm{soil}}(\psi_{\mathrm{soil}}) = \int_{-\infty}^{\psi_{\mathrm{soil}}} K(h'_{\mathrm{soil}})\,dh'_{\mathrm{soil}} . \tag{14}$$

The solution of this integral depends on the functional form of $K(\psi_{\mathrm{soil}})$. Unfortunately, for the Mualem-van-Genuchten parameterization used in our soil water model, no explicit solution is known. Therefore, a closed analytical relationship between water potential h and matric flux potential Φ cannot be established. Nevertheless, within a certain range of h, the matric flux potential can be approximated by the following transfer function

$$\Phi_{\mathrm{soil}}(r_0) = b_1 \exp\left(b_2\,|\psi_{\mathrm{soil}}|^{b_3} + b_4\right) , \tag{15}$$

with b_k soil dependent fitting parameters. For our simulations, the soil parameters b_k of Eq. (15) were fitted to the numerical calculated Φ-h-profile for a sandy soil set up by the Mualem-van-Genuchten parameters given in Table 1.

The solution of Eq. 11 (similar to de Jong van Lier et al., 2008 or Schröder et al., 2009) with given boundary conditions (zero flux at outer boundary, radial flux J_{rad} at inner boundary and a given bulk matric flux potential at a certain radial distance r_{Φ_b}) can be written as

$$\Phi(r_0) = \Phi_b + \frac{J_{\mathrm{rad}}}{2\pi l}\left(\frac{a^2 - \gamma + \gamma\log(a^2\gamma)}{2 - 2\gamma}\right) , \tag{16}$$

with $\gamma = \left(r_{\Phi_b}/r_0\right)^2$, r_0 the root radius, r_{disc} the soil disc radius and $r_{\Phi_b} = a r_{\mathrm{disc}}$, where $a = 0.607$ is proposed by de Jong van Lier et al. (2006). The soil disc radius r_{disc} is linked to the root length in a given soil volume and is set equal for all root segments n within this volume.

Hence, the soil water flow corresponding to all root segments is given by the gradient in matric flux potential between the soil-root interface and the bulk soil multiplied with a function determined by the boundary conditions and hence depending on the segment geometry (given by Eq.16),

$$J^n_{\text{rad}} = g^n \left(\Phi^n_{\text{soil}}(r_0) - \Phi^n_b\right), \tag{17}$$

with

$$g^n = \frac{4\pi l^n (1-\gamma^n)}{a^2 - \gamma^n + \gamma^n \log(a^2\gamma^n)} \,. \tag{18}$$

Writing the radial soil water flow in matrix notation for all N segments with $\mathbf{G}$ the main diagonal matrix containing the functional terms g^n ($\mathbf{G} = \text{diag}\left[g^0, .., g^n, .., g^N\right]$, we receive

$$J_{\text{rad}} = \mathbf{G}(\Phi_{\text{soil}}(r_0) - \Phi_b) \,. \tag{19}$$

2.2.3 Coupling the root and radial soil water flow

The radial root water flow (9) and the radial soil water flow (19) are set equal (coupled directly via flux type condition)

$$\mathbf{W}\psi_{\text{soil}}(r_0) + \boldsymbol{\omega} = \mathbf{G}(\Phi_{\text{soil}}(r_0) - \Phi_b) \,, \tag{20}$$

with Φ given as a nonlinear function of h depending on soil parameters (here given by Eq. (15)) resulting in

$$\mathbf{W}\psi_{\text{soil}}(r_0) + \boldsymbol{\omega} = \mathbf{G}(f(\psi_{\text{soil}}(r_0)) - f(\psi_{\text{b}})) \,. \tag{21}$$

This nonlinear system of equations is solved based on a certain bulk water potential and the given root system with its specific boundary condition at the root collar (forming the matrices $\mathbf{W}$, $\mathbf{G}$ and the vector $\boldsymbol{\omega}$) leading to a distribution of the water potential at the soil-root-interface $\psi_{\text{soil}}(r_0)$.

2.2.4 The sink term for the macroscopic bulk water flow in the unsaturated zone

Figure 1 shows the model scheme we use to implement the sink terms into the bulk soil water flow model and how the bulk soil water potential feeds back to the microscale radial soil water flow model. Our concept underlies the assumption that all soil discs around root segments covering a certain soil volume Ω_{ijk} share uniform bulk water potential ψ_b and soil disc radii r_{disc}.

The sink term S for the bulk soil water flow model is calculated by summing up the radial fluxes J^m_{rad} of all soil discs m belonging to a certain bulk soil volume Ω_{ijk} as

$$S(i,j,k) = \sum_m J^m_{\text{rad}} \quad \forall \;\; J^m_{\text{rad}} \in \Omega_{ijk}$$

$$\Omega_{ijk} = \{(x,y,z) \in \mathbb{R}^3 : a_i \le x \le a_{i+1}, \; b_j \le y \le b_{j+1}, c_k \le z \le c_{k+1}\},$$

with $i, j \in \{1 \ldots N_{\text{hor}}+1\} \subset \mathbb{Z}, k \in \{1 \ldots N_{\text{vert}}+1\} \subset \mathbb{Z}$, where N_{hor} and N_{vert} are the number of bulk soil volumes in the horizontal and vertical direction and the rules for a_i, b_j and c_k are the following

$$a_i = x_{\min} + (i-1)\Delta x; \;\; \Delta x = \tfrac{x_{\max} - x_{\min}}{N_{\text{hor}}};$$
$$b_j = y_{\min} + (j-1)\Delta y; \;\; \Delta y = \tfrac{y_{\max} - y_{\min}}{N_{\text{hor}}};$$
$$c_k = z_{\min} + (k-1)\Delta z; \;\; \Delta z = \tfrac{z_{\max} - z_{\min}}{N_{\text{vert}}}.$$

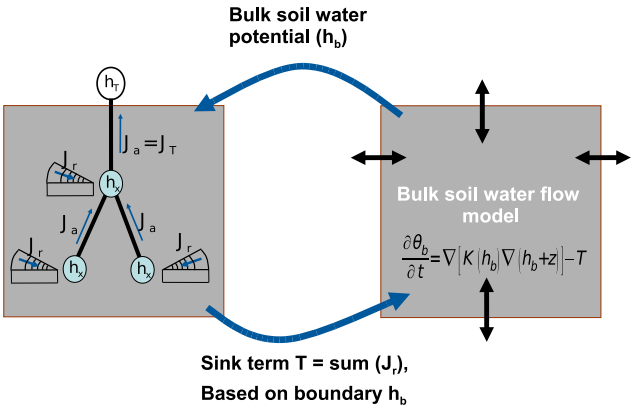

Fig. 1. Concept of coupling microscale radial flow to bulk flow including xylem potentials for a bulk soil volume Ω_{ijk}.

2.3 The root architecture model

The root architecture model used for our simulations is based on the generic model RootTyp by Pagès et al. (2004). The generator creates realizations of the same species by simulating growth as a random process covering root emission, axial and radial growth, sequential branching, reiteration, transition, decay and abscission. The interplay of these processes is parameterized plant specifically. We used a parameter set for plant species of sorghum type, which is a class of numerous grass species. The size of the root system depends on the stage of plant development, hence age. All generated root systems are characterized by their interconnected root segments of a designated order. The order defines the segments axial resistance per length (due to alternating xylem vessel elaboration), specific radial resistivity (due to different stages of suberization) and root radius (see Table 1). Figure 2 shows exemplary a root system for one of the 50 realizations.

2.4 The Feddes model

The RWU function of Feddes (like in Feddes et al., 2001) is the following

$$\varrho(h(x,y,z)) = \beta_{\text{rw}}(h) \frac{L^a_V(x,y,z)}{\int\limits_V L^a_V(x,y,z)dV} \, T_{\text{Pot}} \,, \tag{22}$$

with L^a_V [m m^{-3}] the accumulated root length per volume (RLD) at a point, V the overall volume of the soil-root domain and T_{Pot} [m^3 s^{-1}] the potential transpiration flow

Fig. 2. 2-D-plot of two arbitrarily chosen root system realizations created by the root architecture generator RootTyp.

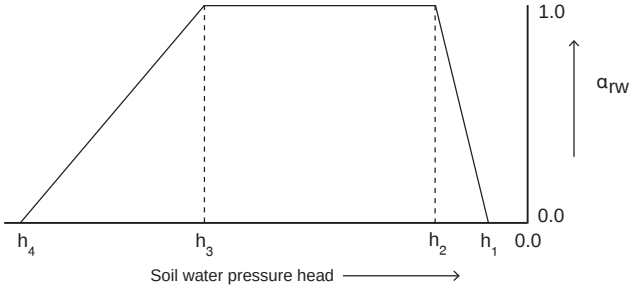

Fig. 3. Water stress function used in the Feddes model: Water uptake above h_1 and below h_4 is set to zero due to oxygen deficit and wilting point. Between h_2 and h_3 water uptake is maximal ($\alpha_{\mathrm{rw}} = 1$). Above h_2 and below h_3, the so-called critical point, water uptake gets limited where the precise value of h_3 is assumed to vary with potential transpiration rate T_{Pot}.

rate. To get the volumetric flow rate $S(x, y, z)$, the extraction rate (of volume of water per volume of soil per time) ϱ [$\mathrm{m^3\,m^{-3}\,s^{-1}}$] has to be applied to a specific soil volume Ω.

The Feddes approach includes a water stress function β_{rw}, where the most common implemented stress function has the form shown in Fig. 3.

2.5 Model input and scenarios

The model exercise was divided into three characteristic cases: (1) the Feddes approach widely applied in current SVAT models based on the RLD neglecting the root systems network character as well as microscopic radial water flow within the soil, the aRoot simulations for (2) Scenario A where higher order roots have higher radial resistances and the aRoot simulations for (3) Scenario B where higher order roots have lower radial resistances (see Table 1). The reason for dividing the aRoot model in two Scenarios (A and B) is the ongoing debate on the range of the radial resistance values (references from Steudle and Peterson, 1998; Zwieniecki et al., 2003).

We performed the simulations for all three cases on 50 root system realizations. The simulation time for root water uptake for all realizations was set to 10 days (with time steps of $\Delta t = 30$ min.) starting from a uniform, initial saturation of $\Theta = 0.4$. The bulk soil water flow model runs on a $2.5 \times 2.5 \times 2.5$ [cm] grid cell size. The overall soil domain size in x-, y- and z-direction is $27.5 \times 27.5 \times 22.5$ [cm] among all root realizations. The plants root system age was set to 1 month (28 days) where there was no further root growth applied within the simulation time.

The transpiration rate was assumed to be time invariant with $T_{\mathrm{Pot}} = -8 \times 10^{-10}\,\mathrm{m^3\,s^{-1}}$ over the 10 days of unlimited uptake, as long as the root collar potential has not exceeded a given threshold. If the corresponding variable collar potential drops below this critical value $\psi_{\mathrm{xylem}}^{\mathrm{crit}}$, then the boundary switches from a flux type to a potential type condition and transpirational flux gets variant.

The specific radial resistance ζ_p (as a material constant for root order k with a given thickness of the roots radial pathway) is assumed to decline with increasing k caused by less suberization, where ζ_p is calculated by multiplying the materials resistivity χ_{pr} with the roots radial thickness r_c. Radial resistance R_{r} is the ratio of ζ_p to the root outer surface area ($R_{\mathrm{r}} = \zeta_p/(2\pi r_0 l)$ [$\mathrm{s\,m^{-2}}$]). Also, we assume that axial resistance per length $\mathcal{R}_l$ increases with root order (due to decreasing root radius), multiplied by the root segment length l_{r} it gives the axial resistance $R_{\mathrm{ax}} = \mathcal{R}_l \times l_{\mathrm{r}}$ [$\mathrm{s\,m^{-2}}$].

Parameters of Scenario A are in agreement with measurements by Steudle and Peterson (1998)(page 778): Root properties of segment order 2 are referenced by the mature late metaxylem measurements whereas for root order 4 characteristics are given by the early metaxylem. For Scenario B radial resistance was decreased, but only for higher order roots, so that $R_{\mathrm{ax}}/R_{\mathrm{r}}$ is in the range of 0.025 in accordance to the results of Zwieniecki et al. (2003).

3 Results

3.1 Influence of root architecture and hydraulic root parameters on root water uptake behavior

Figure 4 shows the modeled root water uptake (RWU) versus root length density (RLD). The plotted points represent entities on the bulk scale where the RLD was calculated by counting root segment lengths in each bulk soil grid cells and RWU is the given sink term of the bulk soil water flow in Eq. (1). We plotted all model runs (50 realizations of each, the Feddes approach, aRoot Scenario A and aRoot Scenario B) at three different time steps (0, 5 and 10 days).

For the initial time step plot (Fig. 4a), all model runs provided very similar results. The results of the Feddes approach match perfectly the 1:1 line which was expected from the model assumption. For later time steps (Fig. 4b and c), we

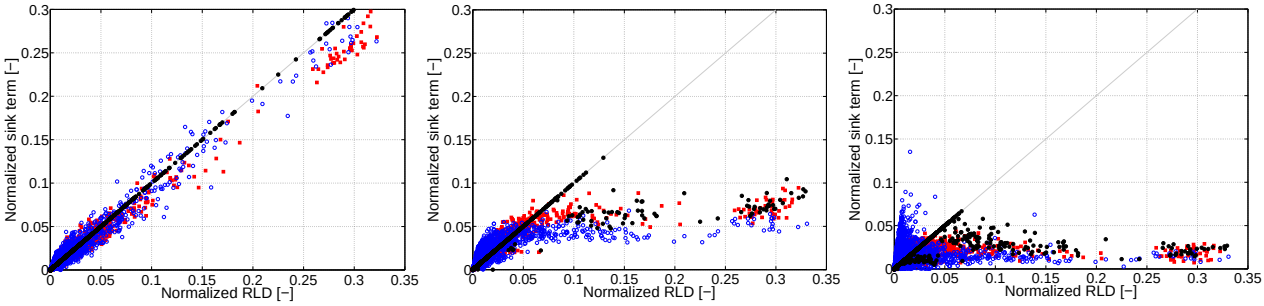

(a) 0 days (b) 5 days (c) 10 days

Fig. 4. Sink term vs. RLD for 50 Realizations of Scenario A (red square), Scenario B (blue circle) and Feddes (black dot) at **(a)** initial time step $t = 0$, **(b)** after 5 days and **(c)** after 10 days (sink terms are normalized by the potential transpiration rate T_{Pot} and RLD by total root length)

see that Scenarios A and B of aRoot show some compensation effects: water uptake from areas of higher RLD is decreased and this decline is compensated by increased uptake from lower RLD regions where Scenario B shows a stronger compensation than Scenario A does. Also, at $t = 5$ and $t = 10$ days, the sink terms of the Feddes approach and the aRoot Scenarios A and B were comparably similar for higher RLD (between 0.1 and 0.35). Within the range of lower RLD (normalized values from 0 to 0.2), water uptake was highest for the Feddes model and lowest for Scenario B. However, in the part of lower RLD (up to 0.1) the sink terms for the Feddes model remained mostly at the 1:1 line with no compensational effects. This missing effects are a straight result of the Feddes model assumptions.

3.2 Influence of root architecture on vertical uptake profiles

In Fig. 7, we plotted the vertical profiles for RLD and RWU. For this, both variables were averaged over the horizontal soil domain and normalized by the total root length respectively the potential transpiration rate T_{Pot}.

All 50 root system realizations showed a similar RLD profile resulting in a narrow 90% confidence band. For the aRoot Scenarios A and B, the RWU profiles showed larger confidence bands than the RLD profile. Moreover, during the simulation, the confidence intervals for the water uptake profiles increased in all three cases. The strongest spread could be seen for Scenario B, while the Feddes approach showed only very little variation.

At the initial time step, $t = 0$ days, the mean water uptake profile for both aRoot Scenarios was in the range of the mean RLD profile. The confidence bands showed a slightly higher spread for the uptake profiles than for the RLD profiles. At t=10 days, the mean uptake at layers with high RLD was for Scenario B only 40% of what would be expected by the RLD profile. At the same time, it was up to 300% higher than RLD at deeper soil layers of lower rooting density. The same trends were observed for Scenario A but with smaller differences between vertical RWU and RLD because of already limited uptake.

Furthermore, the vertical water uptake profiles of Scenarios A and B showed a moving uptake front from layers of high RLD to layers of lower RLD for both scenarios. This shift was faster for Scenario B than for A. Also for Scenario A, RWU was limited earlier than for Scenario B resulting in a slighter compensation of decreased uptake from higher layers (already drier) by increased uptake from lower rooted layers (still wet).

Compared to the aRoot model, we see important differences in the Feddes model: at timestep $t = 0$ days the profiles of vertical uptake do perfectly match the RLD profiles as can already be seen in Fig. 4a. With time the uptake in the layers of higher RLD decreases but with no compensation of water uptake from less densely rooted layers. The width of the confidence bands remains almost constant in the layers of decreased uptake while they still match the RLD profiles in the nonlimited deeper layers. This general uptake behavior leads to early limitation of water uptake compared to the aRoot model.

3.3 Influence of root architecture on critical point of water uptake limitation

Another important factor for modeling root water uptake is the relation between transpirational demand and resulting collar potential (or vice versa). This can only be investigated with a model where xylem potentials are resolved, which is the case for aRoot but not for the Feddes model.

Figure 5 shows the evolution of the root collar potentials over simulation time for all 50 realizations. The influence of root radial resistance on collar potential becomes obvious by comparing Fig. 5a (Scenario A) and b (Scenario B). We see that plants in Scenario A would exhibit a more negative xylem pressure than in Scenario B. This is due to the larger resistance in the flow path from soil to xylem. The curves

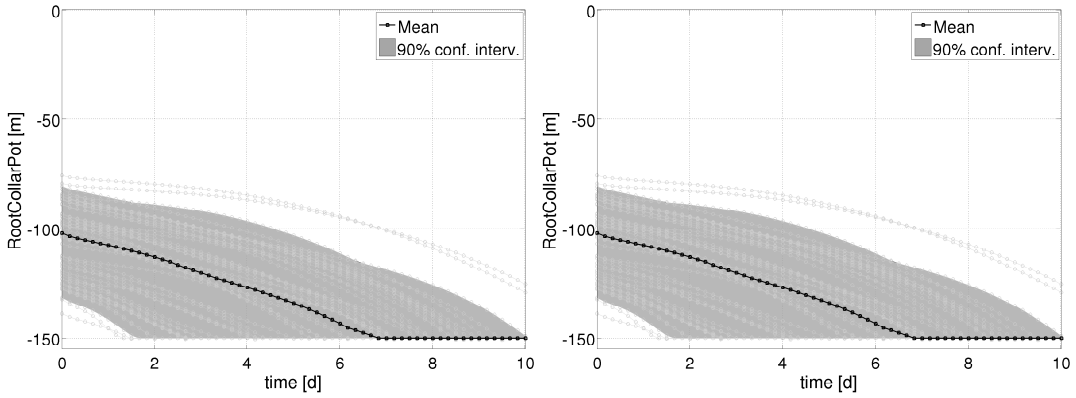

(a) Scenario A (b) Scenario B

Fig. 5. Temporal evolution of collar potentials for **(a)** Scenario A and **(b)** Scenario B. The black dotted line is the mean xylem water potential at the root collar for all 50 realizations. The gray band denotes the 90% confidence interval and the light gray lines are the individual collar potential curves.

also show a high variability among the realizations for Scenario A where for B, the confidence interval is narrow for most of the simulation. We also see that plants in Scenario A reach the critical point of limited water uptake much earlier than in Scenario B. There, water uptake is still unlimited at the end of the 10 day long simulations for all realizations.

In Fig. 6, we plotted only for Scenario A mean soil saturation versus resulting actual transpiration. We observed a wide spread of expected water uptake from individual root architectures. While in early limited root systems uptake was reduced by 40 %, other systems were still not limited after 10 days of transpiration.

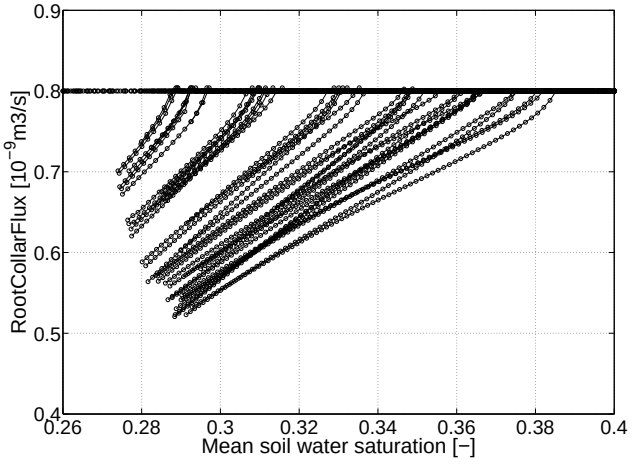

Fig. 6. Individual collar fluxes (black dotted line) for all 50 realizations of Scenario A over mean soil saturation defined as the integral of the entire soil domain (regarding the soil domain as a simple bucket).

4 Discussion

In this model exercise we generated 50 root architectures using the model RootTyp of Pagès (Pagès et al., 2004). These realizations could be interpreted as 50 different individuals of the same plant species and age. The obtained root systems show similar root length density profiles, as indicated by the narrow confidence intervals shown in Fig. 7. Root length density decreases exponentially with depth for all individuals. This is in accordance to observations not only for grasses, but for all biomes (Schenk and Jackson, 2002).

For these root systems, root water uptake was simulated over 10 days of transpiration by three model cases: the architecture based aRoot model by Scenarios A and B and the root length based SVAT approach by Feddes. We implemented Scenarios A and B both based on current literature in plant physiology (see Steudle and Peterson, 1998; Zwieniecki et al., 2003). For Scenario A, the specific radial resistivity of higher order roots is set within the higher range, where for Scenario B it is at the lower limit. The model results for both Scenarios differ, but both show a confidence spread over all modeled individuals, either regarding the evolved collar potential and reaching limiting soil water conditions (Scenario A) or regarding the distribution of vertical uptake profiles over soil depth (Scenario B).

While Scenario A gives vertical uptake profiles that do differ less among the 50 realizations than Scenario B, it shows a high variability in xylem potentials that need to be applied at the root collar. The temporal evolution of collar potential differs among the realizations for Scenario A already at early times, which emphasizes the role of higher root radial resistances. The opposite holds for Scenario B: We see more scattering among the vertical uptake profiles than for Scenario A but less scatter in the evolution of root collar potentials. This variability in the vertical RWU profiles is due to the effects of local soil water depletion. Thus, the influence of root architecture on RWU is either more on the plants side

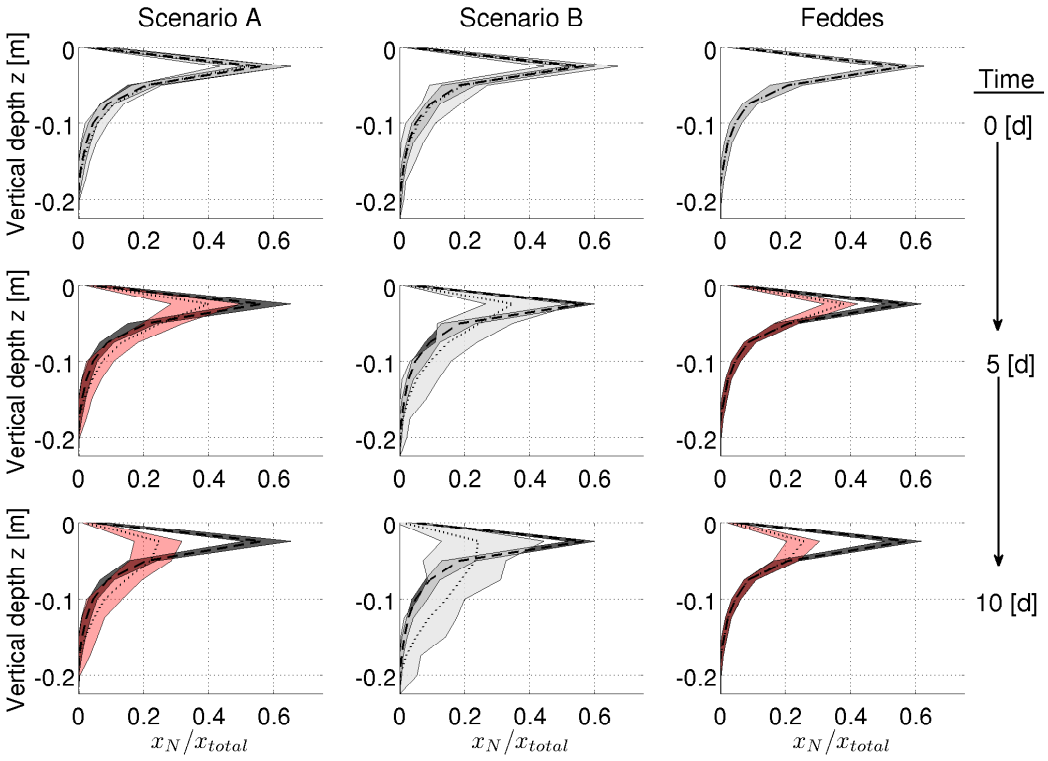

Fig. 7. Vertical Profiles of RLD (dashed) and RWU (dotted) over soil depth for 50 Realizations of Scenario A (left), B (middle) and Feddes (right) at time steps $t = 0$ (up), 5 (middle) and 10 (bottom) days. The dark gray band is the 90% confidence interval for the vertical RLD profile, where the light gray band is the 90% confidence interval for the RWU profile (transparent red bands denote limited water uptake).

(concerning the temporal evolution of collar potentials, Scenario A) or on the soils side (concerning the vertical uptake profiles, Scenario B).

In our aRoot simulations the modeled root water uptake moves from densely to less densely rooted layers with time. This is in agreement with observation (Garrigues et al., 2006; Lai and Katul, 2000) as well as with results from detailed 3-D models for root water uptake (Doussan et al., 2006; Javaux et al., 2008). Our results suggest that the dynamic of this shift depends on the individual root architecture as well as on root properties (here the range of radial resistances). The Feddes approach does not show this moving uptake behavior (as the model does not consider such effects) and additionally lacks the architecture based scattering in water uptake rates versus RLD. Javaux et al. (2008) already pointed out, the parameterization of the Feddes model seems to have little biophysical basis. Our results support this interpretation.

Our simulations show that the occurrence of decreasing water uptake is not at a unique critical point in soil water potential (corresponding to point ψ_3 in Fig. 3). This was the case, although we used the same soil environment and same plant species (with similar RLD profiles). Rather, this study shows that root architecture influences the critical point of bulk soil water content where water uptake becomes limiting. The diverse access of the root systems hydraulic active roots to the soil water storage explains this model result.

The proposed model aRoot underlies certain assumptions or simplifications. Schröder et al. (2008) has shown, that the local soil hydraulic conductivity drop around the roots becomes important when increasing the size of the bulk soil grid cells. We accounted for this by implementing a microscale radial flow model coupled to the bulk soil water flow. In their model study, Schröder et al. (2009) concluded that for coarser soil discretization, separating the microscale (radial) flow from bulk soil water flow as done in aRoot (similar to their method C) gave the best results compared to fine discretized RWU models. The assumption of uniform bulk water content and soil disc radii for all soil discs covering a certain soil volume is discussed in de Jong van Lier et al. (2006). Further work would be necessary to quantify the influence of this assumption.

Further on, within the current model version of aRoot no root growth occurs within the 10 days long simulation. Although we have not implemented root growth, our simulations can be regarded as a stepwise analysis of water uptake related to a certain soil water distribution. Coupling root growth to soil water availability would change the focus of this chapter from the role of root architecture on RWU to adaptivity issues. Nevertheless, root growth can be implemented into aRoot later.

Table 2. List of Variables and Abbreviations.

Symbol	Units	Description
r	m	radial distance
x, y, z	m	cartesian coordinates
l_r	m	root segment length
t	s	time
ψ	m	matric potential
Φ	$m^2\,s^{-1}$	matric flux potential
θ	$m^3\,m^{-3}$	volumetric water content
J, T, S	$m^3\,s^{-1}$	volumetric flow rates
K	$m\,s^{-1}$	hydraulic conductivity
R	$s\,m^{-2}$	hydraulic resistance
κ	$m^2\,s^{-1}$	hydraulic conductance
L_V^a	$[m\,m^{-3}]$	accumulated root length per volume (RLD)
RLD		*r*oot *l*ength *d*ensity
RWU		*r*oot *w*ater *u*ptake

5 Conclusions

In this chapter we developed a simplified model, that captures small scale features of plant-water uptake but is still computationally fast. Although our model currently runs with a 3-D Richards Model it is intended for later implementation in SVAT schemes and for testing hypotheses on optimal root behavior in different environments.

With our model, we found a wide range of vertical water uptake profiles even for very similar vertical RLD profiles, which is a result of the individual behavior of each root architecture and its hydraulic parameters. Root architecture becomes more important for the spatial distribution of uptake with time as shown by the increase of confidence bands for the vertical uptake profiles.

The model predictions with the architecture based model aRoot show different behavior than the Feddes Model. The Feddes model distributes and limits root water uptake based on two key properties of the plant or plant community: (1) the root length density profile, and (2) the critical point where water uptake starts to be limited by soil moisture (see ψ_3 in Fig. 3). Our modeling results with aRoot suggest that both of these properties are not suitable for describing the distribution of real water uptake. While the root length density distribution was similar for all 50 root system realizations, root water uptake profiles differed considerably between individuals. This was especially the case, when assuming relatively low values of root radial resistance (scenario B). Also, transpiration started to be limited at a wide range of bulk water contents, particularly for scenario A, where large root radial resistance was assumed.

Our results suggest that root water uptake behavior might vary greatly between individuals of a particular species. More research is necessary to support this conclusion, and to identify such root properties, which are suitable for describing root water uptake profiles. Also, roots have a complex effect on soil water content and the flow of water through the soil by roots, especially if the interaction between root growth and the surrounding soil is considered. In case of roots clustering in a certain soil volume this might significantly affect the pore space distribution, further impacting on the water holding and soil water movement characteristics.

Acknowledgements. We thank Doris Vetterlein, Andrea Carminati, Mathieu Javaux, Tom Schröder, Vanessa Dunbabin and Jan W. Hopmans for early discussion and comments. This work was kindly supported by Helmholtz Impulse and Networking Fund through Helmholtz Interdisciplinary Graduate School for Environmental Research (HIGRADE).

Edited by: N. Romano and C. Hinz

References

Amenu, G. G. and Kumar, P.: A model for hydraulic redistribution incorporating coupled soil-root moisture transport, Hydrol. Earth Syst. Sci., 12, 55–74, 2008, http://www.hydrol-earth-syst-sci.net/12/55/2008/.

Clausnitzer, V. and Hopmans, J. W.: Simultaneous modeling of transient three-dimensional root growth and soil water flow, Plant Soil, 164, 299–314, 1994.

de Jong van Lier, Q., Metselaar, K., and van Dam, J. C.: Root water extraction and limiting soil hydraulic conditions estimated by numerical simulation, Vadose Zone J., 5, 1264–1277, doi: 10.2136/vzj2006.0056, 2006.

de Jong van Lier, Q., van Dam, J. C., Metselaar, K., de Jong, R., and Duijnisveld, W. H. M.: Macroscopic Root Water Uptake Distribution Using a Matric Flux Potential Approach, Vadose Zone J., 7, 1065–1078, 2008.

De Willigen, P. and van Noordwijk, M.: Root, Plant. Production and Nutrient Use Efficiency, Ph.D. thesis, Agricultural University, Wageningen, The Netherlands, 1987.

Desborough, C. E.: The impact of root weighting on the response of transpiration to moisture stress in land surface schemes, Mon. Weather Rev., 125(8), 1920–1930, doi:10.1175/1520-0493(1997)125⟨1920:TIORWO⟩2.0.CO;2, 1997.

Doussan, C., Pagès, L., and Vercambre, G.: Modelling of the Hydraulic Architecture of Root Systems: an Integrated Approach to Water Absorption – Model Description, Ann. Bot.-London, 81, 213–223, 1998.

Doussan, C., Pierret, A., Garrigues, E., and Pagès, L.: Water uptake by plant roots: II – Modelling of water transfer in the soil root-system with explicit account of flow within the root system – Comparison with experiments, Plant Soil, 283(1–2), 99–117, doi:10.1007/s11104-004-7904-z, 2006.

Feddes, R., Kowalik, P., Kolinska-Malinka, K., and Zaradny, H.: Simulation of field water uptake by plants using a soil water dependent root extraction function, J. Hydrol., 31, 13–26, 1976.

Feddes, R. A., Hoff, H., Bruen, M., Dawson, T., de Rosnay, P., Dirmeyer, P., Jackson, R. B., Kabat, P., Kleidon, A., Lilly, A., and Pitman, A. J.: Modeling Root Water Uptake in Hydrological and Climate Models, B. Am. Meteorol. Soc., 82, 2797–2809, 2001.

Gardner, W. R.: Dynamics aspects of water availability to plants, Soil Sci., 89, 63–73, 1960.

Gardner, W. R.: Relation of root distribution to water uptake and availabilty, Agron. J., 56, 41–45, 1964.

Garrigues, E., Doussan, C., and Pierret, A.: Water Uptake by Plant Roots: I - Formation and Propagation of a Water Extraction Front in Mature Root Systems as Evidenced by 2-D Light Transmission Imaging, Plant Soil, 283(1–2), 83–98, doi:10.1007/s11104-004-7903-0, 2006.

Green, S. R. and Clothier, B.: Root water uptake by kiwifruit vines following partial wetting of the root zone, Plant Soil, 173, 317–328, doi:10.1007/BF00011470, 1995.

Jacobsen, B.: Water and phosphate transport to plant roots, Acta Agr. Scand., 24, 55–60, 1974.

Javaux, M., Schröder, T., Vanderborght, J., and Vereecken, H.: Use of a Three-Dimensional Detailed Modeling Approach for Predicting Root Water Uptake, Vadose Zone J., 7, 1079–1089, doi:10.2136/vzj2007.0115, 2008.

Kolditz, O., Delfs, J.-O., Bürger, C., Beinhorn, M., and Park, C.-H.: Numerical analysis of coupled hydrosystems based on an object-oriented compartment approach, J. Hydroinform., 10(3), 227–244, doi:DOI:10.2166/hydro.2008.003, 2008.

Lai, C.-T. and Katul, G.: The dynamic role of root-water uptake in coupling potential to actual transpiration, Adv. Water Resour., 23(4), 427–439, doi:doi:10.1016/S0309-1708(99)00023-8, 2000.

Levin, A., Shaviv, A., and Indelman, P.: Influence of root resistivity on plant water uptake mechanism, part I: numerical solution, Transport Porous Med., 70, 63–79, doi:10.1007/s11242-006-9084-1, 2007.

Li, K., Jong, R. D., and Boisvert, J.: An exponential root-water-uptake model with water stress compensation, J. Hydrol., 252, 189–204, 2001.

Pagès, L., Vercambre, G., Drouet, J.-L., Lecompte, F., Collet, C., and Bot, J. L.: Root Typ: a generic model to depict and analyse the root system architecture, Plant Soil, 258, 103–119, 2004.

Schenk, H. and Jackson, R.: The global biogeography of roots, Ecol. Monogr., 72(3), 311–328, 2002.

Schröder, T., Javaux, M., Vanderborght, J., Körfgen, B., and H. Vereecken, H.: Effect of local soil hydraulic conductivity drop using a 3-D root water uptake model, Vadose Zone J., 7, 1089–1098, doi:10.2136/vzj2007.0114, 2008.

Schröder, T., Javaux, M., Vanderborght, J., Körfgen, B., and H. Vereecken, H.: Implementation of a microscopic soil-root hydraulic conductivity drop function in a 3-D soil-root architecture water transfer model, Vadose Zone J., 8, 783–792, 2009.

Schymanski, S. J., Sivapalan, M., Roderick, M. L., Beringer, J., and Hutley, L. B.: An optimality-based model of the coupled soil moisture and root dynamics, Hydrol. Earth Syst. Sci., 12, 913–932, 2008, http://www.hydrol-earth-syst-sci.net/12/913/2008/.

Sharp, R. E. and Davies, W. J.: Root Growth and Water Uptake by Maize Plants in Drying Soil, http://jxb.oxfordjournals.org/cgi/content/abstract/36/9/1441, J. Exp. Bot., 36(170), 1441–1456, 1985.

Siqueira, M., Katul, G., and Porporato, A.: Onset of water stress, hysteresis in plant conductance, and hydraulic lift: Scaling soil water dynamics from millimeters to meters, Water Resour. Res., 44, W01432, doi:10.1029/2007WR006094, 2008.

Šimůnek, J., van Genuchten, M. Th., and Šejna, M.: The HYDRUS Software Package for Simulating Two- and Three-dimensional Movement of Water, Heat, and Multiple Solutes in Variably-saturated Media, Technical Manual, Version 1.0, PC Progress, Prague, Czech Republic, p. 241, 2006.

Šimůnek, J., Šejna, M., Saito, H., Sakai, M., and van Genuchten, M. Th.: The HYDRUS-1D Software Package for Simulating the Movement of Water, Heat, and Multiple Solutes in Variably Saturated Media, Version 4.0, HYDRUS Software Series 3, Department of Environmental Sciences, University of California Riverside, Riverside, California, USA, p. 315, 2008.

Šimůnek, J. and Hopmans, J. W.: Modeling compensated root water and nutrient uptake, Ecol. Model., 220, 505–520, doi:10.1016/j.ecolmodel.2008.11.004, 2009.

Sperry, J. S., Stiller, V., and Hacke, U. G.: Xylem hydraulics and the Soil-Plant-Atmosphere Continuum: Opportunities and Unresolved Issues, http://agron.scijournals.org/cgi/content/abstract/95/6/1362, Agron. J., , 95(6), 1362–1370, 2003.

Steudle, E.: Water uptake by plant roots: An integration of views, Plant Soil, 226, 45–56, 2000.

Steudle, E. and Peterson, C. A.: How does water get through roots?, http://jxb.oxfordjournals.org/cgi/content/abstract/49/322/775, J. Exp. Bot., 49(322), 775–788, 1998.

Teuling, A. J., Uijlenhoet, R., Hupet, F., and Troch, P. A.: Impact of plant water uptake strategy on soil moisture and evapotranspiration dynamics during drydown, Geophys. Res. Lett., 33, L03401, doi:10.1029/2005GL025019, 2006.

Tuzet, A., Perrier, A., and Leuning, R.: A coupled model of stomatal conductance, photosynthesis and transpiration, Plant Cell Environ., 26, 1097–1116, doi:10.1046/j.1365-3040.2003.01035.x, 2003.

van Genuchten, M.: A closed-form equation for predicting the hydraulic conductivity of unsaturated soils, Soil Sci. Soc. Am. J., 44, 892–898, 1980.

Vrugt, J. A., van Wijk, M. T., Hopmans, J. W., and Šimunek, J.: One-, two-, and three-dimensional root water uptake functions for transient modeling, http://www.agu.org/journals/wr/v037/i010/2000WR000027/, Water Resour. Res., 37 (10), 2457–2470, 2001.

Wan, C., Yilmaz, I., and Sosebee, R.: Seasonal soil-water availability influences snakeweed root dynamics, J. Arid Environ., 51, 255–264, doi:10.1016/jare.2001.0942, 2002.

Zeng, X., Dai, Y., Dickinson, R., and Shaikh, M.: The role of root distribution for climate simulation over land, http://www.agu.org/pubs/crossref/1998/1998GL900216.shtml, Geophys. Res. Lett., 25(24), 4533–4536, 1998.

Zwieniecki, M. A., Thompson, M. V., and Holbrook, N. M.: Understanding the Hydraulics of Porous Pipes: Tradeoffs Between Water Uptake and Root Length Utilization, J. Plant Growth Regul., 21, 315–323, doi:10.1007/s00344-003-0008-9, 2003.